2021

The Receptor Basis of Serotonergic Modulation in an Olfactory Network

Tyler Ryan Sizemore
West Virginia University, tsizemo2@mix.wvu.edu

The Receptor Basis of Serotonergic Modulation in an Olfactory Network

Tyler R. Sizemore

Dissertation submitted to the Eberly College of Arts and Sciences at West Virginia University in partial fulfillment of the requirements for the degree of

Doctor of Philosophy
in
Biology

Andrew M. Dacks, Ph.D., Committee Chairperson

Kevin C. Daly, Ph.D.

Clifton P. Bishop, Ph.D.

Sarah M. Farris, Ph.D.

Eric S. Tucker, Ph.D.

Department of Biology

Morgantown, West Virginia

July 2021

Keywords: neuromodulation, olfaction, *Drosophila*, serotonin, myoinhibitory peptide, neuropeptides

ABSTRACT

The Receptor Basis of Serotonergic Modulation in an Olfactory Network

Tyler R. Sizemore

Neuromodulation is a nearly ubiquitous process that endows the nervous system with the capacity to alter neural function at every level (synaptic, circuit, network, etc.) without necessarily adding new neurons. Through the actions of neuromodulators, the existing neural circuitry can be adaptively tuned to achieve flexible network output and similarly dynamic behavioral output. However, despite their near ubiquity in all sensory modalities, the mechanisms underlying neuromodulation of sensory processing remain poorly understood. In this dissertation, I address three main questions regarding the mechanisms of one modulator (serotonin) within one sensory modality (olfaction). I begin by establishing a “functional atlas” of which principal neuron types express which of the five serotonin receptors in the highly-tractable *Drosophila* primary olfactory center, the antennal lobe. Later, I use this “functional atlas” to determine how the activity of one serotonin receptor shapes the activity of a specialized neuropeptidergic signaling pathway. However, before I can address how the activity of this serotonin receptor adjusts the activity of this neuropeptidergic pathway, I demonstrate how this neuropeptidergic pathway shapes olfactory processing. Altogether, my work establishes several key insights that expand our understanding of neuromodulation of sensory processing.

DEDICATIONS

To Mom, Lana S. Sizemore:

It's only because of your sacrifices and support that I am here today. I can only hope to be half of the parent and person you are one day. Seeing how hard you worked to give me and Dakota a great chance at a good life is the inspiration for my drive and dedication. Thank you for your unconditional love and support – I love you.

To my Father, Michael W. Duncan:

I wish I could set down at the breakfast table with you and show you this document. I wish I could see your smile and get a big hug. I miss texting you and hearing about what Karma was " wild'n'out " over recently. I wish you could be here for all of my future "big life events". I'll always love and miss you.

To Kristyn:

You are my best friend and the love of my life, and without graduate school we may have never met. I am truly lucky to have you in my life. Thank you for always being there, and being "my bean".

ACKOWLEDGEMENTS

Thank you to everyone who has supported, counseled, instructed, or sacrificed for me. I've been incredibly fortunate in that I'm surrounded by spectacular people.

To Andrew Dacks: Whether regarding science or life in-general, I am immensely grateful for your teachings, counsel, and encouragement over the years. I could not ask for a better mentor. I am only where I am thanks to your "lateral thinking", your constant support, and the spark of fascination for the natural world that you instill. Thank you for everything.

To my Mom, Dad, mawmaw (Patsy Sizemore), pawpaw (Dennis Sizemore, Sr.), and Lenny: You all are my personal heroes. You've taught me the meaning of hard work and humility. You've given me nothing but unconditional love and support throughout my life and education. There's not a day that goes by that I don't think about the sacrifices you've both made to give Dakota and I the best possible shot at life. I wouldn't be here without you all.

To Kristyn Lizbinski: You are my rock, my person, "my bean". You make me a better person and a better scientist. I'm incredibly fortunate to have someone like you in my life.

Thank you to all of the wonderful friends I have made during my time in graduate school and my longtime friends, Tim Squires and Peter Murto, for always being there.

Thank you to all of the Dacks lab members that I've had the pleasure of working with over the years. I couldn't have asked for better colleagues.

Thank you to my graduate committee members Kevin Daly, Clif Bishop, Sarah Farris, and Eric Tucker for your constant support, pushing me to be a better scientist, and great questions.

Thank you to the WVU Department of Biology. Richard Thomas, who was the department's chair for nearly my entire doctorate, was the best department chair anyone could have asked for. The department (me included) would not be where it is without your unwavering advocacy, and unrelenting dedication to its students.

Thank you Mickey Sackett for always being there to support the grad students with food, support, and a seemingly unlimited amount of kindness.

I have been incredibly fortunate to work within a scientific community filled with spectacular people. To those individuals I have had the pleasure of learning from and working with, thank you.

TABLE OF CONTENTS

CHAPTER 1

Introduction

(portions of this chapter are based on my publication Sizemore, T.R., Hurley, L.M., and Dacks, A.M. (2020). Serotonergic modulation across sensory modalities. Journal of Neurophysiology, 123, 6.)

INTRODUCTION

Every animal's ability to interpret and properly traverse its ecology depends on information from the environment being internalized and processed by the animal's sensory modalities. These sensory systems translate complex stimulus information in serial and parallel to form a neural-/biochemical-code capable of specifying stimulus identity, intensity/concentration, and valence. However, all animals experience fluctuations in their ecology and internal state, and therefore require operational flexibility in sensory processing so that the proper behavioral response(s) are initiated. One way in which nervous systems contextualizes neural processing according to such fluxes in external and internal demands is through neuromodulation. Neuromodulation is a nearly ubiquitous process that endows the nervous system with the capacity to alter neural function at every level (synaptic, circuit, network, etc.) without necessarily adding new neurons (Kupfermann, 1979, 1980; Getting, 1989; Harris-Warrick and Marder, 1991; Katz, 1999; Hökfelt et al., 2000). Through the actions of neuromodulators, the existing neural circuitry can be adaptively tuned to achieve flexible network output and similarly dynamic behavioral output (Daur et al., 2016; Kim et al., 2017). However, our current understanding of neuromodulatory mechanisms largely comes from seminal and ongoing work in motor systems such as the stomatogastric ganglion of decapod crustaceans. Consequently, the mechanisms underlying neuromodulation of sensory processing has classically been underexplored. Therefore, in this dissertation, I leverage the unparalleled genetic access and numerically-reduced central brain of the fruit fly (*Drosophila melanogaster*) to determine critical aspects that underlie the actions of one neuromodulator, serotonin.

In this dissertation, I address three main questions regarding the mechanisms of serotonergic modulation of one sensory modality, olfaction. Olfaction is an optimal modality to serve as a platform for determining a given neuromodulator's mechanisms

given the extensive knowledge of each principal neuron's developmental origin, neurotransmitter content, anatomy, and physiology (Chou et al., 2010; Wilson, 2013; Sakuma et al., 2014; Kim et al., 2017; Lee, 2017; Bates et al., 2020; Schmidt and Benton, 2020; Schlegel et al., 2021). I will begin by establishing a "functional atlas" of which principal neuron types express which of the five serotonin receptors in the *Drosophila* primary olfactory center, the antennal lobe **(Chapter 2)**. Later, I use this "functional atlas" to determine how the activity of one serotonin receptor shapes the activity of a specialized neuropeptidergic signaling pathway **(Chapter 4)**. However, before I can address how the activity of this serotonin receptor adjusts the activity of this neuropeptidergic pathway, I determine how this neuropeptidergic pathway shapes olfactory processing **(Chapter 3)**. Altogether, my work establishes several key insights that expand our understanding of neuromodulation of sensory processing.

In this introductory chapter, I introduce the fundamental concepts behind the later chapters of this dissertation **(Chapters 2-4)**. I first describe signaling molecules that have neuromodulatory actions and some the mechanisms underlying those actions. Then, I detail the principal neurons that constitute my chosen platform for studying neuromodulation of sensory processing, the *Drosophila* olfactory system. This leads into our discussion of two of the neuromodulators present within this network, serotonin and the neuropeptide myoinhibitory peptide, and their influence on olfactory processing. Then, I end the chapter by discussing the consequences of one neuromodulator modulating another, a process termed "metamodulation". Occasionally, I describe and contrast across modalities and/or taxa so as to illustrate important correspondences/unique solutions nervous systems use to solve similar computational problems. This emphasis towards "comparative thinking" (i.e., presenting these concepts as they relate to any nervous system/sensory modality) is especially important as our goal as neuroscientists is not to understand how a single brain type operates, but instead how any and all brains operate.

A. NEUROMODULATION: MECHANISMS AND SIGNALING FACTORS

A fundamental concept explored by work in motor systems, such as the

stomatogastric ganglion (STG) of decapod crustaceans, is that modulatory substances represent a diverse tool set to alter network activity. Neuromodulatory substances include – but are not limited to - the amines (e.g., serotonin), neuropeptides (e.g., myoinhibitory peptide), gaseous transmitters, and other substances that act on individual neurons/synapses through intracellular receptors or G-protein coupled receptors (GPCRs) (Bargmann, 2012; Marder, 2012; Taghert and Nitabach, 2012). Neuromodulators can have immediate, and/or latent, effects on the biophysical or synaptic properties of a neuron across adjacent synapses, and/or non-adjacent synapses, and these effects do not necessarily change the membrane potential (Levitan, 1988; Katz, 1999; Marder, 2012; Bargmann and Marder, 2013; Bucher and Marder, 2013; Nadim and Bucher, 2014). Modulators can alter neuronal excitability by adjusting the neuron's voltage- and time-dependent channel conductances [e.g., (Prinz et al., 2004)]. Modulators can also change synapse strength/quantal content, typically by acting on potassium and/or calcium conductances (Hochner and Kandel, 1992; Braha et al., 1993). However, because modulators can alter the neuronal excitability and/or synapse strength, the modulator's effect(s) are dependent on the neuron's or synapse's recent activity. For example, depending on the recent history of network activity of the *Tritonia* escape response circuit, release of the neuromodulator serotonin (5-HT) will either cause a short-term potentiation or a long-term depotentiation on the targeted neuron (Sakurai and Katz, 2003, 2009). This particular example also demonstrates how neuromodulation can cause state changes in neurons and synapses. We can also observe similar phenomena in the rat hippocampus, where glial-derived glutamate acts on AMPA receptors along CA3 pyramidal neuron axons to potentiate/extend transmitter release (Sasaki et al., 2011). Here glutamate, a signaling molecule best known for its actions as a neurotransmitter, acts as a neuromodulator by potentiating the pyramidal neurons via extending the potassium channel inactivation epoch (Sasaki et al., 2011). This example also illustrates another key point: neuromodulators are not necessarily distinct substances from neurotransmitters. In fact, many modulators have non-modulatory effects on a given target neuron, such as GABA's effect on local interneurons in the *Drosophila* primary olfactory center (Wilson and Laurent, 2005; Lizbinski and Dacks, 2018). Moreover, the same signaling molecule released from the same presynaptic partner can have

modulatory and non-modulatory effects on the same downstream partner. Again, in the *Tritonia* escape response circuit, 5-HT from the dorsal swim interneurons (DSI) has both modulatory and non-modulatory effects on the postsynaptic dorsal flexion neurons (DFN) (Katz and Frost, 1995). Altogether, these diverse and nuanced effects of neuromodulation allow neural networks, even those with relatively few neurons, to produce a wide range of different functional outputs. Ultimately, by expanding the computational capacity of any neural network in this way, neuromodulators acting within sensory networks can endow the animal with tremendous behavioral flexibility [e.g., (Tsuda et al., 2021)].

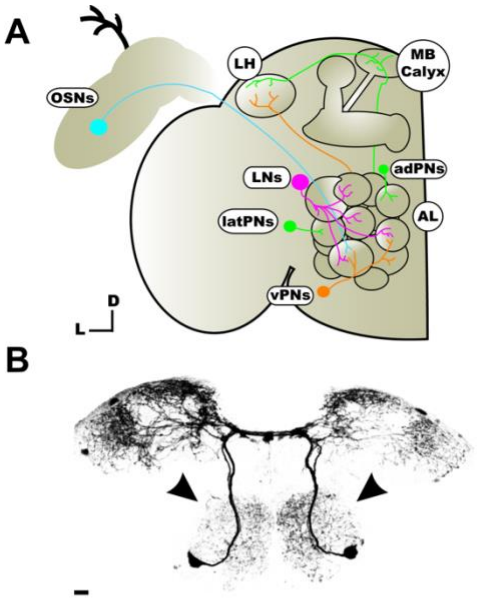

Figure 1. The *Drosophila melanogaster* olfactory network principal neuron types and the sole source of synaptic 5-HT within the antennal lobe, the CSDns.
(A) Olfaction for the fly begins when odorant molecules bind to and activate olfactory receptors expressed by olfactory sensory neurons (OSNs; cyan). The axon terminals of OSNs that express similar olfactory receptors terminate in similar olfactory channels ("glomeruli") within the animal's primary olfactory center, the antennal lobe (AL). Within each glomerulus, OSNs form excitatory synapses with other principal neuron types: projection neurons (PNs; green and orange) and local interneurons (LNs; magenta). Olfactory information is adjusted within and between different glomeruli by these LNs before being carried to higher-order structures (the mushroom body calyx, "MB Calyx"; and, lateral horn, "LH") by PN axons.
(B) In addition to OSNs, PNs, and LNs, the *Drosophila* AL is widely-innervated by a single pair of 5-HTergic neurons, the CSDns. An individual CSDn ramifies throughout the entire olfactory network, and therefore all olfactory regions (e.g., the AL, LH, etc.) are innervated by both CSDns.
Arrowheads indicate CSDn innervation within the AL. Scale bar = 10um.

B. THE *DROSOPHILA* OLFACTORY SYSTEM

Bi. Neuroanatomical Architecture and Signaling Factors

The organization of the *Drosophila* olfactory system shares many core features to those of other invertebrates and vertebrates (Hildebrand and Shepherd, 1997; Strausfeld and Hildebrand, 1999; Eisthen, 2002; Ache and Young, 2005; Bargmann, 2006; Hansson and Stensmyr, 2011; Martin et al., 2011; Wilson, 2013). As with other insects, olfaction for the fly begins when odorants from the external environment enter small pores found along the ~1,000 sensillae on the fly's 3rd-antennal segment and ~60 sensillae on the maxillary palp (Stocker et al., 1983; Venkatesh and Singh, 1984; Stocker, 1994; Shanbhag et al., 1999; Vosshall, 2000; Grabe et al., 2016) **(Figure 1A)**. Here, the

odorant molecules diffuse, bind to, and activate their cognate chemosensory receptor(s) expressed along the dendrites of the 1-4 cholinergic olfactory sensory neurons (OSNs) housed within each sensillum (Stocker et al., 1990; Carlson, 1996; De Bruyne et al., 1999; Vosshall, 2000; Vosshall et al., 2000; Missbach et al., 2014). The chemosensory receptors expressed by the ~1,200 OSNs can belong to one of three distinct gene families: odorant receptors (ORs; ~62 members), ionotropic receptors (IRs; ~60 members), or gustatory receptors (GRs; ~68 members) (Stocker et al., 1990; Benton et al., 2009; Su et al., 2009; Joseph and Carlson, 2015; Grabe et al., 2016). Olfactory sensory neurons are rapidly activated upon odorant binding, in part due to the fact that chemosensory receptors form a ligand-gated heteromultimer ion channel in association to their obligate co-receptor (Neuhaus et al., 2005; Butterwick et al., 2018). Upon activation, OSN signals are relayed to the fly's central brain into the primary olfactory center, the antennal lobe (AL), where the axons of ~10-65 OSNs that express the same/similar chemosensory receptor(s) converge on one or few of the ~51 glomeruli (Couto et al., 2005; Fishilevich and Vosshall, 2005; Benton et al., 2009; Grabe et al., 2016; Bates et al., 2020; Task et al., 2020). Within a glomerulus, OSN axons form excitatory connections with the other two principal neuron types of the AL: second-order relay neurons (projection neurons; PNs) and local processing neurons (local interneurons; LNs).

The cell bodies of PNs - the insect analog of mitral and tufted cells of the vertebrate olfactory bulb - form several distinct clusters defined by their development origins and their location relative to the AL (Yu et al., 2010; Sakuma et al., 2014; Lee, 2017). There are ~345 PNs in the *Drosophila* AL that are divided into the anterodorsal (adPNs), lateral (latPNs), ventrolateral (vlPNs), and ventral (vPNs) cell clusters (Sakuma et al., 2014; Bates et al., 2020). Neurons from the anterodorsal and lateral cell clusters tend to innervate a single glomerulus (uniglomerular; uPNs - ~164 PNs), while neurons from the ventrolateral and ventral clusters generally innervate multiple glomeruli (multiglomerular; mPNs - ~181 PNs) (Lai et al., 2008; Lin et al., 2012; Bates et al., 2020; Schlegel et al., 2021). Neurons of these subtypes can be further divided based on transmitter identity; uPNs and mPNs generally express acetylcholine and GABA, respectively (Yasuyama et al., 2003; Wilson et al., 2004; Okada et al., 2009). Even further still, axons from the

excitatory uPNs and inhibitory mPNs generally travel through distinct fascicles in the brain before terminating in the mushroom body (MB) and/or the lateral horn (LH), where the odor encountered is contextualized based on learned and innate associations, respectively (Heisenberg, 2003; Strutz et al., 2014; Schultzhaus et al., 2017; Cognigni et al., 2018; Amin and Lin, 2019; Das Chakraborty and Sachse, 2021). However, before PN axons relay their signals to the MB and/or LH, the signal is adjusted within- and between-glomeruli by several diverse classes of LNs.

There are ~200 diverse LNs in the *Drosophila* AL, which interconnect and adjust network activity based on the ongoing activity across glomeruli and the animal's current needs (Wilson and Laurent, 2005; Olsen et al., 2007; Root et al., 2008; Ignell et al., 2009; Okada et al., 2009; Chou et al., 2010; Yaksi and Wilson, 2010; Seki et al., 2010; Das et al., 2011; Ko et al., 2015; Schlegel et al., 2021). From developmental origins, transmitter identity, neuroanatomy, and physiology, AL LNs are highly heterogeneous. Antennal lobe LNs can be divided into two major cell clusters based on their soma location and the neuroblast they derive from: the lateral and ventral cell clusters (Stocker et al., 1997; Das et al., 2008, 2011; Lai et al., 2008; Chou et al., 2010; Sen et al., 2014). The majority of LNs (~125) are lateral LNs (latLNs) that are mostly GABAergic LNs (Wilson and Laurent, 2005; Okada et al., 2009; Tanaka et al., 2009; Chou et al., 2010). In addition to GABAergic latLNs, there are also latLNs that are cholinergic (~8-15 LNs), electrically-coupled, and release the inhibitory neuropeptides tachykinin (TKK; ~15-20 LNs) and myoinhibitory peptide (MIP; ~10 LNs) (Shang et al., 2007; Ignell et al., 2009; Carlsson et al., 2010; Chou et al., 2010; Huang et al., 2010; Seki et al., 2010; Yaksi and Wilson, 2010). The ~65 ventral LNs (vLNs) are glutamatergic, which has inhibitory actions on AL neurons (Das et al., 2011; Liu and Wilson, 2013), a stark contrast to glutamate's general role in vertebrate systems. Approximately two tyrosine hydroxylase-immunoreactive LNs are in both the latLN and vLN cell clusters, suggesting there are >4 dopaminergic LNs in the *Drosophila* AL, but dopamine's actions in the AL remain untested (Chou et al., 2010). Additionally, different subgroups of AL LNs display distinct morphological characteristics (Chou et al., 2010). Furthermore, these distinct morphological subtypes tend to act on different aspects of network processing - not unlike interneurons in vertebrate networks (Shipley and Ennis, 1996; Markram et al., 2004; Chou et al., 2010; Nagayama et al., 2014; Lizbinski and

Dacks, 2018). The names for these distinct morphological classes derive from how much of the AL the given LN innervates or the LN's neurite morphology, and are: "panglomerular", "multiglomerular", "few glomeruli", "continuous", and "patchy" (Chou et al., 2010). Further still, nearly half of all AL LNs innervate both the ipsilateral and contralateral AL, and therefore have the potential to process and adjust olfactory information in serial (Chou et al., 2010). Altogether, the diversity of transmitter identity and anatomical features of AL LNs is – at least in part – what enables complex and nuanced processing of olfactory stimuli.

In addition to these principal neuron types, the *Drosophila* AL also receives broad input from two contralaterally projecting, serotonin-immunoreactive deutocerebral neurons (CSDns) **(Figure 1B)** (Dacks et al., 2006; Roy et al., 2007). The CSDns represent the sole source of 5-HT within the *Drosophila* AL and are highly conserved across other insects (Salecker and Distler, 1990; Sun et al., 1993; Wegerhoff, 1999; Hill et al., 2002; Dacks et al., 2006; Zhang and Gaudry, 2016; Coates et al., 2017). Moreover, the *Drosophila* and moth CSDns are odor-responsive (Hill et al., 2002; Zhang and Gaudry, 2016; Coates et al., 2017; Zhang et al., 2019a) and receive direct synaptic input from AL principal neurons (Sun et al., 1993; Berck et al., 2016; Zhang and Gaudry, 2016; Coates et al., 2017, 2020). A single *Drosophila* CSDn projects spans the entire olfactory network (both ALs, both MB calyces, and both LHs), and less well-defined areas which integrate inputs from many modalities (the superior lateral protocerebrum and both antlers) (Roy et al., 2007; Coates et al., 2017, 2020; Suver et al., 2019; Musso et al., 2021; Pacheco et al., 2021). The CSDns' actions in these different regions, as discussed below, appears to vary in these different regions due to compartment-specific inputs and variable synaptic density across glomeruli (Coates et al., 2017, 2020; Zhang et al., 2019a). Although the active zone density does vary across AL glomeruli, all glomeruli have CSDn active zones (Coates et al., 2017) and serotonin receptors are widely expressed across AL principal neuron types (Sizemore and Dacks, 2016). Together, these results suggest nearly all AL neurons are subject to – *or, at least indirectly impacted by* - serotonergic modulation.

Bii. Functional Architecture with Emphasis on Interneuron Computations

Olfactory sensory neuron spiking activity nearly completely depends on the odor-tuning properties of their constituent chemosensory receptor(s) (De Bruyne et al., 2001; Hallem et al., 2004; Larsson et al., 2004; Hallem and Carlson, 2006; Nagel and Wilson, 2011). Structural differences and ligand binding affinity variability across these constituent chemosensory receptors also confer unique patterns of spontaneous activity across OSNs (De Bruyne et al., 1999; Hallem et al., 2004; Olsen et al., 2007; Nagel and Wilson, 2011; Saberi et al., 2016). However, the odor-tuning properties across different OSNs are statistically correlated (Haddad et al., 2010); a feature that has, until recently, complicated experimental dissection of the behavioral contributions of different OSNs (Bell and Wilson, 2016). This feature is, in part, why even a monomolecular odorant can drive activity in a multitude of OSNs (Hallem and Carlson, 2006; Benton et al., 2009; Su et al., 2009; Haddad et al., 2010). In addition to these features of OSN responses conferred by OR properties, there is also a linear relationship between odor concentration and the number of ORs activated. That is, exposure to high odor concentrations enables nonselective binding at the OR binding site, ultimately enabling the given odor to produce a response in OSNs it would not under other circumstances (De Bruyne et al., 1999, 2001; Ng et al., 2002; Hallem and Carlson, 2006; Silbering et al., 2008; Semmelhack and Wang, 2009; Saberi et al., 2016). Interestingly, some odorants drive inhibition in OSNs simply through local ion sequestration by neighboring OSNs activated by the odorant, a phenomenon termed “ephaptic coupling” (Su et al., 2012; Zhang et al., 2019b). Olfactory sensory neuron activity is terribly “noisy”, such that OSNs are quick to respond and exhaust themselves. For instance, OSNs spike even in the absence of odorants (De Bruyne et al., 1999, 2001). Moreover, OSN spike rates are fastest at odor-onset followed by a bout of tonic activity before they deplete their vesicle reserves (Bhandawat et al., 2007; Nagel and Wilson, 2011). Altogether, these observations suggest that OSN activity alone - while useful for discerning stimulus identity and concentrations as the animal traverses its environment – cannot efficiently encode all features of the animal’s olfactory world.

Projection neurons are far less selective in terms of their odor-tuning properties than their presynaptic OSNs (Bhandawat et al., 2007; Olsen and Wilson, 2008). Every “sister” PN within a glomerulus pools input from all OSNs that innervate the given glomerulus, and consequently sister PNs show similar spontaneous and odor-evoked response properties (Kazama and Wilson, 2008). An additional consequence of OSN pooling by projection neurons, PN peak responses occur earlier than OSN responses at odor-onset (Bhandawat et al., 2007; Olsen et al., 2010). More specifically, low OSN firing rates induce a large change in their postsynaptic PNs’ firing rates, but PN spiking becomes desensitized as OSN firing rates climb (Bhandawat et al., 2007; Olsen and Wilson, 2008; Olsen et al., 2010). Even further, PNs can display different patterns of responses as more OSNs are recruited, or if more/different sets of glomeruli are recruited (Ng et al., 2002; Root et al., 2008; Silbering et al., 2008; Semmelhack and Wang, 2009; Olsen et al., 2010). These observations suggest that PN responses are poorly predicted by OSN responses (Wilson et al., 2004). This claim is best exemplified by PNs in the glomerulus VM7, which do not respond to odorants that stimulate VM7 OSNs (Olsen and Wilson, 2008). There is also growing evidence that some ePNs and iPNs form recurrent cholinergic and electrical synapses within the AL (Wang et al., 2014; Shimizu and Stopfer, 2017), but form an antagonistic circuit at their axon terminals in the LH (Liang et al., 2013; Strutz et al., 2014). In this latter instance, appetitive odors activate iPNs, which will then inhibit ePN axons in the LH, thus shunting excitatory drive onto third-order neurons from the ventrolateral protocerebrum and initiating an attractive behavioral program (Liang et al., 2013; Strutz et al., 2014). This, therefore, illustrates how distinct neural output from the AL (iPN vs. ePN output) can initiate distinct behavioral programs. However, before these signals are relayed to higher-order structures (like the LH), different features of these signals are adjusted by the activity of heterogeneous AL LNs.

Local interneurons, much like their morphological heterogeneity, have diverse and complex physiological properties. Antennal lobe LNs can have bursty and/or tonic stimulus responses, and individual LNs can display different patterns of intraglomerular odor-evoked responses to different odorants (Silbering et al., 2008; Chou et al., 2010; Seki et al., 2010). Moreover, LN activation linearly scales with odor concentration (Yaksi and Wilson, 2010; Hong and Wilson, 2015) and different AL LNs show different temporal

odor-evoked response properties (Chou et al., 2010; Nagel and Wilson, 2016). For instance, some LNs respond fastest at odor-onset, some LNs respond fastest at odor-offset, and some LNs respond indifferently to either extreme of the stimulus trial (Nagel and Wilson, 2016). Furthermore, these response properties (in addition to the diversity of morphological subtypes and transmitters used) enable AL LN activity to adjust the gain, resolution, and temporal aspects of stimulus features encoding within the AL.

Recall sensory systems, olfaction included, play an essential role in the animal's ability to detect, identify, and discriminate amongst the rich stimulus diversity they experience. To ensure the animal can do this, sensory systems employ several strategies to dynamically adjust the range of individual stimulus features that they encode. For instance, the animal may experience fluctuations in stimulus intensity as they navigate their environment. In such cases where the animal experiences intense sensory input (e.g., bright lighting, high odor concentration, etc.), the neurons may fail to properly encode the given stimulus as a result of saturation. Conversely, animals may fail to detect ecologically important stimuli (e.g., the scent of a predator) if they are present at low intensities. To overcome these hurdles, sensory systems typically use a suite of computations, such as "gain control" (Abbott et al., 1997; Carandini and Heeger, 2012; Ferguson and Cardin, 2020), to adaptively adjust the sensory input-to-output ratio of a network. In the AL, GABAergic and TKKinergic LNs target OSN axons to reduce the gain of OSN input (Olsen and Wilson, 2008; Root et al., 2008; Ignell et al., 2009; Olsen et al., 2010). Here, GABAergic LNs (for example) activate inhibitory $GABA_B$ receptors expressed along OSN axons in an odor concentration-dependent manner such that PN output is normalized (Bhandawat et al., 2007; Olsen and Wilson, 2008; Root et al., 2008; Olsen et al., 2010). Moreover, the ability of such LNs to perform this function plays a vital role in the animal's ability to efficiently and effectively reproduce. For instance, decreasing GABAergic gain control by reducing expression of $GABA_B$ receptors in pheromone-sensing OSNs impairs the fly's ability to locate a mate (Root et al., 2008). This suggests that GABAergic gain control in pheromone-sensing glomeruli is necessary for this glomerulus' PNs to faithfully represent the stimulus to downstream partners. Additionally, the degree of GABAergic or TKKinergic presynaptic inhibition varies from glomerulus-to-glomerulus due to the differential GABA and/or TKK receptor expression, LN

morphological variability, and the animal's state (Root et al., 2008; Ignell et al., 2009; Hong and Wilson, 2015; Ko et al., 2015). Perhaps different selective pressures fostered different levels of gain control across the various olfactory channels as a trade-off for output speed vs. output information degeneration. For example, by installing fewer inhibitory "nodes" that impinge on afferent input to a channel associated with responding to a predator's scent, then this channel has less feedback inhibition to overcome, and therefore output from this channel can be sent to the relevant downstream neurons faster to initiate the appropriate avoidance response. However, this would require a balance to be struck wherein there is not too little presynaptic inhibition. If such channels - that are clearly imperative to the animal's survival - are too easily activated, then the animal may mistakenly initiate an avoidance response and forgo vital resources they might not have access to later on. Additionally, differential receptor expression to produce variable amounts of gain control across the various olfactory channels may be an ingenious means for conserving circuit topology across closely related species, but adaptively adjusting circuit outcome according to pressures from the specific species' ecological niche. This adaptive adjustment of gain control mechanisms would be different from those observed in visual circuits, like the retina, but this difference would not be surprising given the greater diversity of stimuli encoded by chemosensory systems. Regardless of the adaptive strategies underlying such circuit variability, LN-mediated gain control is an important means for adjusting the strength of afferent input to avoid corrupting output signal information.

In addition to compensating for variations in stimulus intensity, animals may also need to adjust their ability to resolve different stimuli. At the neuronal level, AL LNs can use lateral inhibition for sharpening the resolution with which they encode stimulus identity (Wilson et al., 2004; Silbering et al., 2008; Martin et al., 2011). Here, PNs express both $GABA_A$ and $GABA_B$, while LNs express $GABA_A$ (Wilson and Laurent, 2005). Therefore, if a given odorant stimulates a glomerulus that houses a GABAergic LN that innervates multiple glomeruli, then PNs in those other glomeruli will experience a fast and prolonged inhibitory epoch (Wilson and Laurent, 2005). Lateral inhibition, here, can be used to restrict network responses to a strong stimulus (for instance), while filtering/depressing weaker PN responses. Conversely, if the activated GABAergic LN targets other LNs then

more olfactory channels can be rapidly recruited in the response via disinhibition. This change both in terms of which olfactory channels are recruited, as well as the temporal patterns of their responses, would likely summate within higher-order brain centers in a distinct manner that has important consequences for encoding odorant identity and concentration.

Similar to disinhibition, LNs can also perform lateral excitation as a means for broadening the resolution with which the AL encodes odorant identity and concentration (Shang et al., 2007; Huang et al., 2010; Olsen et al., 2010; Yaksi and Wilson, 2010). The first circumstantial evidence for lateral excitation in the *Drosophila* AL arose from the observation that DM2 PNs responded to odors that did not stimulate their cognate OSNs, suggesting extraglomerular excitatory inputs to DM2 PNs (Wilson et al., 2004). This was later confirmed by others that tested DM2 PN responses in animals that DM2 OSNs lack their cognate ORs, and therefore enabled them to test DM2 PN responses in the absence of input from their presynaptic OSNs (Shang et al., 2007). However, these later investigations could not rule out disinhibition as PN EPSPs remained even in the presence of GABA receptor antagonists and with no OSN input (Shang et al., 2007). Similar results were discovered by separate groups that recorded PN responses with electrophysiology in the presence of GABA receptor antagonists and in an OR-null mutant background (Olsen et al., 2007; Root et al., 2007). Eventually, multiple groups found that this lateral excitation arises from a small population of excitatory LNs (eLNs) that form excitatory synapses with many of the AL principal neurons (Shang et al., 2007; Huang et al., 2010; Yaksi and Wilson, 2010). These eLNs are electrically-coupled (and in some instances also form cholinergic synapses) to iLNs, other eLNs, and most PNs. This is, in part, why the amount of iLN activation linearly scales with increasing odor concentration (see above) (Yaksi and Wilson, 2010). Excitatory LNs can be inhibited by iLNs (via both $GABA_A$ & $GABA_B$), stimulated by reciprocal PN acetylcholine release, and receive monosynaptic connections from OSNs (Huang et al., 2010; Yaksi and Wilson, 2010). Moreover, different subsets of eLNs have different intrinsic properties, which presumably confers differential odor-tuning properties across the various eLNs. Taken together, eLN activity can enable redistribution of olfactory information throughout the AL, while simultaneously increasing the strength of PN activity in response to weaker stimuli (e.g.,

low odor concentration).

In addition to using fast-acting transmitters like GABA or acetylcholine adjust different computations, AL LNs can use slower-acting neuropeptides (e.g., TKK) to adjust many of these aforementioned computations over longer epochs. However, the role(s) LN-mediated neuropeptide release in olfactory processing has been severely understudied in comparison to faster-acting transmitters used by LNs. This dissertation exposes a novel peptidergic signaling pathway within the AL implemented by one such neuropeptide, myoinhibitory peptide (MIP).

C. MYOINHIBITORY PEPTIDE (MIP)

Myoinhibitory peptide (MIP; formerly designated “B-type allatostatins”) was first isolated from the *Locusta* nervous system (“LOM-MIP”) and shown to suppress spontaneous contractions in the *Locusta* and *Leucophaea* hindgut, and the *Locusta* oviduct (Schoofs et al., 1991). Soon after, MIP was isolated from the *Manduca sexta* nervous system (“MsMIP”), where it was shown to near-completely abolish hindgut contractions (Blackburn et al., 1995, 2001). Around this time, homologous neuropeptides were isolated from *Gryllus* nervous system, but were designated as a new member of the allatostatin family of peptides (Allatostatin B, or AstB) due to MIP’s ability to suppress juvenile hormone biosynthesis in *Gryllus* (Lorenz et al., 1995). Since then, MIP has been found in many insects, such as *Periplaneta* (“Pea-MIP”) (Predel et al., 2001), *Drosophila* (Williamson et al., 2001; Baggerman et al., 2002; Yew et al., 2009), *Calliphora* (Kolodziejczyk and Nässel, 2011), *Aedes* (Predel et al., 2010), and *Bombyx* (“PTSP-1”) (Hua et al., 1999). To date, no vertebrate analog for MIP has been definitively identified, although there are suggestions that MIP shares sufficient enough sequence homology to galanin (i.e., $W(X_6)W$-amide motif) that the two may be homologous [see (Lundquist et al., 1991)]. This supposition is somewhat supported by the observation that mutating the amino acids between the two tryptophan residues does not hinder MIP’s ability to bind its cognate receptor, the inhibitory sex peptide receptor (SPR) (Yapici et al., 2008; Kim et al., 2010). Regardless, these comparative studies have revealed MIP’s high degree of evolutionary conservation and that MIP’s allatostatic activity may be unique to few insects

(e.g., *Gryllus*) (Nässel and Winther, 2010; Coast and Schooley, 2011). Consequently, in the interest of having a unifying nomenclature, investigators have recommended the name “myoinhibitory peptide” be used when referring to this neuropeptide or any member of this neuropeptide family (Coast and Schooley, 2011; Yeoh et al., 2017).

Most of what we know about the mechanism underlying MIP’s effect(s) on a network comes from work done in the *Drosophila* circadian and gustatory systems (Kim et al., 2010; Oh et al., 2014; Min et al., 2016). In the circadian system, MIP decreases the activity of wake-promoting pigment-dispersing factor (PDF) neurons throughout the night by activating its inhibitory GPCR, sex peptide receptor (SPR) (Kim et al., 2010; Oh et al., 2014; Shafer and Yao, 2014). Here, MIP release is highest just before and during sleep, which allows it to therefore maintain a sleep-promoting network state over the course of the night (Oh et al., 2014). In the gustatory system, MIP-SPR signaling controls food intake and body weight maintenance (Min et al., 2016). Here, flies will overeat (relative to the relevant controls) to the point of engorgement when the MIPergic neurons are inactivated, or if experiments are performed in a MIP-null mutant background (Min et al., 2016). Conversely, flies tend to eat less when MIPergic neurons are constitutively activated by misexpression of the heat-activated TRPA1 channel in all MIPergic neurons and extended heat exposure (Min et al., 2016). These investigators also found several notable results that suggest MIP-SPR signaling not only controls the balance between hunger and satiety, but directly influences the excitability of food-derived odor associated channels. More specifically, animals that have their MIPergic neurons inactivated will choose the arm of a two-choice olfactory assay (a T-maze apparatus) that houses a food-derived odorant (Min et al., 2016). The same effect was observed in similar behavioral experiments that were performed in a MIP-null mutant background, and was rescued by MIP overexpression in all MIP neurons in this mutant background (Min et al., 2016). Conversely, animals choose the food-odor arm of the T-maze far less when MIPergic neurons are overactivated. It’s notable that these particular animals actually display odor-induced aversion (attraction index of -5% to -30%), whereas the relevant controls display odor-induced attraction (attraction index of 10% to 40%), across multiple food odors (Min et al., 2016). Moreover, sensillae associated with food-odor olfactory sensation spike more frequently when all MIPergic neurons are inactivated (Min et al., 2016). Together,

these results suggest MIP-SPR signaling controls the animal's sensitivity to food-associated odors and drive to search for food.

D. SEROTONERGIC MODULATION OF OLFACTORY PROCESSING

Di. Serotonin (5-HT) Sources

Serotonin is an ancient and pervasive signaling molecule that acts in nearly every sensory system across diverse taxa (Peroutka and Howell, 1994; Hay-Schmidt, 2000; Gaspar and Lillesaar, 2012). Concordantly, this single substance has been implicated in a variety of broad state descriptors such as arousal, mood, and motivation (Cools et al., 2008; Monti, 2011; Miyazaki et al., 2012; Luo et al., 2016). In general, there are two major sources of 5-HT in mammals: gut-derived and brain-derived. The majority of the 5-HT in the mammals is produced in the gut by enterochromaffin cells, then absorbed by platelets and circulated throughout the periphery (Ni and Watts, 2006; Bertrand and Bertrand, 2010; Gershon, 2013; Matthes and Bader, 2018). However, gut-derived 5-HT does not appear to cross the blood-brain-barrier (Berger et al., 2009; El-Merahbi et al., 2015), therefore I will only consider brain-derived 5-HT here. There are ~26,000 neurons in the mouse and rat brain that produce 5-HT, but the majority of these 5-HTergic neurons (~17,000 neurons) are collectively referred to as the raphe nuclei (Steinbusch, 1981; Ishimura et al., 1988; Vertes and Crane, 1997). The raphe nuclei can be further divided into several subpopulations, such as the dorsal raphe nucleus (DRN). In mice, the DRN constitutes the majority of 5-HTergic neurons in the brain (~9,000 5-HTergic neurons) (Ishimura et al., 1988; Hornung, 2010; Ren et al., 2018). These DRN neurons, together with neurons from the median raphe nucleus (MRN), innervate and modulate every sensory processing center (Azmitia and Segal, 1978; Takeuchi et al., 1982; Doty, 1983; Mclean and Shipley, 1987; Tork, 1990; Hurley et al., 2004; Muzerelle et al., 2016; Jacob and Nienborg, 2018).

Invertebrate brains typically contain far fewer neurons than vertebrate brains. For instance, the central nervous system of *C. elegans* has 302 neurons and *Drosophila* has ~200,000 neurons relative to ~70 x 10^6 neurons estimated in mice (White et al., 1986; Herculano-Houzel et al., 2006; Meinertzhagen, 2018; Cook et al., 2019; Raji and Potter,

2021). Despite having orders of magnitude fewer neurons, invertebrate sensory systems must accomplish the same fundamental neural computations as vertebrates. This notion extends to invertebrate 5-HTergic modulatory networks, where there are typically far fewer 5-HTergic neurons, but many of the mechanisms for how 5-HT modulates sensory processing are conserved. The *Drosophila* central brain, for instance, contains only ~90 serotonergic neurons (Vallés and White, 1988), and only 2 widely-projecting neurons (the "CSDns") provide synaptic 5-HT to the AL **(Figure 1B)** (Dacks et al., 2006; Roy et al., 2007). Despite having only two 5-HTergic neurons, compared to >100 neurons that innervate the vertebrate olfactory bulb from the DRN (Ren et al., 2018) and MRN (Muzerelle et al., 2016), 5-HT modulates similar aspects of olfactory encoding in these taxa (see below). Thus, because vertebrate and invertebrate sensory systems must solve similar problems, comparing across taxa can reveal fundamental motifs of neuromodulation of sensory processing.

Although much of my dissertation deals with the consequences of a presynaptic 5-HTergic neuron acting on a direct postsynaptic partner, 5-HTergic neurons do not have to form a synapse with a given cell in order to modulate the cell's activity (Eid et al., 2013; Fuxe et al., 2015). Serotonergic neurons have long been noted to use volume or bulk transmission as a means to release 5-HT over large distances (sometimes >100microns), and extended epochs (on the order of seconds) (Descarries et al., 1982; Chazal and Ralston, 1987; Agnati et al., 1995; Bunin and Wightman, 1998; Hornung, 2010; Gaudry, 2018). For instance, in the cat auditory cortex, most of the 5-HTergic boutons lack conventional synapses (DeFelipe et al., 1991). This principle extends across taxa, such as in the visual system of the house fly, *Calliphora*. Here, 5-HTergic processes are separated from other neurons by glia, lack synaptic specializations, and are dense core vesicle-rich (a hallmark of bulk transmission) (Nässel and Cantera, 1985; Nassel, 1988).

Blood-borne 5-HT, similar to bulk-released 5-HT, also contributes to sensory processing. For instance, in *Drosophila* blood-borne 5-HT activates nociceptors (Kaneko et al., 2017) and is implicated in enhanced olfactory gain control (Zhang and Gaudry, 2016; Suzuki et al., 2020). Moreover, evidence suggests that blood-borne 5-HT acts on excitatory 5-HT2B receptors on OSN dendrites/somata likely as a way of enhancing OSN excitability. This inference derives from evidence that the *Drosophila* CSDns do not

directly synapse onto OSNs (Coates et al., 2017), yet OSNs broadly express the excitatory 5-HT2B receptor (Sizemore and Dacks, 2016; Deanhardt et al., 2021; McLaughlin et al., 2021). In addition, in experiments where the OSN somata were removed for performing antennal nerve shock, exogenous 5-HT did not directly affect activity measured at the axon terminals of OSNs (Dacks et al., 2009). These lines of evidence suggest then that the 5-HT2B receptor likely localizes to OSN dendrites/somata in the periphery, where 5-HT in the haemolymph can act on them. Indeed, there are 5-HTergic fibers in the periphery (Vallés and White, 1988) and the antennal hearts of many insects constantly circulates haemolymph into these olfactory appendages (Pass, 2000; Zhukovskaya and Polyanovsky, 2017). Ultimately, blood-borne 5-HT might act to coordinate the activity of certain OSN according to the fly's needs. This mechanism would be particularly advantageous for increasing the sensitivity of OSNs that respond to food or pheromones when the fly is hungry or aroused, respectively.

Dii. Serotonergic Neurons: Heterogeneous in Nearly Every Way

The 5-HTergic system has the capacity to influence olfactory processing in complex, and stimulus-specific ways, across a multitude of behavioral contexts. This is, in part, achieved through the heterogeneous properties of the neurons that release 5-HT (Okaty et al., 2019). For instance, individual DRN neurons have different electrical properties due to differential ion channel expression levels (Calizo et al., 2011; Templin et al., 2012). This suggests that two given DRN neurons receiving identical synaptic input can still differentially modulate the same sensory network. To the best of our knowledge, ion channel expression profiles of 5-HTergic neurons have not been compared in invertebrates. However, the intrinsic properties and region-specific synaptic inputs (the AL vs. LH) onto the CSDns enable this single 5-HTergic neuron to perform multiple operations across different olfactory processing regions (Zhang et al., 2019a; Coates et al., 2020). Thus, whether biophysical or connectivity-specific, these features of 5-HTergic neurons expand the complexities underlying 5-HTergic modulation of sensory processing.

In addition to these heterogeneous features, individual 5-HTergic neurons can also

release more than just 5-HT onto a downstream neuron. Though such “co-transmitters” have not been identified for the *Drosophila* CSDns (Sizemore et al., 2020), there are examples of the heterogeneous computational consequences of 5-HTergic neurons using multiple transmitters in the vertebrate olfactory bulb. For example, subpopulations of 5-HTergic DRN neurons co-express either glutamate, GABA, several neuropeptides, and nitric oxide synthase (Fu et al., 2010; Liu et al., 2014; Sengupta et al., 2017; Ren et al., 2018; Huang et al., 2019). This feature can enable even a single co-transmitting DRN neuron to affect a downstream target on multiple timescales, which can have a large impact on the targeted neuron’s stimulus-response properties. For instance, when DRN projections to the olfactory bulb are activated, DRN-derived 5-HT and glutamate differentially act on both mitral and tufted cells. The glutamate acts to directly enhance the odor-evoked responses in both output neurons subtypes, while the 5-HT enhances decorrelation of only mitral cell odor-responses (Kapoor et al., 2016). The observed enhancement is further increased by pharmacologically blocking 5-HT receptors, and nearly abolished when glutamate receptors are similarly blocked (Kapoor et al., 2016). Although 5-HT may be acting through polysynaptic interactions in this particular case (Hardy et al., 2005; Liu et al., 2012; Brill et al., 2015), the overall consequence is that co-transmission allows raphe neurons to affect their targets on different timescales through ionotropic and metabotropic receptors, respectively. This allows raphe neurons to both quickly alter a given downstream target’s neuronal activity, but also leave that target’s activity altered for extended epochs.

The non-uniform anatomical projections of 5-HTergic neurons, like the other features of 5-HTergic neurons previously discussed, also make determining the mechanisms behind 5-HTergic modulation of olfaction non-trivial. Moreover, these heterogeneous projections often reflect multiple “functional domains”, wherein the 5-HTergic neuron may be acting more/less based on innervation density. For instance, the *Manduca sexta* CSDns likely do not directly act on OSNs, since they do not innervate the regions of the AL occupied by OSNs (Sun et al., 1993; Lizbinski et al., 2016). In vertebrates, the olfactory bulb is innervated by 5-HTergic processes from both the MRN and DRN, but these processes are most dense in distinct synaptic layers (Mclean and Shipley, 1987; Gracia-Llanes et al., 2010; Muzerelle et al., 2016). Here, processes from

the MRN are most dense in the region occupied mostly by periglomerular cells (a subclass of LN), while processes from the DRN are densest in regions occupied by mitral and tufted cells (the vertebrate analog of insect PNs) and granule cells (another subclass of LN) (Muzerelle et al., 2016). Within the *Drosophila* AL, the CSDns innervate different glomeruli to varying degrees and differentially connect with the various principal neuron types from animal-to-animal (Singh et al., 2013; Coates et al., 2017). Altogether, these heterogeneous intrinsic, extrinsic, and morphological features of 5-HTergic neurons enable them to distinctly target different processing layers and/or stimulus-specific microcircuits.

Diii. The Serotonin Receptor (5-HTR) Family Across Taxa

Just as 5-HTergic neurons are themselves diverse, there is a diversity of serotonin receptors (5-HTRs) that vary in their affinity for 5-HT, time course of action and the secondary messenger system to which they couple (Nichols and Nichols, 2008). This receptor diversity allows 5-HT to differentially target neuronal populations that support distinct sensory computations across modalities.

An array of 5-HTRs are encoded in nearly every animal's genome (Peroutka and Howell, 1994; Ribeiro et al., 2005; Azmitia, 2006; Vleugels et al., 2015; Ishita et al., 2019). The first 5-HTR emerged ~700-800 million years ago (Peroutka and Howell, 1994) and there are seven major 5-HTR families in vertebrates (5-HT1-7) and at least three across the invertebrates (5-HT1, 2, and 7). However, there are notable clade-specific exceptions such as the MOD-1 ionotropic 5-HTR in *C. elegans* (Ranganathan et al., 2000), the 5-HT8 receptor in *P. rapae*, the 5-HT4 and 6 receptors in some molluscs (Nagakura et al., 2010; Tamvacakis et al., 2015, 2018; Kim et al., 2019), the non-functional 5-HT5B receptor subtype in humans (Grailhe et al., 2001), the absence of these receptors in the Ctenophora genome (Moroz et al., 2014), and the 5-HT4 receptor in *A. japonicus* (Wang et al., 2017). Invertebrate 5-HTRs are typically named for the vertebrate 5-HTR family with which they share the most sequence homology, but the pharmacological properties of these counterparts can differ. Methysergide, for example, acts as a broad-spectrum 5-HTR antagonist in vertebrates, but agonizes or has no effect on select invertebrate 5-

HTRs (Röser et al., 2012; Dacks et al., 2013; Blenau et al., 2017). There are fourteen subtypes of vertebrate 5-HTRs (e.g., within the 5-HT2 family there are 5-HT2A-C), some of which can have several isoforms as result of post-transcriptional modifications to the nascent 5-HTR transcript (Burns et al., 1997; Bockaert et al., 2006; Hannon and Hoyer, 2008; Tanaka and Watanabe, 2020). Conversely, invertebrate 5-HTR subtypes are generally encoded at distinct genomic loci and each 5-HTR has a single predicted isoform. For example, the five *Drosophila melanogaster* 5-HTRs **(Figure 2A)** derive from five separate genomic loci and encode a single spliceform (Witz et al., 1990; Saudou et al., 1992; Colas et al., 1995; Gasque et al., 2013). Of these different 5-HTR subtypes, most if-not-all all are expressed by neurons within sensory processing centers across phyla.

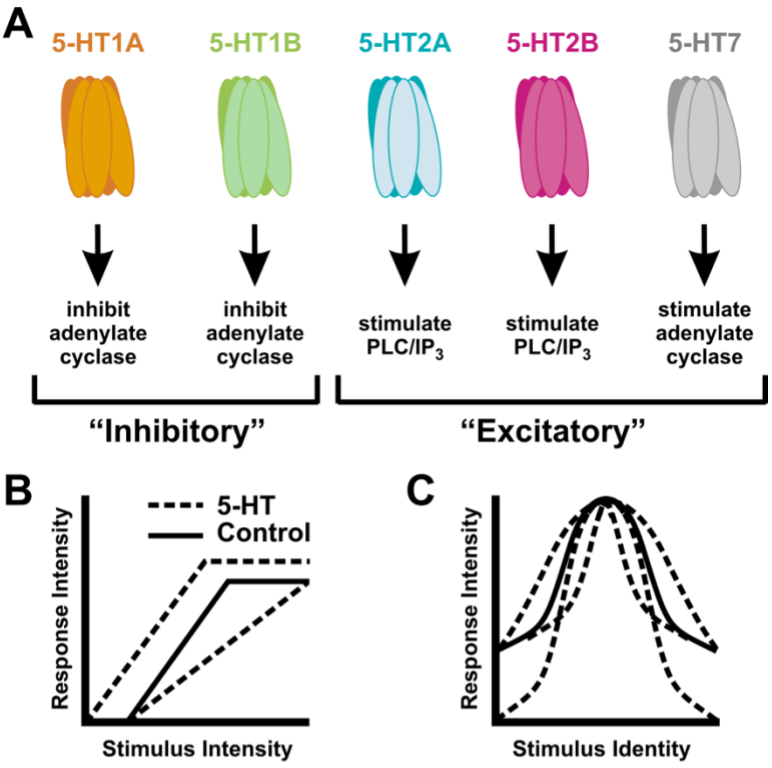

Figure 2. The *Drosophila* 5-HT receptor family members and olfactory computations modulated by 5-HT.
(A) The *Drosophila* genome encodes five distinct 5-HT receptors (5-HTRs): 5-HT1A (orange), 5-HT1B (green), 5-HT2A (blue), 5-HT2B (red), and 5-HT7 (grey). The 1-subtype receptors are negatively coupled to adenylate cyclase, and thus decrease intracellular cAMP. While the 2-subtypes and 7-subtype receptors are positively coupled to PLC/IP_3 signaling and positively coupled to adenylate cyclase, respectively. For these reasons, we generally refer to the two 1-subtype receptors as "inhibitory" and the 2-subtypes and 7-subtype as "excitatory", based on the terminal consequences on the cell's excitability/biophysical properties.
(B) Serotonin (5-HT) can alter stimulus intensity encoding by shifting the slope of the input-output relationship, modulating response strength, or offsetting the threshold for activation.
(C) Serotonin (5-HT) can alter stimulus identity encoding by altering the tuning breadth or by decreasing spontaneous activity to increase the signal-to-noise ratio.
For **B** and **C**: "Control" refers to the neuron's response (albeit, based on stimulus intensity or identity) before 5-HTergic modulation ("5-HT" traces).

Div. Olfactory Transformations via Serotonin Receptor Signaling

Like in other modalities (Sizemore et al., 2020), 5-HTRs expressed by LNs can enable *indirect* modulation of OSN activity to modulate the gain of sensory input. For example, 5-HT stimulates 5-HT2C expressing juxtaglomerular cells in the olfactory bulb to increase the amount of presynaptic inhibition exerted upon OSNs (Petzold et al., 2009). In doing so, 5-HT reduces the gain of OSN responses and thus the amount of sensory input entering the olfactory bulb (Petzold et al., 2009). Moreover, 5-HT can also *indirectly* enhance presynaptic inhibition by activating 5-HT2A receptors expressed by excitatory external tufted cells, which in turn provide excitatory drive to inhibitory short axon and periglomerular cells (Liu et al., 2012; Brill et al., 2015). In this way, 5-HT can potentiate inhibitory inputs to OSNs as a means of decreasing the gain of sensory input. Serotonin similarly *indirectly* decreases the strength of OSN input in the *Drosophila* AL by enhancing presynaptic inhibition (Dacks et al., 2009; Gaudry, 2018), presumably by activating excitatory 5-HT7 receptor along GABAergic LNs (Suzuki et al., 2020).

Recall that, at the synaptic level, lateral inhibition and excitation can be used to sharpen or broaden the resolution with which they encode stimulus identity, respectively (Martin et al., 2011). Not surprisingly, 5-HT also targets these aspects of sensory encoding **(Figure 2B-C)**. Such is the case in the vertebrate piriform cortex, where 5-HT sharpens neuronal representations of odors by decreasing certain mitral/tufted cells' spontaneous activity but leaving their odor-evoked responses unaffected (Lottem et al., 2016). In addition to sharpening responses, 5-HT can also broaden the receptive range of neurons in a given sensory system. In the olfactory bulb, 5-HT activates excitatory 5-HT2A receptors expressed by LNs to enhance the amount of feedforward excitation mitral cells (Liu et al., 2012; Brill et al., 2015; Huang et al., 2017). The combined actions of both 5-HT and glutamate released by DRN neurons increase the sensitivity of tufted cells and decorrelate odor-evoked responses of mitral cells, presumably increasing the separation of representations of different odors (Kapoor et al., 2016). In the *Drosophila* AL, 5-HT has the potential to affect the breadth of odor-evoked representations in a similar way, as the cholinergic and electrically-coupled LNs that broaden odor-tuning properties express excitatory 5-HTRs (Shang et al., 2007; Huang et al., 2010; Yaksi and Wilson, 2010; Sizemore and Dacks, 2016). Serotonin can also *directly* modulate the excitability of second-order neurons within a sensory system to similarly modulate stimulus tuning

breadth. For example, application of exogenous 5-HT increases insect PN excitability (Kloppenburg and Hildebrand, 1995; Kloppenburg et al., 1999; Dacks et al., 2009; Zhang and Gaudry, 2016). This effect, however, is at least partially polysynaptic and depends on the method of delivery as activation of *Drosophila* CSDns can have little-to-no effect on the odor-evoked responses of output neurons depending on the glomerulus (Zhang and Gaudry, 2016). This discrepancy could arise from cell class-specific receptor expression in the AL (Sizemore and Dacks, 2016), differences between 5-HTR binding affinities (Gasque et al., 2013), or differences in the time course of receptor activation and inactivation. Regardless, there appear to be a variety of means by which 5-HT can affect the resolution with which stimulus identity is encoded.

E. METAMODULATION: MODULATING THE ACTIONS OF ANOTHER MODULATOR

Ei. Serotonergic Metamodulation In Sensory Processing

All sensory systems are influenced by multiple neuromodulators released from intrinsic/extrinsic neurons, whose collective concentrations at any given time can be thought to represent the “modulatory tone” of the network at that time (Katz and Edwards, 1999; Iwano and Kanzaki, 2005; Berg et al., 2009; Carlsson et al., 2010; Chalasani et al., 2010; Marder et al., 2014; Jacob and Nienborg, 2018; Lizbinski et al., 2018; Nassel, 2018; Nässel and Zandawala, 2019). Much like how changes in the collective concentrations of intrinsic/extrinsic factors can have profound consequences on a cell’s development (Pearson and Doe, 2004; Doe, 2008), changes in even individual modulators can have profound consequences on the network’s ability to rapidly/efficiently adjust activity. These changes in modulatory tone might, therefore, reflect dramatic shifts in the animal’s behavior state as it relates to a given sensory experience. Therefore, an individual modulator, such as 5-HT, can profoundly alter network-wide activity by simply adjusting existing network-intrinsic modulatory circuitry to rapidly adjust behavioral output.

As outlined above, 5-HT influences interneuron-mediated GABAergic modulation in both vertebrate and invertebrate primary olfactory systems (see above) [see also (Lizbinski and Dacks, 2018)]. Interneurons, more generally, are an ideal target for

modulation given their central role in network processing in serial and parallel, and the diversity of heterogeneous subtypes (see above). Moreover, when the interneurons being modulated also co-release multiple transmitters [e.g., (Lizbinski et al., 2018)], then the computations these LNs adjust can be nonlinearly transformed and layered atop one another to produce nearly exponential network outputs. More specifically, 5-HT can have heterogeneous and complex effects on olfactory processing by leveraging the properties of this single circuit node (GABAergic LNs).

Serotonergic modulation of peptidergic signaling has not been studied in olfactory systems, but has been shown in other systems. For instance, interneurons of the vertebrate sensory cortex that release vasoactive intestinal peptide (VIP) also express the excitatory ionotropic 5-HT3 receptor (Lee et al., 2010; Rudy et al., 2011; Cardin, 2018). Activating 5-HT3 receptors in VIP interneurons causes a hyperpolarization in 5-HT3-negative inhibitory interneurons, which subsequently disinhibits pyramidal neurons (Pfeffer et al., 2013; Jiang et al., 2015). Moreover, serotonergic stimulation of VIP interneurons also produces a latent, $GABA_B$-receptor mediated hyperpolarization in these same pyramidal cells (Takesian et al., 2018). Therefore, by acting through these interneurons, serotonin can have a large impact on network dynamics and even modulate distinct aspects of sensory processing [e.g., (Pi et al., 2013)]. Moreover, the activity of the VIP interneurons appears to be at least one determinant for the changes observed in the activity of visual cortex circuitry according to the animal's ongoing behavioral state (Bennett et al., 2013; Polack et al., 2013; Fu et al., 2014; Pakan et al., 2016; Batista-Brito et al., 2017). Collectively, these results suggest that there may be a serotonin-induced contingency switching module in visual cortex, wherein the animal's locomotor activity induces serotonergic activation of VIP interneurons. Then, perhaps after some epoch post-behavior initiation, negative feedback terminates this serotonin-induced module. This instance nicely illustrates the striking reflection between changes in a network's modulatory tone and dramatic shifts in the animal's behavioral state (in-rest vs. mobile), as well as the important role metamodulation plays in network processing and output. However, perhaps as a consequence of neuromodulation being classically understudied in sensory processing, the consequences of metamodulation remain largely untested.

Therefore, in this dissertation I address three main questions regarding 5-HTergic

metamodulation of olfactory processing. First, I establish a “functional atlas” of which neurons in the *Drosophila* AL express which of the five serotonin receptors **(Chapter 2)**. Later, I leverage this “atlas” to resolve how the activity of one serotonin receptor shapes the activity of a specialized neuropeptidergic signaling pathway **(Chapter 4)**. However, before I can address how the activity of this serotonin receptor adjusts the activity of this neuropeptidergic pathway, I determine the circuit and signaling logic underlying the actions of this peptidergic pathway’s on olfactory processing **(Chapter 3)**. Altogether, my work establishes several key insights that expand our understanding of neuromodulation of sensory processing.

WORKS CITED:

Abbott LF, Varela JA, Sen K, Nelson SB (1997) Synaptic depression and cortical gain control. Science (80-) 275:220–224.

Ache BW, Young JM (2005) Olfaction: Diverse species, conserved principles. Neuron 48:417–430.

Agnati LF, Bjelke B, Fuxe K (1995) Volume versus wiring transmission in the brain: A new theoretical frame for neuropsychopharmacology. Med Res Rev 15:33–45.

Amin H, Lin AC (2019) Neuronal mechanisms underlying innate and learned olfactory processing in Drosophila. Curr Opin Insect Sci 36:9–17.

Azmitia EC (2006) Serotonin and Brain: Evolution, Neuroplasticity, and Homeostasis. Int Rev Neurobiol 77:31–56.

Azmitia EC, Segal M (1978) An autoradiographic analysis of the differential ascending projections of the dorsal and median raphe nuclei in the rat. J Comp Neurol 179:641–667.

Baggerman G, Cerstiaens A, De Loof A, Schoofs L (2002) Peptidomics of the larval Drosophila melanogaster central nervous system. J Biol Chem 277:40368–40374.

Bargmann CI (2006) Comparative chemosensation from receptors to ecology. Nature 444:295–301.

Bargmann CI (2012) Beyond the connectome: How neuromodulators shape neural circuits. BioEssays 34:458–465.

Bargmann CI, Marder E (2013) From the connectome to brain function. Nat Methods 10:483–490.

Bates AS, Schlegel P, Roberts RJV, Drummond N, Tamimi IFM, Turnbull R, Zhao X, Marin EC, Popovici PD, Dhawan S, Jamasb A, Javier A, Serratosa Capdevila L, Li F, Rubin GM, Waddell S, Bock DD, Costa M, Jefferis GSXE (2020) Complete Connectomic Reconstruction of Olfactory Projection Neurons in the Fly Brain. Curr Biol 30:3183-3199.e6.

Batista-Brito R, Vinck M, Ferguson KA, Chang JT, Laubender D, Lur G, Mossner JM, Hernandez VG, Ramakrishnan C, Deisseroth K, Higley MJ, Cardin JA (2017) Developmental Dysfunction of VIP Interneurons Impairs Cortical Circuits. Neuron 95:884-895.e9.

Bell JS, Wilson RI (2016) Behavior Reveals Selective Summation and Max Pooling among Olfactory Processing Channels. Neuron 91:425–438.

Bennett C, Arroyo S, Hestrin S (2013) Subthreshold mechanisms underlying state-dependent modulation of visual responses. Neuron 80:350–357.

Benton R, Vannice KS, Gomez-Diaz C, Vosshall LB (2009) Variant Ionotropic Glutamate Receptors as Chemosensory Receptors in Drosophila. Cell 136:149–162.

Berck ME, Khandelwal A, Claus L, Hernandez-nu L, Si G, Tabone CJ, Li F, Truman JW, Fetter RD, Louis M, Samuel ADT, Cardona A (2016) The wiring diagram of a glomerular olfactory system. Elife:7–9.

Berg BG, Schachtner J, Homberg U (2009) γ-Aminobutyric acid immunostaining in the antennal lobe of the moth Heliothis virescens and its colocalization with neuropeptides. Cell Tissue Res 335:593–605.

Berger M, Gray JA, Roth BL (2009) The expanded biology of serotonin. Annu Rev Med 60:355–366.

Bertrand PP, Bertrand RL (2010) Serotonin release and uptake in the gastrointestinal tract. Auton Neurosci Basic Clin 153:47–57.

Bhandawat V, Olsen SR, Gouwens NW, Schlief ML, Wilson RI (2007) Sensory processing in the Drosophila antennal lobe increases reliability and separability of ensemble odor representations. Nat Neurosci 10:1474–1482.

Blackburn MB, Jaffe H, Kochansky J, Raina AK (2001) Identification of four additional myoinhibitory peptides (MIPs) from the ventral nerve cord of Manduca sexta. Arch Insect Biochem Physiol 48:121–128.

Blackburn MB, Wagner RM, Kochansky JP, Harrison DJ, Thomas-Laemont P, Raina AK (1995) The identification of two myoinhibitory peptides, with sequence similarities to the galanins, isolated from the ventral nerve cord of Manduca sexta. Regul Pept 57:213–219.

Blenau W, Daniel S, Balfanz S, Thamm M, Baumann A (2017) Dm5-HT2B: Pharmacological Characterization of the Fifth Serotonin Receptor Subtype of Drosophila melanogaster. Front Syst Neurosci 11:28.

Bockaert J, Claeysen S, Bécamel C, Dumuis A, Marin P (2006) Neuronal 5-HT

metabotropic receptors: Fine-tuning of their structure, signaling, and roles in synaptic modulation. Cell Tissue Res 326:553–572.

Braha O, Edmonds B, Sacktor T, Kandel ER, Klein M (1993) The contributions of protein kinase A and protein kinase C to the actions of 5-HT on the L-type Ca2+ current of the sensory neurons in Aplysia. J Neurosci 13:1839–1851.

Brill J, Shao Z, Puche AC, Wachowiak M, Shipley MT (2015) Serotonin increases synaptic activity in olfactory bulb glomeruli. J Neurophysiol:jn.00847.2015.

Bucher D, Marder E (2013) SnapShot: Neuromodulation. Cell 155:482-482.e1.

Bunin MA, Wightman RM (1998) Quantitative evaluation of 5-hydroxytryptamine (serotonin) neuronal release and uptake: An investigation of extrasynaptic transmission. J Neurosci 18:4854–4860.

Burns CM, Chu H, Rueter SM, Hutehinson LK, Canton H, Sanders-bush E, Emeson RB (1997) Regulation of serotonin-2C receptor G-protein coupling by RNA editing Sequence analysis of clones isolated from a rat striatum cDNA. Nature 387115:303–308.

Butterwick JA, del Mármol J, Kim KH, Kahlson MA, Rogow JA, Walz T, Ruta V (2018) Cryo-EM structure of the insect olfactory receptor Orco. Nature 560:447–452.

Calizo LH, Akanwa A, Ma X, Pan YZ, Lemos JC, Craige C, Heemstra LA, Beck SG (2011) Raphe serotonin neurons are not homogenous: Electrophysiological, morphological and neurochemical evidence. Neuropharmacology 61:524–543.

Carandini M, Heeger DJ (2012) Normalization as a canonical neural computation. Nat Rev Neurosci 13:51–62.

Cardin JA (2018) Inhibitory Interneurons Regulate Temporal Precision and Correlations in Cortical Circuits. Trends Neurosci 41:689–700.

Carlson JR (1996) Olfaction in Drosophila: From odor to behavior. Trends Genet 12:175–180.

Carlsson M a., Diesner M, Schachtner J, Nässel DR (2010) Multiple neuropeptides in the Drosophila antennal lobe suggest complex modulatory circuits. J Comp Neurol 518:3359–3380.

Chalasani SH, Kato S, Albrecht DR, Nakagawa T, Abbott LF, Bargmann CI (2010) Neuropeptide feedback modifies odor-evoked dynamics in Caenorhabditis elegans

olfactory neurons. Nat Neurosci 13:615–621.

Chazal G, Ralston HJ (1987) Serotonin-containing structures in the nucleus raphe dorsalis of the cat: An ultrastructural analysis of dendrites, presynaptic dendrites, and axon terminals. J Comp Neurol 259:317–329.

Chou Y-H, Spletter ML, Yaksi E, Leong JCS, Wilson RI, Luo L (2010) Diversity and wiring variability of olfactory local interneurons in the Drosophila antennal lobe. Nat Neurosci 13:439–449.

Coast GM, Schooley DA (2011) Toward a consensus nomenclature for insect neuropeptides and peptide hormones. Peptides 32:620–631.

Coates K, Calle-Schuler S, Helmick L, Knotts V, Martik B, Salman F, Warner L, Valla S, Bock D, Dacks A (2020) The wiring logic of an identified serotonergic neuron that spans sensory networks. J Neurosci 40:6309–6327.

Coates KE, Majot AT, Zhang X, Michael CT, Spitzer SL, Gaudry Q, Dacks AM (2017) Identified Serotonergic Modulatory Neurons Have Heterogeneous Synaptic Connectivity within the Olfactory System of *Drosophila*. J Neurosci 37:7318–7331.

Cognigni P, Felsenberg J, Waddell S (2018) Do the right thing: neural network mechanisms of memory formation, expression and update in Drosophila. Curr Opin Neurobiol 49:51–58.

Colas JF, Launay JM, Kellermann O, Rosay P, Maroteaux L (1995) Drosophila 5-HT2 serotonin receptor: coexpression with fushi-tarazu during segmentation. Proc Natl Acad Sci U S A 92:5441–5445.

Cook SJ, Jarrell TA, Brittin CA, Wang Y, Bloniarz AE, Yakovlev MA, Nguyen KCQ, Tang LTH, Bayer EA, Duerr JS, Bülow HE, Hobert O, Hall DH, Emmons SW (2019) Whole-animal connectomes of both Caenorhabditis elegans sexes. Nature 571:63–71.

Cools R, Roberts AC, Robbins TW (2008) Serotoninergic regulation of emotional and behavioural control processes. Trends Cogn Sci 12:31–40.

Couto A, Alenius M, Dickson BJ (2005) Molecular , Anatomical , and Functional Organization of the Drosophila Olfactory System. 15:1535–1547.

Dacks AM, Christensen T a., Hildebrand JG (2006) Phylogeny of a Serotonin-Immunoreactive Neuron in the Primary Olfactory Center of the Insect Brain. J

Comp Neurol 498:727–746.

Dacks AM, Green DS, Root CM, Nighorn AJ, Wang JW (2009) Serotonin modulates olfactory processing in the antennal lobe of Drosophila. J Neurogenet 23:366–377.

Dacks AM, Reale V, Pi Y, Zhang W, Dacks JB, Nighorn AJ, Evans PD (2013) A Characterization of the Manduca sexta Serotonin Receptors in the Context of Olfactory Neuromodulation. PLoS One 8:1–15.

Das A, Chiang A, Davla S, Priya R, Reichert H, VijayRaghavan K, Rodrigues V (2011) Identification and analysis of a glutamatergic local interneuron lineage in the adult Drosophila olfactory system. Neural Syst Circuits 1:4.

Das A, Sen S, Lichtneckert R, Okada R, Ito K, Rodrigues V, Reichert H (2008) Drosophila olfactory local interneurons and projection neurons derive from a common neuroblast lineage specified by the empty spiracles gene. Neural Dev 3:33.

Das Chakraborty S, Sachse S (2021) Olfactory processing in the lateral horn of Drosophila. Cell Tissue Res 383:113–123.

Daur N, Nadim F, Bucher D (2016) The complexity of small circuits: the stomatogastric nervous system. Curr Opin Neurobiol 41:1–7.

De Bruyne M, Clyne PJ, Carlson JR (1999) Odor coding in a model olfactory organ: The Drosophila maxillary palp. J Neurosci 19:4520–4532.

De Bruyne M, Foster K, Carlson JR (2001) Odor coding in the Drosophila antenna. Neuron 30:537–552.

Deanhardt B, Duan Q, Du C, Soeder C, Jones C, Volkan P (2021) Changes in splicing and neuromodulatory gene expression programs in sensory neurons with pheromone signaling and social experience. bioRxiv.

DeFelipe J, Hendry SHC, Hashikawa T, Jones EG (1991) Synaptic relationships of serotonin-Immunoreactive terminal baskets on GABA neurons in the cat auditory cortex. Cereb Cortex 1:117–133.

Descarries L, Watkins K, Garcia S, Beaudet A (1982) The serotonin neurons in nucleus raphe dorsalis of adult rat: a light and electron microscope radioautographic study. J Comp Neurol 207:239–254.

Doe CQ (2008) Neural stem cells: balancing self-renewal with differentiation.

Development 135:1575–1587.

Doty RW (1983) Nongeniculate afferents to striate cortex in macaques. J Comp Neurol 218:159–173.

Eid L, Champigny MF, Parent A, Parent M (2013) Quantitative and ultrastructural study of serotonin innervation of the globus pallidus in squirrel monkeys. Eur J Neurosci 37:1659–1668.

Eisthen HL (2002) Why are olfactory systems of different animals so similar? Brain Behav Evol 59:273–293.

El-Merahbi R, Löffler M, Mayer A, Sumara G (2015) The roles of peripheral serotonin in metabolic homeostasis. FEBS Lett 589:1728–1734.

Ferguson KA, Cardin JA (2020) Mechanisms underlying gain modulation in the cortex. Nat Rev Neurosci 21:80–92.

Fishilevich E, Vosshall LB (2005) Genetic and Functional Subdivision of the Drosophila Antennal Lobe Genetic and Functional Subdivision of the Drosophila Antennal Lobe. Curr Biol 15:1548–1553.

Fu W, Le Maître E, Fabre V, Bernard JF, Xu ZQD, Hökfelt T (2010) Chemical neuroanatomy of the dorsal raphe nucleus and adjacent structures of the mouse brain. J Comp Neurol 518:3464–3494.

Fu Y, Tucciarone JM, Espinosa JS, Sheng N, Darcy DP, Nicoll RA, Huang ZJ, Stryker MP (2014) A cortical circuit for gain control by behavioral state. Cell 156:1139–1152.

Fuxe K, Agnati LF, Marcoli M, Borroto-Escuela DO (2015) Volume Transmission in Central Dopamine and Noradrenaline Neurons and Its Astroglial Targets. Neurochem Res 40:2600–2614.

Gaspar P, Lillesaar C (2012) Probing the diversity of serotonin neurons. Philos Trans R Soc B Biol Sci 367:2382–2394.

Gasque G, Conway S, Huang J, Rao Y, Vosshall LB (2013) Small molecule drug screening in Drosophila identifies the 5HT2A receptor as a feeding modulation target. Sci Rep 3:srep02120.

Gaudry Q (2018) Serotonergic modulation of olfaction in rodents and insects. Yale J Biol Med 91:23–32.

Gershon MD (2013) 5-Hydroxytryptamine (serotonin) in the gastrointestinal tract. Curr Opin Endocrinol Diabetes Obes 20:14–21.

Getting P (1989) Emerging Principles Governing the Operation of Neural Networks. Annu Rev Neurosci 12:185–204.

Grabe V, Baschwitz A, Dweck HKM, Lavista-Llanos S, Hansson BS, Sachse S (2016) Elucidating the Neuronal Architecture of Olfactory Glomeruli in the Drosophila Antennal Lobe. Cell Rep 16:3401–3413.

Gracia-Llanes FJ, Blasco-Ibáñez JM, Nácher J, Varea E, Liberia T, Martínez P, Martínez-Guijarro FJ, Crespo C (2010) Synaptic connectivity of serotonergic axons in the olfactory glomeruli of the rat olfactory bulb. Neuroscience 169:770–780.

Grailhe R, Grabtree GW, Hen R (2001) Human 5-HT5 receptors: The 5-HT5A receptor is functional but the 5-HT5B receptor was lost during mammalian evolution. Eur J Pharmacol 418:157–167.

Haddad R, Weiss T, Khan R, Nadler B, Mandairon N, Bensafi M, Schneidman E, Sobel N (2010) Global features of neural activity in the olfactory system form a parallel code that predicts olfactory behavior and perception. J Neurosci 30:9017–9026.

Hallem EA, Carlson JR (2006) Coding of Odors by a Receptor Repertoire. Cell 125:143–160.

Hallem EA, Ho MG, Carlson JR (2004) The molecular basis of odor coding in the Drosophila larva. Cell 117:965–979.

Hannon J, Hoyer D (2008) Molecular biology of 5-HT receptors. Behav Brain Res 195:198–213.

Hansson BS, Stensmyr MC (2011) Evolution of insect olfaction. Neuron 72:698–711.

Hardy a., Palouzier-Paulignan B, Duchamp a., Royet JP, Duchamp-Viret P (2005) 5-Hydroxytryptamine action in the rat olfactory bulb: In vitro electrophysiological patch-clamp recordings of juxtaglomerular and mitral cells. Neuroscience 131:717–731.

Harris-Warrick R, Marder E (1991) Modulation of Neural Networks for Behavior. Annu Rev Neurosci 14:39–57.

Hay-Schmidt A (2000) The evolution of the serotonergic nervous system. Proc R Soc B Biol Sci 267:1071–1079.

Heisenberg M (2003) Mushroom body memoir: from maps to models. Nat Rev Neurosci 4:266–275.

Herculano-Houzel S, Mota B, Lent R (2006) Cellular scaling rules for rodent brains. Proc Natl Acad Sci U S A 103:12138–12143.

Hildebrand JG, Shepherd GM (1997) MECHANISMS OF OLFACTORY DISCRIMINATION: Converging Evidence for Common Principles Across Phyla. Annu Rev Neurosci 20:595–631.

Hill ES, Iwano M, Gatellier L, Kanzaki R (2002) Morphology and physiology of the serotonin-immunoreactive putative antennal lobe feedback neuron in the male silkmoth Bombyx mori. Chem Senses 27:475–483.

Hochner B, Kandel ER (1992) Modulation of a transient K+ current in the pleural sensory neurons of Aplysia by serotonin and cAMP: Implications for spike broadening. Proc Natl Acad Sci U S A 89:11476–11480.

Hökfelt T, Broberger C, Xu ZQD, Sergeyev V, Ubink R, Diez M (2000) Neuropeptides - An overview. Neuropharmacology 39:1337–1356.

Hong EJ, Wilson RI (2015) Simultaneous Encoding of Odors by Channels with Diverse Sensitivity to Inhibition. Neuron 85:573–589.

Hornung JP (2010) The Neuronatomy of the Serotonergic System. Handb Behav Neurosci 21:51–64.

Hua YJ, Tanaka Y, Nakamura K, Sakakibara M, Nagata S, Kataoka H (1999) Identification of a prothoracicostatic peptide in the larval brain of the silkworm, Bombyx mori. J Biol Chem 274:31169–31173.

Huang J, Zhang W, Qiao W, Hu A, Wang Z (2010) Functional connectivity and selective odor responses of excitatory local interneurons in drosophila antennal lobe. Neuron 67:1021–1033.

Huang KW, Ochandarena NE, Philson AC, Hyun M, Birnbaum JE, Cicconet M, Sabatini BL (2019) Molecular and anatomical organization of the dorsal raphe nucleus. Elife 8:1–34.

Huang Z, Thiebaud N, Fadool DA (2017) Differential serotonergic modulation across the main and accessory olfactory bulbs. J Physiol 11:3515–3533.

Hurley LM, Devilbiss DM, Waterhouse BD (2004) A matter of focus: Monoaminergic

modulation of stimulus coding in mammalian sensory networks. Curr Opin Neurobiol 14:488–495.

Ignell R, Root CM, Birse RT, Wang JW, Nässel DR, Winther AME (2009) Presynaptic peptidergic modulation of olfactory receptor neurons in Drosophila. Proc Natl Acad Sci U S A 106:13070–13075.

Ishimura K, Takeuchi Y, Fujiwara K, Tominaga M, Yoshioka H, Sawada T (1988) Quantitative analysis of the distribution of serotonin-immunoreactive cell bodies in the mouse brain. Neurosci Lett 91:265–270.

Ishita Y, Chihara T, Okumura M (2019) Serotonergic modulation of feeding behavior in Caenorhabditis elegans and other related nematodes. Neurosci Res.

Iwano M, Kanzaki R (2005) Immunocytochemical Identification of Neuroactive Substances in the Antennal Lobe of the Male Silkworm Moth Bombyx mori. Zoolog Sci 22:199–211.

Jacob SN, Nienborg H (2018) Monoaminergic Neuromodulation of Sensory Processing. Front Neural Circuits 12:1–17.

Jiang X, Shen S, Cadwell CR, Berens P, Sinz F, Ecker AS, Patel S, Tolias AS (2015) Principles of connectivity among morphologically defined cell types in adult neocortex. Science (80-) 350.

Joseph RM, Carlson JR (2015) Drosophila Chemoreceptors: A Molecular Interface Between the Chemical World and the Brain. Trends Genet 31:683–695.

Kaneko T, Macara AM, Li R, Hu Y, Iwasaki K, Firestone E, Horvatic S, Guntur A, Shafer OT, Yang H, Zhou J, Ye B, Arbor A, Arbor A (2017) Serotonergic modulation enables pathway-specific plasticity in a developing sensory circuit in Drosophila. Neuron 95:623–638.

Kapoor V, Provost AC, Agarwal P, Murthy VN (2016) Activation of raphe nuclei triggers rapid and distinct effects on parallel olfactory bulb output channels. Nat Neurosci:1–14.

Katz PS (1999) What are we talking about? Modes of neuronal communication Paul.

Katz PS, Edwards DH (1999) Metamodulation: the control and modulation of neuromodulation.

Katz PS, Frost WN (1995) Intrinsic neuromodulation in the Tritonia swim CPG:

Serotonin mediates both neuromodulation and neurotransmission by the dorsal swim interneurons. J Neurophysiol 74:2281–2294.

Kazama H, Wilson RI (2008) Homeostatic Matching and Nonlinear Amplification at Identified Central Synapses. Neuron 58:401–413.

Kim KS, Kim MA, Sohn YC (2019) Molecular characterization, expression analysis, and functional properties of multiple 5-hydroxytryptamine receptors in Pacific abalone (Haliotis discus hannai). Gen Comp Endocrinol 276:52–59.

Kim SM, Su C-Y, Wang JW (2017) Neuromodulation of Innate Behaviors in Drosophila. Annu Rev Neurosci 40:annurev-neuro-072116-031558.

Kim Y-JY-C, Bartalska K, Audsley N, Yamanaka N, Yapici N, Lee J-Y, Markovic M, Isaac E, Tanaka Y, Dickson BJ (2010) MIPs are ancestral ligands for the sex peptide receptor. Proc Natl Acad Sci 107:6520–6525.

Kloppenburg P, Ferns D, Mercer a R (1999) Serotonin enhances central olfactory neuron responses to female sex pheromone in the male sphinx moth manduca sexta. J Neurosci 19:8172–8181.

Kloppenburg P, Hildebrand JG (1995) Neuromodulation by 5-hydroxytryptamine in the antennal lobe of the sphinx moth Manduca sexta. J Exp Biol 198:603–611.

Ko KI, Root CM, Lindsay SA, Zaninovich OA, Shepherd AK, Wasserman SA, Kim SM, Wang JW (2015) Starvation promotes concerted modulation of appetitive olfactory behavior via parallel neuromodulatory circuits. Elife 4:1–17.

Kolodziejczyk A, Nässel DR (2011) Myoinhibitory peptide (MIP) immunoreactivity in the visual system of the blowfly Calliphora vomitoria in relation to putative clock neurons and serotonergic neurons. Cell Tissue Res 345:125–135.

Kupfermann I (1979) Modulatory Actions of Neurotransmitters. Annu Rev Neurosci 2:447–465.

Kupfermann I (1980) Role of cyclic nucleotides in excitable cells. Annu Rev Neurosci 42:629–641.

Lai S-L, Awasaki T, Ito K, Lee T (2008) Clonal analysis of Drosophila antennal lobe neurons: diverse neuronal architectures in the lateral neuroblast lineage. Development 135:2883–2893.

Larsson MC, Domingos AI, Jones WD, Chiappe ME, Amrein H, Vosshall LB (2004)

Or83b encodes a broadly expressed odorant receptor essential for Drosophila olfaction. Neuron 43:703–714.

Lee SH, Hjerling-Leffler J, Zagha E, Fishell G, Rudy B (2010) The largest group of superficial neocortical GABAergic interneurons expresses ionotropic serotonin receptors. J Neurosci 30:16796–16808.

Lee T (2017) Wiring the Drosophila Brain with Individually Tailored Neural Lineages. Curr Biol 27:R77–R82.

Levitan I (1988) MODULATION OF ION CHANNELS IN NEURONS AND OTHER CELLS. Annu Rev Neurosci 11:119–136.

Liang L, Li Y, Potter C, Yizhar O, Deisseroth K, Tsien R, Luo L (2013) GABAergic Projection Neurons Route Selective Olfactory Inputs to Specific Higher-Order Neurons. Neuron 79:917–931.

Lin S, Kao C-F, Yu H-H, Huang Y, Lee T (2012) Lineage Analysis of Drosophila Lateral Antennal Lobe Neurons Reveals Notch-Dependent Binary Temporal Fate Decisions. PLoS Biol 10:e1001425.

Liu S, Aungst JL, Puche a. C, Shipley MT (2012) Serotonin modulates the population activity profile of olfactory bulb external tufted cells. J Neurophysiol 107:473–483.

Liu WW, Wilson RI (2013) Glutamate is an inhibitory neurotransmitter in the Drosophila olfactory system. Proc Natl Acad Sci 110:10294–10299.

Liu Z, Zhou J, Li Y, Hu F, Lu Y, Ma M, Feng Q, Zhang J en, Wang D, Zeng J, Bao J, Kim JY, Chen ZF, ElMestikawy S, Luo M (2014) Dorsal raphe neurons signal reward through 5-HT and glutamate. Neuron 81:1360–1374.

Lizbinski KM, Dacks AM (2018) Intrinsic and Extrinsic Neuromodulation of Olfactory Processing. Front Cell Neurosci 11:1–11.

Lizbinski KM, Marsat G, Dacks AM (2018) Systematic analysis of transmitter coexpression reveals organizing principles of local interneuron heterogeneity. eNeuro 5.

Lizbinski KM, Metheny JD, Bradley SP, Kesari A, Dacks AM (2016) The anatomical basis for modulatory convergence in the antennal lobe of Manduca sexta. J Comp Neurol 524:1859–1875.

Lorenz MW, Kellner R, Hoffmann KH (1995) A family of neuropeptides that inhibit

juvenile hormone biosynthesis in the cricket, Gryllus bimaculatus. J Biol Chem 270:21103–21108.

Lottem E, Lorincz ML, Mainen ZF (2016) Optogenetic Activation of Dorsal Raphe Serotonin Neurons Rapidly Inhibits Spontaneous But Not Odor-Evoked Activity in Olfactory Cortex. J Neurosci 36:7–18.

Lundquist CT, Rökaeus Å, Nässel DR (1991) Galanin immunoreactivity in the blowfly nervous system: Localization and chromatographic analysis. J Comp Neurol 312:77–96.

Luo M, Li Y, Zhong W (2016) Do dorsal raphe 5-HT neurons encode “beneficialness”? Neurobiol Learn Mem 135:40–49.

Marder E (2012) Neuromodulation of Neuronal Circuits: Back to the Future. Neuron 76:1–11.

Marder E, O’Leary T, Shruti S (2014) Neuromodulation of Circuits with Variable Parameters: Single Neurons and Small Circuits Reveal Principles of State-Dependent and Robust Neuromodulation. Annu Rev Neurosci 37:329–346.

Markram H, Toledo-Rodriguez M, Wang Y, Gupta A, Silberberg G, Wu C (2004) Interneurons of the neocortical inhibitory system. Nat Rev Neurosci 5:793–807.

Martin JP, Beyerlein A, Dacks AM, Reisenman CE, Riffell J a., Lei H, Hildebrand JG (2011) The neurobiology of insect olfaction: Sensory processing in a comparative context. Prog Neurobiol 95:427–447.

Matthes S, Bader M (2018) Peripheral Serotonin Synthesis as a New Drug Target. Trends Pharmacol Sci 39:560–572.

McLaughlin CN, Brbić M, Xie Q, Li T, Horns F, Kolluru SS, Kebschull JM, Vacek D, Xie A, Li J, Jones RC, Leskovec J, Quake SR, Luo L, Li H (2021) Single-cell transcriptomes of developing and adult olfactory receptor neurons in drosophila. Elife 10:1–37.

Mclean JH, Shipley T (1987) Serotonergic Afferents to the Rat Olfactory Bulb : I . Origins and Laminar Specificity of Serotonergic Inputs in the Adult Rat. J Neurosci 7.

Meinertzhagen IA (2018) Of what use is connectomics? A personal perspective on the Drosophila connectome. J Exp Biol 221.

Min S, Chae HS, Jang YH, Choi S, Lee S, Jeong YT, Jones WD, Moon SJ, Kim YJ, Chung J (2016) Identification of a peptidergic pathway critical to satiety responses in drosophila. Curr Biol 26:814–820.

Missbach C, Dweck HKM, Vogel H, Vilcinskas A, Stensmyr MC, Hansson BS, Grosse-Wilde E (2014) Evolution of insect olfactory receptors. Elife 2014:1–22.

Miyazaki K, Miyazaki KW, Doya K (2012) The role of serotonin in the regulation of patience and impulsivity. Mol Neurobiol 45:213–224.

Monti JM (2011) Serotonin control of sleep-wake behavior. Sleep Med Rev 15:269–281.

Moroz LL et al. (2014) The ctenophore genome and the evolutionary origins of neural systems. Nature 510:109–114.

Musso P-Y, Junca P, Gordon MD (2021) A neural circuit linking two sugar sensors regulates satiety-dependent fructose drive in Drosophila. bioRxiv:2021.04.08.439043.

Muzerelle A, Scotto-Lomassese S, Bernard JF, Soiza-Reilly M, Gaspar P (2016) Conditional anterograde tracing reveals distinct targeting of individual serotonin cell groups (B5–B9) to the forebrain and brainstem. Brain Struct Funct 221:535–561.

Nadim F, Bucher D (2014) Neuromodulation of neurons and synapses. Curr Opin Neurobiol 29:48–56.

Nagakura I, Dunn TW, Farah CA, Heppner A, Li FF, Sossin WS (2010) Regulation of protein kinase C Apl II by serotonin receptors in Aplysia. J Neurochem 115:994–1006.

Nagayama S, Homma R, Imamura F (2014) Neuronal organization of olfactory bulb circuits. Front Neural Circuits 8:1–19.

Nagel KI, Wilson RI (2011) Biophysical mechanisms underlying olfactory receptor neuron dynamics. Nat Neurosci 14:208–218.

Nagel KI, Wilson RI (2016) Mechanisms Underlying Population Response Dynamics in Inhibitory Interneurons of the Drosophila Antennal Lobe. J Neurosci 36:1–14.

Nassel D (1988) Serotonin and Serotonin-Immunoreactive Neurons in the Nervous System of Insects. Prog Neurobiol 30.

Nassel DR (2018) Substrates for neuronal cotransmission with neuropeptides and small molecule neurotransmitters in drosophila. Front Cell Neurosci 12:1–26.

Nässel DR, Cantera R (1985) Mapping of serotonin-immunoreactive neurons in the larval nervous system of the flies Calliphora erythrocephala and Sarcophaga bullata - A comparison with ventral ganglia in adult animals. Cell Tissue Res 239:423–434.

Nässel DR, Winther ÅME (2010) Drosophila neuropeptides in regulation of physiology and behavior. Prog Neurobiol 92:42–104.

Nässel DR, Zandawala M (2019) Recent advances in neuropeptide signaling in Drosophila, from genes to physiology and behavior. Prog Neurobiol 179:101607.

Neuhaus EM, Gisselmann G, Zhang W, Dooley R, Störtkuhl K, Hatt H (2005) Odorant receptor heterodimerization in the olfactory system of Drosophila melanogaster. Nat Neurosci 8:15–17.

Ng M, Roorda RD, Lima SQ, Zemelman B V., Morcillo P, Miesenböck G (2002) Transmission of olfactory information between three populations of neurons in the antennal lobe of the fly. Neuron 36:463–474.

Ni W, Watts SW (2006) 5-Hydroxytryptamine in the cardiovascular system: Focus on the serotonin transporter (SERT). Clin Exp Pharmacol Physiol 33:575–583.

Nichols DE, Nichols CD (2008) Serotonin Receptors. Chem Rev 108:1614–1641.

Oh Y, Yoon SE, Zhang Q, Chae HS, Daubnerová I, Shafer OT, Choe J, Kim YJ (2014) A Homeostatic Sleep-Stabilizing Pathway in Drosophila Composed of the Sex Peptide Receptor and Its Ligand, the Myoinhibitory Peptide. PLoS Biol 12.

Okada R, Awasaki T, Ito K (2009) Gamma-aminobutyric acid (GABA)-mediated neural connections in the Drosophila antennal lobe. J Comp Neurol 514:74–91.

Okaty BW, Commons KG, Dymecki SM (2019) Embracing diversity in the 5-HT neuronal system. Nat Rev Neurosci 20:397–424.

Olsen SR, Bhandawat V, Wilson RI (2007) Excitatory Interactions between Olfactory Processing Channels in the Drosophila Antennal Lobe. Neuron 54:89–103.

Olsen SR, Bhandawat V, Wilson RI (2010) Divisive normalization in olfactory population codes. Neuron 66:287–299.

Olsen SR, Wilson RI (2008) Lateral presynaptic inhibition mediates gain control in an olfactory circuit. Nature 452:956–960.

Pacheco DA, Thiberge SY, Pnevmatikakis E, Murthy M (2021) Auditory activity is

diverse and widespread throughout the central brain of Drosophila. Nat Neurosci 24:93–104.

Pakan JMP, Lowe SC, Dylda E, Keemink SW, Currie SP, Coutts CA, Rochefort NL (2016) Behavioral-state modulation of inhibition is context-dependent and cell type specific in mouse visual cortex. Elife 5:1–18.

Pass G (2000) Accessory pulsatile organs: evolutionary innovations in insects. Annu Rev Entomol 45:495–518.

Pearson BJ, Doe CQ (2004) Specification of Temporal Identity in the Developing Nervous System. Annu Rev Cell Dev Biol 20:619–647.

Peroutka SJ, Howell TA (1994) The molecular evolution of G protein-coupled receptors: focus on 5-hydroxytryptamine receptors. Neuropharmacology 33:319–324.

Petzold GC, Hagiwara A, Murthy VN (2009) Serotonergic modulation of odor input to the mammalian olfactory bulb. Nat Neurosci 12:784–791.

Pfeffer CK, Xue M, He M, Huang ZJ, Scanziani M (2013) Inhibition of inhibition in visual cortex: The logic of connections between molecularly distinct interneurons. Nat Neurosci 16:1068–1076.

Pi HJ, Hangya B, Kvitsiani D, Sanders JI, Huang ZJ, Kepecs A (2013) Cortical interneurons that specialize in disinhibitory control. Nature 503:521–524.

Polack PO, Friedman J, Golshani P (2013) Cellular mechanisms of brain state-dependent gain modulation in visual cortex. Nat Neurosci 16:1331–1339.

Predel R, Neupert S, Garczynski SF, Crim JW, Brown MR, Russell WK, Kahnt J, Russell DH, Nachman RJ (2010) Neuropeptidomics of the mosquito Aedes aegypti. J Proteome Res 9:2006–2015.

Predel R, Rapus J, Eckert M (2001) Myoinhibitory neuropeptides in the American cockroach. Peptides 22:199–208.

Prinz AA, Bucher D, Marder E (2004) Similar network activity from disparate circuit parameters. Nat Neurosci 7:1345–1352.

Raji JI, Potter CJ (2021) The number of neurons in Drosophila and mosquito brains. PLoS One 16:e0250381.

Ranganathan R, Cannon SC, Horvitz HR (2000) MOD-1 is a serotonin-gated chloride channel that modulates locomotory behaviour in C. elegans. Nature 408:470–475.

Ren J, Friedmann D, Xiong J, Liu CD, Ferguson BR, Weerakkody T, DeLoach KE, Ran C, Pun A, Sun Y, Weissbourd B, Neve RL, Huguenard J, Horowitz MA, Luo L (2018) Anatomically Defined and Functionally Distinct Dorsal Raphe Serotonin Sub-systems. Cell 175:472-487.e20.

Ribeiro P, El-Shehabi F, Patocka N (2005) Classical transmitters and their receptors in flatworms. Parasitology 131.

Root CM, Masuyama K, Green DS, Enell LE, Nässel DR, Lee CH, Wang JW (2008) A Presynaptic Gain Control Mechanism Fine-Tunes Olfactory Behavior. Neuron 59:311–321.

Root CM, Semmelhack JL, Wong AM, Flores J, Wang JW (2007) Propagation of olfactory information in Drosophila. Proc Natl Acad Sci U S A 104:11826–11831.

Röser C, Jordan N, Balfanz S, Baumann A, Walz B, Baumann O, Blenau W (2012) Molecular and Pharmacological Characterization of Serotonin 5-HT2α and 5-HT7 Receptors in the Salivary Glands of the Blowfly Calliphora vicina. PLoS One 7.

Roy B, Singh AP, Shetty C, Chaudhary V, North A, Landgraf M, Vijayraghavan K, Rodrigues V (2007) Metamorphosis of an identified serotonergic neuron in the Drosophila olfactory system. Neural Dev 2:20.

Rudy B, Fishell G, Lee SH, Hjerling-Leffler J (2011) Three groups of interneurons account for nearly 100% of neocortical GABAergic neurons. Dev Neurobiol 71:45–61.

Saberi M et al. (2016) Odorant receptors of Drosophila are sensitive to the molecular volume of odorants. Sci Rep 6:25103.

Sakuma C, Anzo M, Miura M, Chihara T (2014) Development of olfactory projection neuron dendrites that contribute to wiring specificity of the Drosophila olfactory circuit. Genes Genet Syst 89:17–26.

Sakurai A, Katz PS (2003) Spike Timing-Dependent Serotonergic Neuromodulation of Synaptic Strength Intrinsic to a Central Pattern Generator Circuit. J Neurosci 23:10745–10755.

Sakurai A, Katz PS (2009) State-, timing-, and pattern-dependent neuromodulation of synaptic strength by a serotonergic interneuron. J Neurosci 29:268–279.

Salecker I, Distler P (1990) Serotonin-immunoreactive neurons in the antennal lobes of

the American cockroach Periplaneta americana: light- and electron-microscopic observations. Histochemistry 94:463–473.

Sasaki T, Matsuki N, Ikegaya Y (2011) Action-potential modulation during axonal conduction. Science (80-) 331:599–601.

Saudou F, Boschert U, Amlaiky N, Plassat JL, Hen R (1992) A family of Drosophila serotonin receptors with distinct intracellular signalling properties and expression patterns. EMBO J 11:7–17.

Schlegel P, Bates AS, Stürner T, Jagannathan SR, Drummond N, Hsu J, Capdevila LS, Javier A, Marin EC, Barth-Maron A, Tamimi IFM, Li F, Rubin GM, Plaza SM, Costa M, Jefferis G (2021) Information flow, cell types and stereotypy in a full olfactory connectome. Elife.

Schmidt HR, Benton R (2020) Molecular mechanisms of olfactory detection in insects: Beyond receptors: Insect olfactory detection mechanisms. Open Biol 10.

Schoofs L, Holman M, Hayes T, Nachman R, De Loof A (1991) Isolation, identification and synthesis of locustmyoinhibiting peptide (LOM-MIP), a novel biologically active neuropeptide from Locusta migratoria. Regul Pept 36:111–119.

Schultzhaus JN, Saleem S, Iftikhar H, Carney GE (2017) The role of the Drosophila lateral horn in olfactory information processing and behavioral response. J Insect Physiol 98:29–37.

Seki Y, Rybak J, Wicher D, Sachse S, Hansson BS (2010) Physiological and morphological characterization of local interneurons in the Drosophila antennal lobe. J Neurophysiol 104:1007–1019.

Semmelhack JL, Wang JW (2009) Select Drosophila glomeruli mediate innate olfactory attraction and aversion. Nature 459:218–223.

Sen S, Biagini S, Reichert H, VijayRaghavan K (2014) Orthodenticle is required for the development of olfactory projection neurons and local interneurons in Drosophila. Biol Open 3:711–717.

Sengupta A, Bocchio M, Bannerman DM, Sharp T, Capogna M (2017) Control of amygdala circuits by 5-HT neurons via 5-HT and glutamate cotransmission. J Neurosci 37:1785–1796.

Shafer OT, Yao Z (2014) Pigment-Dispersing Factor Signaling and Circadian Rhythms

in Insect Locomotor Activity. Curr Opin Insect Sci 1:73–80.

Shanbhag SR, Müller B, Steinbrecht RA (1999) Atlas of olfactory organs of Drosophila melanogaster 1. Types, external organization, innervation and distribution of olfactory sensilla. Int J Insect Morphol Embryol 28:377–397.

Shang Y, Claridge-Chang A, Sjulson L, Pypaert M, Miesenböck G (2007) Excitatory Local Circuits and Their Implications for Olfactory Processing in the Fly Antennal Lobe. Cell 128:601–612.

Shimizu K, Stopfer M (2017) A Population of Projection Neurons that Inhibits the Lateral Horn but Excites the Antennal Lobe through Chemical Synapses in Drosophila. Front Neural Circuits 11:30.

Shipley MT, Ennis M (1996) Functional Organization of Olfactory System. J Neurobiol 30:123–176.

Silbering AF, Okada R, Ito K, Galizia CG (2008) Olfactory information processing in the Drosophila antennal lobe: anything goes? J Neurosci 28:13075–13087.

Singh AP, Das RN, Rao G, Aggarwal A, Diegelmann S, Evers JF, Karandikar H, Landgraf M, Rodrigues V, VijayRaghavan K (2013) Sensory Neuron-Derived Eph Regulates Glomerular Arbors and Modulatory Function of a Central Serotonergic Neuron. PLoS Genet 9.

Sizemore TR, Dacks AM (2016) Serotonergic Modulation Differentially Targets Distinct Network Elements within the Antennal Lobe of Drosophila melanogaster. Sci Rep 6:37119.

Sizemore TR, Hurley LM, Dacks A (2020) Serotonergic Modulation Across Sensory Modalities. J Neurophysiol:2406–2425.

Steinbusch HW. (1981) Distribution of serotonin-immunoreactivity in the central nervous system of the rat - cell bodies and terminals. Neuroscience 6:557–618.

Stocker RF (1994) The organization of the chemosensory system in Drosophila melanogaster: a review. Cell Tissue Res 275:3–26.

Stocker RF, Heimbeck G, Gendre N, de Belle JS (1997) Neuroblast ablation in Drosophila P[GAL4] lines reveals origins of olfactory interneurons. J Neurobiol 32:443–456.

Stocker RF, Lienhard MC, Borst A, Fischbach KF (1990) Neuronal architecture of the

antennal lobe in Drosophila melanogaster. Cell Tissue Res 262:9–34.

Stocker RF, Singh RN, Schorderet M, Siddiqi O (1983) Projection patterns of different types of antennal sensilla in the antennal glomeruli of Drosophila melanogaster. Cell Tissue Res 232:237–248.

Strausfeld NJ, Hildebrand JG (1999) Olfactory systems: Common design, uncommon origins? Curr Opin Neurobiol 9:634–639.

Strutz A, Soelter J, Baschwitz A, Farhan A, Grabe V, Rybak J, Knaden M, Schmuker M, Hansson BS, Sachse S (2014) Decoding odor quality and intensity in the Drosophila brain. Elife 3:e04147.

Su CY, Menuz K, Carlson JR (2009) Olfactory Perception: Receptors, Cells, and Circuits. Cell 139:45–59.

Su CY, Menuz K, Reisert J, Carlson JR (2012) Non-synaptic inhibition between grouped neurons in an olfactory circuit. Nature 492:66–71.

Sun XJ, Tolbert LP, Hildebrand JG (1993) Ramification pattern and ultrastructural characteristics of the serotonin-immunoreactive neuron in the antennal lobe of the moth Manduca sexta: A laser scanning confocal and electron microscopic study. J Comp Neurol 338:5–16.

Suver MP, Matheson AMM, Sarkar S, Damiata M, Schoppik D, Nagel KI (2019) Encoding of Wind Direction by Central Neurons in Drosophila. Neuron 102:828-842.e7.

Suzuki Y, Schenk JE, Tan H, Gaudry Q (2020) A Population of Interneurons Signals Changes in the Basal Concentration of Serotonin and Mediates Gain Control in the Drosophila Antennal Lobe Report A Population of Interneurons Signals Changes in the Basal Concentration of Serotonin and Mediates Gain Co. Curr Biol:1–9.

Taghert PH, Nitabach MN (2012) Peptide Neuromodulation in Invertebrate Model Systems. Neuron 76:82–97.

Takesian AE, Bogart LJ, Lichtman JW, Hensch TK (2018) Inhibitory circuit gating of auditory critical-period plasticity. Nat Neurosci 21:218–227.

Takeuchi Y, Kimura H, Sano Y (1982) Immunohistochemical demonstration of serotonin nerve fibers in the olfactory bulb of the rat, cat, and monkey. Histochemistry 75:461–471.

Tamvacakis AN, Senatore A, Katz PS (2015) Identification of genes related to learning and memory in the brain transcriptome of the mollusc, Hermissenda crassicornis. Learn Mem 22:617–621.

Tamvacakis AN, Senatore A, Katz PS (2018) Single neuron serotonin receptor subtype gene expression correlates with behaviour within and across three molluscan species. Proc R Soc B Biol Sci 285.

Tanaka M, Watanabe Y (2020) RNA Editing of Serotonin 2C Receptor and Alcohol Intake. Front Neurosci 13:1–8.

Tanaka NK, Ito K, Stopfer M (2009) Odor-evoked neural oscillations in Drosophila are mediated by widely branching interneurons. J Neurosci 29:8595–8603.

Task D, Lin C, Afify A, Li H, Vulpe A, Menuz K, Potter CJ (2020) Widespread Polymodal Chemosensory Receptor Expression in Drosophila Olfactory Neurons. BioRxiv:1–37.

Templin JS, Bang SJ, Soiza-Reilly M, Berde CB, Commons KG (2012) Patterned expression of ion channel genes in mouse dorsal raphe nucleus determined with the Allen Mouse Brain Atlas. Brain Res 1457:1–12.

Tork I (1990) Anatomy of the Serotonergic System. Ann N Y Acad Sci 600:9–34.

Tsuda B, Pate SC, Tye KM, Siegelmann HT, Sejnowski TJ (2021) Neuromodulators enable overlapping synaptic memory regimes and nonlinear transition dynamics in recurrent neural networks. bioRxiv.

Vallés AM, White K (1988) Serotonin-containing neurons in Drosophila melanogaster: Development and distribution. J Comp Neurol 268:414–428.

Venkatesh S, Singh RN (1984) Sensilla on the third antennal segment of Drosophila melanogaster Meigen (Diptera: Drosophilidae). Int J Insect Morphol Embryol 13:1.

Vertes RP, Crane AM (1997) Distribution, quantification, and morphological characteristics of serotonin-immunoreactive cells of the supralemniscal nucleus (B9) and pontomesencephalic reticular formation in the rat. J Comp Neurol 378:411–424.

Vleugels R, Verlinden H, Broeck J Vanden (2015) Serotonin, serotonin receptors and their actions in insects. Neurotransmitter.

Vosshall LB (2000) Olfaction in Drosophila. Curr Opin Neurobiol 10:498–503.

Vosshall LB, Wong a M, Axel R (2000) An olfactory sensory map in the fly brain. Cell 102:147–159.

Wang K, Gong J, Wang Q, Li H, Cheng Q, Liu Y, Zeng S, Wang Z (2014) Parallel pathways convey olfactory information with opposite polarities in Drosophila. Proc Natl Acad Sci U S A 111:3164–3169.

Wang T, Yang Z, Zhou N, Sun L, Lv Z, Wu C (2017) Identification and functional characterisation of 5-HT4 receptor in sea cucumber Apostichopus japonicus (Selenka). Sci Rep 7:1–12.

Wegerhoff R (1999) GABA and serotonin immunoreactivity during postembryonic brain development in the beetle Tonebrio molitor. Microsc Res Tech 45:154–164.

White J, Southgate E, Thomson J, Brenner S (1986) The structure of the nervous system of the nematode Caenorhabditis elegans. Science (80-) 314:1–340.

Williamson M, Lenz C, Winther ME, Nässel DR, Grimmelikhuijzen CJP (2001) Molecular cloning, genomic organization, and expression of a B-type (cricket-type) allatostatin preprohormone from Drosophila melanogaster. Biochem Biophys Res Commun 281:544–550.

Wilson RI (2013) Early Olfactory Processing in Drosophila: Mechanisms and Principles. Annu Rev Neurosci 36:217–241.

Wilson RI, Laurent G (2005) Role of GABAergic inhibition in shaping odor-evoked spatiotemporal patterns in the Drosophila antennal lobe. J Neurosci 25:9069–9079.

Wilson RI, Turner GC, Laurent G (2004) Transformation of Olfactory Representations in the Drosophila Antennal Lobe. Science 303:366–371.

Witz P, Amlaiky N, Plassat JL, Maroteaux L, Borrelli E, Hen R (1990) Cloning and characterization of a Drosophila serotonin receptor that activates adenylate cyclase. Proc Natl Acad Sci U S A 87:8940–8944.

Yaksi E, Wilson RI (2010) Electrical Coupling between Olfactory Glomeruli. Neuron 67:1034–1047.

Yapici N, Kim Y-J, Ribeiro C, Dickson BJ (2008) A receptor that mediates the post-mating switch in Drosophila reproductive behaviour. Nature 451:33–37.

Yasuyama K, Meinertzhagen I a., Schürmann FW (2003) Synaptic Connections of Cholinergic Antennal Lobe Relay Neurons Innervating the Lateral Horn Neuropile in

the Brain of Drosophila melanogaster. J Comp Neurol 466:299–315.

Yeoh JGC, Pandit AA, Zandawala M, Nässel DR, Davies SA, Dow JAT (2017) DINeR: Database for Insect Neuropeptide Research. Insect Biochem Mol Biol 86:9–19.

Yew JY, Wang Y, Barteneva N, Dikler S, Kutz-Naber KK, Li L, Kravitz EA (2009) Analysis of neuropeptide expression and localization in adult Drosophila melanogaster central nervous system by affinity cell-capture mass spectrometry (Journal of Proteome Research (2009) 8, (1271-1284)). J Proteome Res 8:3786.

Yu H-H, Kao C-F, He Y, Ding P, Kao J-C, Lee T (2010) A Complete Developmental Sequence of a Drosophila Neuronal Lineage as Revealed by Twin-Spot MARCM. PLoS Biol 8:e1000461.

Zhang X, Coates K, Dacks A, Günay C, Lauritzen JS, Li F, Calle-Schuler SA, Bock D, Gaudry Q (2019a) Local synaptic inputs support opposing, network-specific odor representations in a widely projecting modulatory neuron. Elife 8:1–17.

Zhang X, Gaudry Q (2016) Functional integration of a serotonergic neuron in the drosophila antennal lobe. Elife 5:1–24.

Zhang Y, Tsang TK, Bushong EA, Chu LA, Chiang AS, Ellisman MH, Reingruber J, Su CY (2019b) Asymmetric ephaptic inhibition between compartmentalized olfactory receptor neurons. Nat Commun 10:1–16.

Zhukovskaya MI, Polyanovsky AD (2017) Biogenic amines in insect antennae. Front Syst Neurosci 11:1–9.

CHAPTER 2

Serotonergic Modulation Differentially Targets Distinct Network Elements within the Antennal Lobe of *Drosophila melanogaster*

SUMMARY:

Sensory systems internalize and process information from the environment to form the animal's internal representation of its surroundings. These systems typically consist of several interconnected neural networks, wherein information regarding a single stimulus (e.g., stimulus identity or strength) are extracted and contextualized with other stimuli present in the environment (e.g., the scent of a predator) and the animal's internal needs (e.g., satiation state). In this way, even the same stimulus can produce divergent behaviors across different animals. One nearly-ubiquitous mechanism nervous systems employ to adjust neural network activity according to the animal's internal needs and external demands is neuromodulation.

Neuromodulation promotes behavioral flexibility from anatomically restricted neural networks by altering the biophysical and synaptic properties of individual neurons (Kandel and Schwartz, 1982; Destexhe and Marder, 2004; Marder, 2012; Nadim and Bucher, 2014; Kim et al., 2017). A single neuromodulator can have short- and/or long-lasting effects on individual network members that can suppress and/or expand the number of network members participating in information processing. These multi-dimensional effects of a single neuromodulator are, in part, a direct consequence of the diversity and distribution of receptor subtypes activated by the given neuromodulator. Thus, to predict the mechanisms underlying the actions of any given neuromodulator in a network, we must first determine the functional class and spatial organization of neurons that express each receptor for that given neuromodulator. This problem is well-illustrated by earlier investigations that sought to determine the mechanism underlying the actions of serotonin (5-HT) in the first olfactory processing center in the *Drosophila* brain, the antennal lobe (AL) (Dacks et al., 2009).

Olfaction for *Drosophila* begins when odorants bind to odorant receptors (ORs) expressed along one or more of the ~1,200 olfactory sensory neurons (OSNs) housed within sensillae along their antennae and maxillary palps (Stocker, 2001; Grabe et al., 2016). A chemical-to-electrical signal transformation occurs upon odorant binding to its cognate OR, thus activating the given OSN. Depending on the OR expressed by the activated OSN, the OSN axons will relay this electrical signal to one or more of the ~51

glomeruli that comprise the AL (Vosshall et al., 2000; Couto et al., 2005; Bates et al., 2020; Marin et al., 2020) where they form excitatory synapses with second-order relay and local processing neurons (projection neurons (PNs) and local interneurons (LNs), respectively). The initial OSN electrical signal is then extracted, decoded, and recoded in an as-of-yet-undetermined manner before (& likely concurrently) the signal is sent via PN projections to the mushroom body and lateral horn (de Belle and Heisenberg, 1994; Yasuyama et al., 2003; Jefferis et al., 2007; Jeanne and Wilson, 2015; Jeanne et al., 2018; Dolan et al., 2019; Frechter et al., 2019; Bates et al., 2020). Within the *Drosophila* AL, there exists only one source of synaptic 5-HT; the contralaterally projecting, serotonin-immunoreactive deutocerebral neurons (CSDns) (Dacks et al., 2006; Roy et al., 2007; Coates et al., 2017, 2020). Moreover, much like in other insects (Hill et al., 2002; Dacks et al., 2008), exogenous application of 5-HT alters *Drosophila* AL principal neuron activity (Dacks et al., 2009; Zhang and Gaudry, 2016). For instance, exogenous application of 5-HT increases PN sensitivity, and enhances PN odor-evoked responses in a stimulus-dependent manner in the *Drosophila* AL (Dacks et al., 2009). However, this observation could equally result from 5-HT acting directly on these PNs to enhance their excitability, or 5-HT altering the synaptic input these PNs receive (albeit by increasing excitation or decreasing inhibition) depending on 5-HTR expression within the AL. Therefore, in this chapter, I leverage the genetic-accessibility and anatomically-tractable of the *Drosophila melanogaster* olfactory system to establish a “functional atlas” of 5-HTR expression within the AL. More specifically, I use immunocytochemistry, intersectional genetics, and transgenics that couple the production of a given 5-HTR to the production of GFP, to determine the number and functional identities of every AL neuron that expresses each of the five 5-HTRs. I found that each 5-HTR is expressed by specific subsets of neurons, suggesting 5-HT targets multiple levels of olfactory processing. Generally, the inhibitory 5-HTRs are expressed by inhibitory neurons including GABAergic PNs and a subpopulation of LNs. Conversely, excitatory 5-HTRs are expressed by OSNs and cholinergic PNs. This suggests serotonin’s effects on olfactory processing within the AL are mediated by a combination of network-wide disinhibition and glomerulus-specific enhancement. More specifically, I found that OSNs exclusively express 5-HT2B, which suggests that 5-HT has cell-class specific effects on OSN activity.

In contrast to OSN 5-HTR expression, I also found that the ventral PNs (vPNs) express all five 5-HTRs, therefore suggesting 5-HT diversely affects vPN activity. Moreover, this suggests that 5-HT likely plays an important role in behavioral attraction to innately appetitive odors as vPN activity has been implicated in promoting olfactory attraction (Masse et al., 2009; Liang et al., 2013; Strutz et al., 2014; Das Chakraborty and Sachse, 2021). Ultimately, this “functional atlas” of 5-HTR expression in the *Drosophila* AL provides a mechanistic framework for the effects of 5-HT on olfactory processing in this network.

WORKS CITED:

Bates AS, Schlegel P, Roberts RJ V, Drummond N, Tamimi IFM, Turnbull RG, Zhao X, Marin EC, Popovici PD, Dhawan S, Jamasb AR, Javier A, Li F, Rubin GM, Waddell S, Bock DD, Costa M, Jefferis GSXE (2020) Complete connectomic reconstruction of olfactory projection neurons in the fly brain. Curr Biol 30:1–17.

Coates K, Calle-Schuler S, Helmick L, Knotts V, Martik B, Salman F, Warner L, Valla S, Bock D, Dacks A (2020) The wiring logic of an identified serotonergic neuron that spans sensory networks. J Neurosci 40:6309–6327.

Coates KE, Majot AT, Zhang X, Michael CT, Spitzer SL, Dacks AM, Spitzer SL, Gaudry Q, Dacks AM (2017) Identified serotonergic modulatory neurons have heterogeneous synaptic connectivity within the olfactory system of Drosophila Title : Identified serotonergic modulatory neurons have heterogeneous synaptic connectivity within the olfactory system of Drosop.

Couto A, Alenius M, Dickson BJ (2005) Molecular , Anatomical , and Functional Organization of the Drosophila Olfactory System. 15:1535–1547.

Dacks a M, Christensen T a, Hildebrand JG (2008) Modulation of olfactory information processing in the antennal lobe of Manduca sexta by serotonin. J Neurophysiol 99:2077–2085.

Dacks AM, Christensen T a., Hildebrand JG (2006) Phylogeny of a Serotonin-Immunoreactive Neuron in the Primary Olfactory Center of the Insect Brain. J Comp Neurol 498:727–746.

Dacks AM, Green DS, Root CM, Nighorn AJ, Wang JW (2009) Serotonin modulates olfactory processing in the antennal lobe of Drosophila. J Neurogenet 23:366–377.

Das Chakraborty S, Sachse S (2021) Olfactory processing in the lateral horn of Drosophila. Cell Tissue Res 383:113–123.

de Belle JS, Heisenberg M (1994) Associative odor learning in Drosophila abolished by chemical ablation of Mushroom Bodies. Science (80-) 263:692–695.

Destexhe A, Marder E (2004) Plasticity in single neuron and circuit computations. Nature 431:789–795.

Dolan M et al. (2019) Neurogenetic dissection of the Drosophila lateral horn reveals major outputs, diverse behavioural functions, and interactions with the mushroom body.

Elife:1–45.

Frechter S, Bates AS, Tootoonian S, Dolan MJ, Manton J, Jamasb AR, Kohl J, Bock D, Jefferis G (2019) Functional and anatomical specificity in a higher olfactory centre. Elife 8:1–39.

Grabe V, Baschwitz A, Dweck HKM, Lavista-Llanos S, Hansson BS, Sachse S (2016) Elucidating the Neuronal Architecture of Olfactory Glomeruli in the Drosophila Antennal Lobe. Cell Rep 16:3401–3413.

Hill ES, Iwano M, Gatellier L, Kanzaki R (2002) Morphology and physiology of the serotonin-immunoreactive putative antennal lobe feedback neuron in the male silkmoth Bombyx mori. Chem Senses 27:475–483.

Jeanne JM, Fis M, Wilson RI, Jeanne JM, Fis M (2018) The Organization of Projections from Olfactory Glomeruli onto Higher-Order Neurons. Neuron:1198–1213.

Jeanne JM, Wilson RI (2015) Convergence, Divergence, and Reconvergence in a Feedforward Network Improves Neural Speed and Accuracy. Neuron 88:1014–1026.

Jefferis GSXE, Potter CJ, Chan AM, Marin EC, Rohlfing T, Maurer CR, Luo L (2007) Comprehensive maps of Drosophila higher olfactory centers: spatially segregated fruit and pheromone representation. Cell 128:1187–1203.

Kandel ER, Schwartz JH (1982) Molecular biology of learning: modulation of transmitter release. Science 218:433–443.

Kim SM, Su C-Y, Wang JW (2017) Neuromodulation of Innate Behaviors in Drosophila. Annu Rev Neurosci 40:annurev-neuro-072116-031558.

Liang L, Li Y, Potter C, Yizhar O, Deisseroth K, Tsien R, Luo L (2013) GABAergic Projection Neurons Route Selective Olfactory Inputs to Specific Higher-Order Neurons. Neuron 79:917–931.

Marder E (2012) Neuromodulation of Neuronal Circuits: Back to the Future. Neuron 76:1–11.

Marin EC, Büld L, Theiss M, Sarkissian T, Roberts RJV, Turnbull R, Tamimi IFM, Pleijzier MW, Laursen WJ, Drummond N, Schlegel P, Bates AS, Li F, Landgraf M, Costa M, Bock DD, Garrity PA, Jefferis GSXE (2020) Connectomics Analysis Reveals First-, Second-, and Third-Order Thermosensory and Hygrosensory Neurons in the Adult Drosophila Brain. Curr Biol 30:3167-3182.e4.

Masse NY, Turner GC, Jefferis GSXE (2009) Olfactory Information Processing in Drosophila. Curr Biol 19:R700–R713.

Nadim F, Bucher D (2014) Neuromodulation of neurons and synapses. Curr Opin Neurobiol 29:48–56.

Roy B, Singh AP, Shetty C, Chaudhary V, North A, Landgraf M, Vijayraghavan K, Rodrigues V (2007) Metamorphosis of an identified serotonergic neuron in the Drosophila olfactory system. Neural Dev 2:20.

Stocker RF (2001) Drosophila as a focus in olfactory research: Mapping of olfactory sensilla by fine structure, odor specificity, odorant receptor expression, and central connectivity. Microsc Res Tech 55:284–296.

Strutz A, Soelter J, Baschwitz A, Farhan A, Grabe V, Rybak J, Knaden M, Schmuker M, Hansson BS, Sachse S (2014) Decoding odor quality and intensity in the Drosophila brain. Elife 3:e04147.

Vosshall LB, Wong a M, Axel R (2000) An olfactory sensory map in the fly brain. Cell 102:147–159.

Yasuyama K, Meinertzhagen I a., Schürmann FW (2003) Synaptic Connections of Cholinergic Antennal Lobe Relay Neurons Innervating the Lateral Horn Neuropile in the Brain of Drosophila melanogaster. J Comp Neurol 466:299–315.

Zhang X, Gaudry Q (2016) Functional integration of a serotonergic neuron in the drosophila antennal lobe. Elife 5:1–24.

(this chapter is taken directly from my publication "Sizemore, T.R. & Dacks A.M. (2016). Serotonergic Modulation Differentially Targets Distinct Network Elements within the Antennal Lobe of Drosophila melanogaster. Sci Rep 6, 37119".)

ABSTRACT

Neuromodulation confers flexibility to anatomically-restricted neural networks so that animals are able to properly respond to complex internal and external demands. However, determining the mechanisms underlying neuromodulation is challenging without knowledge of the functional class and spatial organization of neurons that express individual neuromodulatory receptors. Here, we describe the number and functional identities of neurons in the antennal lobe of *Drosophila melanogaster* that express each of the receptors for one such neuromodulator, serotonin (5-HT). Although 5-HT enhances odor-evoked responses of antennal lobe projection neurons (PNs) and local interneurons (LNs), the receptor basis for this enhancement is unknown. We used endogenous reporters of transcription and translation for each of the five 5-HT receptors (5-HTRs) to identify neurons, based on cell class and transmitter content that express each receptor. We find that specific receptor types are expressed by distinct combinations of functional neuronal classes. For instance, the excitatory PNs express the excitatory 5-HTRs, while distinct classes of LNs each express different 5-HTRs. This study therefore provides a detailed atlas of 5-HT receptor expression within a well-characterized neural network, and enables future dissection of the role of serotonergic modulation of olfactory processing.

INTRODUCTION

Animals continually alter their behavior to meet dynamic internal and external demands. Neuromodulation promotes behavioral flexibility from anatomically restricted neural networks by altering the biophysical and synaptic properties of individual neurons (Katz, 1999; Marder, 2012; Nadim and Bucher, 2014). Typically, neuromodulators activate G-protein coupled receptors (GPCRs) (Gudermann et al., 1997) with ligand binding initiating an intracellular signaling cascade that dictates the effect of a

neuromodulator on a neuron. Depending on the G-protein associated with a given neuromodulatory receptor, a single neuromodulator can differentially affect the excitability and the synaptic strength of individual neurons in a network (Destexhe and Marder, 2004; Villalobos et al., 2005; Blenau and Thamm, 2011; Nadim and Bucher, 2014). Moreover, these receptors can be expressed by multiple cell types within a sensory circuit (Hen, 1992; Villalobos et al., 2005; Andrade, 2011; Blenau and Thamm, 2011), and/or concertedly expressed by the same cell (Beique et al., 2004) thus compounding the effects of a single neuromodulator. The multi-dimensional effects of a single neuromodulator acting on individual neurons within a network increases the dynamic range of network activity, ultimately promoting depth to behavioral output. Within the antennal lobe (AL) of *Drosophila*, the first olfactory processing center of the brain, the neuromodulator serotonin (5-HT) has widespread effects on odor-evoked responses of different neuronal classes (Dacks et al., 2009). However, it is difficult to determine how 5-HT modulates olfactory processing without knowing which functional neuron classes express each 5-HT receptor (5-HTR). Here, we exploit recent technological advances to generate a comprehensive atlas of 5-HTR expression in the well-characterized AL of *Drosophila*.

In the AL of *Drosophila* there are three major neuron classes that each perform distinct functions (**Fig. 1a**); olfactory sensory neurons (OSNs), projection neurons (PNs), and local interneurons (LNs) (Wilson, 2013). The dendrites and soma of odor-detecting OSNs are housed in the antennae and maxillary palps and, generally, each OSN expresses one chemosensory receptor protein endowing them with sensitivity to a particular set of odorants (Joseph and Carlson, 2015). The axon terminals of OSNs that express the same chemosensory protein converge in the same glomerulus (Vosshall et al., 2000; Couto et al., 2005; Fishilevich and Vosshall, 2005) where they form excitatory synapses with PNs and LNs. Projection neuron cell bodies surround the AL in 3 distinct cell clusters: ventral, lateral, and anterodorsal cell clusters (Ito et al., 2014; Sakuma et al., 2014) Projection neurons, the second-order neurons of the AL, express acetylcholine (e-PNs) (Yasuyama et al., 2003) or GABA (i-PNs) (Okada et al., 2009). Recent evidence suggests that these PN types may respond to different categories of odors based on the odor's attractiveness (Liang et al., 2013; Parnas et al., 2013; Strutz et al., 2014). PNs

project to two higher-order brain structures, the mushroom bodies and lateral horn (de Belle and Heisenberg, 1994; Yasuyama et al., 2003; Jefferis et al., 2007). Projection neuron spiking activity is refined by several distinct classes of AL LNs that act upon PNs directly, as well as the input that they receive from OSNs and other LNs. LNs are remarkably diverse in their morphology and physiology (Chou et al., 2010; Seki et al., 2010). In terms of transmitter content, subsets of LNs express GABA (Jackson et al., 1990; Python and Stocker, 2002), acetylcholine (Shang et al., 2007; Huang et al., 2010), glutamate (Das et al., 2011; Liu and Wilson, 2013), neuropeptides (Ignell et al., 2009; Carlsson et al., 2010) and can be electrically coupled (Yaksi and Wilson, 2010). Thus, even within these major AL neuron classes, there is a large degree of diversity which may also be indicative of differences in their expression of modulatory receptors.

Within the AL of *Drosophila* there are two 5-HT immunoreactive neurons; the contralaterally projecting, serotonin-immunoreactive deutocerebral (CSD) neurons (Dacks et al., 2006; Roy et al., 2007). Each CSD neuron innervates both ALs, as well as both lateral horns. Exogenous application of 5-HT in *Drosophila* increases PN sensitivity, and enhances PN responses in an odor-dependent manner (Dacks et al., 2009). Serotonin also decreases the strength of OSN responses to antennal nerve stimulation by enhancing GABAergic presynaptic inhibition of OSNs. However, 5-HT could enhance the activity of a given neuron by directly affecting excitability or by altering the synaptic input that a neuron receives either by increasing excitation or decreasing inhibition depending on 5-HTR expression within the network. The *Drosophila* genome encodes five 5-HTR genes (5-HT1A, 1B, 2A, 2B, and 7) that target distinct second-messenger pathways. 5-HT1-type, 2-type, and 7-type receptors are negatively coupled to adenylate cyclase, positively coupled to phospholipase C, and positively coupled to adenylate cyclase, respectively (Witz et al., 1990; Saudou et al., 1992; Colas et al., 1995; Gasque et al., 2013). Therefore, the 5-HT1 type receptors are generally inhibitory, while the 5-HT2 type and 7 are generally excitatory (Nichols and Nichols, 2008). Thus, to determine the receptor basis for the effects of 5-HT on individual neuronal classes within the AL we made use of the newly available 5-HTR MiMIC T2A-GAL4 protein-trap and gene-trap transgenic fly lines (Gnerer et al., 2015) in combination with immunocytochemistry. These fly lines have undergone recombinase-mediated cassette exchange (RMCE) in order to

replace their 5′ non-coding (“gene-trap”) or coding-intronic (“protein-trap”) MiMIC cassette with a GAL4 containing cassette (Bateman et al., 2006; Venken et al., 2011; Gnerer et al., 2015). In the case of the gene-trap lines, the MiMIC cassette is replaced with a cassette encoding a universal splice-acceptor and GAL4. In the case of the protein-trap lines, the MiMIC cassette is replaced with one that encodes a universal splice acceptor followed by a self-cleaving T2A peptide (González et al., 2011; Diao and White, 2012) fused to the GAL4 coding sequence [see (Gnerer et al., 2015)] for a detailed description of cassette insertion sites). Thus, the gene-trap and protein-trap 5-HTR lines represent endogenous 5-HTR gene transcription and translation, respectively. However, with the exception of 5-HT7, we rely on protein-trap 5-HTR lines to determine what neuronal populations express a given 5-HTR. It should be noted that this approach relies on endogenous 5-HTR translation or transcription to produce GAL4, and subsequently GFP throughout a 5-HTR expressing neuron. Thus, GFP expression does not reflect the distribution of individual 5-HTR proteins along a cell, but rather that a given neuron expressed a 5-HTR. We find that different protein-trap lines for the same 5-HTR highlight neurons of the same functional class (**Fig. 1b–f** and **Table 1**). However, in some instances, we note subtle differences between the number of neurons labeled by T2A-GAL4 lines for the same 5-HTR (see **Supplementary Information Fig. S1**). At the extreme, the difference between two T2A-GAL4 lines for 5-HT2B is ~2–4 PNs out of a population of ~51 PNs (~4–8% of the entire population). More importantly, coding-intronic insertion lines for the same 5-HTR were expressed by the same combinations of neuronal populations (i.e., OSNs, latPNs, vPNs, etc.) and sub-population (i.e., TKKinergic LNs, MIPergic LNs, etc.) (**Supplementary Information Fig. S1**).

In general, we found that each 5-HTR is expressed by distinct neuronal populations suggesting that 5-HT differentially modulates separate features of olfactory coding. For the most part, the excitatory 5-HTRs (5-HT2A, 2B, and 7) were expressed by excitatory AL neurons, whereas distinct classes of LNs expressed different sets of 5-HTRs. This suggests that 5-HT has both direct effects on PN excitability, as well as indirect effects on PN responses via modulation of the lateral interactions exerted within and between glomeruli by LNs. Our results represent the first steps towards understanding the mechanistic basis for serotonergic modulation on *Drosophila* olfactory

processing.

RESULTS

Antennae and Maxillary Palp OSNs express 5-HT2B

In *Drosophila*, OSN axons cross the midline via the antennal commissure to innervate a specific glomerulus in both the ipsilateral and contralateral AL (Stocker, 1994). Thus, neurites crossing the midline via the antennal commissure provide a reliable anatomical marker for OSNs. We observed a large amount of GFP-expressing fibers crossing through the antennal commissure in both 5-HT2B T2A-GAL4 lines (**Fig. 2a**) that were not apparent in other 5-HTR lines. The exception to this was the 5-HT7 T2A-GAL4, in which there were a small number of fibers with extremely faint GFP expression (data not shown). Additionally, there were a large number of GFP-expressing cell bodies in both the antennae (**Fig. 2b**) and the maxillary palps (**Fig. 2c**), suggesting that OSNs express the 5-HT2B receptor. To confirm that the 5-HT2B T2A-GAL4 driven GFP-expression in axons crossing the antennal commissure originated from OSNs within the antennae and maxillary palps, we ablated either or both appendages of newly eclosed adult flies and examined for the presence of GFP in the antennal commissure. Removal of either the antennae (**Fig. 2d**) or maxillary palps (**Fig. 2e**) on their own only partially eliminated the expression of GFP within the antennal commissure. However, removal of both the antennae and maxillary palps resulted in total loss of GFP-positive arbors crossing the antennal commissure (**Fig. 2f**), indicating that OSNs in both the antennae and maxillary palps express the 5-HT2B receptor.

Lateral PNs and Anterodorsal PNs express excitatory 5-HTRs

The majority of the excitatory PNs (ePNs) reside in the lateral and anterodorsal cell clusters (latPNs and adPNs, respectively). Previous reports have identified ~35 latPNs (Jefferis et al., 2001) (based on latPNs expressed by GH146-GAL4) and ~73 adPNs (Lai et al., 2008), the majority of which are cholinergic (Yasuyama et al., 2003). 14.59 ± 1.01 ($n = 11$) latPNs express 5-HT2A (**Fig. 3a**, **b**), while 12.04 ± 0.86 ($n = 13$)

latPNs express 5-HT7 (**Fig. 3c**, **d**). The 5-HT2B is expressed by 9.67 ± 0.13 (n* = 2 transgenic lines, n = 13 and 10 brains per line) latPNs (**Fig. 3e**, **f**). To a lesser extent, 4.58 ± 0.90 (n* = 3 transgenic lines, n = 6–11 brains per line) latPNs express 5-HT1A (data not shown). Within the adPNs, 19.3 ± 0.53 (n = 10) cells express 5-HT7 (**Fig. 3g–h**), while 7.88 ± 0.67 (n* = 2 transgenic lines, n = 9 and 7 brains per line) cells express 5-HT2B (**Fig. 3i**, **j**). Similar to the number of 5-HT2B expressing adPNs, 5-HT1A is expressed by 8.12 ± 0.62 (n* = 3 transgenic lines, n = 8–9 brains per line) adPNs (data not shown). Exogenous application of 5-HT increases the odor-evoked responses of ePNs within these two cell clusters (Dacks et al., 2009), therefore this enhancement is at least in part direct in nature, as 5-HT2A and 5-HT7 are positively coupled to IP_3 and cAMP pathways, respectively.

Widespread 5-HTR Expression within the Ventral PNs

Cells of the vPN cell cluster project into the AL through a characteristic fascicle, which we refer to as the “ventral AL fascicle” (see **Supplementary Information Fig. S1**), and send their axons to the lateral horn through the mediolateral antennal lobe tract (mlALT) (Ito et al., 2014). However, the glutamatergic LNs that are ventral to the AL (Das et al., 2011) also project into the AL through the ventral AL fascicle (see **Supplementary Information Fig. S2**). Therefore, we defined every non-glutamatergic neuron with a soma ventral to the AL that projects into the AL through the ventral AL fascicle as a vPN. Previous reports have identified ~51 vPNs; ~45 vPNs labeled by MZ699-GAL4 (Lai et al., 2008) and 6 labeled by GH146-GAL4 (Wilson and Laurent, 2005). In terms of transmitter content, ~36 vPNs are GABAergic based on vPNs expressed by GH146-GAL4 (Jefferis et al., 2007) and MZ699-GAL4 (Liang et al., 2013), and while cholinergic vPNs have been described (Yasuyama et al., 2003), the number of cholinergic vPNs has not been quantified.

Within the vPNs, there are subsets of cells that express each of the 5-HTRs, although the total number of vPNs expressing each receptor did vary between receptor types (**Fig. 4**). Furthermore, each 5-HTR is expressed by a combination of GABAergic and cholinergic vPNs. The two 5-HT1 type receptors are similarly expressed within the

vPNs. 5-HT1A is expressed by 21.70 ± 1.10 (n* = 3 transgenic lines, n = 18–22 brains per line) vPNs, of which 13.84 ± 1.14 are GABAergic and 7.87 ± 0.36 are cholinergic (**Fig. 4a–c**), while 5-HT1B is expressed by 25.33 ± 1.02 (n = 18) vPNs, of which 15.5 ± 1.02 (n = 9) are GABAergic and 9.83 ± 1.13 (n = 9) are cholinergic (**Fig. 4d–f**). The 5-HT2A is the least widely expressed receptor within the vPNs, with only 6.73 ± 0.75 (n = 22) vPNs, of which 2.95 ± 0.40 (n = 11) are GABAergic and 3.77 ± 0.69 (n = 11) are cholinergic (**Fig. 4g–i**). Finally, 5-HT2B and 5-HT7 are expressed in similar numbers of vPNs to the 5-HT1 type receptors. The 5-HT2B is expressed by 19.81 ± 1.30 (n* = 2 transgenic lines, n = 20 and 25 brains per line) vPNs, of which 12.33 ± 1.03 are GABAergic and 7.47 ± 0.75 are cholinergic (**Fig. 4j–l**). Similarly, 5-HT7 is expressed by 23.55 ± 1.13 (n = 19) vPNs, of which 16.67 ± 2.0 (n = 6) are GABAergic and 6.88 ± 0.52 (n = 13) are cholinergic (**Fig. 4m–o**). These results suggest that while 5-HT likely has a widespread effect on vPNs, these effects will be heterogeneous as both excitatory and inhibitory 5-HTRs are expressed by both GABAergic and cholinergic vPNs. Moreover, when combined with the observed diversity in 5-HTR expression, these results suggest that the vPN neuronal class is likely more diverse than previously described.

Distinct Populations of LNs express 5-HTRs

The majority of GABAergic cell bodies within the lateral neuroblast cluster are LNs. However, there have been reports of a small number (~1–2) of GABAergic latPNs (Okada et al., 2009). Our approach could not objectively distinguish a GABAergic LN from a GABAergic latPN. Therefore, we make the assumption that GABAergic cell bodies in the lateral cell cluster are likely LNs, knowing that there are a small number of GABAergic latPNs (Okada et al., 2009). However, there is a small subset of cholinergic LNs ventrolateral to the AL that are easily discernable, based on soma size, from cholinergic PNs (Yaksi and Wilson, 2010). There are ~200 LNs within the AL (Stocker et al., 1990) that express a diverse array of transmitters (Chou et al., 2010) including glutamate (Das et al., 2011) and neuropeptides such as tachykinin (TKK) and myoinhibitory peptide (MIP) (Ignell et al., 2009; Carlsson et al., 2010), and vary in their synaptic connectivity with other AL neuron classes (Root et al., 2008; Huang et al., 2010; Olsen et al., 2010; Yaksi and

Wilson, 2010).

Distinct subcategories of LNs, based on transmitter content, express distinct 5-HTRs (**Fig. 5**). The 5-HT1A is expressed by 13.63 ± 0.55 (n* = 3 transgenic lines, n = 17–18 brains per line) lateral LNs (**Fig. 5a**) whose cell bodies are consistently located in close proximity to the AL. Of these LNs, 12.40 ± 0.86 are GABAergic (**Fig. 5b**). In addition, a significant proportion of the 5-HT1A expressing LNs are peptidergic, with 8.62 ± 0.01 LNs expressing MIP (**Fig. 5c**) and 7.00 ± 0.26 expressing TKK (**Fig. 5d**). The 5-HT2A receptor is expressed by a smaller number of lateral LNs (4.27 ± 0.96, n = 11) relative to the 5-HT1A LNs (**Fig. 5e**). Of these, 3.73 ± 0.81 (n = 11) are GABAergic (**Fig. 5f**), 1.14 ± 0.10 (n = 11) are cholinergic (**Fig. 5g**), and none of the 5-HT2A LNs were TKKinergic (**Fig. 5h**). The 5-HT2B expressing lateral LNs (**Fig. 5i**), of which there are 12.42 ± 0.93 (n* = 2 transgenic lines, n = 25 and 20 brains per line), are primarily GABAergic (10.12 ± 0.78; **Fig. 5j**), although 2.30 ± 0.15 are cholinergic (**Fig. 5k**), and roughly a single (0.87 ± 0.68) TKKinergic LN (**Fig. 5l**). Finally, the 5-HT7 receptor is also expressed by lateral LNs (**Fig. 5m**; 12.19 ± 0.71, n = 16) which are predominantly GABAergic (**Fig. 5n**; 11.25 ± 0.69, n = 8), although a small number (4.64 ± 0.21, n = 7) are MIPergic (**Fig. 5o**) and 1.72 ± 0.15 (n = 9) TKKinergic (**Fig. 5p**).

To assess 5-HTR expression within the glutamatergic LNs that are ventral to the AL (Das et al., 2011), we performed RFP-GFP dual-expression experiments. In these cases, a Trojan-LexA::QFAD protein-trap line for vesicular glutamate transporter (VGlut) was used to produce GFP in all cells that produce VGlut (Diao et al., 2015), simultaneously RFP is produced in all cells that produce a given 5-HTR via the T2A-GAL4 5-HTR driver (**Fig. 6a**). The 5-HT1A is expressed by 7.75 ± 0.43 (n* = 5-HT1A$^{1468\text{-T2A-G4}}$, n = 10 brains) glutamatergic LNs (**Fig. 6b**). Similarly, the 5-HT1B is expressed by 6.89 ± 0.48 (n = 9 brains) glutamatergic LNs (**Fig. 6c**). The 5-HT2A is expressed by 3.72 ± 0.19 (n = 9 brains) glutamatergic LNs (**Fig. 6d**), while 5-HT2B is expressed by 9.75 ± 0.40 (n* = 5-HT2B$^{5208\text{-T2A-G4}}$, n = 10 brains) glutamatergic LNs (**Fig. 6e**). Finally, 5-HT7 is expressed by 9.50 ± 0.54 (n = 8 brains) glutamatergic LNs (**Fig. 6f**).

DISCUSSION

Neuromodulators often act through diverse sets of receptors expressed by distinct network elements and in this manner, differentially affect specific features of network dynamics. Knowing which network elements express each receptor for a given neuromodulator provides a framework for making predictions about the mechanistic basis by which a neuromodulator alters network activity. In this study, we provide an "atlas" of 5-HTR expression within the AL of *Drosophila*, thus revealing network elements subject to the different effects of serotonergic modulation. In summary, we find that different receptors are predominantly expressed by distinct neuronal populations (**Fig. 7a–d**). For example, the 5-HT2B is expressed by OSNs (**Fig. 7a**), while the 5-HT2A and 7 are expressed by cholinergic PNs (**Fig. 7b**). Additionally, we find that each receptor is expressed by diverse populations of LNs, with the exception the 5-HT1B. For instance, 5-HT1A is expressed by GABAergic and peptidergic (TKK and MIP) LNs, while 5-HT2A and 2B are not expressed by peptidergic LNs (**Fig. 7d**). However, the vPNs are the exception to the general observation that distinct neuronal classes differ from each other in the 5-HTRs (**Fig. 7c**) and we discuss the implications of this below. Together, our results suggest that within the AL, 5-HT differentially modulates distinct populations of neurons that undertake specific tasks in olfactory processing.

A recurring theme of neuromodulation is that the expression of distinct receptor types by specific neural populations allows a single modulatory neuron to differentially affect individual coding features. For instance, GABAergic medium spiny neurons (MSNs) in the nucleus accumbens express either the D1 or D2 dopamine receptor allowing dopamine to have opposite effects on different MSNs via coupling to different G_{α} subunits [reviewed in (Russo and Nestler, 2013)]. MSNs that differ in dopamine receptor expression also differ in their synaptic connectivity. Dopamine activates D1-expressing MSNs that directly inhibit dopaminergic neurons in the ventral tegmental area (VTA), and inhibits D2-expressing MSNs that inhibit GABAergic VTA interneurons thus inducing suppression of dopamine release. In this manner, a single neuromodulator differentially affects two populations of principal neurons via different receptors to generate coordinated network output. This principle also holds true for the effects of 5-HT within

the olfactory bulb. For instance, 5-HT enhances presynaptic inhibition of olfactory sensory neurons by 5-HT2C-expressing juxtaglomerular cells (Petzold et al., 2009), while increasing excitatory drive to mitral/tufted cells and periglomerular cells via 5-HT2A-expressing external tufted cells (Liu et al., 2012). Similarly, we observed that distinct classes of AL neurons differ in their expression of 5-HTRs. For instance, ePNs express the 5-HT2A, 5-HT2B and 5-HT7 receptors (**Fig. 3**), while peptidergic LNs predominantly express the 5-HT1A receptor (**Fig. 5c**, **d**). This suggests that the cumulative effect of 5-HT results from a combination of differential modulation across neuronal populations within the AL.

Interestingly, although we find that 5-HT2B is expressed by OSNs, previous reports found that 5-HT does not directly affect *Drosophila* OSNs (Dacks et al., 2009). In this study, OSNs were stimulated using antennal nerve shock in which the antennae were removed in order to place the antennal nerve within a suction electrode (Dacks et al., 2009). Thus, if 5-HT2B is localized to the OSN cell body, removal of the antennae would eliminate any effect of 5-HT on OSNs. In several insects, 5-HT within the antennal haemolymph modulates OSN odor-evoked responses (Dolzer et al., 2001; Grosmaitre et al., 2001). Therefore, it is plausible OSNs are modulated by a source of 5-HT other than the CSD neurons within the AL.

Serotonergic modulation of LN activity has widespread, and sometimes odor specific, effects on olfactory processing. LNs allow ongoing activity across the AL to shape the activity of individual AL neurons, often in a glomerulus specific manner creating non-reciprocal relationships (Olsen et al., 2007; Root et al., 2008; Silbering et al., 2008; Reisenman et al., 2011). It is fairly clear that 5-HT directly modulates LNs, although 5-HT almost certainly affects synaptic input to LNs. Serotonin modulates isolated *Manduca sexta* LNs *in vitro* (Mercer et al., 1995) and, consistent with our results, a small population of GABAergic LNs in the AL of *Manduca* also express the 5-HT1A receptor (Dacks et al., 2013). Furthermore, 5-HT has odor-dependent effects on PN odor-evoked activity (Dacks et al., 2008, 2009), suggesting that odor specific sets of lateral interactions are modulated by 5-HT. We found that different populations of LNs expressed different sets of 5-HT receptors, however we categorized LNs based on transmitter type, so it is possible that these categories could be even further sub-divided based on morphological type, synaptic

connectivity or biophysical characteristics (Chou et al., 2010; Huang et al., 2010; Seki et al., 2010; Yaksi and Wilson, 2010). Regardless, our results suggest that 5-HT modulates lateral interactions within the AL by selectively affecting LN populations that undertake different tasks. For instance, the TKKergic LNs that express the 5-HT1A receptor provide a form of gain control by presynaptically inhibiting OSNs (Ignell et al., 2009). Our results suggest that 5-HT may affect TKK mediated gain control differently relative to processes undertaken by other LN populations. Furthermore, the expression of the TKK receptor by OSNs is regulated by hunger, allowing the effects of TKK to vary with behavioral state (Ko et al., 2015). It would be interesting to determine if the expression of 5-HTRs themselves also vary with behavioral state as a means of regulating neuromodulation within the olfactory system.

Although we primarily found that individual populations of AL neurons chiefly expressed a single or perhaps two 5-HTR types, the vPNs appear to be an exception. As a population, the vPNs express all of the 5-HTRs (**Fig. 4**) and the vPNs that express each 5-HTR did not appear to differ in terms of the proportion of those neurons that were GABAergic or cholinergic (roughly 3:2). Unfortunately, our approach does not allow us to determine the degree to which individual vPNs co-express 5-HTRs. However, it is estimated that there are ~51 vPNs and even if this is an underestimate, there is likely some overlap of receptor types as a large number of vPNs expressed the 5-HT1A, 1B, 2B and 7 receptors. It is possible that a single vPN expresses one 5-HTR in the AL and a different 5-HTR in the lateral horn. However, our approach only allows us to identify which neurons express a given 5-HTR, not where that receptor is expressed. The CSD neurons ramify throughout both ALs and both lateral horns (Dacks et al., 2006; Roy et al., 2007), thus vPNs could have differential spatial expression of individual 5-HTRs. Individual neurons expressing multiple 5-HTRs has been demonstrated in several neural networks. For instance, pyramidal cells in prefrontal cortex express both the 5-HT1A and 5-HT2A (Andrade, 2011). This allows 5-HT to have opposing effects that differ in their time course in the same cell (Beique et al., 2004; Villalobos et al., 2005). In terms of the vPNs, our results suggest that the current understanding of the diversity of this neuron class is limited. The expression of receptors for different signaling molecules could potentially be a significant component to vPN diversity.

Neuromodulators are often released by a small number of neurons within a network, yet they can have extremely diverse effects depending upon patterns of receptor expression. For the most part, individual populations of AL neurons differed in the receptor types that they expressed. This suggests that 5-HT differentially acts on classes of neurons that undertake distinct tasks in olfactory processing. In the case of the vPNs, this differential modulation may be fairly complex due to the diversity within this neuronal class. Our goal was to establish a functional atlas of 5-HTR expression in the AL of *Drosophila*. This dataset therefore provides a mechanistic framework for the effects of 5-HT on olfactory processing in this network.

METHODS

Fly Stocks. Flies were maintained on standard cornmeal at 24°C and under a 12:12 light:dark cycle. MiMIC T2A-GAL4 protein- and gene-trap stocks were graciously provided by Dr. H.A. Dierick and have been previously described (Gnerer et al., 2015). These include: 5-HT1A-T2A-GAL4^{MI04464}, 5-HT1A-T2A-GAL4^{MI01140}, 5-HT1A-T2A-GAL4^{MI01468}, 5-HT1B-T2A-GAL4^{MI05213}, 5-HT2A-T2A-GAL4^{MI00459}, 5-HT2B-T2A-GAL4^{MI05208}, 5-HT2B-T2A-GAL4^{MI06500}, and 5-HT7-GAL4^{MI00215}. All 5-HT receptor protein-trap and gene-trap lines were crossed to membrane-targeted UAS-IVS-mCD8::GFP (Pfeiffer et al., 2010) (BL#32185). Dr. Tzumin Lee kindly provided the MZ699-GAL4 and GH146-LexA stocks (Lai et al., 2008). The Trojan-LexA::QFAD VGlut protein-trap line (Diao et al., 2015) (BL#60314) recombined with y, w,10xUAS-RFP, LexAop-GFP (BL#32229) was generously provided by Dr. Quentin Gaudry.

Immunocytochemistry. Brains were dissected in Drosophila external saline (CSHL recipe) fixed in 4% paraformaldehyde for 30 minutes on ice, washed with phosphate buffered saline with 0.5% Triton-X 100 (PBST), and blocked for 1 hour in PBST with either 2% IgG-free BSA (Jackson Immunoresearch; Cat#001-000-162), or 5% NGS (for GABA & ChAT labeling; Jackson Immunoresearch; Cat#005-000-121). In many instances, an ascending-descending ethanol wash series (30%, 50%, 70%, 95%, 100%, 95%, 70%, 50%, and 30%) was used prior to blocking to clear air from residual trachea. Brains were

incubated at 4°C in primary antibody diluted with blocking solution and 5mM sodium azide. Primary antibody dilutions used include: 1:50 mouse anti-Bruchpilot [DSHB; mAbnc82 (Wagh et al., 2006)], 1:500 rabbit anti-GABA (Sigma; Cat#A2052), 1:200 mouse anti-ChAT [DSHB; ChAT4B1 (Yasuyama et al., 1995)], 1:5,000 rabbit anti-TKK [provided by Dr. Jan Veenstra; (Veenstra et al., 1995)], 1:4,000 rabbit anti-MIP [provided by Dr. Christian Wegener; (Predel et al., 2001)], and 1:1,000 rabbit anti-GFP (Life Technologies; Cat#A-11122). Brains were then washed in PBST, blocked as above, and incubated at 4°C in secondary antibody diluted with blocking solution and 5mM sodium azide. All secondary antibodies were purchased from Life Technologies and include: goat anti-rabbit Alexa-488 (Cat#A-11008), donkey anti-rabbit Alexa-488 (Cat#A-21206), donkey anti-mouse Alexa-546 (Cat#A-10036), goat anti-mouse Alexa-546 (Cat#A-11030), goat anti-rabbit Alexa-633 (Cat#A-21070), and goat anti-mouse Alexa-633 (Cat#A-21050). Brains were then washed in PBST and PBS, then cleared via an ascending glycerol series (40%, 60%, 80%), and finally mounted on well slides in Vectashield® (Vector Laboratories, Burlingame, CA; Cat#H-1200).

Image Acquisition and Analysis. Brains were imaged using an Olympus BX61 (Shinjuku, Tokyo, Japan) confocal microscope running the Fluoview FV1000 software with a 40x UPlanFL-N or 60x PlanApo-N oil-immersion objective. In some cases, brightness and contrast were manually adjusted in Adobe Photoshop v.14.2 (San Jose, CA). GFP-positive and additional primary labeled cell bodies were recorded in VAA3D (v.3.20) (Peng et al., 2010). Anterodorsal, lateral, and ventral PN and LNs were defined by cell body location (Lai et al., 2008) and, in the case of the lateral PNs and LNs, transmitter content.

OSN Ablations. To demonstrate that 5-HT2B is expressed in both antennae and maxillary palp OSNs, the antennae, maxillary palps, or both were removed 4–5 hours post-eclosion. Animals were kept under standard conditions and media until 10-days later when they were processed for immunocytochemistry.

Statistical Analysis. All statistics were performed in GraphPad Prism v.5.01 (GraphPad

Software, La Jolla, CA). For simplicity, we use the average of the averages for multiple transgenic lines used for the same receptor (i.e., 5-HT1A and 5-HT2B) when reporting results. In these cases, data are presented as mean of the mean of each individual line ± mean of the s.e.m of each individual line (n* = total number of transgenic lines for a receptor, n = total number of brains for each transgenic line). All other data are presented as mean ± s.e.m (n = total number of brains). A D'Agostino and Pearson omnibus normality test ($\alpha = 0.05$) was used to confirm normal distribution of neuronal classes highlighted between the multiple lines for 5-HT1A and 2B. A one-way ANOVA followed by a Tukey's multiple comparison test ($\alpha = 0.05$) was used to test for significant differences between the number of neurons within a neuronal class highlighted by the different 5-HT1A T2A-GAL4 lines. An unpaired Student's t-test ($\alpha = 0.05$) was performed to test for significant differences between the number of neurons within a neuron class highlighted by the different 5-HT2B T2A-GAL4 lines for the same 5-HTR.

ACKNOWLEDGEMENTS

We would like to thank Dr. Herman Dierick for providing the MiMIC T2A-GAL4 fly stocks, Dr. Jan Veenstra for providing the TKK antibody and Dr. Christian Wegener for providing the MIP antibody which was developed by Dr. Manfred Eckert. We thank Dr. Tzumin Lee for providing the MZ699-GAL4 and GH146-LexA fly stocks. We also would like to thank Dr. Quentin Gaudry for the 10xUAS-RFP, LexAop-GFP;Trojan-LexA::QFAD VGlut protein-trap fly stock. Dr. Jing Wang provided insightful technical advice. Additionally, we would like to thank Dr. Christopher Potter, Kristyn M. Lizbinski and Kaylynn Coates for helpful comments on the manuscript.

WORKS CITED:

Andrade R (2011) Serotonergic regulation of neuronal excitability in the prefrontal cortex. Neuropharmacology 61:382–386.

Bateman JR, Lee AM, Wu CT (2006) Site-specific transformation of Drosophila via phiC31 integrase-mediated cassette exchange. Genetics 173:769–777.

Beique J-C, Campbell B, Perring P, Hamblin MW, Walker P, Mladenovic L, Andrade R (2004) Serotonergic Regulation of Membrane Potential in Developing Rat Prefrontal Cortex: Coordinated Expression of 5-Hydroxytryptamine (5-HT)1A , 5-HT2A, and 5-HT7 Receptors. J Neurosci 24:4807–4817.

Blenau W, Thamm M (2011) Distribution of serotonin (5-HT) and its receptors in the insect brain with focus on the mushroom bodies. Lessons from Drosophila melanogaster and Apis mellifera. Arthropod Struct Dev 40:381–394.

Carlsson M a., Diesner M, Schachtner J, Nässel DR (2010) Multiple neuropeptides in the Drosophila antennal lobe suggest complex modulatory circuits. J Comp Neurol 518:3359–3380.

Chou Y-H, Spletter ML, Yaksi E, Leong JCS, Wilson RI, Luo L (2010) Diversity and wiring variability of olfactory local interneurons in the Drosophila antennal lobe. Nat Neurosci 13:439–449.

Colas JF, Launay JM, Kellermann O, Rosay P, Maroteaux L (1995) Drosophila 5-HT2 serotonin receptor: coexpression with fushi-tarazu during segmentation. Proc Natl Acad Sci U S A 92:5441–5445.

Couto A, Alenius M, Dickson BJ (2005) Molecular , Anatomical , and Functional Organization of the Drosophila Olfactory System. 15:1535–1547.

Dacks a M, Christensen T a, Hildebrand JG (2008) Modulation of olfactory information processing in the antennal lobe of Manduca sexta by serotonin. J Neurophysiol 99:2077–2085.

Dacks AM, Christensen T a., Hildebrand JG (2006) Phylogeny of a Serotonin-Immunoreactive Neuron in the Primary Olfactory Center of the Insect Brain. J Comp Neurol 498:727–746.

Dacks AM, Green DS, Root CM, Nighorn AJ, Wang JW (2009) Serotonin modulates olfactory processing in the antennal lobe of Drosophila. J Neurogenet 23:366–377.

Dacks AM, Reale V, Pi Y, Zhang W, Dacks JB, Nighorn AJ, Evans PD (2013) A Characterization of the Manduca sexta Serotonin Receptors in the Context of Olfactory Neuromodulation. PLoS One 8:1–15.

Das A, Chiang A, Davla S, Priya R, Reichert H, VijayRaghavan K, Rodrigues V (2011) Identification and analysis of a glutamatergic local interneuron lineage in the adult Drosophila olfactory system. Neural Syst Circuits 1:4.

de Belle JS, Heisenberg M (1994) Associative odor learning in Drosophila abolished by chemical ablation of Mushroom Bodies. Science (80-) 263:692–695.

Destexhe A, Marder E (2004) Plasticity in single neuron and circuit computations. Nature 431:789–795.

Diao F, Ironfield H, Luan H, Diao F, Shropshire WC, Ewer J, Marr E, Potter CJ, Landgraf M, White BH (2015) Plug-and-Play Genetic Access to Drosophila Cell Types using Exchangeable Exon Cassettes. Cell Rep 10:1410–1421.

Diao F, White BH (2012) A novel approach for directing transgene expression in Drosophila: T2A-Gal4 in-frame fusion. Genetics 190:1139–1144.

Dolzer J, Krannich S, Fischer K, Stengl M (2001) Oscillations of the transepithelial potential of moth olfactory sensilla are influenced by octopamine and serotonin. J Exp Biol 204:2781–2794.

Fishilevich E, Vosshall LB (2005) Genetic and Functional Subdivision of the Drosophila Antennal Lobe Genetic and Functional Subdivision of the Drosophila Antennal Lobe. Curr Biol 15:1548–1553.

Gasque G, Conway S, Huang J, Rao Y, Vosshall LB (2013) Small molecule drug screening in Drosophila identifies the 5HT2A receptor as a feeding modulation target. Sci Rep 3:srep02120.

Gnerer JP, Venken KJT, Dierick H a. (2015) Gene-specific cell labeling using MiMIC transposons. Nucleic Acids Res:1–13.

González M, Martín-Ruíz I, Jiménez S, Pirone L, Barrio R, Sutherland JD (2011) Generation of stable Drosophila cell lines using multicistronic vectors. Sci Rep 1.

Grosmaitre X, Marion-Poll F, Renou M (2001) Biogenic amines modulate olfactory receptor neurons firing activity in Mamestra brassicae. Chem Senses 26:653–661.

Gudermann T, Schoneberg T, Schultz G (1997) Functional and Structural Complexity of

Signal Transduction via G-Protein-Coupled Receptors. Annu Rev Neurosci 20:399–427.

Hen R (1992) Of mice and flies: commonalities among 5-HT receptors. Trends Pharmacol Sci 13:160–165.

Huang J, Zhang W, Qiao W, Hu A, Wang Z (2010) Functional connectivity and selective odor responses of excitatory local interneurons in drosophila antennal lobe. Neuron 67:1021–1033.

Ignell R, Root CM, Birse RT, Wang JW, Nässel DR, Winther AME (2009) Presynaptic peptidergic modulation of olfactory receptor neurons in Drosophila. Proc Natl Acad Sci U S A 106:13070–13075.

Ito K, Shinomiya K, Ito M, Armstrong JD, Boyan G, Hartenstein V, Harzsch S, Heisenberg M, Homberg U, Jenett A, Keshishian H, Restifo LL, Rössler W, Simpson JH, Strausfeld NJ, Strauss R, Vosshall LB (2014) A systematic nomenclature for the insect brain. Neuron 81:755–765.

Jackson FR, Newby LM, Kulkarni SJ (1990) Drosophila GABAergic Systems: Sequence and Expression of Glutamic Acid Decarboxylase. J Neurochem 54:1068–1078.

Jefferis GS, Marin EC, Stocker RF, Luo L (2001) Target neuron prespecification in the olfactory map of Drosophila. Nature 414:204–208.

Jefferis GSXE, Potter CJ, Chan AM, Marin EC, Rohlfing T, Maurer CR, Luo L (2007) Comprehensive maps of Drosophila higher olfactory centers: spatially segregated fruit and pheromone representation. Cell 128:1187–1203.

Joseph RM, Carlson JR (2015) Drosophila Chemoreceptors: A Molecular Interface Between the Chemical World and the Brain. Trends Genet 31:683–695.

Katz PS (1999) What are we talking about? Modes of neuronal communication Paul.

Ko KI, Root CM, Lindsay SA, Zaninovich OA, Shepherd AK, Wasserman SA, Kim SM, Wang JW (2015) Starvation promotes concerted modulation of appetitive olfactory behavior via parallel neuromodulatory circuits. Elife 4:1–17.

Lai S-L, Awasaki T, Ito K, Lee T (2008) Clonal analysis of Drosophila antennal lobe neurons: diverse neuronal architectures in the lateral neuroblast lineage. Development 135:2883–2893.

Liang L, Li Y, Potter C, Yizhar O, Deisseroth K, Tsien R, Luo L (2013) GABAergic

Projection Neurons Route Selective Olfactory Inputs to Specific Higher-Order Neurons. Neuron 79:917–931.

Liu S, Aungst JL, Puche a. C, Shipley MT (2012) Serotonin modulates the population activity profile of olfactory bulb external tufted cells. J Neurophysiol 107:473–483.

Liu WW, Wilson RI (2013) Glutamate is an inhibitory neurotransmitter in the Drosophila olfactory system. Proc Natl Acad Sci 110:10294–10299.

Marder E (2012) Neuromodulation of Neuronal Circuits: Back to the Future. Neuron 76:1–11.

Mercer a R, Hayashi JH, Hildebrand JG (1995) Modulatory effects of 5-hydroxytryptamine on voltage-activated currents in cultured antennal lobe neurones of the sphinx moth Manduca sexta. J Exp Biol 198:613–627.

Nadim F, Bucher D (2014) Neuromodulation of neurons and synapses. Curr Opin Neurobiol 29:48–56.

Nichols DE, Nichols CD (2008) Serotonin Receptors. Chem Rev 108:1614–1641.

Okada R, Awasaki T, Ito K (2009) Gamma-aminobutyric acid (GABA)-mediated neural connections in the Drosophila antennal lobe. J Comp Neurol 514:74–91.

Olsen SR, Bhandawat V, Wilson RI (2007) Excitatory Interactions between Olfactory Processing Channels in the Drosophila Antennal Lobe. Neuron 54:89–103.

Olsen SR, Bhandawat V, Wilson RI (2010) Divisive normalization in olfactory population codes. Neuron 66:287–299.

Parnas M, Lin A, Huetteroth W, Miesenböck G (2013) Odor Discrimination in Drosophila: From Neural Population Codes to Behavior. Neuron 79:932–944.

Peng H, Ruan Z, Long F, Simpson JH, Myers EW (2010) V3D enables real-time 3D visualization and quantitative analysis of large-scale biological image data sets. Nat Biotechnol 28:348–353.

Petzold GC, Hagiwara A, Murthy VN (2009) Serotonergic modulation of odor input to the mammalian olfactory bulb. Nat Neurosci 12:784–791.

Pfeiffer BD, Ngo TTB, Hibbard KL, Murphy C, Jenett A, Truman JW, Rubin GM (2010) Refinement of tools for targeted gene expression in Drosophila. Genetics 186:735–755.

Predel R, Rapus J, Eckert M (2001) Myoinhibitory neuropeptides in the American

cockroach. Peptides 22:199–208.

Python F, Stocker RF (2002) Immunoreactivity against choline acetyltransferase, γ-aminobutyric acid, histamine, octopamine, and serotonin in the larval chemosensory system of Drosophila melanogaster. J Comp Neurol 453:157–167.

Reisenman CE, Dacks AM, Hildebrand JG (2011) Local interneuron diversity in the primary olfactory center of the moth Manduca sexta. J Comp Physiol A Neuroethol Sens Neural Behav Physiol 197:653–665.

Root CM, Masuyama K, Green DS, Enell LE, Nässel DR, Lee CH, Wang JW (2008) A Presynaptic Gain Control Mechanism Fine-Tunes Olfactory Behavior. Neuron 59:311–321.

Roy B, Singh AP, Shetty C, Chaudhary V, North A, Landgraf M, Vijayraghavan K, Rodrigues V (2007) Metamorphosis of an identified serotonergic neuron in the Drosophila olfactory system. Neural Dev 2:20.

Russo SJ, Nestler EJ (2013) The brain reward circuitry in mood disorders. Nat Rev Neurosci 14:609–625.

Sakuma C, Anzo M, Miura M, Chihara T (2014) Development of olfactory projection neuron dendrites that contribute to wiring specificity of the Drosophila olfactory circuit. Genes Genet Syst 89:17–26.

Saudou F, Boschert U, Amlaiky N, Plassat JL, Hen R (1992) A family of Drosophila serotonin receptors with distinct intracellular signalling properties and expression patterns. EMBO J 11:7–17.

Seki Y, Rybak J, Wicher D, Sachse S, Hansson BS (2010) Physiological and morphological characterization of local interneurons in the Drosophila antennal lobe. J Neurophysiol 104:1007–1019.

Shang Y, Claridge-Chang A, Sjulson L, Pypaert M, Miesenböck G (2007) Excitatory Local Circuits and Their Implications for Olfactory Processing in the Fly Antennal Lobe. Cell 128:601–612.

Silbering AF, Okada R, Ito K, Galizia CG (2008) Olfactory information processing in the Drosophila antennal lobe: anything goes? J Neurosci 28:13075–13087.

Stocker RF (1994) The organization of the chemosensory system in Drosophila melanogaster: a review. Cell Tissue Res 275:3–26.

Stocker RF, Lienhard MC, Borst A, Fischbach KF (1990) Neuronal architecture of the antennal lobe in Drosophila melanogaster. Cell Tissue Res 262:9–34.

Strutz A, Soelter J, Baschwitz A, Farhan A, Grabe V, Rybak J, Knaden M, Schmuker M, Hansson BS, Sachse S (2014) Decoding odor quality and intensity in the Drosophila brain. Elife 3:e04147.

Veenstra JA, Lau GW, Agricola HJ, Petzel DH (1995) Immunohistological localization of regulatory peptides in the midgut of the female mosquito Aedes aegypti. Histochem Cell Biol 104:337–347.

Venken KJT, Schulze KL, Haelterman N a, Pan H, He Y, Evans-Holm M, Carlson JW, Levis RW, Spradling AC, Hoskins R a, Bellen HJ (2011) MiMIC: a highly versatile transposon insertion resource for engineering Drosophila melanogaster genes. Nat Methods 8:737–743.

Villalobos C, Beique J-C, Gingrich JA, Andrade R (2005) Serotonergic regulation of calcium-activated potassium currents in rodent prefrontal cortex. Eur J Neurosci 22:1120–1126.

Vosshall LB, Wong a M, Axel R (2000) An olfactory sensory map in the fly brain. Cell 102:147–159.

Wagh DA, Rasse TM, Asan E, Hofbauer A, Schwenkert I, Dürrbeck H, Buchner S, Dabauvalle M-C, Schmidt M, Qin G, Wichmann C, Kittel R, Sigrist SJ, Buchner E (2006) Bruchpilot, a Protein with Homology to ELKS/CAST, Is Required for Structural Integrity and Function of Synaptic Active Zones in Drosophila. Neuron 49:833–844.

Wilson RI (2013) Early Olfactory Processing in Drosophila: Mechanisms and Principles. Annu Rev Neurosci 36:217–241.

Wilson RI, Laurent G (2005) Role of GABAergic inhibition in shaping odor-evoked spatiotemporal patterns in the Drosophila antennal lobe. J Neurosci 25:9069–9079.

Witz P, Amlaiky N, Plassat JL, Maroteaux L, Borrelli E, Hen R (1990) Cloning and characterization of a Drosophila serotonin receptor that activates adenylate cyclase. Proc Natl Acad Sci U S A 87:8940–8944.

Yaksi E, Wilson RI (2010) Electrical Coupling between Olfactory Glomeruli. Neuron 67:1034–1047.

Yasuyama K, Kitamoto T, Salvaterra PM (1995) Immunocytochemical study of choline

acetyltransferase in Drosophila melanogaster: An analysis of cis-regulatory regions controlling expression in the brain of cDNA-transformed flies. J Comp Neurol 361:25–37.

Yasuyama K, Meinertzhagen I a., Schürmann FW (2003) Synaptic Connections of Cholinergic Antennal Lobe Relay Neurons Innervating the Lateral Horn Neuropile in the Brain of Drosophila melanogaster. J Comp Neurol 466:299–315.

Table 1 | 5-HTR MiMIC T2A-GAL4 transgenic lines used and the number of cells in each cluster that express each receptor. With the exception of 5-HT7, our investigation relies solely on MiMIC T2A-GAL4 protein-trap transgenics (PT). In all cases, the number of cells in each cluster that express each receptor are represented as mean ± s.e.m. (n = number of brains). Note that the total number of LNs that express a given 5-HTR line is the total of the GABA, cholinergic (ChAT), and glutamatergic (Glut) LN columns, since peptidergic LNs are also GABAergic. “PT” and “GT” describe which lines are protein-traps and which are gene-trap, respectively. “*N/Ap*” denotes 5-HTR expressing neuron classes that did not co-label for that given transmitter or expressed by that neuronal class. Dashes (“-“) denote lines that were not tested for colabeling.

5-HTR Line	PT	GT	latPNs	adPNs	vPNs		LNs				
					GABA	ChAT	GABA	ChAT	TKK	MIP	Glut
5-HT1A[4464]	■		6.00±0.83 (6)	8.81±1.41 (8)	14.87±1.31 (12)	8.42±0.3 (6)	11.0±0.35 (12)	*N/Ap*	6.31±0.25 (8)	8.6±0.31 (10)	-
5-HT1A[1468]	■		4.82±0.49 (11)	6.87±1.21 (8)	14.64±1.4 (11)	7.59±0.45 (11)	13.95±0.89 (11)	*N/Ap*	7.44±0.27 (9)	8.61±0.29 (9)	7.75±0.43 (10)
5-HT1A[1140]	■		2.91±0.81 (11)	8.67±0.83 (9)	12±0.72 (9)	7.59±0.34 (11)	12.25±0.61 (12)	*N/Ap*	7.25±0.27 (10)	8.64±0.14 (7)	-
5-HT1B[5213]	■		2.06±0.47 (9)	1.00±0.25 (8)	15.5±1.02 (9)	9.83±1.13 (9)	3.61±0.59 (9)	*N/Ap*	2.94±0.33 (9)	1.75±0.42 (10)	6.89±0.48 (9)
5-HT2A[459]	■		14.59±1.01 (11)	*N/Ap*	2.95±0.4 (11)	3.77±0.69 (11)	3.73±0.81 (11)	1.14±0.1 (11)	*N/Ap*	*N/Ap*	3.72±0.19 (9)
5-HT2B[5208]	■		9.54±0.92 (13)	8.56±0.94 (9)	13.92±0.82 (12)	7.19±0.78 (13)	9.33±0.78 (12)	2.15±0.24 (13)	1.55±0.22 (10)	*N/Ap*	9.75±0.4 (10)
5-HT2B[6500]	■		9.80±0.95 (10)	7.21±0.45 (7)	10.75±1.23 (10)	7.75±0.72 (10)	10.9±0.67 (10)	2.45±0.35 (10)	0.19±0.09 (8)	*N/Ap*	-
5-HT7[215]		■	12.04±0.86 (13)	19.30±0.53 (10)	16.67±2 (6)	6.88±0.52 (13)	11.25±0.69 (8)	2.77±0.39 (13)	1.72±0.15 (9)	4.64±0.21 (7)	9.5±0.54 (8)

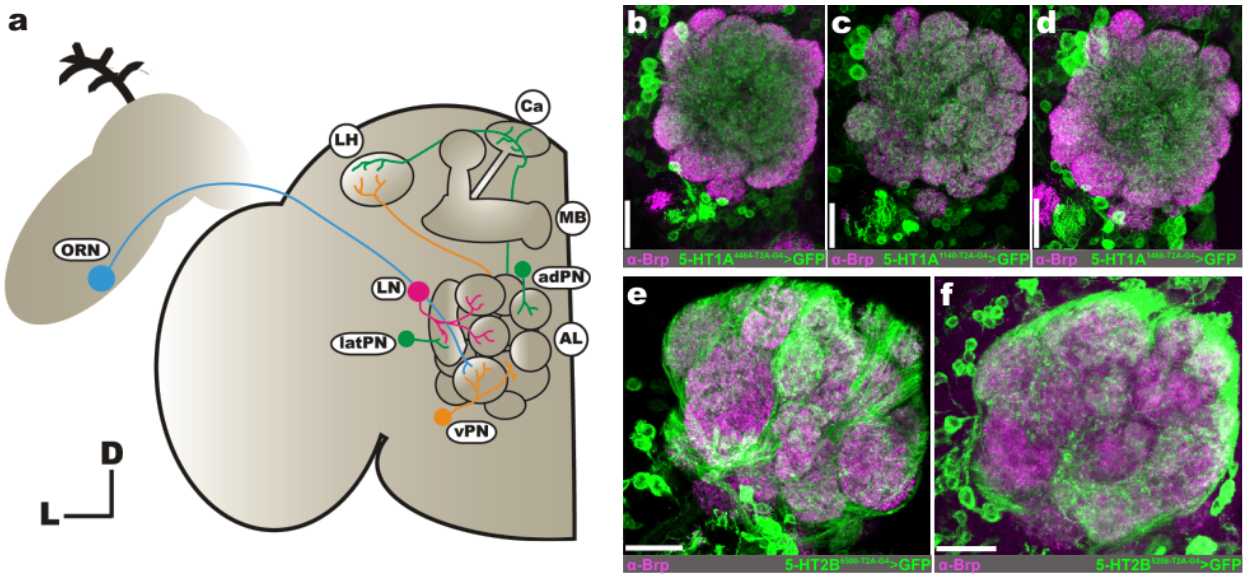

Figure 1 | Consistent neuron labeling from different coding-intronic insertions of 5-HTRs in the antennal lobe of Drosophila melanogaster. (**a**) Olfactory receptor neurons (ORNs; cyan) housed within the antennae and maxillary palps (not depicted here) send axons to a single glomerulus in the antennal lobe (AL). Within a glomerulus, ORNs synapse on projection neurons (PNs; green and orange) and local interneurons (LNs; magenta). LNs interconnect glomeruli and synapse on ORNs, PNs, and other LNs. A given PN is classified as an anterodorsal PN (adPN; green), lateral PN (latPN; green), or ventral PN (vPN; orange) based on its cell body position. PN axons project to the mushroom body (MB) calyx (Ca) and lateral horn (LH). Ellipses indicate neuron type, while circles indicate specific brain regions. (**b-d**) T2A-GAL4 conversion of three separate MiMIC insertions (4464, 1140, and 1468, respectively) in the 5-HT1A locus reveals consistent labeling of LNs and vPNs. (**e** and **f**) T2A-GAL4 conversion of two separate MiMIC insertions (6500 and 5208, respectively) in the 5-HT2B locus consistently labels ORNs. Neuropil in (**b-f**) are delineated by α-Bruchpilot (α-Brp; magenta) labeling. All scale bars=20um.

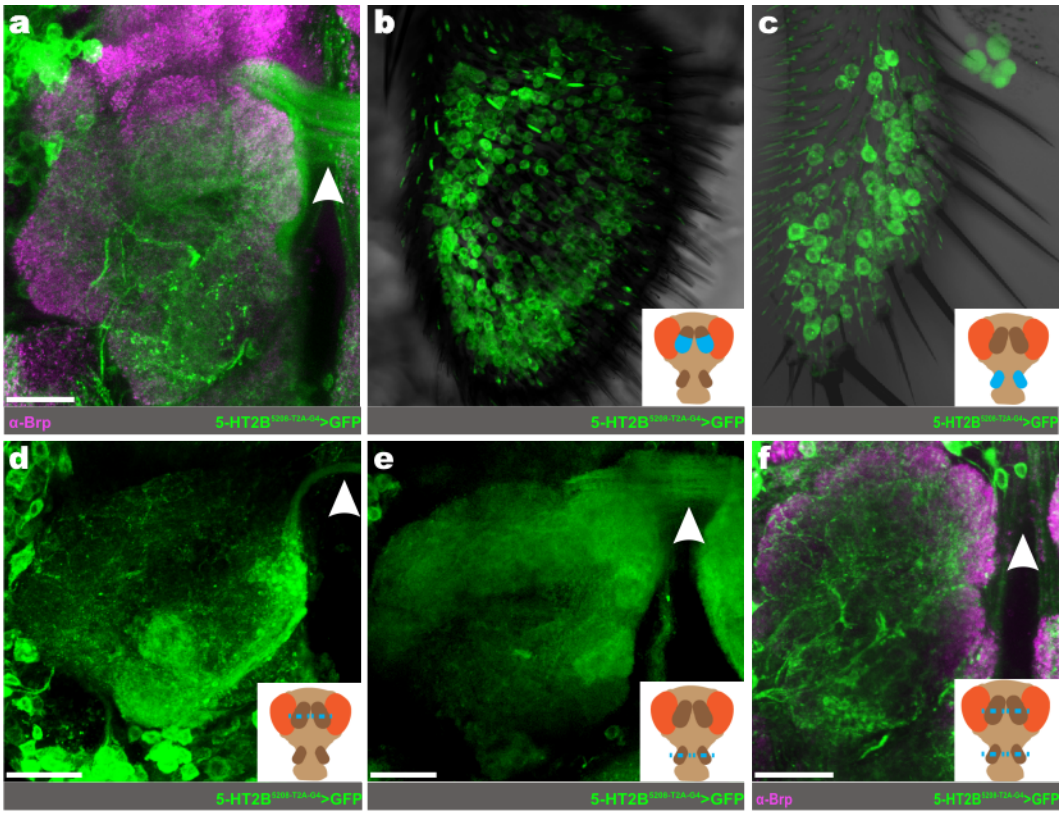

Figure 2 | 5-HT2B is expressed by antennae and maxillary palp ORNs. (**a**) Representative confocal stack of 5-HT2B expressing ORN axons (green) crossing the AL commissure. (**b**) 5-HT2B expressing ORN soma within the antennae. (**c**) 5-HT2B expressing ORN soma within the maxillary palp. To confirm antennae and maxillary palp ORNs express 5-HT2B, one-day old adults' antennae (**d**), maxillary palp (**e**), or both (**f**) were removed. Removal of either structure individually only partially abolishes 5-HT2B ORN axons, while removal of both abolishes 5-HT2B ORN axons. The white arrowhead in (**a**) and (**d-f**) highlights ORN axons crossing the AL commissure. Neuropil in (**a**) and (**f**) are delineated by α-Bruchpilot (α-Brp; magenta) labeling. All scale bars=20um.

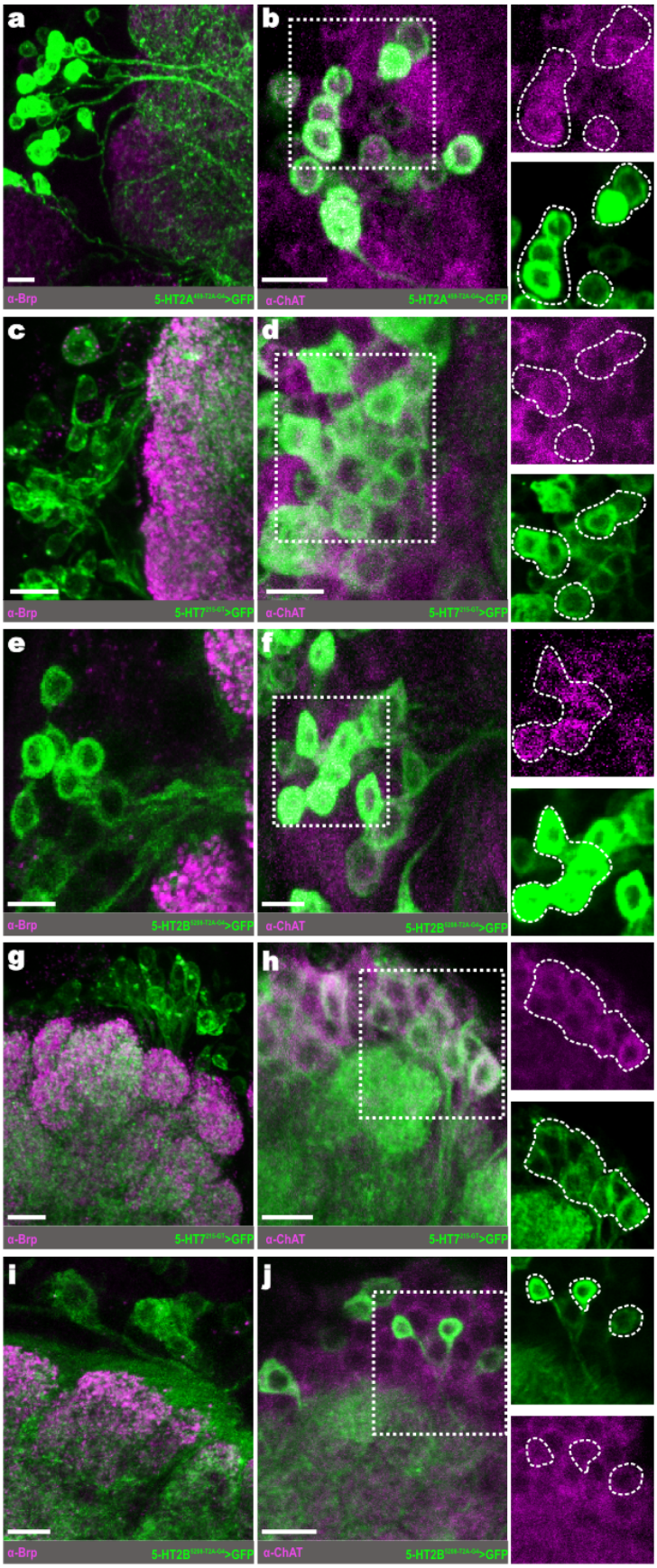

Figure 3 | Excitatory PNs express excitatory serotonin receptors. (**a**) Representative confocal stack of 5-HT2A expressing lateral projection neurons (latPNs; green). (**b**) 5-HT2A expressing latPNs also colabel for choline acetyltransferase (ChAT; magenta). (**c**) Representative confocal stack of 5-HT7 expressing latPNs (green). (**d**) 5-HT7 expressing latPNs also co-label for ChAT (magenta). (**e**) Representative confocal stack of 5-HT2B expressing latPNs (green). (**f**) Lateral PNs that express 5-HT2B also co-label for ChAT (magenta). (**g**) 5-HT7 expressing anterodorsal projection neurons (adPNs; green). (**h**) 5-HT7 expressing adPNs co-label for ChAT (magenta). (**i**) 5-HT2B expressing adPNs (green). (**j**) Anterodorsal PNs that express 5-HT2B also co-label for ChAT (magenta). Neuropil in (**a**), (**c**), (**e**), (**g**), and (**i**) are delineated by α-Bruchpilot (α-Brp; magenta) labeling. All scale bars=10um.

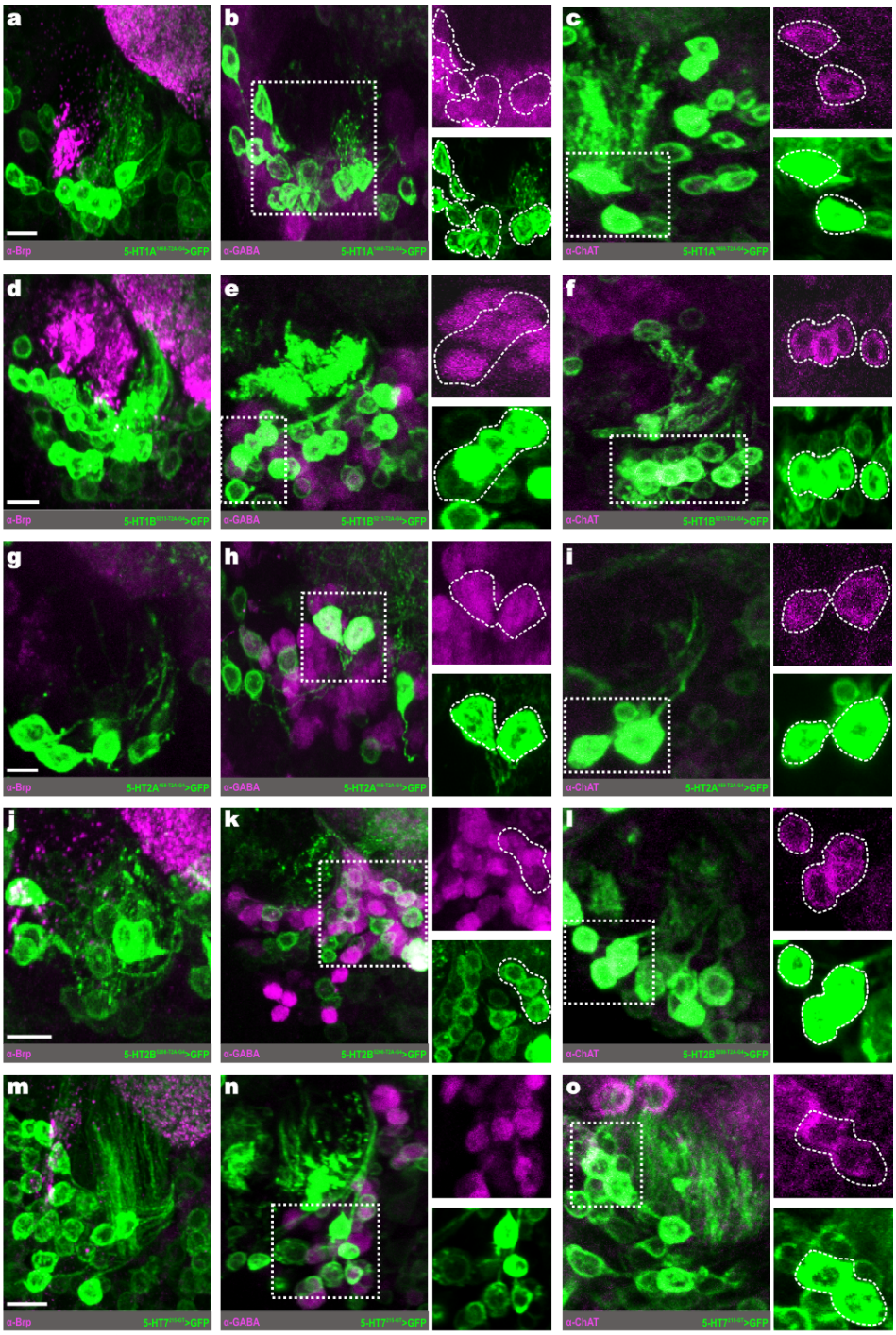

Figure 4 | Ventral PNs express each serotonin receptor. (**a**) 5-HT1A is expressed by vPNs (green). (**b**) 5-HT1A expressing vPNs (green) colabel for GABA (magenta). (**c**) 5-HT1A expressing vPNs colabel for choline acetyltransferase (ChAT; magenta). (**d**) 5-HT1B is expressed by vPNs (green). (**e**) 5-HT1B expressing vPNs (green) colabel for GABA (magenta). (**f**) 5-HT1B expressing vPNs colabel for ChAT (magenta). (**g**) 5-HT2A is expressed by vPNs (green). (**h**) 5-HT2A vPNs (green) colabel for GABA (magenta). (**i**) 5-HT2A vPNs (green) colabel for ChAT (magenta). (**j**) 5-HT2B expressing vPNs (green). (**k**) 5-HT2B vPNs (green) colabel for GABA (magenta). (**l**) 5-HT2B vPNs (green) colabel ChAT (magenta). (**m**) vPNs that express 5-HT7 (green). (**n**) 5-HT7 vPNs (green) co-label for GABA (magenta). (**o**) 5-HT7 vPNs (green) colabel for ChAT (magenta). Regions of neuropil in (**a**), (**d**), (**g**), (**j**) and (**m**) are delineated by α-Bruchpilot (α-Brp; magenta) labeling. All scale bars=10um.

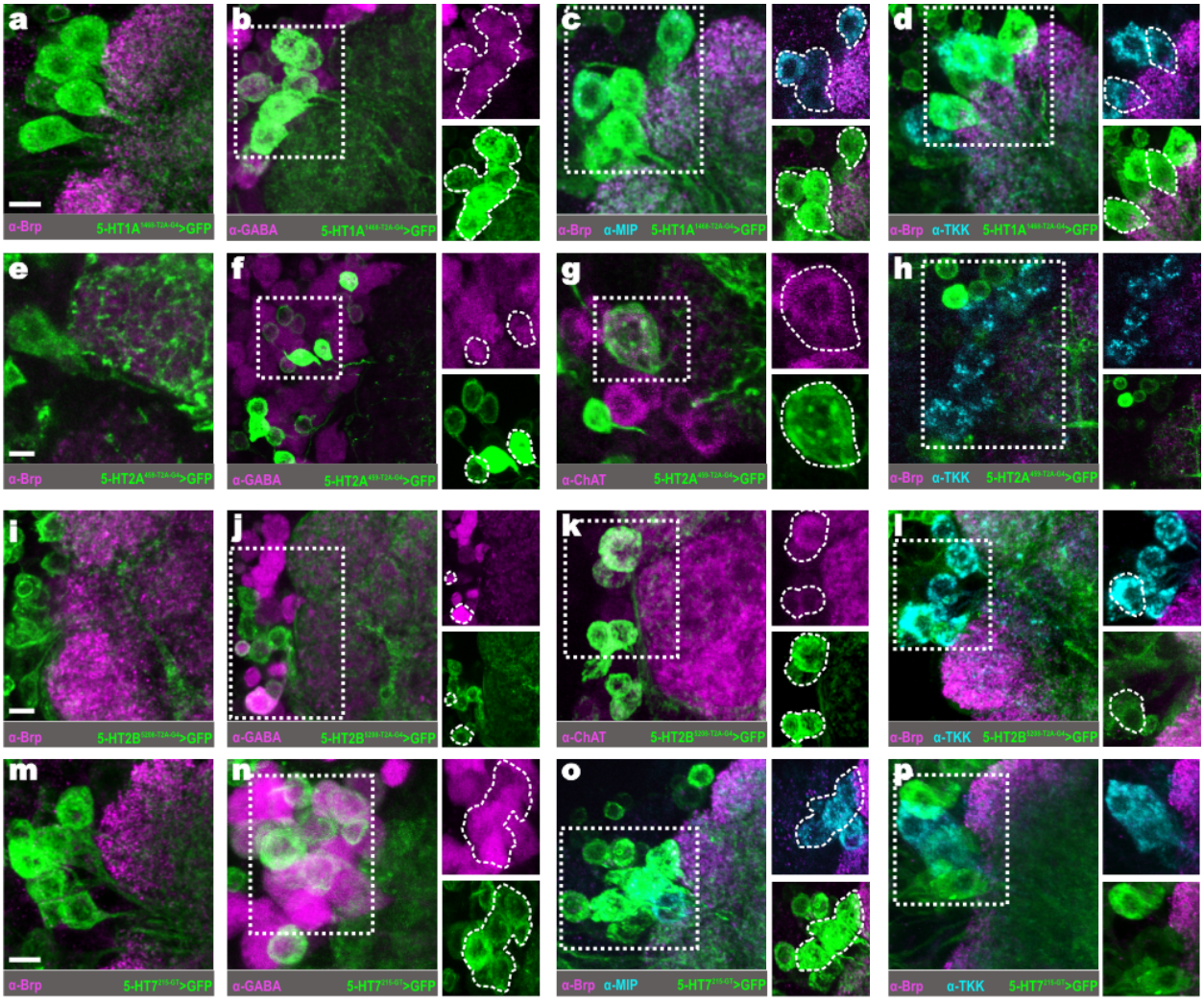

Figure 5 | 5-HTRs are expressed by distinct populations of local interneurons. (**a**) Local interneurons (LNs) that express 5-HT1A. (**b**) 5-HT1A LNs (green) colabel for GABA (magenta). (**c**) 5-HT1A LNs (green) colabel for myoinhibitory peptide (MIP; cyan). (**d**) 5-HT1A LNs colabel for tachykinin (TKK; cyan). (**e**) 5-HT2A expressing LNs (green). (**f**) 5-HT2A LNs (green) colabel for GABA (magenta). (**g**) Cholinergic LNs (ChAT; magenta) express 5-HT2A. (**h**) 5-HT2A (green) is not expressed by any TKKinergic LN (cyan). (**i**) LNs that express 5-HT2B. (**j**) 5-HT2B LNs (green) colabel for GABA (magenta). (**k**) Cholinergic LNs (ChAT; magenta) express 5-HT2B. (l) 5-HT2B (green) is expressed by TKKinergic LNs (cyan). (**m**) 5-HT7 expressing LNs. (**n**) 5-HT7 LNs colabel for GABA (magenta). (**o**) 5-HT7 LNs colabel for MIP (cyan). (**p**) 5-HT7 LNs colabel for TKK (cyan). Neuropil in (**a**), (**c-e**), (**i**), (**l**), (**m**), and (**o-p**) are delineated by α-Bruchpilot (α-Brp; magenta) labeling. All scale bars=10um.

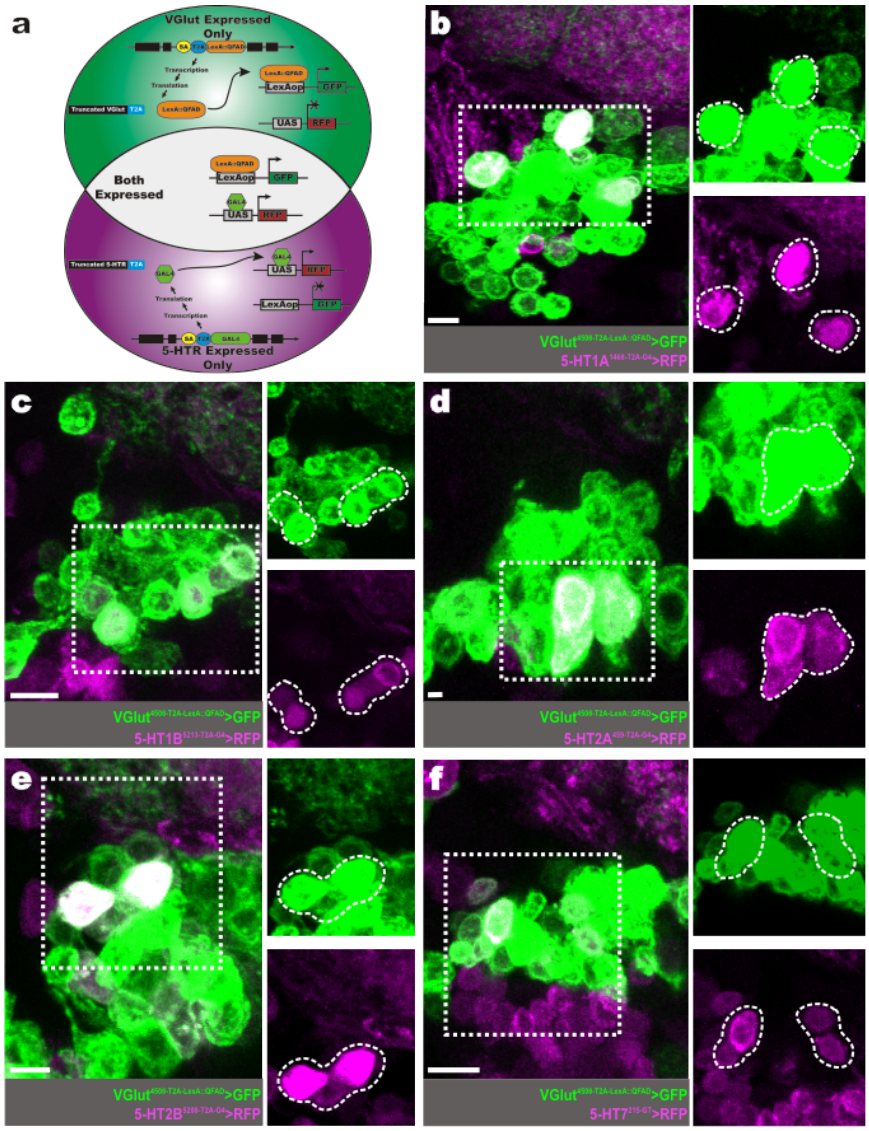

Figure 6 | Glutamatergic LNs express each 5-HTR. (**a**) Schematic of approach used to determine 5-HTR expression within glutamatergic LNs. We used a Trojan T2A-LexA::QFAD protein-trap line for vesicular glutamate transporter (VGlut) to drive the expression of GFP (green) in every glutamatergic neuron. Within the same animal, RFP (magenta) is produced in every neuron that produces a given 5-HTR, depending on the 5-HTR T2A-GAL4 line used. Both GFP and RFP (white) is produced in glutamatergic neurons that express a given 5-HTR. (**b**) Glutamatergic LNs (green) that co-express the 5-HT1A (magenta). (**c**) Glutamatergic LNs (green) that co-express the 5-HT1B (magenta). (**d**) Glutamatergic LNs (green) that co-express the 5-HT2A (magenta). (**e**) Glutamatergic LNs (green) that co-express the 5-HT2B (magenta). (**f**) Glutamatergic LNs (green) that co-express the 5-HT7 (magenta). All scale bars=10um.

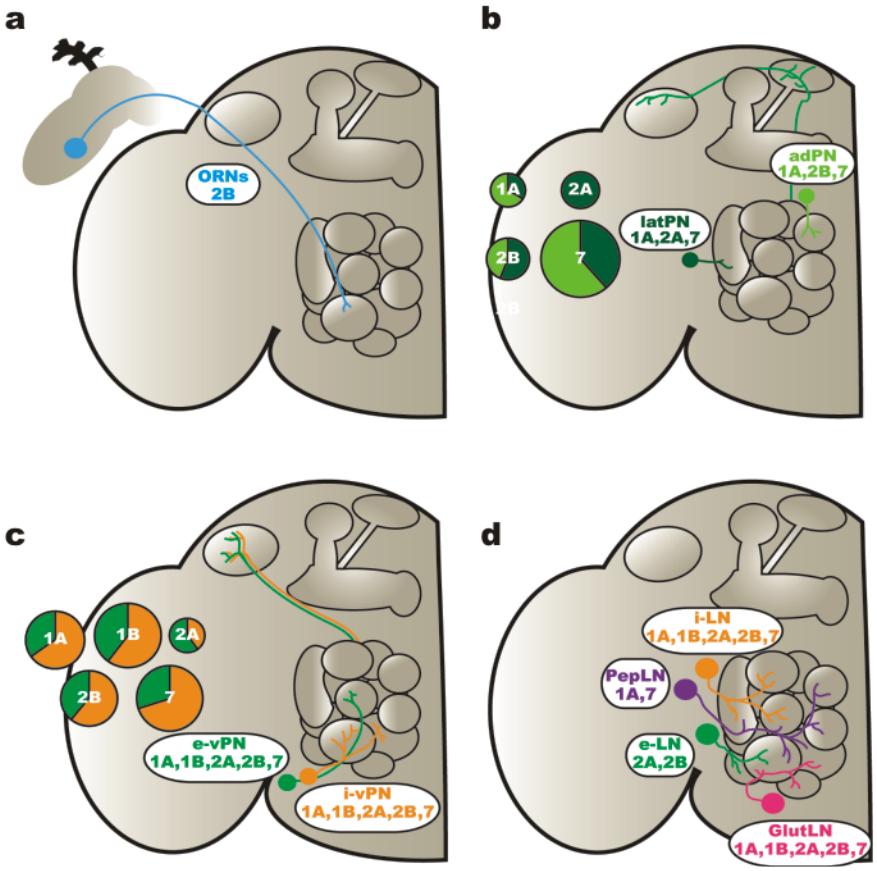

Figure 7 | Serotonin targets distinct network elements within the AL. (**a**) ORNs (blue) within the antennae and maxillary palps express 5-HT2B. (**b**) Excitatory PNs (ePNs) in the lateral (latPNs; dark green) and anterodorsal (adPNs; lime green) clusters express 5-HT2A and 5-HT7, respectively. In all cases, the pie chart diameter represents the total number of ePNs that express a given 5-HTR, and is divided by the relative number of latPNs (dark green slices) and adPNs (lime green slices) that express a given 5-HTR. (**c**) Inhibitory ventral PNs (i-vPN; orange) and excitatory ventral PNs (e-vPN; green) express all 5-HTRs. In all cases, the pie chart diameter represents the total number of vPNs that express a given 5-HTR. Moreover, each pie chart is divided by the relative number of i-vPNs (orange slices) and e-vPNs (green slices) that express a given 5-HTR. (**d**) GABAergic local interneurons (i-LN; orange) express all 5-HTRs. Cholinergic LNs (e-LN; green) express 5-HT2A and 2B. Peptidergic LNs (PepLN; purple) express 5-HT1A and 5-HT7. Glutamatergic LNs (GlutLN; pink) express all 5-HTRs.

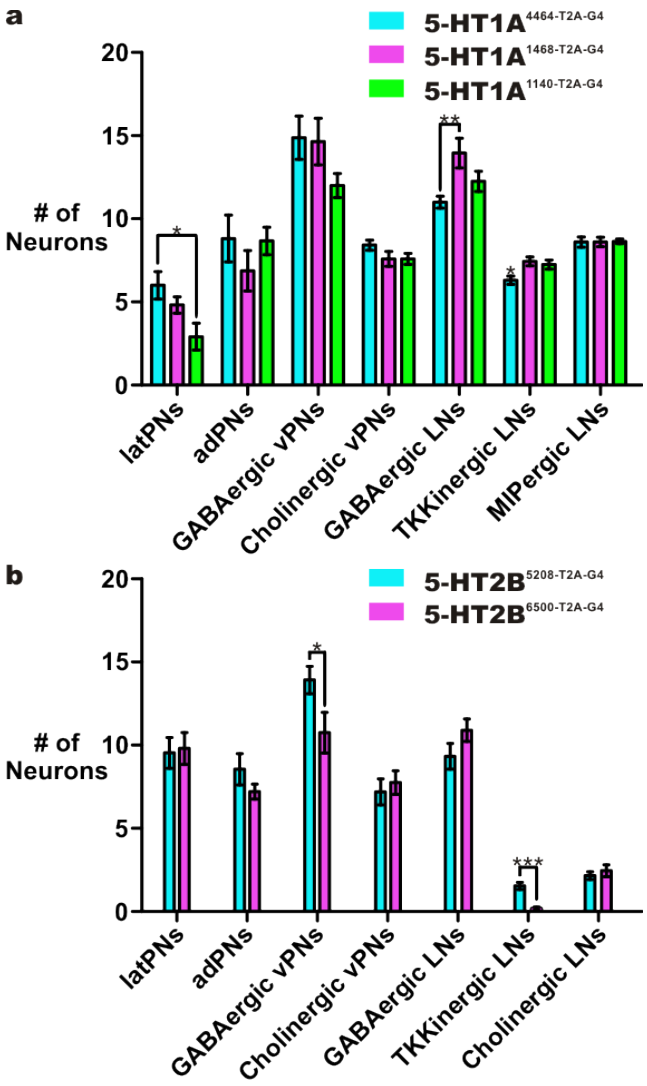

Supplementary Figure 1 | Different coding-intronic insertion drivers for the same locus label similar neurons. (a) Number of latPNs, adPNs, GABAergic vPNs, cholinergic vPNs, TKKinergic LNs, and MIPergic LNs highlighted by each T2A-GAL4 line for 5-HT1A. Data were compared using a 1-Way ANOVA followed by a Tukey's Multiple Comparison Test (α = 0.05). (**b**) Number of latPNs, adPNs, GABAergic vPNs, cholinergic vPNs, TKKinergic LNs, and cholinergic LNs highlighted by each T2A-GAL4 line for 5-HT2B. The difference between the number of TKKinergic LNs highlighted by these two lines is one neuron. The number of glutamatergic LNs labeled by each transgenic line was not tested. Data were compared using an unpaired Student's *t*-test (α = 0.05). In all graphs, error bars are s.e.m. **p* < 0.05; ***p* < 0.005; ****p* < 0.0005.

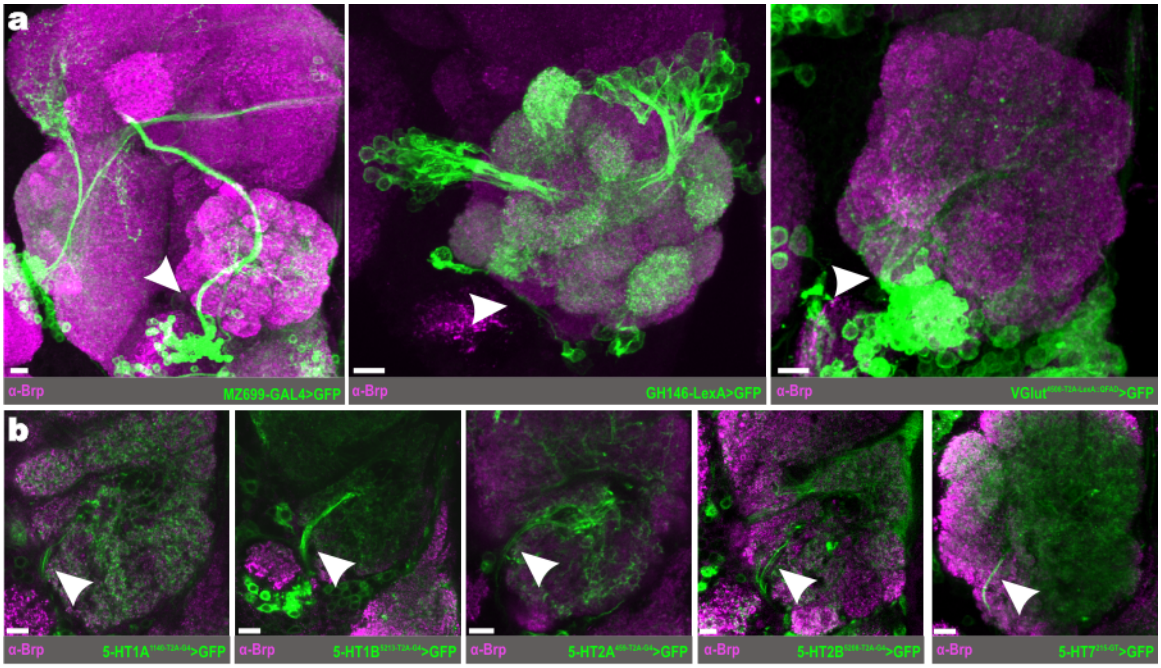

Supplementary Figure 2 | vPNs and glutamatergic LNs enter the AL through the ventral AL fascicle. (**a**) Representative confocal stack of the MZ699 enhancer-trap GAL4, GH146 enhancer-trap LexA, and a T2A-LexA::QFAD protein-trap line for the vesicular glutamate transporter (VGlut) driving the expression of GFP (green). MZ699-GAL4 and GH146-LexA ventral PNs, as well as glutamatergic LNs, project into the AL through the ventral AL fascicle. (**b**) Representative confocal stack of the T2A-GAL4 MiMIC 5-HTR lines driving the expression of GFP (green). Similar to the neurites of MZ699-GAL4, GH146-LexA, and VGlut$^{4508\text{-T2A-LexA::QFAD}}$, 5-HTR expressing ventral neurons enter the AL through the ventral AL fascicle. In all cases, the white arrowhead demarcates the ventral AL fascicle. Neuropil is delineated by α-Bruchpilot (α-Brp; magenta) labeling. All scale bars=10um.

CHAPTER 3

A Peptidergic Pathway for Olfactory Gain Control

ABSTRACT

Detection of food-associated odors is a fundamental action of all olfactory systems. However, properly detecting and encoding food-associated odors likely represents only a portion of all of the odors an animal needs to detect and encode. Moreover, there are times when the animal's need to detect and process odors that are not associated with food far outweigh the need to detect and process food odors (e.g., when the animal encounters the scent of a predator). Such shifts between what stimuli are pertinent to the animal's ongoing needs reflect shifts in neural circuit operations, such that circuit nodes dedicated to detecting and processing one stimulus are downregulated while others are upregulated. To accomplish this, nervous systems typically use neuromodulators to modulate individual neural circuit nodes according to the animal's external demands or internal needs. Neuropeptides are one such class of neuromodulators used across diverse modalities in disparate taxa to transform neural network processing according to such internal demands as satiation state. However, neuropeptides remain severely understudied relative to their classic, smaller, neurotransmitter counterparts. Here, we reveal a novel peptidergic signaling pathway in the highly-tractable *Drosophila* antennal lobe (AL) that modulates the gain of olfactory input to several food-odor associated channels. More specifically, we show that the neuropeptide myoinhibitory peptide (MIP) is released by GABAergic LNs, which through electron microscopy (EM)-level analyses we show form many reciprocal connections with principal AL neurons across glomeruli. We determine which these downstream targets express the MIP receptor (sex peptide receptor, or SPR), and show that MIP-SPR signaling modulates the gain of OSN input to several key food-odor processing glomeruli. Previous behavioral analyses found animals lacking MIP display significantly greater behavioral attraction to food-odors (Min et al., 2016). Therefore, taken together with our results, this suggests MIPergic AL LNs represent one of likely several neural substrates that underly the animal's switch in satiety-state driven behaviors.

INTRODUCTION

Neuropeptides are the largest and most diverse collection of signaling molecules found across Holozoa, and are thought to have arisen at least ~3.5bya with the last unicellular ancestor to all metazoans (Katsukura et al., 2004; Golubovic et al., 2007; Kass-Simon and Pierobon, 2007; Watanabe et al., 2009; Nässel and Winther, 2010; Conzelmann et al., 2011; Donaldson et al., 2013; Smith et al., 2014; Takahashi and Takeda, 2015; Nässel et al., 2019; Zieger et al., 2021; Moroz et al., 2021). As such, it is perhaps unsurprising that recent investigations across disparate taxa have discovered neuropeptidergic signaling plays a fundamental role in nervous system function and plasticity (Yapici et al., 2014; Kim et al., 2017; Nässel and Zandawala, 2019; Flavell et al., 2020; Liessem et al., 2021). For instance, neuropeptide F (NPF) and its vertebrate counterpart neuropeptide Y (NPY) play a conserved role in promoting feeding behaviors in humans, flies, nematodes, mosquitoes, *Aplysia* and rodents (De Bono and Bargmann, 1998; Inui, 1999; Wu et al., 2005; Jing et al., 2007; van den Pol, 2012; Maeda et al., 2015; Ohno et al., 2017; Duvall et al., 2019). However, the circuit logic and mechanistic understanding of neuropeptidergic modulation remains largely elusive within most sensory modalities. This is further confounded by limited reagents to label neuropeptides and their receptors, genetic inaccessibility to manipulate neuropeptide signaling, and unresolved circuit connectivity of most sensory networks.

The *Drosophila* AL is an attractive platform for exploring peptidergic sensory modulation because: (1) many neuropeptides are present in the *Drosophila* AL (Carlsson et al., 2010); (2) the circuit architecture and physiologies of the underlying circuitry are well-characterized (Wilson, 2013; Joseph and Carlson, 2015; Bates et al., 2020b; Clements et al., 2020; Scheffer et al., 2020; Schlegel et al., 2021); and, (3) the behavioral consequences of activating individual olfactory channels and “odor valence” have been well studied (Semmelhack and Wang, 2009; Knaden et al., 2012; Bell and Wilson, 2016). The AL circuit is comprised of several glomeruli (or, “microcircuits”) wherein olfactory sensory neurons (OSNs) that express distinct chemosensory receptors form excitatory synapses with projection neurons (PNs) and local interneurons (LNs) (Wilson, 2013; Joseph and Carlson, 2015; Schmidt and Benton, 2020; Task et al., 2020). Amongst this

circuitry are several principal and centrifugal neurons that release the neuropeptides tachykinin (TKK), short neuropeptide F (sNPF), myoinhibitory peptide (MIP), SIFamide, allatostatin A, IPNamide, and myosuppressin (Carlsson et al., 2010). More recently, TKK and sNPF were found to be released by LNs and OSNs (respectively), and each plays a distinct role in an antagonistic signaling pathway which adjusts AL processing based on the animal's current satiation state (Winther et al., 2006; Ignell et al., 2009; Root et al., 2011; Ko et al., 2015). Similarly, MIP signaling was found to be necessary and sufficient to stimulate the fly's drive towards food-odors (Min et al., 2016).

Previous experiments found that blocking all MIP transmission enhances attraction towards food-odors, while increasing MIP transmission induces strong aversion towards food-odors (Min et al., 2016). These results suggest MIP signaling controls the animal's sensitivity to food-associated odors and drive to search for food. However, the MIPergic neurons responsible for this switch in odor-evoked behavior were not identified. The most parsimonious explanation would be that MIP signaling from neurons closely associated with the olfactory system underlies this switch in food-odor preference. Indeed, there are MIP-immunoreactive (MIP-ir) neurons in the AL (see above), but what type of neuron(s) (LNs, PNs, centrifugal neurons) release MIP in the AL? Do these MIP-ir neurons connect to neurons involved with food-odor associated glomeruli? Do MIP-ir neurons respond to food associated odors directly, or are they responsive to other stimuli that then impinges on the response to food-odors? And, ultimately, does MIP modulate the activity of principal neurons responsible for processing food-odors?

To answer these questions, we first set out to determine which AL principal neurons express MIP, then we leverage transgenic light-microscopy and EM-level data to determine how MIP-ir neurons connect with other AL neurons. We find that MIP is released by patchy GABAergic LNs, which as individual neurons innervate a different compliment of glomeruli from animal-to-animal but innervate all glomeruli across all animals. Additionally, we used MIPergic LN directed synaptic polarity transgenic markers, as well as the densely reconstructed hemibrain EM volume (Clements et al., 2020; Scheffer et al., 2020), to determine the connectivity of these MIPergic LNs across the AL. We find MIPergic LNs broadly connect to and receive input from a vast array of AL principal neurons, and form all-to-all inhibitory connections amongst each other. We, then

tested MIPergic LN odor-evoked responses to a panel of diverse odorants, and find MIPergic LNs are consistently and robustly activated by the food-associated odor apple cider vinegar (ACV). Moreover, we find that the MIP receptor (sex peptide receptor, or SPR) is expressed by OSNs, PNs, and a handful of two different inhibitory LN populations. More specifically, we find SPR is expressed by food-odor associated OSNs and that MIP application reduces the odor-evoked responses in most food-odor associated olfactory channels. Of particular note, we find MIP decreases DM1 OSN responses, which have been shown to be necessary and sufficient for the animal's ability to initiate an attractive olfactory behavioral response (Semmelhack and Wang, 2009; Bell and Wilson, 2016). Together, our results - and those of earlier behavioral experiments (Min et al., 2016) - provide the neural substrates and modulatory mechanisms that likely contributes to the animal's overall shift in behaviors under starved or satiated states.

RESULTS

Patchy GABAergic LNs release MIP within the AL

Previous work found that the varicosities of the AL-associated MIPergic neurons are restricted to the AL, which suggests MIP is released from AL LNs (Carlsson et al., 2010). However, there are ~200 LNs in the *Drosophila* AL, whose distinct roles in AL olfactory processing have been associated to their small-neurotransmitter identity and morphology (Wilson and Laurent, 2005; Olsen et al., 2007; Root et al., 2008; Ignell et al., 2009; Okada et al., 2009; Chou et al., 2010; Yaksi and Wilson, 2010; Seki et al., 2010; Das et al., 2011; Ko et al., 2015; Schlegel et al., 2021). For example, the cholinergic LNs innervate many glomeruli and perform lateral excitation to broaden odor representations in the AL (Huang et al., 2010; Yaksi and Wilson, 2010). Thus, determining the small-neurotransmitter identity of MIP-ir AL neurons can shed light on what functional role MIP-ir LNs likely play in AL olfactory processing. To do so, we used recently established protein-trap transgenics that have been shown to couple the production of a gene-of-interest to the expression of a binary expression factor (Diao et al., 2015; Gnerer et al., 2015; Lee et al., 2018; Deng et al., 2019; Task et al., 2020). More specifically, we determined the overlap of MIP-immunoreactivity with choline acetyltransferase (ChAT; a

proxy for cholinergic neurons), glutamic acid decarboxylase 1 (GAD1; a proxy for GABAergic neurons), and vesicular glutamate transporter (VGlut; a proxy for glutamatergic neurons) Trojan LexA driven GFP (**Figure 1A and Figure S1**). We find that no AL MIP-ir neurons overlap with ChAT or VGlut Trojan LexA, but all MIP-ir neurons in the AL overlap with the GAD1 Trojan LexA (9.1 $\pm$ 0.19 neurons, n = 5) (**Figure 1A**). In accordance with RNA-sequencing results (Menuz et al., 2014; Mohapatra and Menuz, 2019; McLaughlin et al., 2021), we find no detectable MIP-immunoreactivity in the third-antennal segment, nor maxillary palps (data not shown). We also find that MIP-immunoreactivity within the CNS primarily colabels with the VGlut Trojan LexA (**Figure S1**), in agreement with recent single-cell RNA sequencing (scRNA-seq) data (Croset et al., 2018). Altogether, our results and those of previous reports (Carlsson et al., 2010) suggest MIP is released from GABAergic LNs within the *Drosophila* AL.

The *Drosophila* AL houses a variety of distinct GABAergic LNs, which can be subdivided into five major morphological types: panglomerular, multiglomerular, oligoglomerular, continuous, and patchy (Chou et al., 2010). Aside from their distinct morphological characteristics, these different interneuron morphological types play distinct roles in olfactory processing in the AL, not unlike cortical interneurons (Gupta et al., 2000; Markram et al., 2004). To determine the morphological type(s) of neurons that release MIP within the AL, we first visually screened ~6,000 driver lines (Jenett et al., 2012), manually screened ~25 of those lines for MIP-immunoreactivity in-house, and identified a GAL4 driver (R32F10-GAL4) that selectively highlights the MIPergic LNs (**Figure 1B and Figure 1C**). We then combined this driver and the MultiColor FlpOut (MCFO) (Nern et al., 2015) method for stochastically labeling individual neurons, which revealed that all MIPergic LNs have a discontinuous innervation pattern that resemble LNs of the patchy subtype (**Figure 1D**).

There are many AL neurons, including other LNs, whose discontinuous morphology could seem like patchy LNs but are not (Chou et al., 2010). However, individual patchy LNs are unique in that they are the only AL LNs known to innervate different sets of glomeruli from animal-to-animal (Chou et al., 2010). For example, previous reports found 161 different innervation patterns for 161 patchy LN clones (Chou et al., 2010). Therefore, to determine if any LN is truly of the patchy subtype one must

determine if the given LN projects to a different repertoire of glomeruli from animal-to-animal. To determine if MIPergic LNs are bonafide patchy LNs we analyzed the set of glomeruli innervated by 50 individual MIPergic LNs (**Figure 1E**). If MIPergic LNs were not patchy LNs, or if MIPergic LNs were restricted to certain glomeruli because they release a neuropeptide (a relatively specialized transmitter), we would expect to see several distinct combinations of glomeruli innervated by individual MIPergic LNs across animals. However, we find that no individual MIPergic LN innervates the same set of glomeruli across animals (**Figure 1E and Figure S2 & S3**); of the 50 clones analyzed we observed 50 different innervation patterns. Additionally, we find individual MIPergic LNs do not preferentially innervate any one glomerulus over others (**Figure S2A**). We find individual MIPergic LNs also do not preferentially innervate glomeruli based on the glomerulus' reported hedonic valence (**Figure S2B**), nor do they target glomeruli tuned to particular odorant functional groups (**Figure S2C**). Principal components analysis (PCA) of these glomerular innervation data reveals that no individual glomerulus' innervation pattern could explain a large portion of the overall variance. Here, a total of 15/46 principal components are required to explain ~75% of the variance in the data, where PC1 and PC2 account for only 8.7% and 7.8%, respectively (**Figure S2D**). Interestingly, when sister clones were assessed, we found that two individual MIPergic LNs tend to co-innervate ~12 glomeruli on average (n = 5 brains, 5 sister clones) (**Figure S3A & B**), and individual MIPergic LNs consistently innervated at least one of the hygro-/thermosensory associated glomeruli (Gallio et al., 2011; Frank et al., 2017; Marin et al., 2020) (**Figure S3C-E**). If we extrapolate, these results suggest that at least two MIPergic LNs innervate any single glomerulus, including the hygro-/thermosensory domains. Altogether, these observations confirm that MIPergic LNs are indeed patchy LNs, and also suggests that specialized modulatory neurons can have heterogeneity and variability built-into their morphology.

Very few monomolecular odors activate a single glomerulus (Hallem and Carlson, 2006; Silbering et al., 2008; Semmelhack and Wang, 2009; Haddad et al., 2010). Thus, if individual MIPergic LNs innervate different sets of glomeruli from animal-to-animal, might there be pairs of glomeruli that are innervated significantly more than other pairs? And, if so, what ecological relationships exist amongst significantly correlated pairs of

glomeruli? Correlation analysis between pairs of glomeruli (**Figure 1F**) revealed several statistically significant relationships, of which the most significant pairs were DM3-D ($r = 0.49$, $p = 2.7 \times 10^{-4}$) and VL2p-VA6 ($r = -0.47$, $p = 4.9 \times 10^{-4}$). The significant likelihood that when a MIPergic LN innervates DM3 it also innervates D is interesting as both glomeruli's cognate ORs respond to volatiles produced by yeast to attract and defend *Drosophila* from infectious bacteria (Carrau et al., 2005; Sokovicǵ et al., 2010; Liu et al., 2012; Mathew et al., 2013; Mansourian and Stensmyr, 2015; Federman et al., 2016). By co-innervating DM3 and D, MIPergic LNs may act to reduce the probability attractive behavioral responses are inappropriately initiated when these stimuli are absent (i.e., "false positive" behavioral reaction). This supposition is supported by two-choice assay results in which inactivation and rescue of nearly every MIP neuron's activity is necessary and sufficient for constraining behavioral attraction to yeast paste (Min et al., 2016). For similar reasons, the significant probability that when a MIPergic LN innervates VL2p it is less likely to innervate VA6 is intriguing. These glomeruli respond to several attractive volatiles that emanate from ripening fruit where yeast growth is prosperous (Mansourian and Stensmyr, 2015), and output from these glomeruli converge onto similar 3rd-order lateral horn neurons (LHNs) (Jeanne et al., 2018). The integration of output from these glomeruli at the level of these LHNs has been proposed to signal aggregation and/or courtship near food sources (Jeanne et al., 2018). Therefore, it is interesting that a given MIPergic LN that innervates VL2p is statistically unlikely to innervate VA6, as this increases the risk for output from these glomeruli becoming decorrelated. Perhaps, the signals derived from VL2p output generally indicate the presence of fermentation volatiles, while VA6 output contextualizes the specific ripening fruit where these fermentation signals originate. However, this supposition seems less likely as the olfactory receptor expressed by VA6 afferents (OR85b) is broadly tuned to acetate esters (Hallem and Carlson, 2006; Christiaens et al., 2014). In addition to DM3-D and VL2p-VA6, this analysis also revealed a significant probability for MIPergic LN co-innervation amongst several pairs of glomeruli responsive to the innately attractive odor apple cider vinegar (ACV) (Semmelhack and Wang, 2009), such as VM2-DM1 ($r = 0.35$, $p = 0.01$), DM4-DM2 ($r = 0.31$, $p = 0.03$), and DP1m-DM1 ($r = 0.29$, $p = 0.04$). These results indicate that the MIPergic LNs might play a vital role in modulating the balance of activity in ACV-

responsive glomeruli.

MIPergic LNs Provide and Receive Broad Input and Output Across the AL

While no individual MIPergic LN innervates the same set of glomeruli from animal-to-animal (**Figure 2A**), every glomerulus is innervated by at least one MIPergic LN across all animals (**Figure 2B**). However, are the MIPergic ensemble's pre-/post-synaptic sites equally distributed, or are there certain olfactory channels this ensemble preferentially modulates and/or receives input from (**Figure 2C**)? To answer this, we first drove the expression of the dendritic marker DenMark (Nicolaï et al., 2010), the axonal marker synaptotagmin.eGFP (syt.eGFP) (Zhang et al., 2002), and mCD8::GFP in MIPergic LNs, and measured their respective density in each glomerulus (**Figure 2D and Figure 2E**). Additionally, we analyzed anti-MIP immunoreactive puncta density within each glomerulus as a more directed means of determining which glomeruli are preferential targets of MIPergic modulation (**Figure 2E**). We find that the density of each indicator varies across glomeruli but are stereotypic across samples (**Figure 2E and Figure S4**). The density of both output indicators (syt.eGFP and MIP-immunoreactive puncta) were statistically correlated, and nearly every indicator scaled with MIPergic LN cable density within a given glomerulus (**Figure S4**). However, DenMark density did not scale with MIPergic LN cable density, likely owing to the indicator's tendency to concentrate within somata.

These puncta analyses afford the advantages of analyzing MIPergic LN synaptic polarity across many individuals of both sexes and are definitively restricted to MIPergic LNs. However, traditional light microscopy is limited by its ability to resolve fine structures such as axons/dendrites, and the polarity marker effectors used here often do not fully resolve a neuron's dendrites/axons (e.g., **Figure S4**) (Schlegel et al., 2017; Meinertzhagen, 2018). Therefore, we sought to perform similar analyses on individual putative MIPergic LNs (putMIP LNs) within the densely reconstructed hemibrain electron microscopy volume (Clements et al., 2020; Scheffer et al., 2020). More specifically, we analyzed individual putMIP LN connectivity to answer: (1) which glomeruli receive more/less input from putMIP LNs, and therefore which glomeruli are more/less likely

targeted by MIPergic modulation? (2) what neurons are upstream/downstream of putMIP LNs in each glomerulus? and, (3) at which synapses are vesicles associated with neuropeptides (dense core vesicles, or DCVs) (Prokop and Meinertzhagen, 2006; Merighi, 2018) enriched in the given putMIP LN's axon terminal? To answer these questions, we first used several criteria (**see Methods**) for identifying fully traced putMIP LNs and identified 20 ideal candidates (~10% of all AL LNs) (**Figure 2F**).

After identifying several optimal candidates, we wondered whether any putMIP LNs can be separated into axonic/dendritic compartments. If true, this would suggest putMIP LNs make region-specific output/input not unlike what has been suggested for the "heterogeneous LNs" in the honeybee AL (Flanagan and Mercer, 1989; Fonta et al., 1993; Sachse and Galizia, 2002; Galizia and Kimmerle, 2004). Synaptic flow centrality (Schneider-Mizell et al., 2016) and axonal-dendritic segregation indices reveal all putMIP LNs lack clearly definable input and output compartments (**Figure 2F**). Moreover, the low synaptic flow centrality suggests individual putMIP LN arbors act as intraglomerular local processing units within the glomeruli they innervate. This structural feature is similar to interneurons in the crustacean STG and vertebrate nervous system (Carnevale et al., 1997; Chitwood et al., 1999; Otopalik et al., 2017b, 2017a, 2019), and may be a means for MIPergic LNs to manipulate the activity in one glomerulus independent of their activity in the other glomeruli they innervate. Consistent with this supposition, neurites from individual putMIP LNs within a given glomerulus contain nearly identical amounts of dendritic and axonic sites (**Figure 2G**). However, regardless of the balanced input:output site ratios across all glomeruli innervated, putMIP LNs may receive unbalanced amounts of excitatory drive, inhibitory suppression, and modulatory input across the AL. If unbalanced concentrations of these various input types (albeit based on synapse numbers) do exist, this could explain an individual putMIP LN's variable activity in each glomerulus. Moreover, synapse counts strongly predict functional output strength from other systems, including other *Drosophila* AL neurons (Ding et al., 2016; Frechter et al., 2019; Barnes et al., 2020; Lyu et al., 2020; Holler et al., 2021; Schlegel et al., 2021). Therefore, we first assessed general input demographics for each putMIP LN (**Figure 3A and Figure S5**), and the balance of excitatory, inhibitory, and modulatory input each putMIP LN receives across all glomeruli (**Figure 3B**). Then, we assess each putMIP LN's

general output demographics, as well as which of these targets are postsynaptic to DCV enriched putMIP LN presynaptic terminals (**Figure 4B**).

Most putMIP LNs receive more input from OSNs (45% of putMIP LNs; ~31%-54% total input) than other principal neuron categories, while 30% of putMIP LNs receive the most input from PNs (~25%-40% total input) and other LNs (~25% of putMIP LNs; ~26%-41% total input) (**Figure 3A**). Interestingly, every putMIP LN forms strong connectivity with every other putMIP LN (**Figure 3A and Figure S5**). This all-to-all circuit motif suggests depolarizing one MIPergic LN likely drives inhibition across other members of the MIPergic LN ensemble. This motif is reminiscent of the inhibitory connections amongst starburst amacrine cells (SACs) in the vertebrate retina, which help define each SAC's stimulus receptive field (Ding et al., 2016). Perhaps a similar operation is produced by MIPergic LN-to-MIPergic LN inhibition, thus enabling individual MIPergic LNs to act as intraglomerular local processing units within select glomeruli.

Across the entire AL, most putMIP LNs (putMIP LNs 4-6, 8, and 10-20) receive more excitatory drive than inhibitory input (~75% - 100% glomeruli innervated) (**Figure 3B**). The amount of excitation a given putMIP LN receives within a glomerulus can be as high as all of the input to the given putMIP LN (e.g., putMIP LN 2 input in DM4) or as low as no excitatory input (e.g., putMIP LN 5 input in VL1) (**Figure 3B**). There are five putMIP LNs (putMIP LNs 1-3, 7, and 9) that mostly (~84% - 98% glomeruli innervated) receive more inhibitory input across the glomeruli they innervate (**Figure 3B**). Similar to the range of excitatory input, the amount of inhibitory input a given putMIP LN receives can be as high as all of the input a given putMIP LN receives in that glomerulus (e.g., putMIP LN 9 input in DA4l) or as low as no inhibitory input to the given putMIP LN (e.g., putMIP LN 3 input in VM1) (**Figure 3B**). In some instances, the ratio of excitatory vs. inhibitory inputs were equal (10 glomeruli across 6 putMIP LNs), while in one case (putMIP LN 12 input in VM2) the ratio of all three input types were balanced (**Figure 3B**). Moreover, putMIP LN 5 receives twice as much excitatory inputs as inhibitory inputs in VM2, but here the amount of excitatory and modulatory inputs is balanced (**Figure 3B**). More broadly, the ratio of excitatory-to-inhibitory inputs onto each given putMIP LN across glomeruli was generally mixed (i.e., not as straightforward as all, equal, or none), but still excitatory inputs dominate (~1.2-2.5x more) (**Figure 3B**). Altogether, these results show that

MIPergic LNs receive broad excitatory input that generally outweighs inhibitory inputs, thus suggesting activation of a broad-range of olfactory channels can recruit MIPergic LN activity.

To test if these anatomical inputs correspond well with functional supposition, we measured MIPergic LN odor-evoked responses to a panel of diverse odorants (**Figure 3C**). Most odors in our panel drove inhibitory responses in MIPergic LN neurites in several glomeruli, regardless of behavioral valence (**Figure 3C**). For instance, geranyl acetate is behaviorally attractive (Knaden et al., 2012) and evokes an inhibitory response in MIPergic LN neurites in DM4 (mean max %ΔF/F = -37.72%, n = 3) and VM2 (mean max %ΔF/F = -92.29%, n = 3) (**Figure 3C**). In contrast, the behaviorally aversive odor 1-oct-3-ol (Knaden et al., 2012) inhibits MIPergic LN processes in DM1 (mean max %ΔF/F = -55.56%, n = 2), DM2 (mean max %ΔF/F = -263.69%, n = 2), VA2 (mean max %ΔF/F = -305.99%, n = 2), and VM2 (mean max %ΔF/F = -97.62%, n = 2) (**Figure 3C**). Strikingly, we found that in some animals an odor would drive strong inhibitory responses in MIPergic LN neurites, while in other animals the same odor would drive excitatory responses in MIPergic LN neurites in the same glomerulus. For example, ammonium hydroxide activated MIPergic LN neurites in DM1, DM4, DP1m, and VA2 in some animals, but inhibited MIPergic LN neurites in another case (**Figure 3D**). This result may arise from animal-to-animal differences in MIPergic LN connectivity within the AL, just as their morphology varies from animal-to-animal. In contrast, ACV reliably and consistently evoked robust activation of MIPergic LN neurites in nearly every glomerulus tested (mean max %ΔF/F = ~34-148%, n = 4) (**Figure 3C and 3D**). This suggests that, despite variable morphology and odor-evoked responses to certain odorants, consistent activation of MIPergic LNs (and potentially MIP release) in response to ACV persists. However, we acknowledge that these MIPergic LN responses cannot be directly linked to their release of MIP; odor-evoked MIPergic LN activation might evoke the release of GABA or MIP (**Figure 1**). We attempted to determine what olfactory stimuli drove MIPergic LN DCV-release using two different peptide release sensors: preproANF-EMD (Rao et al., 2001) and NPRR-ANP (Ding et al., 2019). However, we were unable to resolve DCV-trafficking or peptide release (i.e., decrease in fluorophore puncta) with either sensor, most likely due to weak expression levels of either sensor when used in combination with our driver.

Regardless, multiple lines of evidence suggest MIP likely plays a role in ACV processing, such as: (1) multiple ACV-responsive glomeruli are statistically likely to be co-innervated by a single MIPergic LN (**Figure 1F**); (2) putMIP LN terminals presynaptic to ACV-responsive OSNs house DCVs (**Figure 4B**); (3) while most odors drive inhibitory responses in MIPergic LNs, ACV consistently drives strong activation in MIPergic LN neurites across several glomeruli (**Figure 3C and 3D**).

MIPergic LN Downstream Partners and Widespread Sex Peptide Receptor Expression Within the AL

Most putMIP LNs generally target other non-putMIP LNs (45% of putMIP LNs; ~27%-40% of total output) and OSNs (35% of putMIP LNs; ~28%-44% of total output) (**Figure 4A**). Notably, for some putMIP LNs a sizeable proportion of synaptic output (putMIP LN 10, 13, 15, and 16; ~26%-35% of total output) targeted members of the "Unknown" category, which includes unidentified neurons and/or fragments of neurons that have yet to be annotated (**Figure 4A**). Together, these results suggest that, generally, MIPergic LNs are likely to be involved in several fast-acting disinhibitory circuits across the AL, as AL LNs express $GABA_A$ (Wilson and Laurent, 2005). To determine which of these downstream partners were likely targets of MIPergic modulation, we determined which postsynaptic partners were downstream of putMIP LN terminals where dense core vesicles (DCVs) could be observed (**Figure 4B**). We observed several instances where DCVs could be found in putMIP LN terminals presynaptic to OSNs, PNs, and ventral LNs (**Figure 4B**). Based on these observations, OSNs, PNs, and ventral LNs are likely targets for MIPergic modulation. However, the presence of DCVs in MIPergic LN presynaptic terminal does not necessarily mean the downstream neuron is modulated by MIP. To determine which downstream partners are subject to MIPergic modulation, we must identify which AL neurons express MIP's cognate receptor, the inhibitory sex peptide receptor (SPR) (Yapici et al., 2008; Yang et al., 2009; Kim et al., 2010; Poels et al., 2010).

To this point, we have demonstrated that MIP is released by an ensemble of GABAergic patchy LNs, which target and receive input from across the entire AL. Electron

microscopy evidence indicates that several AL principal neuron types are plausible targets for MIPergic modulation (**Figure 5A**), but this can only be determined by identifying the AL neurons that express SPR. To determine which AL neurons express SPR, we took advantage of animals with a CRISPR/Cas9-mediated T2A-GAL4 insertion within the endogenous SPR locus (Katow et al., 2019), thus enabling GAL4 expression within SPR-expressing cells (**Figure 5B**). We first noted overlap between SPR-T2A-GAL4 derived GFP and staining for the classic glia marker *reverse polarity* (repo) (**Figure 5C**), which MCFO experiments revealed correspond to: (1) cortical glia, (2) neuropil ensheathing glia, and (3) tract ensheathing glia (**Figure 5D**). However, while these glial subtypes are intimately associated with AL neurons (Hartenstein, 2011; Freeman, 2015; Kremer et al., 2017), there is no evidence directly linking the actions of these glial subtypes with AL processing. Therefore, we turned our attention to AL principal neuron types: OSNs, LNs, and PNs.

Olfactory sensory neuron somata are located within the third-antennal segment and maxillary palp in *Drosophila* (Joseph and Carlson, 2015; Schmidt and Benton, 2020). We find 208.9 ± 11.89 (n = 17 animals, 30 antennae) and 63.42 ± 4.31 (n = 18 animals, 31 maxillary palps) SPR-T2A-GAL4 positive neurons in the third-antennal segment and the maxillary palp, respectively (**Figure 5E & 5F**). Moreover, by performing MCFO experiments where the antennal nerve is left attached to the brain, we find OSN fibers that innervate: DM2, DM5, VA1d, VA1v, VA2, VA5, VA7l, VA7m, VM1, VM2, VM5d, VM5v, and VM6 (**Figure 5G**). Despite the stochastic nature of MCFO, we believe these glomeruli likely capture the total number of SPR-expressing OSNs since there are ~187-203.5 OSNs that innervate these glomeruli, excluding VA7m (Grabe et al., 2016). Interestingly, MIPergic modulation of sensory afferents may be a fundamental feature in *Drosophila* as we find SPR-T2A-GAL4 expression in afferents belonging to each sensory modality (**Figure S6**).

In addition to OSNs, we noted several cells immunopositive for the proneural transcription factor *embryonic lethal abnormal vision* (ELAV) next to the AL, which suggested SPR-expression in either PNs and/or LNs (**Figure 5H**). By using intersectional genetics and MCFO, we find that these neurons consist of: 4.89 ± 0.21 (n = 23) SPR-expressing glutamatergic interneurons (GlutLNs) (**Figure 5H & 5I**); several uniglomerular

PNs, some of which could be identified as belonging to DA4, VA3, VA7m, VC1, and VC2 (**Figure 5J**); and, several lateral LNs (**Figure 5K**). Sex peptide receptor expression in PNs is particularly interesting, especially in glomeruli such as VA7m where OSNs also express SPR, because it suggests certain shared features between GABAergic and MIPergic signaling in the AL. For instance, projection neurons express both $GABA_A$ and $GABA_B$ receptors (Wilson and Laurent, 2005) and computational evidence suggests postsynaptic inhibition can be used to reduce the gain of second-order neurons' responses (Ayaz and Chance, 2009). Assuming broad SPR expression amongst PNs (**Figure 5J**), then MIPergic modulation of PNs may serve as an additional (potentially degenerate) locus for MIPergic modulation of olfactory gain.

In agreement with these results, we find similar neuron types - but not necessarily numbers - using a SPR bacterial artificial chromosome GAL4 driver (SPR-GAL4::VP16) (Ameku et al., 2018) (**Figure S7**), and publicly available scRNA-seq datasets (Li et al., 2017; Croset et al., 2018; Davie et al., 2018) (**Figure S8 and Figure S9**). The discrepancy in the number of neurons of a given type observed between the SPR-T2A-GAL4 versus the SPR-GAL4::VP16 drivers is likely a result of the non-native chromosomal topology, as well as potentially missing enhancer elements, of the SPR-GAL4::VP16 driver. Additionally, we created a $SPR^{MI13553}$-T2A-LexA::QFAD driver strain whose expression in the adult central brain was too weak to resolve neurites, but may still be of interest for those interested in studying SPR in the larval CNS (**Figure S10**).

MIPergic Signaling Adjusts Afferent Gain in Food Odor-Associated Glomeruli

We have shown that: (1) MIPergic LNs significantly co-innervate several ACV-responsive glomeruli; (2) putMIP LNs form many reciprocal connections and receive significant excitation within ACV-responsive glomeruli; (3) MIPergic LNs are consistently activated by ACV; and, (4) many ACV-responsive OSNs express the MIP receptor, SPR. Altogether, these results indicate that ACV-responsive glomeruli are likely influenced by MIPergic modulation. To test whether MIP can alter the odor-evoked responses in ACV-responsive glomeruli, we first recorded from the OSNs in these glomeruli before, during, and after applying synthetic MIP (synMIP) (**see Methods**) (**Figure 6A**). We chose to use

this approach, as oppose to stimulating MIPergic LNs while recording from OSNs, because any changes observed in OSN responses after stimulating MIPergic LNs could be due to GABA and/or MIP (**Figure 1A**). Moreover, as previously stated, we attempted to determine the stimulation intensity necessary for MIP release from MIPergic LNs by stimulating the LNs via P2X2 misexpression and ATP injection (Lima and Miesenböck, 2005), while simultaneously measuring peptide release with a peptide release sensor. However, because of the aforementioned reasons, these sensors could not be used for this purpose.

Olfactory sensory neuron axons display robust responses to both test concentrations of ACV before synMIP application (**Figure 6B**). However, after synMIP was applied (the "during" test) the odor-evoked responses of several glomeruli were altered in an odor-concentration independent manner (albeit, not statistically significantly) (**Figure 6B**). After the washout period (the "after" test), DM1 OSN odor-evoked responses to both odor concentrations are substantially diminished (10^{-2}: $p = 0.040$, $n = 8$, before v. after; 10^{-6}: $p = 0.048$, $n = 6$, before v. after; Bonferroni-corrected repeated-measures pairwise t-tests). Although, we can't rule out likely polysynaptic contributions to this effect, this suggests MIP's effects on OSN odor-evoked responses last for extended epochs. Interestingly, though most OSNs tested showed varying concentration independent decreases in their odor-evoked responses, DM2 OSNs showed a notable (albeit nonsignificant) concentration independent increase in their responses (10^{-2}: ~30%ΔF/F increase in max response; 10^{-6}: ~200%ΔF/F increase in max response) (**Figure 6B**). Much like the effect of MIP on DM1 OSN responses, the increase in DM2 OSN odor-evoked responses persisted even after the ten-minute washout period (the "after" test) (**Figure 6B**). Altogether, these results show that MIP modulates OSN odor-evoked responses in a stimulus concentration independent manner, but these effects may be (and are likely) polysynaptic in-nature. Therefore, we decreased SPR levels in these OSNs to test the necessity of direct MIP-SPR signaling on the observed changes in OSN odor-evoked responses (**Figure 7**).

We find that DM1 OSN odor-evoked responses are no longer decreased by synMIP application when SPR is knocked down (10^{-2}: $p = 0.11$, $n = 7$; 10^{-6}: $p = 0.156$, $n = 8$; repeated-measures one-way ANOVA). These findings are consistent with the idea

that direct MIP-SPR signaling is, at least in part, responsible for the changes in OSN odor-evoked responses after synMIP application. Additionally, we no longer observe any significant change in DM2 OSN odor-evoked responses after synMIP application (10^{-2}: p = 0.678, n = 7, before v. during; p = 0.102, n = 7, before v. after; 10^{-6}: p = 0.56, n = 7, before v. during; p = 1.00, n = 7; Bonferroni-corrected repeated-measures pairwise t-tests) (**Figure 7A**).

DISCUSSION

Altogether, our data reveal a novel neuropeptide signaling pathway that mediates olfactory gain control. We have shown that MIP is released by patchy GABAergic LNs that – as individuals – innervate a different compliment of olfactory channels from animal-to-animal. However, these MIPergic LNs reliably innervate all glomeruli across all animals, where they receive and target many principal neuron types. We have revealed which downstream partners express the MIP receptor (SPR) and are therefore subject to MIPergic modulation. Then, we use a "simple case study" for the consequences of MIPergic modulation by testing MIP's effect on the odor-evoked responses of OSNs in several food-odor associated glomeruli. This "simple case study" reveals that MIP has concentration independent effects on OSN input, wherein most glomeruli tested OSN input is decreased while in one glomerulus OSN input is boosted. As the activity of these OSNs - and MIP itself - has been shown to play a key role in the animal's odor-evoked behavioral responses (see below), the neural substrates and signaling pathway detailed here likely contribute to a key circuit switch for behavioral attraction vs. aversion. Below, we expand upon several of the important circuit features and MIP-SPR signaling properties discovered in this work.

Non-Stereotypical Morphology of Neurons in a Stereotyped Circuit

We found that MIPergic LNs are patchy GABAergic LNs that – as individuals – innervate a different repertoire of glomeruli across animals (**Figure 1**). This data is consistent with that of a seminal tour de force report characterizing all AL LNs wherein patchy LNs were generally described (Chou et al., 2010). We also show that individual

MIPergic LNs do not preferentially innervate any one glomerulus over others, or preferentially innervate individual glomeruli associated with a particular odor-evoked behavioral response or odor-tuning properties (**Figure S1**). These observations beg the question: why is the morphology of neurons that release a specialized modulator (a neuropeptide), which is relatively more energetically demanding to make and use, to innervate different glomeruli from animal-to-animal? One explanation might be that MIPergic LN morphological idiosyncrasy is a byproduct of experience during development. Consistent with this, the initial LN glomerular innervation and dendritic elaboration require during development requires OSN axons and cell-to-cell interactions (Zhu et al., 2006; Chou et al., 2010). However, OSN removal in the adult does not disrupt the animal-to-animal variability of patchy LNs (Chou et al., 2010). To the best of our knowledge, a single locus (albeit environmental experience or heritable trait) that would support animal-to-animal variation in patchy LNs has not been identified, but this line of research remains of large interest (Yang et al., 2019).

Another explanation for animal-to-animal differences in MIPergic LN morphology is that it may not matter which individual MIPergic LN form synapses with which downstream target, as long as all of the MIPergic LN downstream targets are met. Every nervous system is the byproduct of the adaptive pressures demanded by the animal's niche; a place that can be volatile, continually changing in unpredictable ways. Therefore, it's likely a developmental "parameter space" exists, wherein just enough genetic idiosyncrasy is allowed for in a population to help prevent extinction in the face of environmental perturbations. The breadth of this developmental parameter space (or the degree of variability from the "median") would be defined by many generations of selective pressures, wherein subtle changes in genetic idiosyncrasies might equally result in winners and losers. As a consequence of these genetic idiosyncrasies, phenotypic variability in a given developmental program would inevitably accumulate, resulting in the observed animal-to-animal variability in neuronal features (e.g., morphology, ion channel distribution, etc.). Consistent with this idea, animal-to-animal variations in the neural architecture have been noted in grasshoppers (Goodman, 1978), crabs (Goeritz et al., 2013; Otopalik et al., 2017b, 2017a, 2019), lobsters (Thuma et al., 2009; Daur et al., 2012), flies (Chou et al., 2010; Caron et al., 2013; Linneweber et al., 2020), and

vertebrates (Ambros-Ingerson and Holmes, 2005). However, in each case, nervous system functions persist, not unlike MIP's consistent decrease in select OSN responses (**Figure 6**). Moreover, several significant correlations exist between pairs of glomeruli for and against MIPergic LN innervation, such as the significant probability for MIPergic LN co-innervation in ACV-responsive glomeruli (**Figure 1**). This suggests that - to go back to our developmental parameter space supposition – individual MIPergic LNs can innervate different sets of glomeruli from animal-to-animal, as long as the right combinations of downstream targets (e.g., food-odor responsive glomeruli) are met by the ensemble.

Considering Copulatory Changes in MIP-SPR Signaling in the AL

MIP-SPR signaling was previously implicated in a post-mating switch in polyamine olfactory sensitivity, wherein both MIP and SPR expression increases in IR41a-expressing OSNs after females copulate resulting in increased sensitivity to polyamines (Hussain et al., 2016). These investigators found that MIP is expressed by OSNs and is upregulated after post-copulation (Hussain et al., 2016), however in accordance with previous results from RNA-sequencing (Menuz et al., 2014; Mohapatra and Menuz, 2019; McLaughlin et al., 2021) and immunocytochemistry experiments (Carlsson et al., 2010) we did not find evidence for MIP-expression in OSNs. Moreover, we could not find qualitative differences in the number of MIPergic LNs between males, mated females, or virgin females. The MIP-SPR post-mating behavior switch model also supposes copulation induces changes in SPR-expression in OSNs, while other groups have shown that post-mating sensory changes arise from a sex peptide (SP) signaling pathway that's initiated when SP from the male's seminal fluid acts on neurons in the reproductive tract (Chapman et al., 2003; Liu and Kubli, 2003; Yapici et al., 2008; Hasemeyer et al., 2009; Yang et al., 2009; Rezával et al., 2012; Walker et al., 2015). In the latter model, SPR-expression is not altered, but instead SP-SPR signaling eventually inactivates ascending neurons (SP abdominal ganglion, or SAG neurons) which then activates/inactivates central brain circuitry to produce post-mating sensory changes (Walker et al., 2015). Consistent with this, we find no significant difference in the number of SPR-positive neurons in the AL between mated vs. virgin females (**Figure S6 and Figure S7**).

Moreover, our data are consistent with recent experimental evidence using a SPR Tango activity sensor, which also showed that SPR-expression in the brain is not different between mated vs. virgin females (Katow et al., 2019). Altogether, our evidence does not support post-mating changes in MIP-SPR signaling circuitry, but our evidence does support MIP-SPR signaling modulates the gain of OSN input (**Figure 6**). Although we did not test IR41a-expressing OSNs, perhaps MIP from MIPergic LNs also modulates the gain of these OSNs.

Linking MIP-SPR Signaling to Behavioral Outcomes

Each AL glomerulus can be characterized by the particular chemosensory receptor compliment of their cognate OSN(s). This, in part, gave rise to a long-held belief that each olfactory glomerulus represented a “labeled line”, where each glomerulus represented a distinct channel for detecting and processing a particular odor. Decades of evidence has since revealed that there are few labeled lines (e.g., glomeruli V and DA2), and - as was stated above - most odorants elicit a response from several olfactory channels (Hallem and Carlson, 2006; Silbering et al., 2008; Semmelhack and Wang, 2009; Su et al., 2009; Haddad et al., 2010). Previous behavioral experiments have circumvented this limitation by using “optogenetic odors” to selectively activate different OSNs (Bell and Wilson, 2016). These experiments found that DM1 and DM2 coactivation do not summate and co-stimulation of both glomeruli produces a behavioral response that resembles DM1-only activation (Bell and Wilson, 2016). Based on this, the investigators proposed that an antagonistic relationship exists between DM1 and DM2, such that co-stimulation reduces the efficacy of either or both glomeruli (Bell and Wilson, 2016). We find MIP decreases and increases DM1 OSN and DM2 OSN odor-evoked responses in a concentration independent manner (**Figure 6**). Therefore, MIP-SPR signaling in DM1 and DM2 may act as a homeostat such that coactivation of each glomerulus never produces a behavioral response greater than the DM1-only activation response. In doing so, this “buffer” would prevent saturation at the downstream LHN subtype that receives convergent excitatory inputs from each glomerulus (Fişek and Wilson, 2014; Jeanne et al., 2018; Schlegel et al., 2021).

MIP-SPR signaling was previously implicated in the balance of olfactory drive for food-derived odors (Min et al., 2016). These investigators found that inactivating all MIPergic neurons increases the animal's drive for food-derived odors in a two-choice assay (a T-maze assay) (Min et al., 2016). This effect was replicated in similar experiments performed with MIP-genetic null mutants and could be reversed by MIP overexpression in all MIP neurons in this mutant background (Min et al., 2016). Moreover, single sensillum recordings from OSNs associated with food-odor olfactory sensation were found to spike more frequently when all MIPergic neurons are inactivated (Min et al., 2016). In contrast, if all MIPergic neurons were made overly active the animal's drive for food-odors was significantly diminished, so much so that they display odor-induced aversion (attraction index of -5% to -30%) (Min et al., 2016). Together, these behavioral results suggest MIP-SPR signaling controls the animal's sensitivity to food-associated odors and drive to search for food. In accordance with these observations, we found that individual MIPergic LNs significantly co-innervate several food-odor associated glomeruli (**Figure 1**) and neurons from several of these glomeruli express the MIP receptor, SPR (**Figure 5**). Moreover, we found that MIP application significantly diminishes odor-evoked responses from food-odor associated glomeruli in a concentration independent manner (**Figure 6**). Altogether, these results point to a probable role for MIPergic LN-derived MIP signaling to adjust olfactory processing, likely while other MIPergic neurons adjust other sensory/motor elements, in accordance with satiety homeostasis drives. However, this role is likely one of several that the MIPergic LNs play in AL processing as they also release GABA, and form connections with neurons outside of the SPR-expressing neurons identified here. More broadly, these MIPergic LNs may be a critical feature of insect AL processing as MIPergic LNs are found across Arthropoda (Utz et al., 2007; Neupert et al., 2012; Siju et al., 2014; Lizbinski et al., 2018; Habenstein et al., 2021).

METHODS

Key Resources Table

REAGENT or RESOURCE	SOURCE	IDENTIFIER
Antibodies		
Rabbit anti-RFP	Rockland	Catalog #: 600-401-379; RRID: AB_2209751
Rabbit anti-DsRed	Clontech	Catalog #: 632496; RRID: AB_10013483
Rat anti-DN-Cadherin	DSHB, University of Iowa	Catalog #: DN-Ex #8; RRID: AB_528121
Rabbit anti-GFP	Thermo Fisher Scientific, CA	Catalog #: A-11122; RRID: AB_ 221569
Chicken anti-GFP	Abcam	Catalog #: ab13970; RRID: AB_300798
Rabbit anti-Hemagglutinin	Cell Signaling Technology	Catalog #: 3724; RRID: AB_1549585
Mouse anti-V5-Tag::DyLight550	BioRad (formerly AbD Serotec)	Catalog #: MCA1360D550GA; RRID: AB_2687576
Rat anti-FLAG	Novus Bio	Catalog #: NBP1-06712SS; RRID: AB_1625982
Mouse anti-Bruchpilot	DSHB, University of Iowa	Catalog #: nc82; RRID: AB_2314866
Rabbit anti-Myoinhibitory Peptide (MIP)	Dr. Manfred Eckert (gift from Dr. Christian Wegener)	RRID: AB_2314803
Rat anti-Embryonic lethal abnormal vision (Elav)	DSHB, University of Iowa	RRID: AB_528218
Mouse anti-Reversed polarity (Repo)	DSHB, University of Iowa	RRID: AB_528448
Goat anti-Rabbit AlexaFluor 488	Thermo Fisher Scientific, CA	Catalog #: A-11008; RRID: AB_ 143165
Donkey anti-Chicken AlexaFluor 488	Jackson ImmunoResearch Laboratories, Inc.	Catalog #: 703-545-155; RRID: AB_2340375
Donkey anti-Rabbit AlexaFluor 546	Thermo Fisher Scientific, CA	Catalog #: A-10040; RRID: AB_2534016
Goat anti-Mouse AlexaFluor 546	Thermo Fisher Scientific, CA	Catalog #: A-11030; RRID: AB_2534089
Donkey anti-Rat AlexaFluor 647	Abcam	Catalog #: ab150155

Experimental Models: Organisms/Strains		
w^{*};; GAD1^{MI09277} Trojan LexA::QFAD/TM6B, Tb^{1}	Bloomington Stock Center	RRID: BDSC_60324
w^{*};; ChAT ^{MI04508} Trojan LexA::QFAD/TM6B, Tb^{1}	Bloomington Stock Center	RRID: BDSC_60319
w^{*}; VGlut ^{MI04979} Trojan LexA::QFAD/CyO, P{Dfd-GMR-nvYFP}	Bloomington Stock Center	RRID: BDSC_60314
y^{1},w^{*}, 10xUAS-IVS-mCD8::RFP, 13xLexAop-mCD8::GFP	Bloomington Stock Center	RRID: BDSC_32229
w^{-};; GMR32F10-GAL4	Bloomington Stock Center	RRID: BDSC_49725
hs-FlpG5.PEST;; UAS-MCFO-1	Bloomington Stock Center	RRID: BDSC_64085
w^{*}; 10xUAS-IVS-myr::tdTomato	Bloomington Stock Center	RRID: BDSC_32222
w^{*}; 26xLexAop-mCD8::GFP	Bloomington Stock Center	RRID: BDSC_32207
w^{*}; 10xUAS-IVS-mCD8::GFP	Bloomington Stock Center	RRID: BDSC_32185
w^{-}; 20xUAS-IVS-GCaMP6f	Bloomington Stock Center	RRID: BDSC_42747
w^{*}; UAS-SPR-RNAi	Bloomington Stock Center	RRID: BDSC_66888
w^{-}; UAS-DenMark, UAS-syt.eGFP; In(3L)D, $mirr^{SaiD1}$,D^{1}/TM6C, Sb^{1}	Bloomington Stock Center	RRID: BDSC_33064
y^{1},w^{*}, $SPR^{MI13553}$	Bloomington Stock Center	RRID: BDSC_60934
y^{1},w^{*}; wg^{Sp1}/CyO; 13xLexAop2-6xmCherryHA	Bloomington Stock Center	RRID: BDSC_52271
w*,dlg^{14},frt101/FM7a;;$CG11583^{c01124}$,frt80B/TM3, Sb^{1}	Bloomington Stock Center	RRID: BDSC_36283
$SPR^{MI13885}$-T2A-LexA::QFAD	This study.	N/A
y^{1}, w^{-}, SPR-T2A-GAL4	Shu Kondo, Tohoku University	Katow et al., 2019 Flybase ID: FBti0209968
Pebbled-GAL4 (Peb-GAL4)	R. Wilson, Harvard University	N/A
SPR-GAL4::VP16	J. Truman, University of Washington (by way of M. Texada, University of Copenhagen)	Ameku et al., 2018 Flybase ID: FBti0201391
Odors		
Paraffin oil	J.T. Baker, VWR	CAS #: 8012-95-1
Apple Cider Vinegar (ACV)	Heinz	N/A
2-heptanone	Millipore Sigma	Catalog #: 537683; CAS #: 110-43-0
1-hexanol	Millipore Sigma	Catalog #: H13303; CAS #: 111-27-3

1-oct-3-ol	Millipore Sigma	Catalog # 68225; CAS #: 3391-86-4
Ammonium hydroxide	Millipore Sigma	Catalog #: 221228; CAS #: 1336-21-6
Benzaldehyde	Millipore Sigma	Catalog #: 8.01756; CAS #: 100-52-7
Geranyl acetate	Millipore Sigma	Catalog #: 173495; CAS #: 105-87-3
Recombinant DNA		
pBS-KS-attB2-SA(2)-T2A-LexA::QFAD-Hsp70	Daio et al., 2015	Addgene: #62949
Software and Algorithms		
VAA3D (v.3.20)	Peng et al., 2010	RRID: SCR_002609
FluoRender (v.2.22.3)	Wan et al., 2017	RRID: SCR_014303
FIJI (v.2.0.0)	Open-Source	RRID:SCR_002285
R Studio (v.1.4.1103)	Open-Source	www.rstudio.com
MATLAB 2016b	MathWorks	www.mathworks.com
Python 3	Open-Source	RRID: SCR_008394
CorelDRAW 2021	Corel Corp.	www.corel.com
Adobe Illustrator 2020	Adobe Inc.	www.adobe.com
SCope	Davie et al., 2018	http://scope.aertslab.org
natverse	Bates et al., 2020; Schlegel et al., 2021	https://natverse.org/
Connectome-neuprint/neuprint-python	Stuart Berg (JRC)	N/A
CloudVolume	William Silversmith (Princeton)	https://github.com/seung-lab/cloud-volume

Contact for Reagent and Resource Sharing. Further information and reasonable requests for reagents and resources should be directed to - and will be fulfilled by - the Lead Contact, Tyler R. Sizemore (sizemoretyler92@gmail.com).

Experimental Model and Subject Details. Flies were reared on standard cornmeal and molasses media at 24°C and under a 12:12 light:dark cycle. Equal numbers of male and female animals were used when possible, excluding live-imaging experiments. For mating status comparisons: 1) “virgin females” denotes meconium-positive females, 2) non-virgin females were housed with males until processing for immunocytochemistry, and 3) flies were age-matched and kept on the similar media until processed for

immunocytochemistry.

Immunocytochemistry and Imaging. All immunocytochemistry was performed generally as previously described (Sizemore and Dacks, 2016). Briefly, samples were dissected, fixed in 4% paraformaldehyde, then washed with phosphate buffered saline with 0.5% Triton-X 100 (PBST) several times before taking samples through an ascending-descending ethanol was series, then blocking in 4% IgG-free BSA (Jackson Immunoresearch; Cat#001-000-162). Samples were then incubated in primary antibody (see **Key Resources Table**) diluted in blocking solution and 5mM sodium azide. Following primary antibody incubation samples were washed with PBST, blocked, and incubated in secondary antibody diluted in blocking solution and 5mM sodium azide. Finally, samples were washed, cleared using an ascending glycerol series (40%, 60%, 80%), and mounted on well slides in Vectashield® (Vector Laboratories, Burlingame, CA; Cat#H-1200). Images were collected and analyzed as previously described (Sizemore and Dacks, 2016), with the exception of images captured with a 40x/1.25 Silicone UPlanSApo Olympus objective.

Single LN Clone Induction and Glomerular Innervation Analysis. Single LN clones were induced using the MCFO method (Nern et al., 2015). Flies carrying the MCFO cassettes, Flp-recombinase, and GAL4 driver were raised under normal conditions (see above) until heat shock. Adult flies were heat-shocked in a 37°C water bath for 12-25 minutes and returned to normal conditions for ~2-3 days before processing for immunocytochemistry. With the exception of VA1v, glomeruli were defined according to previously published AL maps (Laissue et al., 1999; Couto et al., 2005). Neuropil was stained using anti-DN-cadherin or anti-Bruchpilot (**see Key Resources Table**). Hierarchical clustering and principal components analysis (PCA) of glomerular innervation data were performed as previously described (Chou et al., 2010). PCA was performed without any arbitrary threshold of significance. Data were clustered using Ward's method ("ward.D2") and Euclidian distance using the *ClustVis* package (https://github.com/taunometsalu/ClustVis) (Metsalu and Vilo, 2015). Pairwise Pearson's correlation coefficient of MIPergic LN glomerular innervation were determined using the

"cor" function in the base R *stats* package, and significant correlations were subsequently assessed using the "rcorr" function in the *Hmisc* package. The *corrplot* package was used to create the hierarchically clustered (using Ward's method) representation of these pairwise correlation coefficients depicted in **Figure 1**. In every case used, glomerular "odor scene" information is derived from previous assignments (Bates et al., 2020b).

To determine if MIPergic LNs preferentially innervate glomeruli based on valence, glomeruli were assigned "attractive" or "aversive" based on either: (1) previous reports (Semmelhack and Wang, 2009; Stensmyr et al., 2012; Min et al., 2013; Ebrahim et al., 2015; Mansourian et al., 2016); or, (2) derived from the behavioral valence of the odors (Knaden et al., 2012) that glomerulus' OSNs respond to according to DoOR 2.0 (Münch and Galizia, 2016). Glomeruli whose OSNs respond to neutral (e.g., DL5), or whose valence is state-dependent (i.e., the V glomerulus) (van Breugel et al., 2018), were excluded from this analysis. These methods were also used to determine if MIPergic LNs preferentially innervate glomeruli based on the functional group of a given OR's cognate odorant, with the exception of the V, VA7m, and VM6 glomeruli.

MIPergic LN Anatomical Marker Density Analyses. Analysis of syt.eGFP, DenMark, anti-MIP immunoreactive puncta signal, and LN innervation (via mCD8::GFP signal) density in antennal lobe glomeruli was performed as previously described (Hong and Wilson, 2015). Images of all antennal lobes within a given brain were collected with similar confocal scan settings (laser power, detector offset, etc.) and later imported into FIJI for quantification. Using the Segmentation Editor plugin and a previously described script (graciously provided by Rachel Wilson, Harvard) (Hong and Wilson, 2015), ROIs were manually traced every 2-3 slices around the neuropil boundaries of each glomerulus using the anti-DN-Cadherin or anti-Bruchpilot channel, and then interpolated through the stack to obtain boundaries in adjacent slices. To ensure each brain contributed equally when pooling data across brains, signal density values for all glomeruli were normalized to the maximum density value within the given indicator being analyzed (e.g., all density values for syt.eGFP were normalized to the maximum syt.eGFP value). The "ggscatter" function in the *ggpubr* package was used to determine Pearson's correlation coefficients and p-values when assessing correlations between effector/anti-MIP and MIPergic LN

mCD8::GFP voxel density across all glomeruli. Adjusted R-squared values were calculated using the base-R *stats* package and correspond to how well each data being assessed for the given correlation analysis fit a linear model.

Putative MIPergic LN Connectome Analyses. All connectome analyses leveraged the publicly available Janelia FlyEM *Drosophila* hemibrain electron microscopy volume (version 1.2; https://neuprint.janelia.org/) (Clements et al., 2020; Scheffer et al., 2020), and recently described analysis suites (Bates et al., 2020a; Schlegel et al., 2021). We used several criteria for determining which neurons are most likely MIPergic LNs, the first of which was the candidate neurons must be antennal lobe LNs. Next, we selected those candidate LNs that receive input from the serotonergic CSD neurons as all MIPergic LNs express the 5-HT1A serotonin receptor (Sizemore and Dacks, 2016), and form connections with the serotonergic CSD neurons (Coates et al., 2017). We then used *natverse* (Bates et al., 2020a) to transform the interconnectivity of each candidate neuron into the FCWB template brain three-dimensional space (Chiang et al., 2011; Costa et al., 2016), so we could generate a morphological similarity score between our query neuron and neurons FlyLight project's GMR-GAL4 repository (Jenett et al., 2012) by using the built-in NBLAST package (*nat.nblast*) (Costa et al., 2016). We selected for only those candidates that achieved a GMR32F10-GAL4 NBLAST score of >0.60 ["identical twins"; (Costa et al., 2016)]. Lastly, any remaining candidate MIPergic LNs were filtered for those neurons that are considered "Traced", the hemibrain's highest level of tracing completeness and confidence. Only neurons that met all of these criteria were considered for further analysis.

Most methods for analyzing putMIP LN morphology and connectivity have been described recently (Schlegel et al., 2021). Putative MIPergic LN skeleton meshes (**Figure 2F**) were fetched from the hemibrain data repository by accessing the neuPrint Python API using the *neuprint-python* (https://github.com/connectome-neuprint/neuprint-python) and *Cloud-Volume* (https://github.com/seung-lab/cloud-volume) packages. The *hemibrainr* package (https://github.com/flyconnectome/hemibrainr) was used to fetch each putMIP LN's metadata and calculate each neuron's dendrite-axon segregation index and flow centrality (Schneider-Mizell et al., 2016) using the recommended arguments.

To determine the fraction of a given putMIP LN's total input or output reside within each glomerulus the total number of pre- and postsynaptic sites, and downstream partners, were first extracted from the hemibrain repository using the *neuprintr* "get_roiInfo" function. To represent this data as percentages the given putMIP LN's number of pre-/postsynaptic sites/or downstream partners present within a given glomerulus were then divided by the total number of pre-/postsynaptic sites/or downstream partners across all AL glomeruli, then multiplied by 100%.

To identify and compare the demographics of each putMIP LN's upstream and downstream partners, putMIP LN connectivity data were first extracted using the *hemibrainr* "simple connectivity" function. The demographic of each presynaptic and postsynaptic partner was generally assigned according to the neuron's accompanying "name" or "type" as listed on neuPrint. In cases where a neuron's "name" or "type" was unannotated ("NA"), the neuron would be categorized as "Unknown". We used the following formula to determine the percentage of overall input a given putMIP LN receives from a given neuron category: [*(sum of connections from a given neuron category to the given putMIP LN)/(summed amount of input that given putMIP LN receives from all categories)] x 100%*. Similar methods were applied for determining the percentage of overall output a given neuron category receives from a given putMIP LN.

To determine the amount of excitatory, inhibitory, and modulatory input a given putMIP LN receives within each glomerulus, we first categorized each presynaptic neuron as either excitatory, inhibitory, or modulatory based on the presynaptic neuron's neuPrint "name"/"type", previous immunocytochemistry results (Stocker et al., 1997; Dacks et al., 2006; Okada et al., 2009; Tanaka et al., 2009; Chou et al., 2010; Das et al., 2011; Sen et al., 2014), and/or the category assigned in previous reports (Schlegel et al., 2021). However, we acknowledge several caveats to this analysis, such as: (1) this analysis does not account for co-transmission; (2) several glomeruli are truncated within the hemibrain AL (Schlegel et al., 2021); (3) we consider all LNs as inhibitory as most are either GABAergic or glutamatergic (combined, these represent ~170/200 AL LNs) (Stocker et al., 1997; Okada et al., 2009; Tanaka et al., 2009; Chou et al., 2010; Das et al., 2011; Liu and Wilson, 2013), but there are ~4 tyrosine hydroxylase-immunoreactive (dopaminergic) and ~8-15 cholinergic and/or electrically coupled LNs in the AL (Shang et

al., 2007; Chou et al., 2010; Huang et al., 2010; Yaksi and Wilson, 2010); (4) although GABA can also act as an intrinsic modulator in the AL [reviewed in (Lizbinski and Dacks, 2018)], we only count GABAergic LNs as part of the “inhibitory input” category here; and, (5) we consider all ventral LNs analyzed here as being glutamatergic, but there are ~1-2 dopaminergic (tyrosine hydroxylase-immunoreactive) ventral LNs (Chou et al., 2010). Once each presynaptic neuron’s chemical identity (excitatory, inhibitory, or modulatory) was determined, we used several approaches to assign these synapses to particular glomeruli. In the case of uniglomerular PNs (uPNs) and OSNs, we leveraged the single glomerulus innervation of these presynaptic neuron types to assign their synapse onto a given putMIP LN synapse to the presynaptic neuron’s home glomerulus. That is to say, OSN-to-putMIP LN and uPN-to-putMIP LN synapses were assigned to a glomerulus by: (1) using the home glomerulus assigned to a given presynaptic in the neuron’s neuPrint “name”/”type”, or (2) by the home glomerulus assigned to the neuron in previous reports (Schlegel et al., 2021). For instance, if the presynaptic neuron was a cholinergic PN whose home glomerulus is DA2, and this DA2 PN synapses on a given putMIP LN five times, then those five synapses went to the overall excitatory input the given putMIP LN receives within DA2. Neurons were only excluded from this analysis if the presynaptic neuron’s home glomerulus was not previously identified (Schlegel et al., 2021). Once the polarity of the input type was established, we used previously established 3D meshes for each glomerulus (Schlegel et al., 2021) to determine if the XYZ coordinates of each putMIP LN’s synapse(s) with a given presynaptic partner were located in a given glomerulus. Synapse counts for each putMIP LN partner within the given glomerulus were then summed by type (excitatory, inhibitory, or modulatory), and the resulting total was divided by the total number of synapses the given putMIP LN makes within that glomerulus to establish percent excitatory, inhibitory input, or modulatory input.

SPR^{MI13885}-T2A-LexA::QFAD Generation. The SPR^{MI13885}-T2A-LexA::QFAD fly line was established using previously described injections methods (Diao et al., 2015). We also note that we also attempted to create an SPR-T2A-GAL4 using the pC-(lox2-attB2-SA-T2A-Gal4-Hsp70)3 construct (Addgene #62957), but no founders emerged (potentially owing to lethality when these construct elements are inserted in the SPR locus). Briefly,

pBS-KS-attB2-SA(2)-T2A-LexA::QFAD-Hsp70 and ΦC31 helper plasmid DNA were co-injected into y^1, w^*, Mi{MIC}$SPR^{MI13885}$. pBS-KS-attB2-SA(2)-T2A-LexA::QFAD-Hsp70 (Addgene plasmid #62949) and pC-(lox2-attB2-SA-T2A-Gal4-Hsp70)3 (Addgene #62957) were gifts from Benjamin H. White (NIH). $SPR^{MI13885}$-T2A-LexA::QFAD transformants were isolated as depicted in **Figure S10**.

Single Cell RNA-Sequencing Analysis of SPR expression. Single-cell transcriptomic data were accessed and downloaded from the SCope web interface on 8/14/2018 and 4/7/2021. Projection neuron cluster boundaries were manually redrawn as depicted in each dataset's original report (Li et al., 2017; Croset et al., 2018; Davie et al., 2018). Projection neuron subpopulations were then identified within each scRNA-seq dataset using previously established marker genes (Komiyama et al., 2003; Komiyama and Luo, 2007; Li et al., 2017).

***in vivo* Calcium Imaging – animal preparation.** All calcium imaging experiments were performed on female flies ~1-5 days post-eclosion, and at room temperature. Animals of the proper genotype were collected and briefly anesthetized on ice. Once anesthetized, an animal was affixed to a custom-built holder with UV curable glue (BONDIC, M/N: SK8024). Our custom-built holder consists of a sheet of aluminum foil with a small hole (the imaging window) affixed to a 3D-printed design derived from similar designs described previously (Weir et al., 2016). Once mounted, a small window exposing the dorsal side of the brain was created, and covered with filtered recording saline (in mM: 2 $CaCl_2$, 5 KCl, 5 HEPES, 8.2 $MgCl_2$, 108 NaCl, 4 $NaHCO_3$, 1 NaH_2PO_4, 10 sucrose, and 5 trehalose; adjusted pH: ~7.4) (Root et al., 2008). Following this, the air sacs, fat bodies, and trachea covering the dorsal side of the brain were removed with fine forceps. With the exception of minimal epochs during the synthetic MIP bath application experiments (see below), the brain was continuously perfused with oxygenated (95%O_2/5%CO_2) recording saline using a Cole-Parmer Masterflex C/L (M/N: 77120-62) at a rate of ~2mL/min.

***in vivo* Calcium Imaging – Image Acquisition.** Functional imaging data were acquired

using a Prior Scientific Open Stand (M/N: H175) microscope mounted on Prior Scientific motorized translational stage (M/N: HZPKT1), and equipped with an Olympus 10x/0.30 UPlanFL N objective and an Olympus 60x/1.00 LUMPlanFL N water-immersion objective. A 470nm CoolLED pE-100 (CoolLED Ltd., Hampshire, UK) was used as the light source. Each trial was captured with a Hamamatsu ORCA-4.0LT camera (Hamamatsu Phototonics, Hamamatsu, Japan), and consists of 40 1,024x1,024 frames acquired at a frame rate of ~9 Hz.

***in vivo* Calcium Imaging - Odor Preparation and Delivery.** All odor concentrations are reported as v/v dilutions in paraffin oil (J.T. Baker, VWR #JTS894), or autoclaved and twice-filtered distilled water (for diluting acids). For example, 10^{-2} dilution indicates that one volume of an odor is diluted with 100 volumes of paraffin oil. Dilutions were prepared in 2mL odor vials (SUPELCO; P/N: 6020) that contained a final volume of 1mL of diluted odor in paraffin oil every other day, or after two experiments (whichever came first). Odors were presented as previously described (Bhandawat et al., 2007; Hong and Wilson, 2015; Jeanne et al., 2018). Briefly, a carrier stream of carbon-filtered, dehumidified, air was presented at 2.2 L/min to the fly continuously through an 8mm Teflon tube placed ~1cm away from the fly. A three-way solenoid (The Lee Company, P/N: LHDA1231315H) diverted a small portion of the airstream (0.2 L/min) through the headspace of an odor vial for 200ms after triggering an external voltage command (TTL pulse) at frame 20 of the trial. Considering the above, the odor is diluted further (by 10-fold) prior to delivery to the animal. The odor stream joined the carrier stream 11cm from the end of the tube, and the tube opening measured ~4mm.

Methods for assessing preparation health and performing multiple odor trials generally conform to previous work (Hong and Wilson, 2015; Jeanne et al., 2018). At the start of each experiment, the animal was presented a test odor (10^{-3} 2-heptanone) to assess the preparation's health. Only the data collected from animals whose responses to this test odor were robust and did not dramatically change from baseline over the course of the experiment were used for further analysis. The only exceptions to this were those data collected in synthetic MIP bath application experiments (see below), since bath application of any modulator would likely result in network property changes that

would consequently change olfactory responses. Therefore, the test odor was only initially presented to those animals used for synthetic peptide application experiments, so their initial olfactory response health could be assessed. Each experiment consisted of multiple odor trials (3 for OSNs; 4 for LNs) within a preparation which were then averaged to attain a within-animal response. These within-animal averages were subsequently averaged across many animals for subsequent statistical analysis, and “n” is reported as the number of animals. Each odor trial consisted of five 200ms pulses of odor with a 1ms interpulse interval. The same odor was never presented twice within 2min to prevent depletion of the odor vial's headspace. If multiple odors were to be tested, then they were presented randomly. If multiple concentrations of a given odor were to be tested, then the lower concentration was presented before the higher concentration. Air entered and exited each odor vial through a PEEK one-way check valve (The Lee Company, P/N: TKLA3201112H) connected to the vial by Teflon tubing. The odor delivery tube was flushed with clean air for 2min when changing between odors/concentrations. As an additional preemptive measure, all odor delivery system components were hooked up to the house vacuum line overnight.

***in vivo* Calcium Imaging – Data Analysis.** All calcium imaging data were analyzed using a custom-made script graciously provided by Marco Gallio (Northwestern University) and has been described previously (Frank et al., 2015, 2017). With the exception of any preparations that violated the aforementioned criteria (e.g., movement, diminishing prep health, etc.), no data points or outliers were excluded from our analyses. Generally, the number of flies to be used for experiments are not a limiting factor, therefore no statistical power analyses were used to pre-determine sample sizes. Regardless, with the exception of MIPergic LN odor panel experiments, our sample sizes are similar to those in previous reports that perform similar experiments (Ignell et al., 2009; Oh et al., 2014; Badel et al., 2016; Díaz et al., 2019; Zandawala et al., 2021). Before analyzing the data, a Gaussian low-pass filter (sigma=1), bleach correction (exponential fit), and image stabilizer algorithms were applied to the given trial’s raw $\Delta F/F$ signal. Calcium transients ($\Delta F/F$) were measured as changes in fluorescence (ΔF) normalized to baseline fluorescence (F, averaged over the first 19 frames before odor delivery). By normalizing this way, we could

ensure trivial effects of slight z-axis drifts, GCaMP concentration differences, and variations in the tested neuron's innervation density would be corrected. Responses were pooled for each odor stimulus - and within concentration - by averaging the peak odor-evoked calcium signal across multiple odor presentation trials (3 for OSNs; 4 for LNs). We used the following formula to derive percent ΔF/F: *[(the calcium transients within a given glomerulus)/(the peak odor response averaged across the entire AL tested)] x 100%*. A trial's maximum response (Max %ΔF/F) refers to the average of five consecutive frames centered around that trial's peak response post stimulus presentation. Glomeruli were manually identified post-hoc by comparing acquired images to well-defined three-dimensional maps of the AL (Fishilevich and Vosshall, 2005; Grabe et al., 2015). Only the glomeruli that were reasonably identifiable were considered for analysis.

Synthetic Myoinhibitory Peptide (synMIP) Application Experiments. Synthetic MIP (synMIP; EPTWNNLKGMW-amide) was custom made by GenScript (Piscataway, NJ, USA) at the highest purity available (>75%). The sequence we chose to use for synMIP is identical to the sequence previous investigations have used when discerning the role of MIP in the *Drosophila* circadian system (Oh et al., 2014). To test how synMIP application adjusts odor-evoked responses, a 1,000μM working solution was made by diluting a small portion of the lyophilized peptide in nuclease-free water (Thermo Scientific, #R0581). After testing the initial odor-evoked responses of the neurons being tested for a given experiment, the perfusion system was switched off momentarily so a small portion of our synMIP working solution could be pressure injected into the AL to a final concentration of 10μM. Ten minutes after synMIP pressure injection, the animal's odor-evoked responses were tested as before synMIP injection, and then the perfusion system was switched back on. Ten minutes after turning the perfusion system back on, the animal's odor-evoked responses were once again tested as they were initially. Re-testing the animal's response to the test odor (10^{-3} 2-heptanone) at the end of these experiments could not be used as a reliable means for assessing prep health due to changes in circuit member responses induced by modulator bath application. Therefore, for these experiments no animal was tested for longer than the average time that animals were reliably healthy in the MIPergic LN odor panel experiments (~90min). Furthermore,

we believe these preparations remain healthy throughout the entire experimental epoch as DM2 ACV responses do not diminish over the course of the experimental epoch. The resulting data were generally analyzed as outlined above, but we modified our procedure for deriving percent ΔF/F such that the average peak response within that given glomerulus to both ACV concentrations before synMIP application was used as the dividend across treatment groups.

Quantification and Statistical Analyses. Statistical analyses were performed using R (v.3.6.2) in R Studio (v.1.4.1103). Values to be analyzed were concatenated in Excel before importing into the relevant analysis software. Statistical results are reported in text and in each figure legend. All statistical tests were two-tailed. The *ClustVis* package was used to hierarchically cluster (using Ward's criteria) and perform PCA on individual MIPergic LN innervation patterns. The "cor" function in the base R *stats* package and the "rcorr" function in the *Hmisc* package were used to calculate statistically significant Pearson's correlation coefficients for MIPergic LN pairwise glomerular innervation patterns. The *ggpubr* package's "ggscatter" function was used to determine Pearson's correlation coefficients and p-values when assessing correlations between: (1) effector/anti-MIP and MIPergic LN mCD8::GFP voxel density across all glomeruli, and (2) MIPergic LN glomerular innervation frequency as a function of each glomerulus' volume. Adjusted R-squared values were calculated using the base-R *stats* package and correspond to how well each data being assessed for the given correlation analysis fit a linear model. The Shapiro-Wilk test was used to evaluate any deviations from a normal distribution. We used an unpaired Student's t-test with Welch's correction to determine if MIPergic LNs preferentially innervate glomeruli based on valence. A Kruskal-Wallis rank sum test followed by a Dunn's test with a Bonferroni multiple comparisons correction was used to determine if: (1) MIPergic LNs preferentially innervate based on the functional group found along the odorant that activates the given glomerulus' OR; and, (2) SPR-GAL4::VP16 expression in antennae and maxillary palps between males, mated females, and virgin females. A one-way ANOVA with a Bonferroni multiple comparisons correction was used to assess statistically significant differences in: (1) SPR-T2A-GAL4 expression in antennae and maxillary palps between males, mated females, and virgin females; and,

(2) SPR-GAL4::VP16 expression in glutamatergic LNs between males, mated females, and virgin females. Delta F/F analyses were carried out using the custom MATLAB scripts previously described (Frank et al., 2015, 2017), and are depicted as mean ± SEM. To assess max response (%ΔF/F) differences between OSN odor-evoked synMIP treatments, we first determined if normality could be assumed (as above), then outliers were determined using the "identify_outliers" function in *rstatix* package. If normality could be assumed and no outliers were present, then an omnibus one-way repeated measures ANOVA with a Greenhouse-Geisser sphericity correction was performed ("anova_test" in *rstatix*). If max responses (%ΔF/F) were statistically different at each odor trial, then pairwise paired t-tests with a Bonferroni multiple comparisons correction were performed to identify which groups were statistically different. If normality could not be assumed, then a Kruskal-Wallis rank sum test followed by a pairwise Mann-Whitney U test with a Bonferroni multiple comparisons adjustment were performed. All boxplots display the minimum, 25^{th}-percentile, median, 75^{th}-percentile, and 'maximum' of the given data. Additional analysis details are provided for each set of experiments above. Values are given as means ± SEM. Statistical significance is defined as $p < 0.05$.

Acknowledgements. We are grateful for the Bloomington Drosophila Stock centers (NIH P40OD018537) and the Janelia Fly Light project for flies. We also would like to thank Shu Kondo, Rachel Wilson, David Krantz, Michael Texada, Jim Truman, and Quentin Gaudry for providing fly stocks. Christian Wegener kindly provided the MIP antibody that was developed by Manfred Eckert. Rachel Wilson and Marco Gallio graciously provided analysis scripts. Marta Costa, Greg Jefferis, and Philipp Schlegel gave helpful advice and instruction regarding connectomic analyses, especially for extracting synapse counts within AL glomeruli. Our connectomic analyses also benefited from discussions in the nat-user community (https://groups.google.com/g/nat-user). Fengqiu Diao gave technical advice for creating the $SPR^{MI13885}$-T2A-LexA::QFAD Trojan exon transgenic animals. Kristyn Lizbinski and James Jeanne graciously provided advice and equipment specifications that lead to the construction and use of the olfactometer system described here. Kristyn Lizbinski, James Jeanne, Gaby Maimon, Marco Gallio, and Mehmet Keles provided invaluable technical advice for performing *in vivo* physiology. Kevin Daly kindly

loaned equipment to us for our purposes and gave invaluable technical advice regarding their use. This work was supported by a Grant-In-Aid of Research (G20141015669888) from Sigma Xi, The Scientific Research Society (T.R.S.), and a National Institutes of Health R01 DC016293 (A.M.D.).

Author Contributions. T.R.S. conceived and implemented all experiments, analyzed the subsequent data, prepared figures, and wrote and edited the manuscript. A.M.D. acquired funding and helped with manuscript edits.

WORKS CITED:

Ambros-Ingerson J, Holmes WR (2005) Analysis and comparison of morphological reconstructions of hippocampal field CA1 pyramidal cells. Hippocampus 15:302–315.

Ameku T, Yoshinari Y, Texada MJ, Kondo S, Amezawa K, Yoshizaki G, Shimada-Niwa Y, Niwa R (2018) Midgut-derived neuropeptide F controls germline stem cell proliferation in a mating-dependent manner. PLOS Biol 16:e2005004.

Ayaz A, Chance FS (2009) Gain modulation of neuronal responses by subtractive and divisive mechanisms of inhibition. J Neurophysiol 101:958–968.

Badel L, Ohta K, Tsuchimoto Y, Kazama H (2016) Decoding of Context-Dependent Olfactory Behavior in Drosophila. Neuron 91:155–167.

Barnes CL, Bonnéry D, Cardona A (2020) Synaptic counts approximate synaptic contact area in Drosophila. bioRxiv:2020.10.09.333187.

Bates AS, Manton JD, Jagannathan SR, Costa M, Schlegel P, Rohlfing T, Jefferis GSXE (2020a) The natverse, a versatile toolbox for combining and analysing neuroanatomical data. Elife 9:1–35.

Bates AS, Schlegel P, Roberts RJ V, Drummond N, Tamimi IFM, Turnbull RG, Zhao X, Marin EC, Popovici PD, Dhawan S, Jamasb AR, Javier A, Li F, Rubin GM, Waddell S, Bock DD, Costa M, Jefferis GSXE (2020b) Complete connectomic reconstruction of olfactory projection neurons in the fly brain. Curr Biol 30:1–17.

Bell JS, Wilson RI (2016) Behavior Reveals Selective Summation and Max Pooling among Olfactory Processing Channels. Neuron 91:425–438.

Bhandawat V, Olsen SR, Gouwens NW, Schlief ML, Wilson RI (2007) Sensory processing in the Drosophila antennal lobe increases reliability and separability of ensemble odor representations. Nat Neurosci 10:1474–1482.

Carlsson M a., Diesner M, Schachtner J, Nässel DR (2010) Multiple neuropeptides in the Drosophila antennal lobe suggest complex modulatory circuits. J Comp Neurol 518:3359–3380.

Carnevale NT, Tsai KY, Claiborne BJ, Brown TH (1997) Comparative electrotonic analysis of three classes of rat hippocampal neurons. J Neurophysiol 78:703–720.

Caron SJC, Ruta V, Abbott LF, Axel R (2013) Random convergence of olfactory inputs in

the Drosophila mushroom body. Nature 497:113–117.

Carrau FM, Medina K, Boido E, Farina L, Gaggero C, Dellacassa E, Versini G, Henschke PA (2005) De novo synthesis of monoterpenes by Saccharomyces cerevisiae wine yeasts. FEMS Microbiol Lett 243:107–115.

Chapman T, Bangham J, Vinti G, Seifried B, Lung O, Wolfner MF, Smith HK, Partridge L (2003) The sex peptide of Drosophila melanogaster: Female post-mating responses analyzed by using RNA interference. Proc Natl Acad Sci U S A 100:9923–9928.

Chiang AS et al. (2011) Three-dimensional reconstruction of brain-wide wiring networks in drosophila at single-cell resolution. Curr Biol 21:1–11.

Chitwood RA, Hubbard A, Jaffe DB (1999) Passive electrotonic properties of rat hippocampal CA3 interneurones. J Physiol 515:743–756.

Chou Y-H, Spletter ML, Yaksi E, Leong JCS, Wilson RI, Luo L (2010) Diversity and wiring variability of olfactory local interneurons in the Drosophila antennal lobe. Nat Neurosci 13:439–449.

Christiaens JF, Franco LM, Cools TL, de Meester L, Michiels J, Wenseleers T, Hassan BA, Yaksi E, Verstrepen KJ (2014) The fungal aroma gene ATF1 promotes dispersal of yeast cells through insect vectors. Cell Rep 9:425–432.

Clements J, Dolafi T, Umayam L, Neubarth N, Berg S, Scheffer L, Plaza S (2020) neuPrint: Analysis Tools for EM Connectomics. bioRxiv:1–20.

Coates KE, Majot AT, Zhang X, Michael CT, Spitzer SL, Gaudry Q, Dacks AM (2017) Identified Serotonergic Modulatory Neurons Have Heterogeneous Synaptic Connectivity within the Olfactory System of *Drosophila*. J Neurosci 37:7318–7331.

Conzelmann M, Offenburger SL, Asadulina A, Keller T, Münch TA, Jékely G (2011) Neuropeptides regulate swimming depth of Platynereis larvae. Proc Natl Acad Sci U S A 108.

Costa M, Manton JD, Ostrovsky AD, Prohaska S, Jefferis GSXE (2016) NBLAST: Rapid, Sensitive Comparison of Neuronal Structure and Construction of Neuron Family Databases. Neuron 91:293–311.

Couto A, Alenius M, Dickson BJ (2005) Molecular , Anatomical , and Functional Organization of the Drosophila Olfactory System. 15:1535–1547.

Croset V, Treiber CD, Waddell S (2018) Cellular diversity in the Drosophila midbrain

revealed by single-cell transcriptomics. Elife 7:1–31.

Dacks AM, Christensen T a., Hildebrand JG (2006) Phylogeny of a Serotonin-Immunoreactive Neuron in the Primary Olfactory Center of the Insect Brain. J Comp Neurol 498:727–746.

Das A, Chiang A, Davla S, Priya R, Reichert H, VijayRaghavan K, Rodrigues V (2011) Identification and analysis of a glutamatergic local interneuron lineage in the adult Drosophila olfactory system. Neural Syst Circuits 1:4.

Daur N, Bryan AS, Garcia VJ, Bucher D (2012) Short-term synaptic plasticity compensates for variability in number of motor neurons at a neuromuscular junction. J Neurosci 32:16007–16017.

Davie K et al. (2018) A Single-Cell Transcriptome Atlas of the Aging Drosophila Brain. Cell:982–998.

De Bono M, Bargmann CI (1998) Natural variation in a neuropeptide Y receptor homolog modifies social behavior and food response in C. elegans. Cell 94:679–689.

Deng B, Li Q, Liu X, Cao Y, Li B, Qian Y, Xu R, Mao R, Zhou E, Zhang W, Huang J, Rao Y (2019) Chemoconnectomics: Mapping Chemical Transmission in Drosophila. Neuron 101:876-893.e4.

Diao F, Ironfield H, Luan H, Diao F, Shropshire WC, Ewer J, Marr E, Potter CJ, Landgraf M, White BH (2015) Plug-and-Play Genetic Access to Drosophila Cell Types using Exchangeable Exon Cassettes. Cell Rep 10:1410–1421.

Díaz MM, Schlichting M, Abruzzi KC, Long X, Rosbash M (2019) Allatostatin-C/AstC-R2 Is a Novel Pathway to Modulate the Circadian Activity Pattern in Drosophila. Curr Biol 29:13-22.e3.

Ding H, Smith RG, Poleg-Polsky A, Diamond JS, Briggman KL (2016) Species-specific wiring for direction selectivity in the mammalian retina. Nature 535:105–110.

Ding K, Han Y, Seid TW, Buser C, Karigo T, Zhang S, Dickman DK, Anderson DJ (2019) Imaging neuropeptide release at synapses with a genetically engineered reporter. Elife 8:1–15.

Donaldson ZR, Nautiyal KM, Ahmari SE, Hen R (2013) Genetic approaches for understanding the role of serotonin receptors in mood and behavior. Curr Opin Neurobiol 23:399–406.

Duvall LB, Ramos-Espiritu L, Barsoum KE, Glickman JF, Vosshall LB (2019) Small-Molecule Agonists of Ae. aegypti Neuropeptide Y Receptor Block Mosquito Biting. Cell 176:687-701.e5.

Ebrahim SAM, Dweck HKM, Stökl J, Hofferberth JE, Trona F, Weniger K, Rybak J, Seki Y, Stensmyr MC, Sachse S, Hansson BS, Knaden M (2015) Drosophila Avoids Parasitoids by Sensing Their Semiochemicals via a Dedicated Olfactory Circuit. PLoS Biol 13:1–18.

Federman C, Ma C, Biswas D (2016) Major components of orange oil inhibit staphylococcus aureus growth and biofilm formation, and alter its virulence factors. J Med Microbiol 65:688–695.

Fişek M, Wilson RI (2014) Stereotyped connectivity and computations in higher-order olfactory neurons. Nat Neurosci 17:280–288.

Fishilevich E, Vosshall LB (2005) Genetic and Functional Subdivision of the Drosophila Antennal Lobe Genetic and Functional Subdivision of the Drosophila Antennal Lobe. Curr Biol 15:1548–1553.

Flanagan D, Mercer AR (1989) Morphology and response characteristics of neurones in the deutocerebrum of the brain in the honeybee Apis mellifera. J Comp Physiol A 164:483–494.

Flavell SW, Raizen DM, You YJ (2020) Behavioral states. Genetics 216:315–332.

Fonta C, Sun XJ, Masson C (1993) Morphology and spatial distribution of bee antennal lobe interneurones responsive to odours. Chem Senses 18:101–119.

Frank DD, Enjin A, Jouandet GC, Zaharieva EE, Para A, Stensmyr MC, Gallio M (2017) Early Integration of Temperature and Humidity Stimuli in the Drosophila Brain. Curr Biol 27:2381-2388.e4.

Frank DD, Jouandet GC, Kearney PJ, MacPherson LJ, Gallio M (2015) Temperature representation in the Drosophila brain. Nature 519:358–361.

Frechter S, Bates AS, Tootoonian S, Dolan MJ, Manton J, Jamasb AR, Kohl J, Bock D, Jefferis G (2019) Functional and anatomical specificity in a higher olfactory centre. Elife 8:1–39.

Freeman MR (2015) Drosophila Central Nervous System Glia.

Galizia CG, Kimmerle B (2004) Physiological and morphological characterization of

honeybee olfactory neurons combining electrophysiology, calcium imaging and confocal microscopy. J Comp Physiol A Neuroethol Sensory, Neural, Behav Physiol 190:21–38.

Gallio M, Ofstad TA, Macpherson LJ, Wang JW, Zuker CS (2011) The coding of temperature in the Drosophila brain. Cell 144:614–624.

Gnerer JP, Venken KJT, Dierick H a. (2015) Gene-specific cell labeling using MiMIC transposons. Nucleic Acids Res:1–13.

Goeritz ML, Bowers MR, Slepian B, Marder E (2013) Neuropilar projections of the anterior gastric receptor neuron in the stomatogastric ganglion of the Jonah crab, Cancer borealis. PLoS One 8:1–15.

Golubovic A, Kuhn A, Williamson M, Kalbacher H, Holstein TW, Grimmelikhuijzen CJP, Gründer S (2007) A peptide-gated ion channel from the freshwater polyp Hydra. J Biol Chem 282:35098–35103.

Goodman CS (1978) Isogenic grasshoppers: Genetic variability in the morphology of identified neurons. J Comp Neurol 182:681–705.

Grabe V, Baschwitz A, Dweck HKM, Lavista-Llanos S, Hansson BS, Sachse S (2016) Elucidating the Neuronal Architecture of Olfactory Glomeruli in the Drosophila Antennal Lobe. Cell Rep 16:3401–3413.

Grabe V, Strutz A, Baschwitz A, Hansson BS, Sachse S (2015) Digital in vivo 3D atlas of the antennal lobe of Drosophila melanogaster. J Comp Neurol 523:530–544.

Gupta A, Wang Y, Markram H (2000) Organizing principles for a diversity of GABAergic interneurons and synapses in the neocortex. Science (80-) 287:273–278.

Habenstein J, Schmitt F, Liessem S, Ly A, Trede D, Wegener C, Predel R, Rössler W, Neupert S (2021) Transcriptomic, peptidomic, and mass spectrometry imaging analysis of the brain in the ant Cataglyphis nodus. J Neurochem:1–22.

Haddad R, Weiss T, Khan R, Nadler B, Mandairon N, Bensafi M, Schneidman E, Sobel N (2010) Global features of neural activity in the olfactory system form a parallel code that predicts olfactory behavior and perception. J Neurosci 30:9017–9026.

Hallem EA, Carlson JR (2006) Coding of Odors by a Receptor Repertoire. Cell 125:143–160.

Hartenstein V (2011) Morphological Diversity and Development of Glia in Drosophila.

1252:1237–1252.

Hasemeyer M, Yapici N, Heberlein U, Dickson BJ (2009) Sensory Neurons in the Drosophila Genital Tract Regulate Female Reproductive Behavior. Neuron:511–518.

Holler S, Köstinger G, Martin KAC, Schuhknecht GFP, Stratford KJ (2021) Structure and function of a neocortical synapse. Nature 591:111–116.

Hong EJ, Wilson RI (2015) Simultaneous Encoding of Odors by Channels with Diverse Sensitivity to Inhibition. Neuron 85:573–589.

Huang J, Zhang W, Qiao W, Hu A, Wang Z (2010) Functional connectivity and selective odor responses of excitatory local interneurons in drosophila antennal lobe. Neuron 67:1021–1033.

Hussain A, Üçpunar HK, Zhang M, Loschek LF, Grunwald Kadow IC (2016) Neuropeptides Modulate Female Chemosensory Processing upon Mating in Drosophila. PLOS Biol 14:e1002455.

Ignell R, Root CM, Birse RT, Wang JW, Nässel DR, Winther AME (2009) Presynaptic peptidergic modulation of olfactory receptor neurons in Drosophila. Proc Natl Acad Sci U S A 106:13070–13075.

Inui A (1999) Feeding and body-weight regulation by hypothalamic neuropeptides - Mediation of the actions of leptin. Trends Neurosci 22:62–67.

Ito K, Shinomiya K, Ito M, Armstrong JD, Boyan G, Hartenstein V, Harzsch S, Heisenberg M, Homberg U, Jenett A, Keshishian H, Restifo LL, Rössler W, Simpson JH, Strausfeld NJ, Strauss R, Vosshall LB (2014) A systematic nomenclature for the insect brain. Neuron 81:755–765.

Jeanne JM, Fis M, Wilson RI, Jeanne JM, Fis M (2018) The Organization of Projections from Olfactory Glomeruli onto Higher-Order Neurons. Neuron:1198–1213.

Jenett A et al. (2012) A GAL4-Driver Line Resource for Drosophila Neurobiology. Cell Rep 2:991–1001.

Jiang H, Lkhagva A, Daubnerová I, Chae HS, Šimo L, Jung SH, Yoon YK, Lee NR, Seong JY, Žitňan D, Park Y, Kim YJ (2013) Natalisin, a tachykinin-like signaling system, regulates sexual activity and fecundity in insects. Proc Natl Acad Sci U S A 110.

Jing J, Vilim FS, Horn CC, Alexeeva V, Hatcher NG, Sasaki K, Yashina I, Zhurov Y, Kupfermann I, Sweedler J V., Weiss KR (2007) From hunger to satiety:

Reconfiguration of a feeding network by Aplysia neuropeptide Y. J Neurosci 27:3490–3502.

Joseph RM, Carlson JR (2015) Drosophila Chemoreceptors: A Molecular Interface Between the Chemical World and the Brain. Trends Genet 31:683–695.

Kass-Simon G, Pierobon P (2007) Cnidarian chemical neurotransmission, an updated overview. Comp Biochem Physiol - A Mol Integr Physiol 146:9–25.

Katow H, Takahashi T, Saito K, Tanimoto H (2019) Tango knock-ins visualize endogenous activity of G protein-coupled receptors in Drosophila Tango knock-ins visualize endogenous activity of G protein-coupled receptors. J Neurogenet 0:1–8.

Katsukura Y, Ando H, David CN, Grimmelikhuijzen CJP, Sugiyama T (2004) Control of planula migration by LWamide and RFamide neuropeptides in Hydractinia echinata. J Exp Biol 207:1803–1810.

Kim SM, Su C-Y, Wang JW (2017) Neuromodulation of Innate Behaviors in Drosophila. Annu Rev Neurosci 40:annurev-neuro-072116-031558.

Kim Y-JY-C, Bartalska K, Audsley N, Yamanaka N, Yapici N, Lee J-Y, Markovic M, Isaac E, Tanaka Y, Dickson BJ (2010) MIPs are ancestral ligands for the sex peptide receptor. Proc Natl Acad Sci 107:6520–6525.

Knaden M, Strutz A, Ahsan J, Sachse S, Hansson BS (2012) Spatial Representation of Odorant Valence in an Insect Brain. Cell Rep 1:392–399.

Ko KI, Root CM, Lindsay SA, Zaninovich OA, Shepherd AK, Wasserman SA, Kim SM, Wang JW (2015) Starvation promotes concerted modulation of appetitive olfactory behavior via parallel neuromodulatory circuits. Elife 4:1–17.

Komiyama T, Johnson WA, Luo L, Jefferis GSXE (2003) From lineage to wiring specificity: POU domain transcription factors control precise connections of Drosophila olfactory projection neurons. Cell 112:157–167.

Komiyama T, Luo L (2007) Intrinsic Control of Precise Dendritic Targeting by an Ensemble of Transcription Factors. Curr Biol 17:278–285.

Kremer MC, Jung C, Batelli S, Rubin GM, Gaul U (2017) The Glia of the Adult Drosophila Nervous System.

Laissue PP, Reiter C, Hiesinger PR, Halter S, Fischbach KF, Stocker RF (1999) Three-dimensional reconstruction of the antennal lobe in Drosophila melanogaster. J Comp

Neurol 405:543–552.

Lee P-T et al. (2018) A gene-specific T2A-GAL4 library for Drosophila. Elife 7:1–24.

Li H, Horns F, Wu B, Luginbuhl DJ, Quake SR, Li H, Horns F, Wu B, Xie Q, Li J, Li T, Luginbuhl DJ, Quake SR (2017) Classifying Drosophila Olfactory Projection Neuron Resource Classifying Drosophila Olfactory Projection Neuron Subtypes by Single-Cell RNA Sequencing. Cell 171:1206-1207.e22.

Liessem S, Kowatschew D, Dippel S, Blanke A, Korsching S, Guschlbauer C, Hooper SL, Predel R, Büschges A (2021) Neuromodulation Can Be Simple: Myoinhibitory Peptide, Contained in Dedicated Regulatory Pathways,Is the Only Neurally-Mediated Peptide Modulator of Stick Insect Leg Muscle. J Neurosci 41:2911–2929.

Lima SQ, Miesenböck G (2005) Remote control of behavior through genetically targeted photostimulation of neurons. Cell 121:141–152.

Linneweber GA, Andriatsilavo M, Dutta SB, Bengochea M, Hellbruegge L, Liu G, Ejsmont RK, Straw AD, Wernet M, Hiesinger PR, Hassan BA (2020) A neurodevelopmental origin of behavioral individuality in the Drosophila visual system. Science (80-) 367:1112–1119.

Liu H, Kubli E (2003) Sex-peptide is the molecular basis of the sperm effect in Drosophila melanogaster. Proc Natl Acad Sci U S A 100:9929–9933.

Liu K, Chen Q, Liu Y, Zhou X, Wang X (2012) Isolation and Biological Activities of Decanal, Linalool, Valencene, and Octanal from Sweet Orange Oil. J Food Sci 77.

Liu WW, Wilson RI (2013) Glutamate is an inhibitory neurotransmitter in the Drosophila olfactory system. Proc Natl Acad Sci 110:10294–10299.

Lizbinski KM, Dacks AM (2018) Intrinsic and Extrinsic Neuromodulation of Olfactory Processing. Front Cell Neurosci 11:1–11.

Lizbinski KM, Marsat G, Dacks AM (2018) Systematic analysis of transmitter coexpression reveals organizing principles of local interneuron heterogeneity. eNeuro 5.

Lyu C, Abbott LF, Maimon G (2020) A neuronal circuit for vector computation builds an allocentric traveling-direction signal in the drosophila fan-shaped body. bioRxiv:2020.12.22.423967.

Maeda T, Nakamura Y, Shiotani H, Hojo MK, Yoshii T, Ida T, Sato T, Yoshida M, Miyazato

M, Kojima M, Ozaki M (2015) Suppressive effects of dRYamides on feeding behavior of the blowfly, Phormia regina. Zool Lett 1:1–10.

Mansourian S, Corcoran J, Enjin A, Löfstedt C, Dacke M, Stensmyr MC (2016) Fecal-Derived Phenol Induces Egg-Laying Aversion in Drosophila. Curr Biol 26:2762–2769.

Mansourian S, Stensmyr MC (2015) The chemical ecology of the fly. Curr Opin Neurobiol 34:95–102.

Marin EC, Büld L, Theiss M, Sarkissian T, Roberts RJV, Turnbull R, Tamimi IFM, Pleijzier MW, Laursen WJ, Drummond N, Schlegel P, Bates AS, Li F, Landgraf M, Costa M, Bock DD, Garrity PA, Jefferis GSXE (2020) Connectomics Analysis Reveals First-, Second-, and Third-Order Thermosensory and Hygrosensory Neurons in the Adult Drosophila Brain. Curr Biol 30:3167-3182.e4.

Markram H, Toledo-Rodriguez M, Wang Y, Gupta A, Silberberg G, Wu C (2004) Interneurons of the neocortical inhibitory system. Nat Rev Neurosci 5:793–807.

Mathew D, Martelli C, Kelley-Swift E, Brusalis C, Gershow M, Samuel ADT, Emonet T, Carlson JR (2013) Functional diversity among sensory receptors in a Drosophila olfactory circuit. Proc Natl Acad Sci U S A 110.

McLaughlin CN, Brbić M, Xie Q, Li T, Horns F, Kolluru SS, Kebschull JM, Vacek D, Xie A, Li J, Jones RC, Leskovec J, Quake SR, Luo L, Li H (2021) Single-cell transcriptomes of developing and adult olfactory receptor neurons in drosophila. Elife 10:1–37.

Meinertzhagen IA (2018) Of what use is connectomics? A personal perspective on the Drosophila connectome. J Exp Biol 221.

Menuz K, Larter NK, Park J, Carlson JR (2014) An RNA-Seq Screen of the Drosophila Antenna Identifies a Transporter Necessary for Ammonia Detection. PLoS Genet 10.

Merighi A (2018) Costorage of high molecular weight neurotransmitters in large dense core vesicles of mammalian neurons. Front Cell Neurosci 12:1–7.

Metsalu T, Vilo J (2015) ClustVis: A web tool for visualizing clustering of multivariate data using Principal Component Analysis and heatmap. Nucleic Acids Res 43:W566–W570.

Min S, Ai M, Shin SA, Suh GSB (2013) Dedicated olfactory neurons mediating attraction

behavior to ammonia and amines in Drosophila. Proc Natl Acad Sci 110:E1321–E1329.

Min S, Chae HS, Jang YH, Choi S, Lee S, Jeong YT, Jones WD, Moon SJ, Kim YJ, Chung J (2016) Identification of a peptidergic pathway critical to satiety responses in drosophila. Curr Biol 26:814–820.

Mohapatra P, Menuz K (2019) Molecular profiling of the Drosophila antenna reveals conserved genes underlying olfaction in insects. G3 Genes, Genomes, Genet 9:3753–3771.

Moroz LL, Romanova DY, Kohn AB (2021) Neural versus alternative integrative systems: Molecular insights into origins of neurotransmitters. Philos Trans R Soc B Biol Sci 376.

Münch D, Galizia CG (2016) DoOR 2.0 - Comprehensive Mapping of Drosophila melanogaster Odorant Responses. Sci Rep 6:1–14.

Nässel DR, Winther ÅME (2010) Drosophila neuropeptides in regulation of physiology and behavior. Prog Neurobiol 92:42–104.

Nässel DR, Zandawala M (2019) Recent advances in neuropeptide signaling in Drosophila, from genes to physiology and behavior. Prog Neurobiol 179:101607.

Nässel DR, Zandawala M, Kawada T, Satake H (2019) Tachykinins: Neuropeptides That Are Ancient, Diverse, Widespread and Functionally Pleiotropic. Front Neurosci 13:1–26.

Nern A, Pfeiffer BD, Rubin GM (2015) Optimized tools for multicolor stochastic labeling reveal diverse stereotyped cell arrangements in the fly visual system. Proc Natl Acad Sci U S A 112:E2967–E2976.

Neupert S, Fusca D, Schachtner J, Kloppenburg P, Predel R (2012) Toward a single-cell-based analysis of neuropeptide expression in Periplaneta americana antennal lobe neurons. J Comp Neurol 520:694–716.

Nicolaï LJJ, Ramaekers A, Raemaekers T, Drozdzecki A, Mauss AS, Yan J, Landgraf M, Annaert W, Hassan B a (2010) Genetically encoded dendritic marker sheds light on neuronal connectivity in Drosophila. Proc Natl Acad Sci U S A 107:20553–20558.

Oh Y, Yoon SE, Zhang Q, Chae HS, Daubnerová I, Shafer OT, Choe J, Kim YJ (2014) A Homeostatic Sleep-Stabilizing Pathway in Drosophila Composed of the Sex Peptide

Receptor and Its Ligand, the Myoinhibitory Peptide. PLoS Biol 12.

Ohno H, Yoshida M, Sato T, Kato J, Miyazato M, Kojima M, Ida T, Iino Y (2017) Luqin-like RYamide peptides regulate food-evoked responses in C. Elegans. Elife 6:1–23.

Okada R, Awasaki T, Ito K (2009) Gamma-aminobutyric acid (GABA)-mediated neural connections in the Drosophila antennal lobe. J Comp Neurol 514:74–91.

Olsen SR, Bhandawat V, Wilson RI (2007) Excitatory Interactions between Olfactory Processing Channels in the Drosophila Antennal Lobe. Neuron 54:89–103.

Otopalik AG, Goeritz ML, Sutton AC, Brookings T, Guerini C, Marder E (2017a) Sloppy morphological tuning in identified neurons of the crustacean stomatogastric ganglion. Elife 6:1–32.

Otopalik AG, Pipkin J, Marder E (2019) Neuronal morphologies built for reliable physiology in a rhythmic motor circuit. Elife 8:1–24.

Otopalik AG, Sutton AC, Banghart M, Marder E (2017b) When complex neuronal structures may not matter. Elife 6:1–29.

Poels J, Van Loy T, Vandersmissen HP, Van Hiel B, Van Soest S, Nachman RJ, Van Den Broeck J (2010) Myoinhibiting peptides are the ancestral ligands of the promiscuous Drosophila sex peptide receptor. Cell Mol Life Sci 67:3511–3522.

Prokop A, Meinertzhagen IA (2006) Development and structure of synaptic contacts in Drosophila. Semin Cell Dev Biol 17:20–30.

Rao S, Lang C, Levitan ES, Deitcher DL (2001) Visualization of neuropeptide expression, transport, and exocytosis in Drosophila melanogaster. J Neurobiol 49:159–172.

Rezával C, Pavlou HJ, Dornan AJ, Chan YB, Kravitz EA, Goodwin SF (2012) Neural circuitry underlying Drosophila female postmating behavioral responses. Curr Biol 22:1155–1165.

Root CM, Ko KI, Jafari A, Wang JW (2011) Presynaptic Facilitation by Neuropeptide Signaling Mediates Odor-Driven Food Search. Cell 145:133–144.

Root CM, Masuyama K, Green DS, Enell LE, Nässel DR, Lee CH, Wang JW (2008) A Presynaptic Gain Control Mechanism Fine-Tunes Olfactory Behavior. Neuron 59:311–321.

Sachse S, Galizia CG (2002) Role of inhibition for temporal and spatial odor representation in olfactory output neurons: A calcium imaging study. J Neurophysiol

87:1106–1117.

Scheffer L et al. (2020) A connectome and analysis of the adult drosophila central brain. Elife:1–83.

Schlegel P, Bates AS, Stürner T, Jagannathan SR, Drummond N, Hsu J, Capdevila LS, Javier A, Marin EC, Barth-Maron A, Tamimi IFM, Li F, Rubin GM, Plaza SM, Costa M, Jefferis G (2021) Information flow, cell types and stereotypy in a full olfactory connectome. Elife.

Schlegel P, Costa M, Jefferis GSXE (2017) Learning from connectomics on the fly. Curr Opin Insect Sci 24:96–105.

Schmidt HR, Benton R (2020) Molecular mechanisms of olfactory detection in insects: Beyond receptors: Insect olfactory detection mechanisms. Open Biol 10.

Schneider-Mizell CM, Gerhard S, Longair M, Kazimiers T, Li F, Zwart MF, Champion A, Midgley FM, Fetter RD, Saalfeld S, Cardona A (2016) Quantitative neuroanatomy for connectomics in Drosophila. Elife 5:1–36.

Seki Y, Rybak J, Wicher D, Sachse S, Hansson BS (2010) Physiological and morphological characterization of local interneurons in the Drosophila antennal lobe. J Neurophysiol 104:1007–1019.

Semmelhack JL, Wang JW (2009) Select Drosophila glomeruli mediate innate olfactory attraction and aversion. Nature 459:218–223.

Sen S, Biagini S, Reichert H, VijayRaghavan K (2014) Orthodenticle is required for the development of olfactory projection neurons and local interneurons in Drosophila. Biol Open 3:711–717.

Shang Y, Claridge-Chang A, Sjulson L, Pypaert M, Miesenböck G (2007) Excitatory Local Circuits and Their Implications for Olfactory Processing in the Fly Antennal Lobe. Cell 128:601–612.

Siju KP, Reifenrath A, Scheiblich H, Neupert S, Predel R, Hansson BS, Schachtner J, Ignell R (2014) Neuropeptides in the antennal lobe of the yellow fever mosquito, Aedes aegypti. J Comp Neurol 522:592–608.

Silbering AF, Okada R, Ito K, Galizia CG (2008) Olfactory information processing in the Drosophila antennal lobe: anything goes? J Neurosci 28:13075–13087.

Sizemore TR, Dacks AM (2016) Serotonergic Modulation Differentially Targets Distinct

Network Elements within the Antennal Lobe of Drosophila melanogaster. Sci Rep 6:37119.

Smith CL, Varoqueaux F, Kittelmann M, Azzam RN, Cooper B, Winters CA, Eitel M, Fasshauer D, Reese TS (2014) Novel cell types, neurosecretory cells, and body plan of the early-diverging metazoan Trichoplax adhaerens. Curr Biol 24:1565–1572.

Sokovicǵ M, Glamočlija J, Marin PD, Brkić D, Van Griensven LJLD (2010) Antibacterial effects of the essential oils of commonly consumed medicinal herbs using an in vitro model. Molecules 15:7532–7546.

Stensmyr MC, Dweck HKM, Farhan A, Ibba I, Strutz A, Mukunda L, Linz J, Grabe V, Steck K, Lavista-Llanos S, Wicher D, Sachse S, Knaden M, Becher PG, Seki Y, Hansson BS (2012) A conserved dedicated olfactory circuit for detecting harmful microbes in drosophila. Cell 151:1345–1357.

Stocker RF, Heimbeck G, Gendre N, de Belle JS (1997) Neuroblast ablation in Drosophila P[GAL4] lines reveals origins of olfactory interneurons. J Neurobiol 32:443–456.

Su CY, Menuz K, Carlson JR (2009) Olfactory Perception: Receptors, Cells, and Circuits. Cell 139:45–59.

Takahashi T, Takeda N (2015) Insight into the molecular and functional diversity of cnidarian neuropeptides. Int J Mol Sci 16:2610–2625.

Tanaka NK, Ito K, Stopfer M (2009) Odor-evoked neural oscillations in Drosophila are mediated by widely branching interneurons. J Neurosci 29:8595–8603.

Task D, Lin C, Afify A, Li H, Vulpe A, Menuz K, Potter CJ (2020) Widespread Polymodal Chemosensory Receptor Expression in Drosophila Olfactory Neurons. BioRxiv:1–37.

Thuma JB, White WE, Hobbs KH, Hooper SL (2009) Pyloric neuron morphology in the stomatogastric ganglion of the lobster, Panulirus interruptus. Brain Behav Evol 73:26–42.

Utz S, Huetteroth W, Wegener C, Kahnt J, Predel R, Schachtner J (2007) Direct Peptide Profiling of Lateral Cell Groups of the Antennal Lobes of Manduca sexta Reveals Specific Composition and Changes in Neuropeptide Expression during Development. Dev Neurobiol 67.

van Breugel F, Huda A, Dickinson MH (2018) Distinct activity-gated pathways mediate attraction and aversion to CO2 in Drosophila. Nature 564:420–424.

van den Pol AN (2012) Neuropeptide Transmission in Brain Circuits. Neuron 76:98–115.

Walker SJ, Corrales-Carvajal VM, Ribeiro C (2015) Postmating Circuitry Modulates Salt Taste Processing to Increase Reproductive Output in Drosophila. Curr Biol 25:2621–2630.

Watanabe H, Fujisawa T, Holstein TW (2009) Cnidarians and the evolutionary origin of the nervous system. Dev Growth Differ 51:167–183.

Weir PT, Henze MJ, Bleul C, Baumann-Klausener F, Labhart T, Dickinson MH (2016) Anatomical reconstruction and functional imaging reveal an ordered array of skylight polarization detectors in drosophila. J Neurosci 36:5397–5404.

Wilson RI (2013) Early Olfactory Processing in Drosophila: Mechanisms and Principles. Annu Rev Neurosci 36:217–241.

Wilson RI, Laurent G (2005) Role of GABAergic inhibition in shaping odor-evoked spatiotemporal patterns in the Drosophila antennal lobe. J Neurosci 25:9069–9079.

Winther ÅME, Acebes A, Ferrús A (2006) Tachykinin-related peptides modulate odor perception and locomotor activity in Drosophila. Mol Cell Neurosci 31:399–406.

Wu Q, Zhao Z, Shen P (2005) Regulation of aversion to noxious food by Drosophila neuropeptide Y- and insulin-like systems. Nat Neurosci 8:1350–1355.

Yaksi E, Wilson RI (2010) Electrical Coupling between Olfactory Glomeruli. Neuron 67:1034–1047.

Yang C-J, Tsai K-T, Liou N-F, Chou Y-H (2019) Interneuron Diversity: Toward a Better Understanding of Interneuron Development In the Olfactory System. J Exp Neurosci 13:117906951982605.

Yang C hui, Rumpf S, Xiang Y, Gordon MD, Song W, Jan LY, Jan YN (2009) Control of the Postmating Behavioral Switch in Drosophila Females by Internal Sensory Neurons. Neuron 61:519–526.

Yapici N, Kim Y-J, Ribeiro C, Dickson BJ (2008) A receptor that mediates the post-mating switch in Drosophila reproductive behaviour. Nature 451:33–37.

Yapici N, Zimmer M, Domingos AI (2014) Cellular and molecular basis of decision-making. EMBO Rep 10:1023–1035.

Zandawala M, Nguyen T, Segura MB, Johard HAD, Amcoff M, Wegener C, Paluzzi JP, Nässel DR (2021) A neuroendocrine pathway modulating osmotic stress in

Drosophila.

Zhang YQ, Rodesch CK, Broadie K (2002) Living synaptic vesicle marker: Synaptotagmin-GFP. Genesis 34:142–145.

Zhu H, Hummel T, Clemens JC, Berdnik D, Zipursky SL, Luo L (2006) Dendritic patterning by Dscam and synaptic partner matching in the Drosophila antennal lobe. Nat Neurosci 9:349–355.

Zieger E, Robert NSM, Calcino A, Wanninger A (2021) Ancestral Role of Ecdysis-Related Neuropeptides in Animal Life Cycle Transitions. Curr Biol 31:1–7.

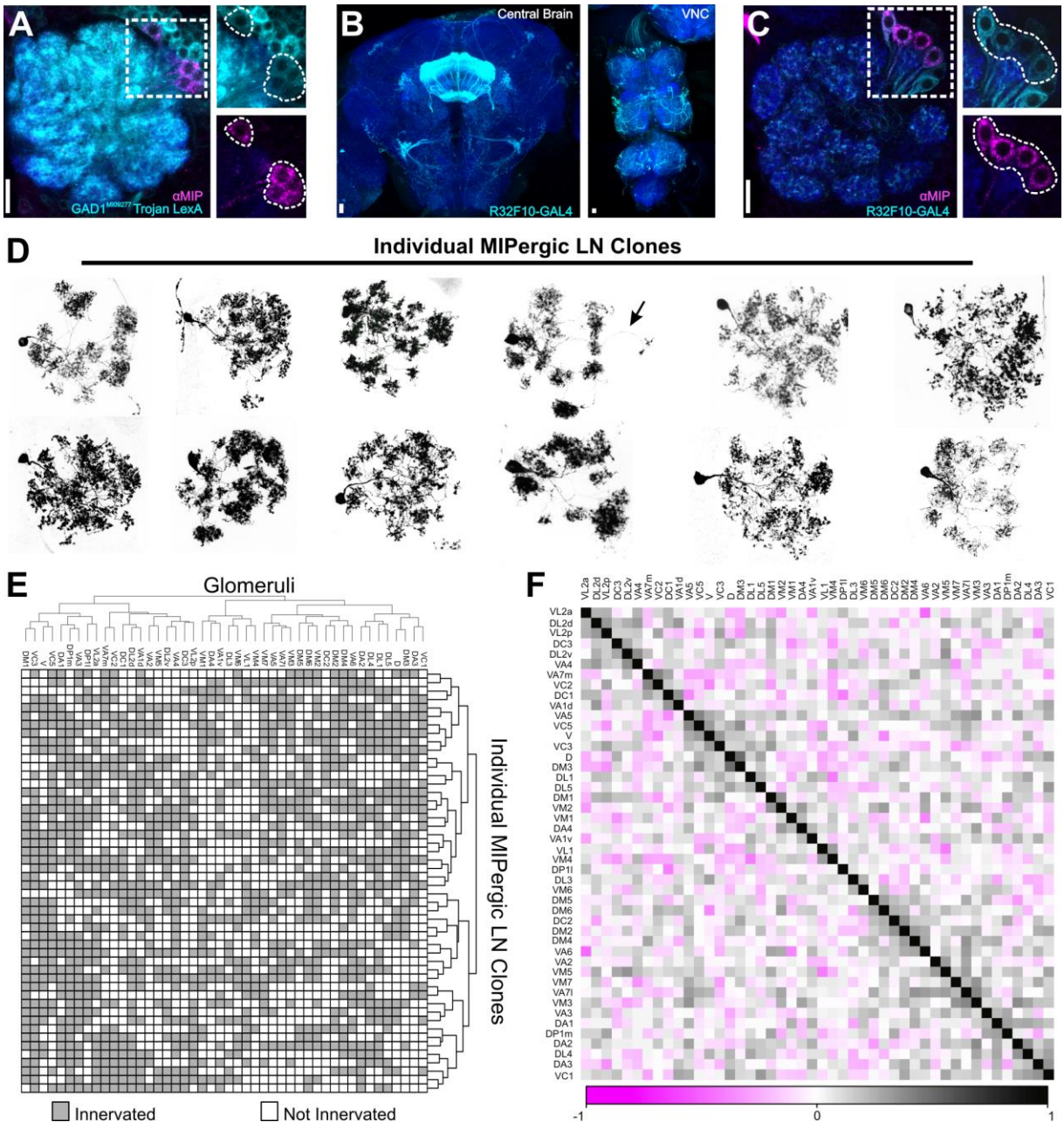

Figure 1. Myoinhibitory peptide is released by GABAergic patchy LNs in the AL.
(A) A protein-trap Trojan LexA driver for glutamic acid decarboxylase (GAD1), the rate-limiting enzyme for GABA, highlights all myoinhibitory peptide (MIP) immunoreactive neurons in the AL. Cell count estimates, n = 5 brains, 10 ALs.
(B) R32F10-GAL4 expression in the central brain and ventral nerve cord (VNC).
(C) R32F10-GAL4 highlights ~13.2 (±0.68) AL neurons, which includes all MIP immunoreactive neurons (~8.7±0.3 neurons) and ~4.5 (±0.68) non-MIPergic LNs. Cell count estimates, n = 5 brains, 9 ALs.
(D) Representative individual MIPergic LNs reveals MIP is released by patchy LNs. Arrow indicates a projection into the contralateral AL.
(E) Glomerular innervation patterns of 50 individual MIPergic LN clones organized by

hierarchical clustering similarity. Each row represents the innervation pattern of a single clone, and each column represents a given glomerulus. Although it is not explicitly highlighted here, glomeruli do not cluster by “odor scene” as previously defined (Bates et al., 2020). We note that in some cases a given clone might project into the contralateral AL, but here only the ipsilateral innervation patterns were included for analysis.
(F) All pairwise correlations of MIPergic LN innervation patterns between AL glomeruli. Values correspond to the Pearson’s correlation coefficient.
In all cases: neuropil was delineated by anti-DN-Cadherin staining; scale bars = 10um.

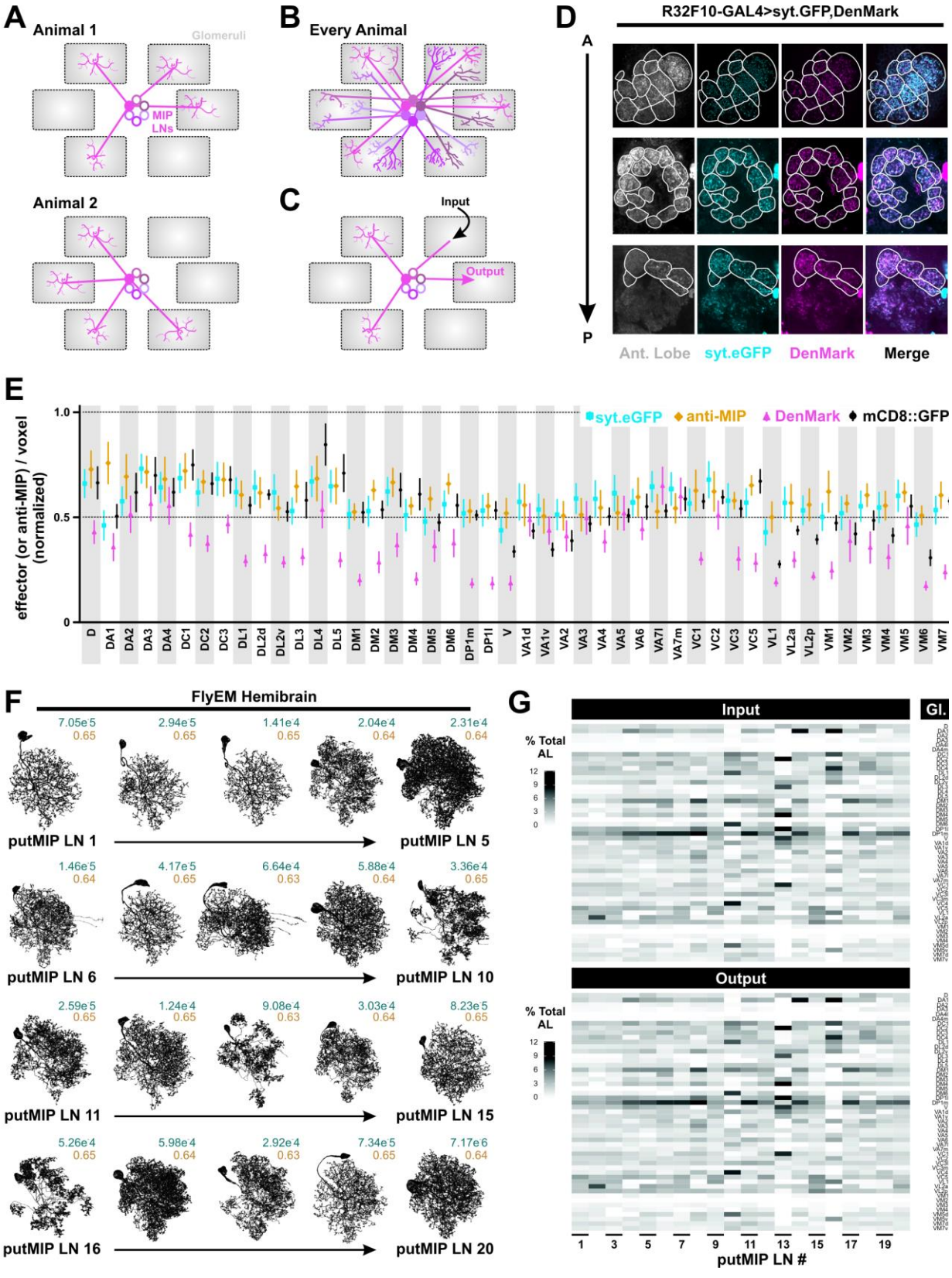
A
Animal 1
Glomeruli
MIP LNs
Animal 2
B
Every Animal
C
Input
Output
D
R32F10-GAL4>syt.GFP,DenMark
A
P
Ant. Lobe
syt.eGFP
DenMark
Merge
E
syt.eGFP
anti-MIP
DenMark
mCD8::GFP
effector (or anti-MIP) / voxel (normalized)
1.0
0.5
0
D DA1 DA2 DA3 DA4 DC1 DC2 DC3 DL1 DL2d DL2v DL3 DL4 DL5 DM1 DM2 DM3 DM4 DM5 DM6 DP1m DP1l V VA1d VA1v VA2 VA3 VA4 VA5 VA6 VA7l VA7m VC1 VC2 VC3 VC5 VL1 VL2a VL2p VM1 VM2 VM3 VM4 VM5 VM6 VM7
F
FlyEM Hemibrain
7.05e-5 0.65
2.94e-5 0.65
1.41e-4 0.65
2.04e-4 0.64
2.31e-4 0.64
putMIP LN 1
putMIP LN 5
1.46e-5 0.64
4.17e-5 0.65
6.64e-4 0.63
5.88e-4 0.64
3.36e-4 0.65
putMIP LN 6
putMIP LN 10
2.59e-5 0.65
1.24e-4 0.65
9.08e-4 0.63
3.03e-4 0.64
8.23e-5 0.65
putMIP LN 11
putMIP LN 15
5.26e-4 0.65
5.98e-4 0.64
2.92e-4 0.63
7.34e-5 0.65
7.17e-6 0.64
putMIP LN 16
putMIP LN 20
G
Input
Output
% Total AL
12
9
6
3
0
Gl.
1 3 5 7 9 11 13 15 17 19
putMIP LN #

Figure 2. MIPergic LNs integrate and dispense signaling throughout the entire AL.
(A) Individual MIPergic LNs project to different glomeruli from animal-to-animal.
(B) The MIPergic LN ensemble covers the entire AL in every animal.
(C) Do MIPergic LNs receive input from particular sets of glomeruli? Are there particular sets of glomeruli subject to more/less MIPergic LN output than others?
(D) Representative image of glomerular voxel density analysis. Here, the effectors synaptotagmin.eGFP (syt.eGFP; cyan) and DenMark (magenta) are expressed in all MIPergic LNs, and the antennal lobe glomeruli (Ant. Lobe; grey) are delineated by anti-DN-Cadherin immunostaining (**see Methods**). Glomeruli outlined in white.
(E) Effector (e.g., syt.eGFP, DenMark, or mCD8::GFP) or anti-myoinhibitory peptide (anti-MIP; orange) puncta density per voxel within each AL glomerulus. Each indicator is normalized to the highest value within that indicator. Data are represented as the mean ± SEM of each indicator's voxel density being measured within a given glomerulus. For each indicator, n = 7 (syt.eGFP), 7 (DenMark), 4 (mCD8::GFP), 4 (anti-MIP).
(F) Putative MIPergic LN mesh skeletons identified from the FlyEM FIB-SEM hemibrain connectome volume. Values in the upper right-hand corner of each mesh skeleton are that neuron's synaptic flow centrality index (blue-green) and GMR32F10-GAL4 NBLAST similarity score (light brown).
(G) Putative MIPergic LN postsynaptic and presynaptic sites across all AL glomeruli represented as a function of the total number of postsynaptic/presynaptic sites in each putMIP LN. These data only consider putMIP LN connections within the ipsilateral AL.

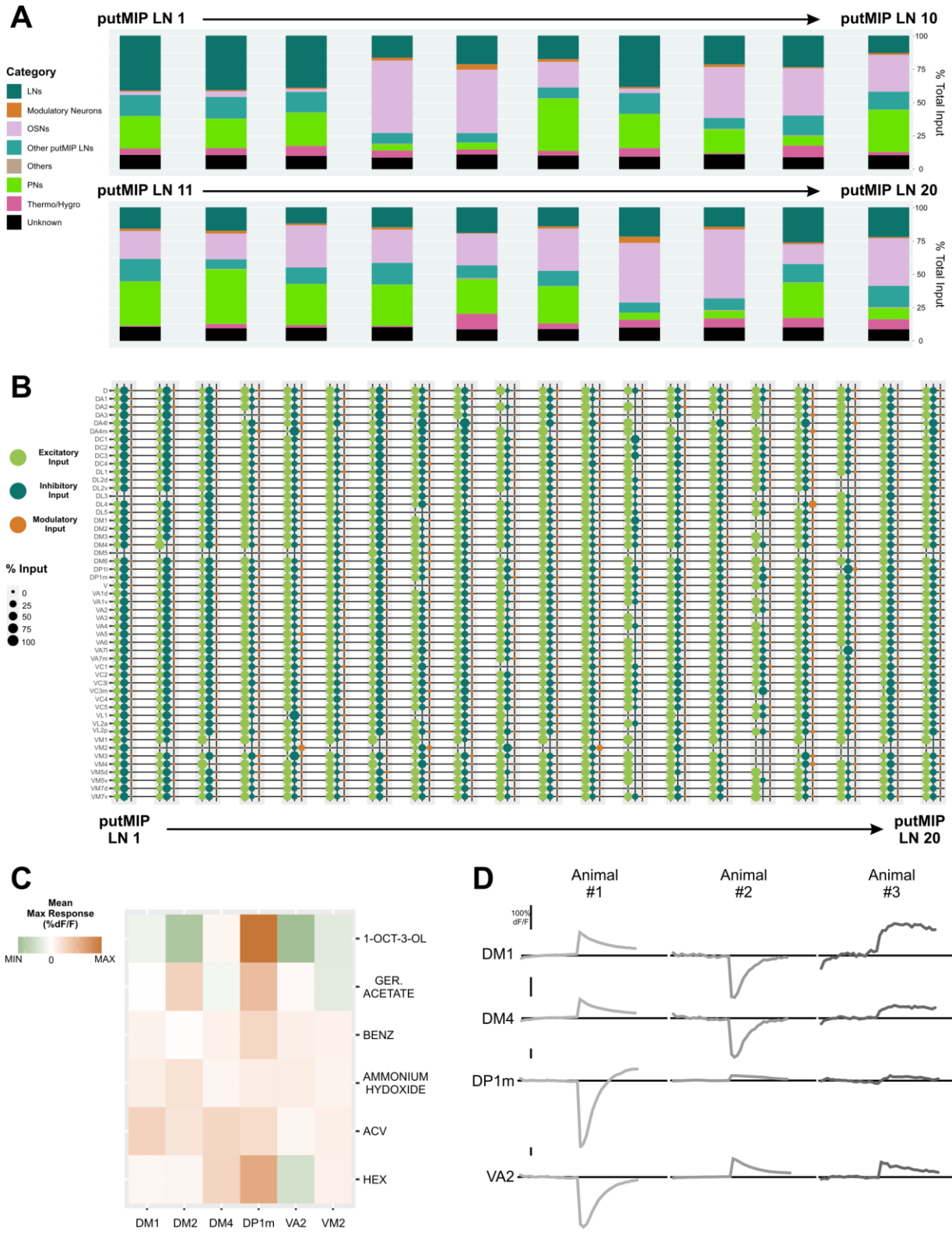
A
putMIP LN 1
putMIP LN 10
putMIP LN 11
putMIP LN 20
Category
LNs
Modulatory Neurons
OSNs
Other putMIP LNs
Others
PNs
Thermo/Hygro
Unknown
% Total Input
B
Excitatory Input
Inhibitory Input
Modulatory Input
% Input
putMIP LN 1
putMIP LN 20
C
Mean Max Response (%dF/F)
MIN
0
MAX
1-OCT-3-OL
GER. ACETATE
BENZ
AMMONIUM HYDOXIDE
ACV
HEX
DM1
DM2
DM4
DP1m
VA2
VM2
D
Animal #1
Animal #2
Animal #3
100% dF/F
DM1
DM4
DP1m
VA2

Figure 3. Anatomical inputs to putMIP LNs and functional glomerular outputs from identified MIPergic LNs.
(A) Putative MIPergic LN upstream partners' demographics. Data are represented as a function of the total amount of input a putMIP LN receives from all categories.
(B) The amount of excitatory, inhibitory, and modulatory inputs each putMIP LN receives within every glomerulus as a function of the total amount of inputs a given putMIP LN receives within the glomerulus.
(C) Mean max responses (%ΔF/F) of MIPergic LN neurites in DM1, DM2, DM4, DP1m, VA2, and VM2 in response to 1-hexanol (HEX), apple cider vinegar (ACV), ammonium hydroxide, benzaldehyde (BENZ), geranyl acetate (GER. ACETATE), and 1-octen-3-ol. Data are represented as the average max %ΔF/F over many animals and several odor trials within each animal (4 trials). For each stimulus, n = 3-4 animals.
(D) Example traces of animal-to-animal variability in MIPergic LN glomerular responses to 10^{-2} ammonium hydroxide. Each column represents three distinct animals, each row corresponds to the glomerulus where GCaMP activity in MIPergic LN processes is being measured, and each trace represents the within-animal response to the odor (the average of 4 odor trials). For each glomerular response, scale bar = 100%ΔF/F.

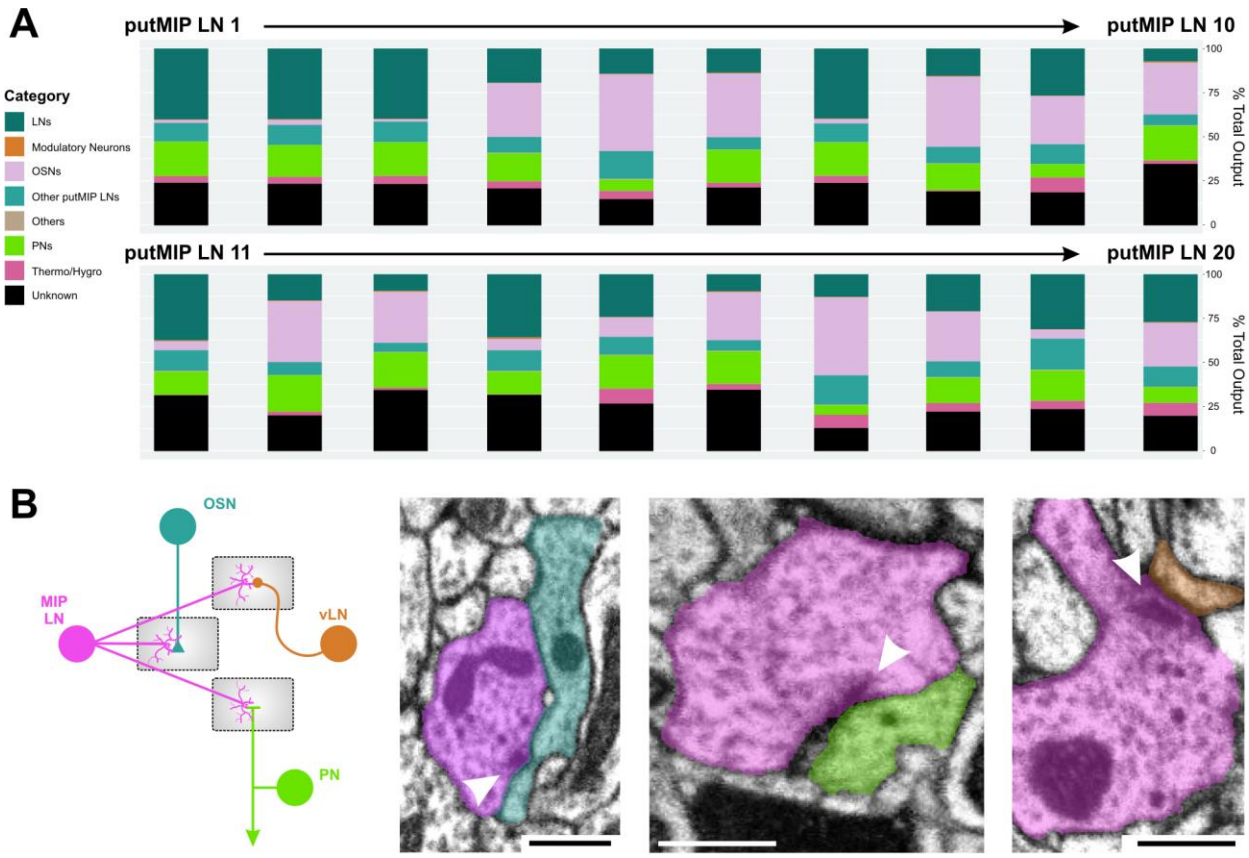

Figure 4. Downstream postsynaptic targets of each putMIP LN and representative putMIP LN presynaptic terminals with dense core vesicles (DCVs).
(A) Demographics analysis of all putMIP LN postsynaptic targets by neuron type. Data are represented as a function of the total amount of output a putMIP LN sends to all categories.
(B) Representative images of DCVs present in a given putMIP LN's presynaptic terminal. From left to right: DCVs are found in putMIP LN presynaptic terminals upstream of OSNs (blue), PNs (green), and ventral LNs (vLN; orange). These particular examples include putMIP LNs 6, 14, and 19 with a DM1 OSN (blue) and a DC4 anterodorsal PN (green).
In all cases: white arrowheads indicate the putMIP LN's presynaptic site; scale bars = 500nm.

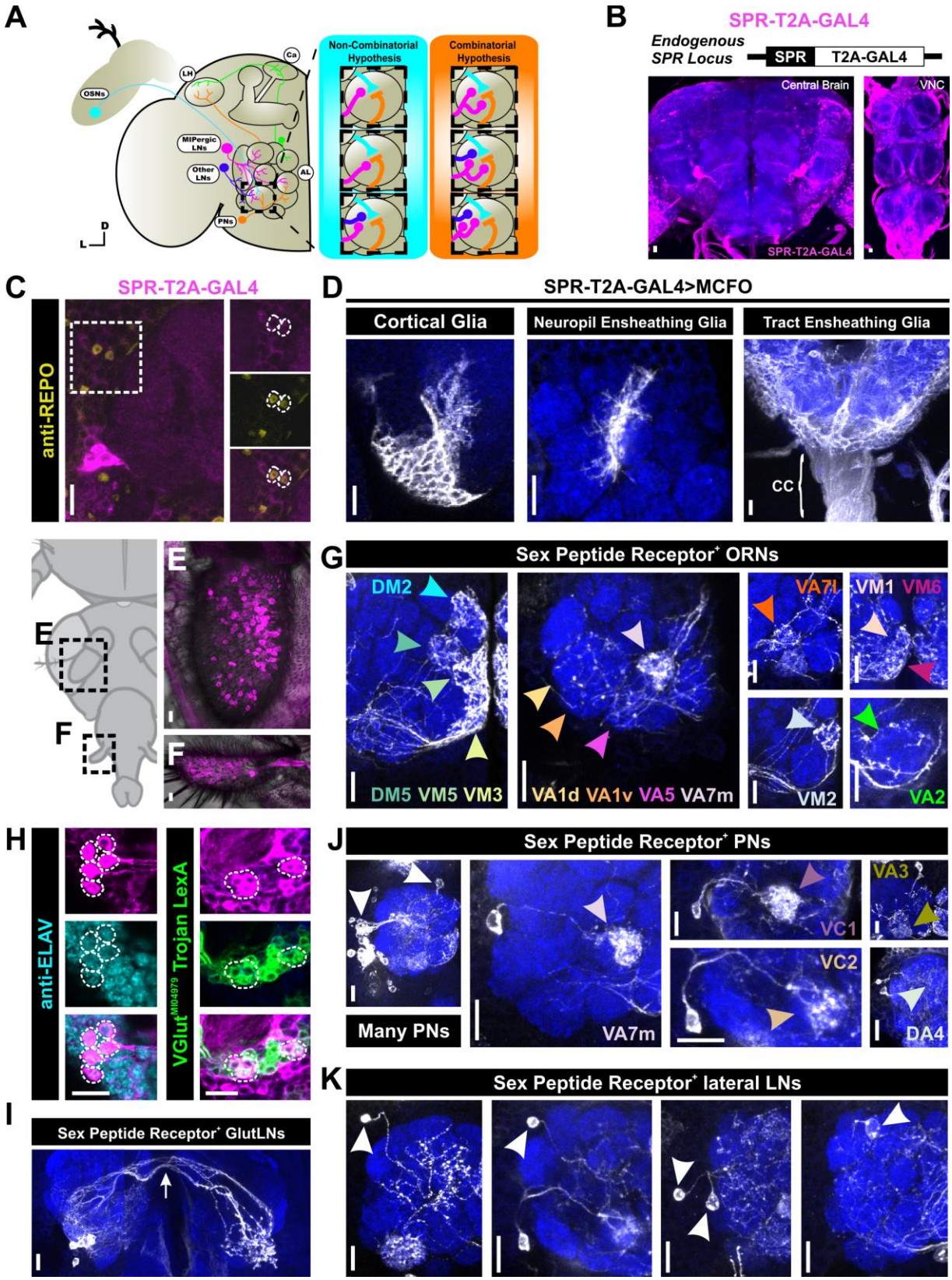
A
OSNs
LH
Ca
MIPergic LNs
Other LNs
AL
PNs
D
L
Non-Combinatorial Hypothesis
Combinatorial Hypothesis
B
SPR-T2A-GAL4
Endogenous SPR Locus
SPR
T2A-GAL4
Central Brain
VNC
SPR-T2A-GAL4
C
SPR-T2A-GAL4
anti-REPO
D
SPR-T2A-GAL4>MCFO
Cortical Glia
Neuropil Ensheathing Glia
Tract Ensheathing Glia
CC
E
F
G
Sex Peptide Receptor+ ORNs
DM2
DM5 VM5 VM3
VA1d VA1v VA5 VA7m
VA7l
VM1 VM6
VM2
VA2
H
anti-ELAV
VGlut MI04979 Trojan LexA
J
Sex Peptide Receptor+ PNs
Many PNs
VA7m
VC1
VA3
VC2
DA4
K
Sex Peptide Receptor+ lateral LNs
I
Sex Peptide Receptor+ GlutLNs

Figure 5. Widespread sex peptide receptor (SPR) expression throughout the AL.
(A) MIPergic LNs form synaptic connections with all principal neuron types in the AL; OSNs (cyan), PNs (orange and green), and other LNs (blue). Therefore, within a single glomerulus, MIPergic modulation might target any one of these neuron types (so called, "Non-combinatorial Hypothesis"), or multiple neuron types ("Combinatorial Hypothesis").
(B) Sex peptide receptor expression (magenta) as revealed using a CRISPR/Cas9 T2A-GAL4 insertion in the SPR coding intron.
(C) SPR-T2A-GAL4 colocalizes with the general glial marker *reverse polarity* (anti-REPO; yellow).
(D) MCFO labeling using the SPR-T2A-GAL4 reveals expression in several glial subtypes, including cortical, neuropil ensheathing, and tract ensheathing glia.
(E & F) SPR-T2A-GAL4 expression in OSNs housed in the third-antennal segment and maxillary palp.
(G) SPR-T2A-GAL4 MCFO experiments where the antennal nerve remains intact reveals SPR-expressing OSNs include those that belong to: DM2, DM5, VM5v, VM5d, VM3, VA1d, VA1v, VA5, VA7m, VA7l, VM1, VM6, VM2, and VA2.
(H) SPR-T2A-GAL4 colocalizes with several neurons immunopositive for the proneural marker *embryonic lethal abnormal vision* (anti-ELAV; cyan), a subset of which is also positive for the glutamate marker, $VGlut^{MI04979}$ Trojan LexA (green).
(I) SPR-T2A-GAL4 MCFO experiments reveal SPR-expression in bilaterally-projecting ventral glutamatergic LNs (GlutLNs). Bilateral projection indicated by the white arrow.
(J) SPR-T2A-GAL4 MCFO labeling reveals SPR-expression in several lateral and anterodorsal PNs (white arrowheads), some of which were identifiable as belonging to: VA7l, VC1, VC2, VA3, and DA4.
(K) Several (at least ~5) lateral LNs express SPR as identified through SPR-T2A-GAL4 MCFO labeling.
In all cases: neuropil was delineated by anti-DN-Cadherin staining; scale bars = 10um.

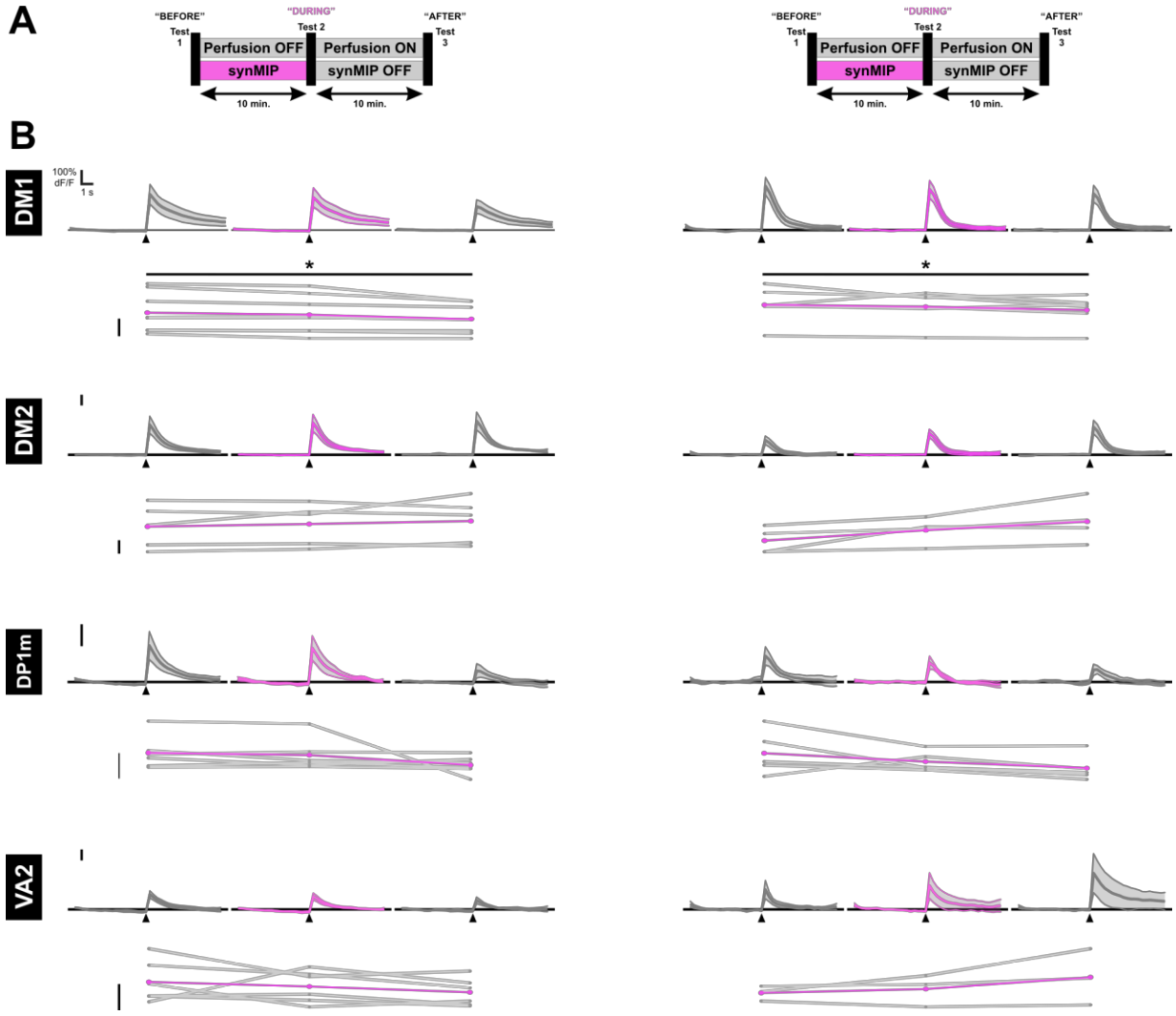

Figure 6. Myoinhibitory peptide reduce OSN responses to apple cider vinegar (ACV).

(A) OSN responses are initially tested under constant perfusion (Test 1; "BEFORE"), then the perfusion system is shut off and synthetic MIP (synMIP) is pressure injected into the AL. After a 10min incubation period, OSN responses are tested again (Test 2; "DURING"), after which the perfusion system is turned back on. OSN responses are tested once more after a 10min washout period (Test 3; "AFTER").

(B) DM1, DM2, DP1m, and VA2 OSN responses (mean ± SEM) to 10^{-2} (left column) and 10^{-6} (right column) ACV before 10um synMIP application (most left traces in each column), 10min after 10um synMIP pressure injection (middle trace in each column), and after a 10min washout epoch (far right trace in each column). Synthetic MIP significantly decreases DM1 OSN responses independent of ACV concentration (black bars; 10^{-2}: p = 0.040, n = 8, BEFORE v. AFTER; 10^{-6}: p = 0.048, n = 6, BEFORE v. AFTER; Bonferroni-corrected repeated-measures pairwise t-tests).

For **B**: 10^{-2}: n = 8 (DM1), 5 (DM2), 6 (DP1m), 6 (VA2); 10^{-6}: n = 6 (DM1), 4 (DM2), 5 (DP1m), 3 (VA2).

In all cases: Traces represent mean ± SEM of the data; scale bars = 100%ΔF/F; repeated measures scatter plot represents each animal's max response (%ΔF/F; black dots) connected across treatments (black lines), and the mean of each test's max response (%ΔF/F) across all animals (magenta dots and lines).

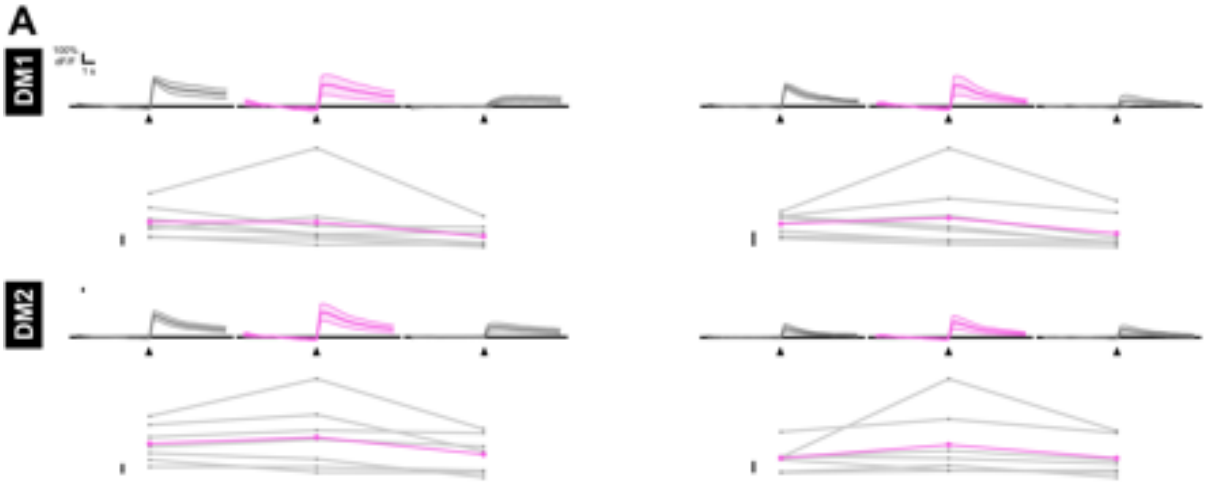

(A) OSN-directed SPR knockdown relieves the effect of synMIP on DM1 and DM2 OSN odor-evoked responses (DM1: 10^{-2}: p = 0.11, n = 7; repeated-measures one-way ANOVA; 10^{-6}: p = 0.06, n = 4, before v. during; p = 0.156, n = 8, before v. after; Bonferroni-corrected repeated-measures pairwise Wilcoxon tests; DM2: 10^{-2}: p = 0.678, before v. during; p = 0.102, before v. after, n = 7; Bonferroni-corrected repeated measures pairwise t-tests; 10^{-6}: p = 0.201, n = 7; repeated-measures one-way ANOVA). For **A**: 10^{-2}: n = 7 (DM1), 7 (DM2); 10^{-6}: n = 8 (DM1), 7 (DM2).

In all cases: Traces represent mean ± SEM of the data; scale bars = 100%ΔF/F; repeated measures scatter plot represents each animal's max response (%ΔF/F; black dots) connected across treatments (black lines), and the mean of each test's max response (%ΔF/F) across all animals (magenta dots and lines).

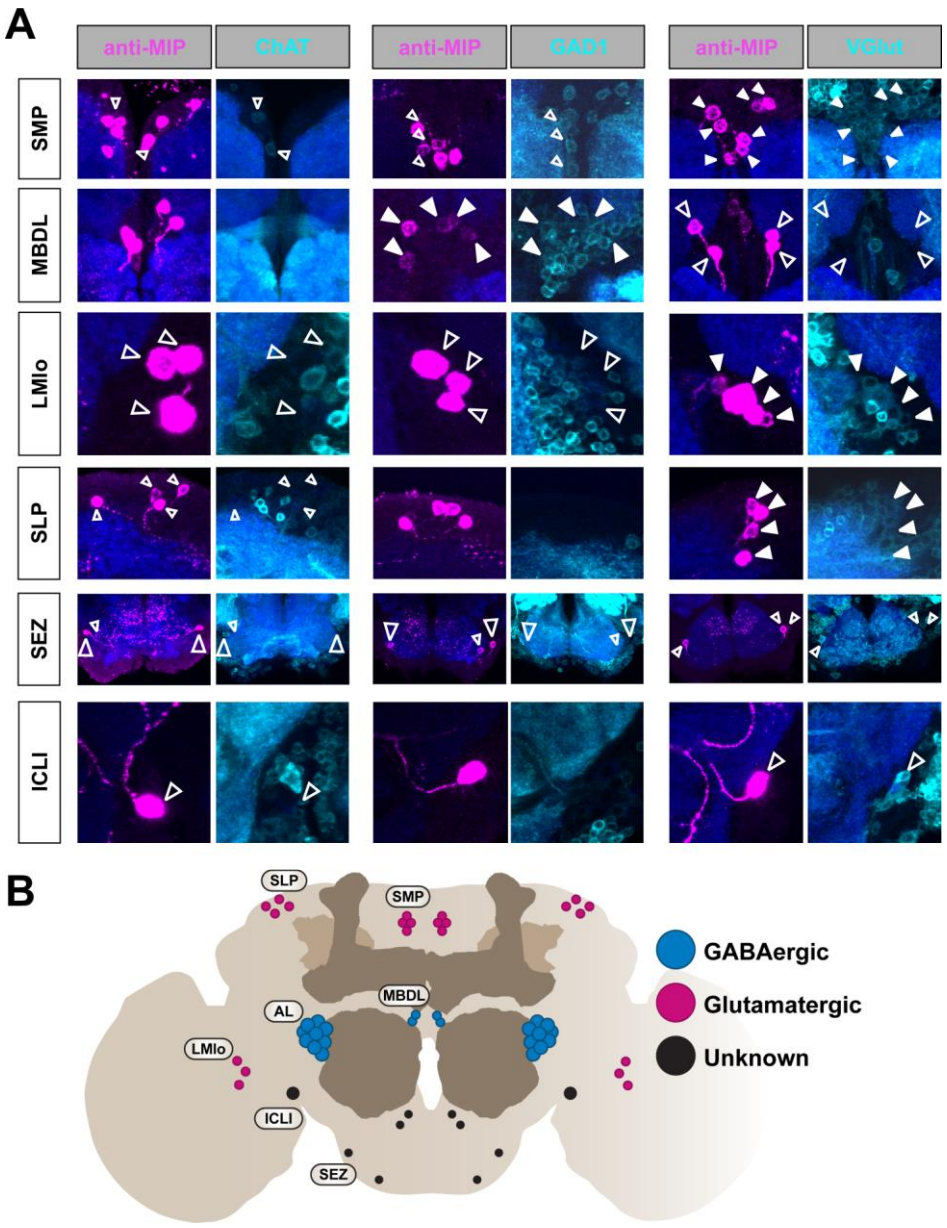

Figure S1. Myoinhibitory peptide (MIP) colabeling with transgenic markers for GABAergic, cholinergic, and glutamatergic neurons in the *Drosophila* central brain.

(A) MIPergic neurons in the antennal lobe (AL) (**see Figure 1**) and near the median bundle (MBDL) colabel with glutamic acid decarboxylase 1 (GAD1). MIPergic neurons in the superior medial and lateral protocerebrum (SMP and SLP, respectively) and near the lateral medial lobula (LMlo) colabel with vesicular glutamate transporter (VGlut). MIPergic neurons within the inferior contralateral interneuron cluster (ICLI) (Jiang et al., 2013) and SEZ do not colabel for ChAT, GAD1, or VGlut, and are most likely tyraminergic (Tyr) based on scRNA-seq data (Croset et al., 2018).

(B) Cartoon schematic summarizing data from **A**, wherein several populations of MIP-immunoreactive neurons are also glutamatergic (MIP^+-$VGlut^+$ neurons in the SMP, LMlo, and SLP; magenta), two populations are also GABAergic (MIP^+-$GAD1^+$ neurons

in the MBDL and AL) (**see also Figure 1**), and no MIP-immunoreactive neurons are cholinergic (colabel with ChAT).
Except for the ICLI interneurons, soma locations are labeled according to the closest neuropil, or fascicle, according to established nomenclature (Ito et al., 2014).
In all cases: neuropil was delineated by anti-DN-cadherin staining; open arrowheads = no colocalization; closed arrowheads = colocalization.

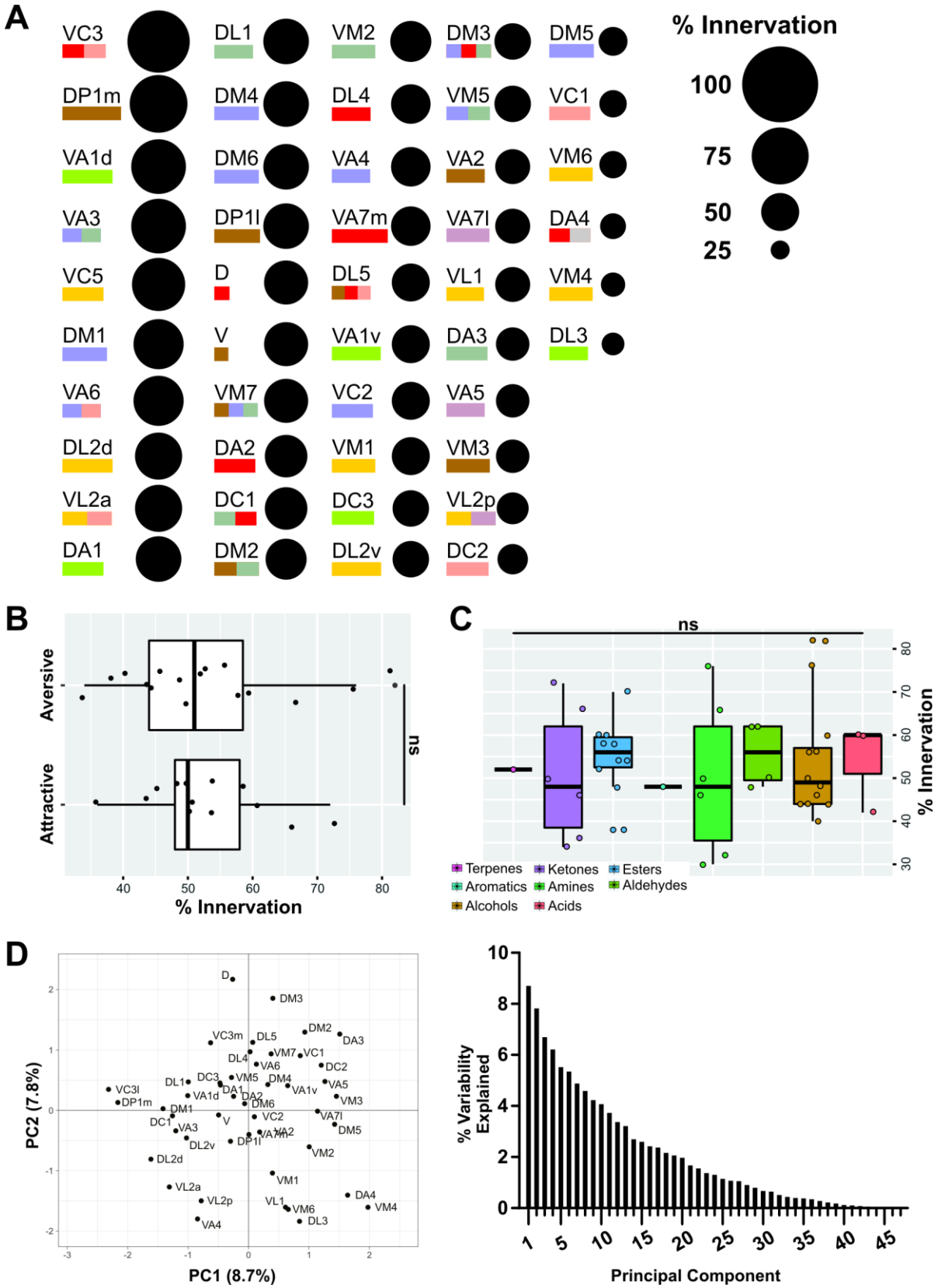

Supplementary Figure 2. MIPergic LNs do not preferentially innervate olfactory glomeruli based on odor-evoked behavioral valence, nor the odor-tuning

properties of a given glomeruli's olfactory receptor neuron(s).
(A) Dot plot representation of the frequency we find a given glomerulus is innervated by a single MIPergic LN clone. Rectangles underneath each glomerulus' name represents the "odor scene" of that glomerulus (Bates et al., 2020). These are: alcoholic fermentation (brown); yeasty (blue); fruity (faded green); decaying fruit (yellow); plant matter (pink); animal matter (pale purple); pheromones (chartreuse); dangerous (red); and, unknown (gray).
(B) MIPergic LNs do not preferentially innervate glomeruli whose activity has been linked to attractive or aversive behavioral responses ($p = 0.991$, $n = 13$ ("attractive"), 16 ("aversive"), unpaired t-test with Welch's correction).
(C) MIPergic LNs do not preferentially innervate glomeruli tuned to any particular odorant molecules ($p = 0.9455$, Bonferroni-corrected Dunn's test). Odorant molecule functional groups are color coded as follows: terpenes (magenta), ketones (purple), esters (blue), aromatics (aqua marine), amines (chartreuse), aldehydes (green), alcohols (brown), and acids (deep pink).
(D) Principal components analysis of MIPergic LN innervation patterns, where each data point represents MIPergic LN innervation patterns for each glomerulus. Bar graph represents the percentage of the variance explained by each principal component.
In all cases, boxplots display the minimum, 25^{th}-percentile, median, 75^{th}-percentile, and 'maximum' of the given data.

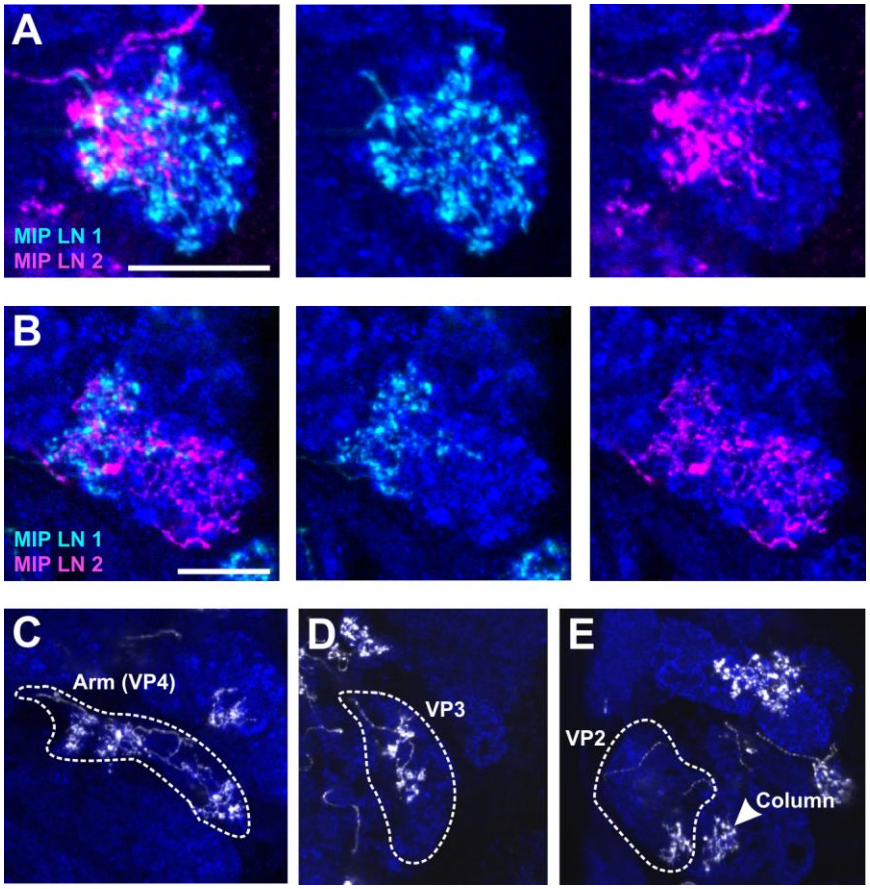

Supplementary Figure 3. MIPergic LNs co-innervate olfactory glomeruli and individual MIPergic LNs innervate thermo-/hygrosensory glomeruli, suggesting thermal and hygrosensory signals may integrate with olfactory signals in the antennal lobe.

(A-B) On average, ~12 glomeruli are co-innervated by sister MIPergic LN clones. In these examples, two distinct MIPergic LNs co-innervate DL2d and DP1l (respectively). For comparing sister MIPergic LN co-innervation patterns, n = 5 brains.

(C) Single MIPergic LN branching in the dry-responsive glomerulus VP4 (formerly, “the arm”; hatched outline).

(D) Neurites of a single MIPergic LN innervating the cold-responsive VP3 glomerulus (hatched outline).

(E) An individual MIPergic LN innervating both the hot-responsive VP2 glomerulus (hatched outline) and the column (arrowhead).

In all cases: neuropil was delineated by anti-DN-Cadherin staining; all scale bars = 10um.

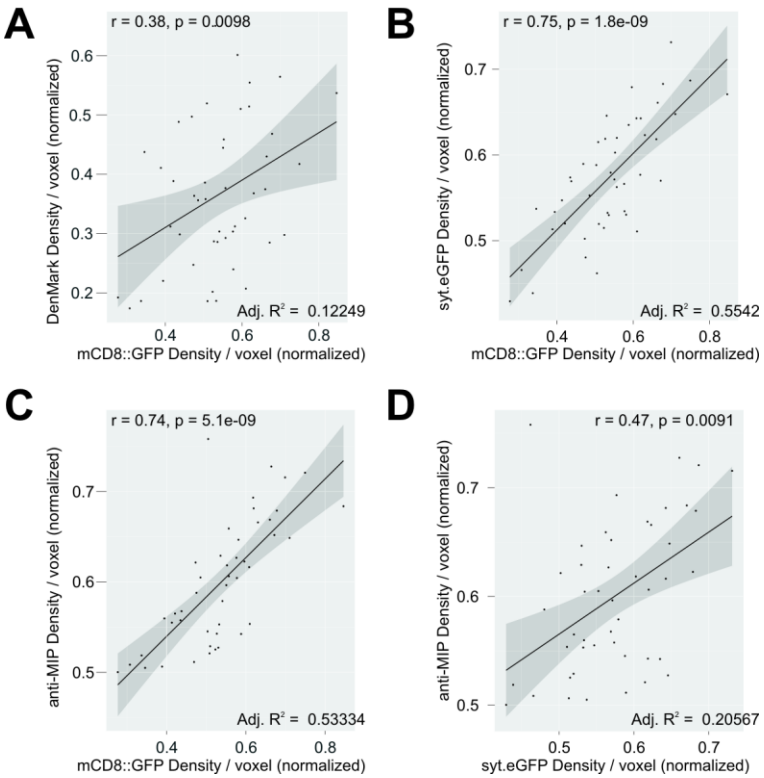

Supplementary Figure 4. The voxel density of synaptic polarity markers expressed in MIPergic LNs generally scales with the voxel density of total MIPergic LN cable within glomeruli.

(A) DenMark (a postsynaptic marker) voxel density variations across glomeruli are significantly weakly correlated to the voxel density of total MIPergic LN cable within each glomerulus ($r = 0.38$, $p = 0.0098$). However, variations in DenMark voxel density across glomeruli do not correlate (adjusted $R^2 = 0.12249$).

(B) Synaptotagmin-eGFP (a presynaptic marker) voxel density variations across glomeruli are significantly strongly correlated to the voxel density of total MIPergic LN cable within each glomerulus ($r = 0.75$, $p = 1.8 \times 10^{-9}$).

(C) The voxel density of anti-myoinhibitory peptide immunoreactive punctate (anti-MIP) is significantly correlated with the voxel density of total MIPergic LN neurite volume ($r = 0.74$, $p = 5.1 \times 10^{-9}$).

(D) The density of syt.eGFP in MIPergic LNs significantly scales with anti-MIP density ($p = 0.0091$), but variations across glomeruli do not correlate (adjusted $R^2 = 0.20567$).

In all cases, each data point represents the normalized mean for indicator density within each glomerulus and each line represents the linear regression model.

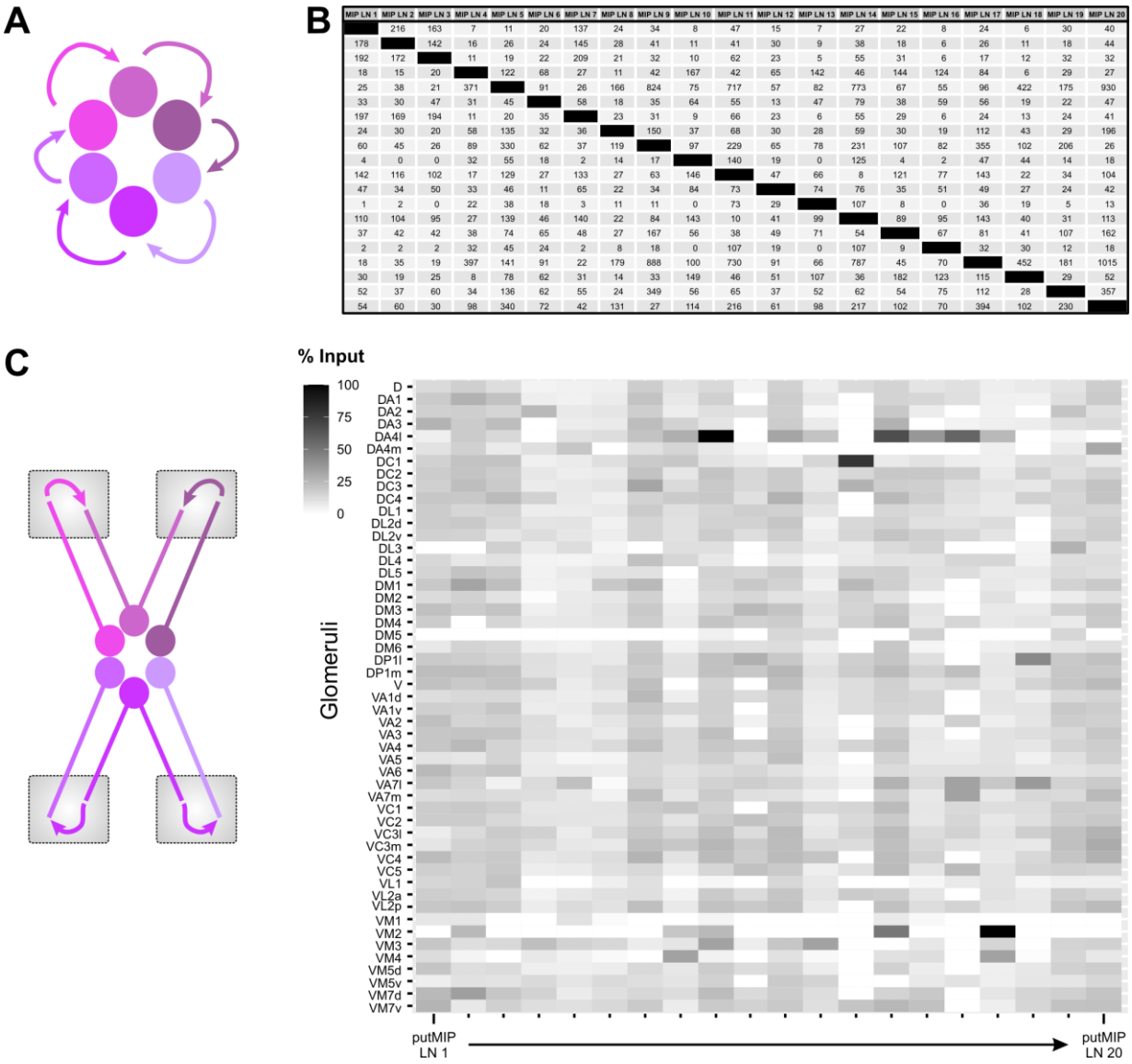

MIP LN 1	MIP LN 2	MIP LN 3	MIP LN 4	MIP LN 5	MIP LN 6	MIP LN 7	MIP LN 8	MIP LN 9	MIP LN 10	MIP LN 11	MIP LN 12	MIP LN 13	MIP LN 14	MIP LN 15	MIP LN 16	MIP LN 17	MIP LN 18	MIP LN 19	MIP LN 20
	216	163	7	11	20	137	24	34	8	47	15	7	27	22	8	24	6	30	40
178		142	16	26	24	145	28	41	11	41	30	9	38	18	6	26	11	18	44
192	172		11	19	22	209	21	32	10	62	23	5	55	31	6	17	12	32	32
18	15	20		122	68	27	11	42	167	42	65	142	46	144	124	84	6	29	27
25	38	21	371		91	26	166	824	75	717	57	82	773	67	55	96	422	175	930
33	30	47	31	45		58	18	35	64	55	13	47	79	38	59	56	19	22	47
197	169	194	11	20	35		23	31	9	66	23	6	55	29	6	24	13	24	41
24	30	20	58	135	32	36		150	37	68	30	28	59	30	19	112	43	29	196
60	45	26	89	330	62	37	119		97	229	65	78	231	107	82	355	102	206	26
4	0	0	32	55	18	2	14	17		140	19	0	125	4	2	47	44	14	18
142	116	102	17	129	27	133	27	63	146		47	66	8	121	77	143	22	34	104
47	34	50	33	46	11	65	22	34	84	73		74	76	35	51	49	27	24	42
1	2	0	22	38	18	3	11	11	0	73	29		107	8	0	36	19	5	13
110	104	95	27	139	46	140	22	84	143	10	41	99		89	95	143	40	31	113
37	42	42	38	74	65	48	27	167	56	38	49	71	54		67	81	41	107	162
2	2	2	32	45	24	2	8	18	0	107	19	0	107	9		32	30	12	18
18	35	19	397	141	91	22	179	888	100	730	91	66	787	45	70		452	181	1015
30	19	25	8	78	62	31	14	33	149	46	51	107	36	182	123	115		29	52
52	37	60	34	136	62	55	24	349	56	65	37	52	62	54	75	112	28		357
54	60	30	98	340	72	42	131	27	114	216	61	98	217	102	70	394	102	230	

Supplementary Figure 5. All putMIP LNs make reciprocal connections with all other putMIP LNs.

(A-B) All putMIP LNs are synaptically connected to each other. Table of the number of synapses from one putMIP LN to all other putMIP LNs.

(C-D) The amount of putative MIPergic LN reciprocal connectivity assessed within each glomerulus. Heatmap of the amount of input a given putMIP LN receives from all other putMIP LNs within every AL glomerulus as a function of the total amount of input that putMIP LN receives within a glomerulus.

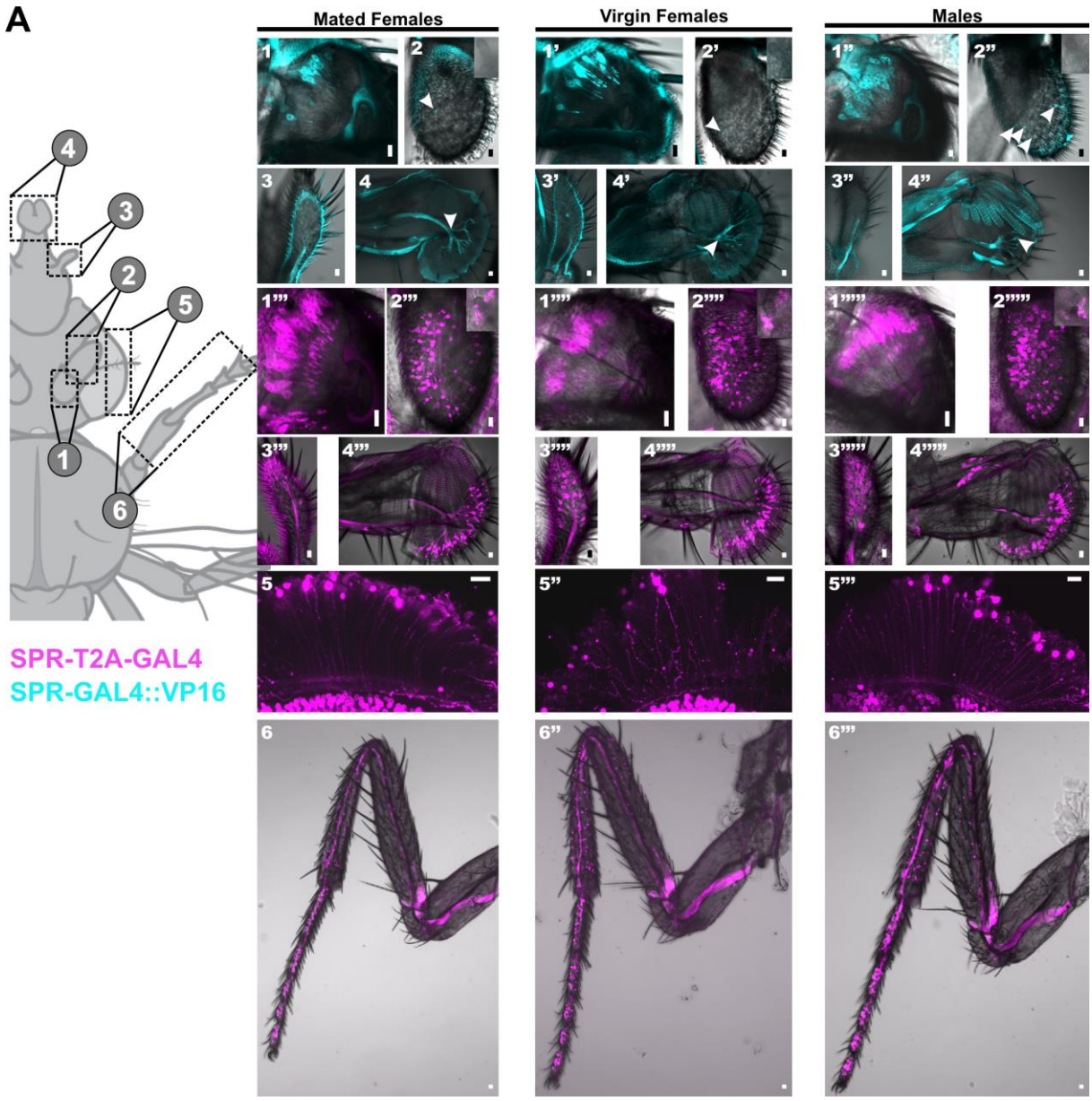

Supplementary Figure 6. SPR-GAL4::VP16 and SPR-T2A-GAL4 expression throughout all primary sensory neurons.

(A) Expression patterns of the bacterial artificial chromosome derived element SPR-GAL4::VP16 (cyan) and a CRISPR-Cas9 T2A-GAL4 insertion in the coding-intron of the sex peptide receptor (SPR-T2A-GAL4, magenta) in all sensory afferents in mated females, virgin females, and males. The left most diagram represents imaging plane for all images to the right, wherein: 1-1’’’’’ = auditory afferents; 2-2’’’’’ = olfactory, thermal, and hygrosensory afferents; 3-3’’’’’ = olfactory afferents; 4-4’’’’’ = gustatory afferents; 5-5’’’ = visual afferents; 6-6’’’ = proprioceptive and gustatory afferents. Driver expression in visual afferents and proprioceptive/gustatory afferents (in T1) were only tested for SPR-T2A-GAL4. Arrowhead(s) in 2-2’’’ and 4-4’’’ highlight the few neurons the express SPR-GAL4::VP16 in the third-antennal segment (olfactory, thermal, and hygrosensory afferents), and the labellum (gustatory afferents), respectively. Neuron(s)

that innervate the sacculus, a thermal/hygrosensory organ in the third-antennal segment, are presented in the insets in the top right of 2-2’’’’’.
In all cases, scale bar = 10um.

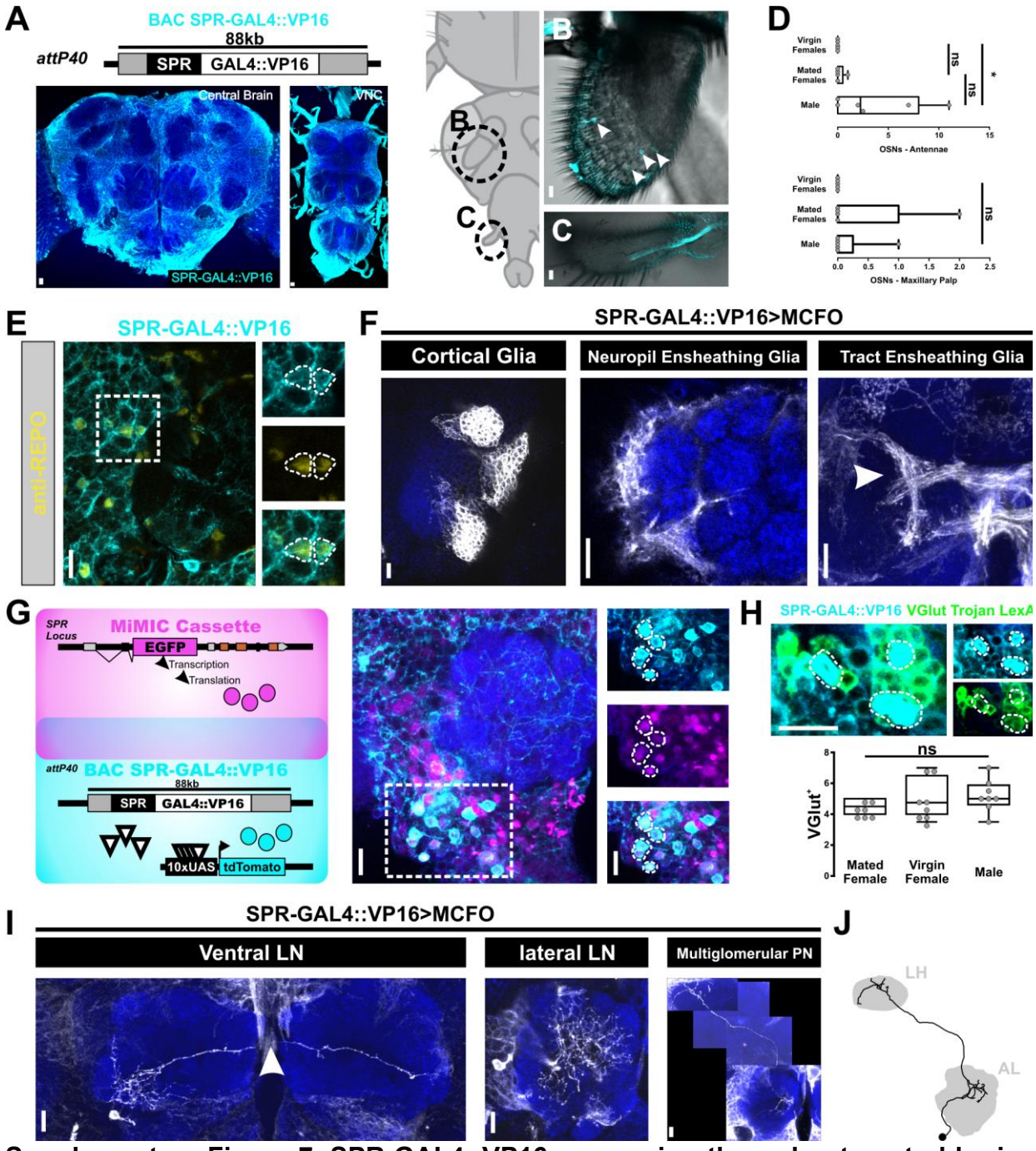

Supplementary Figure 7. SPR-GAL4::VP16 expression throughout central brain circuitry with emphasis on AL expression.

(A) Sex peptide receptor expression (SPR; cyan) as revealed using a bacterial artificial chromosome derived GAL4::VP16 element (Ameku et al., 2018). Note that this element contains the SPR locus and much of the surrounding genomic locus (~88kb total), and the GAL4::VP16 coding sequence was later inserted before the SPR stop site (Ameku et al 2018). This element was then reintroduced at the attp40 landing site (Ameku et al 2018).

(B-D) SPR-GAL4::VP16 expression (cyan) in OSNs housed in the third-antennal

segment and maxillary palp. Female mating status does not affect the number of SPR-GAL4::VP16-positive cells in antennae, but males have significantly more SPR-GAL4::VP16-positive cells in their antennae than virgin females (antennal OSNs: virgin vs. mated females: $p = 0.942$, $n = 5$; males vs virgin females: $p = 0.025$, $n = 6$ (males), 5 (virgin females); Dunn's test with a Bonferroni multiple comparisons correction). However, the number of SPR-GAL4::VP16-positive cells in the maxillary palp does not differ based on sex or mating status (maxillary palp OSNs: $p = 0.59$, $n = 5$ (virgin females), 5 (mated females), and 6 (males), Kruskal-Wallis rank sum test).
(E) SPR-GAL4::VP16 (cyan) colocalizes with the general glial marker *reverse polarity* (anti-REPO; yellow).
(F) MCFO labeling using the SPR-GAL4::VP16 reveals expression in several glial subtypes, including cortical, neuropil ensheathing, and tract ensheathing glia.
(G) Several ventral AL neurons are labeled through intersectional genetics experiments between an EGFP-insertion in the endogenous non-coding intron of SPR (MiMIC Cassette; magenta) and SPR-GAL4::VP16 (cyan).
(H) At least a portion of the ventral AL neurons labeled by SPR-GAL4::VP16 are ventral glutamatergic LNs. The number of vesicular glutamate transporter-positive ($VGlut^+$) SPR-GAL4::VP16 neurons does not statistically differ based on sex or mating status ($p = 0.546$, $n = 8$ (virgin females), 7 (mated females), and 8 (males), one-way ANOVA with a Bonferroni multiple comparisons correction).
(I) Later MCFO experiments confirm SPR-GAL4::VP16 expression in ventral LNs, and in at least one instance, a lateral LN and a ventral multiglomerular PN could be resolved.
(J) Skeleton representation of the aforementioned SPR-GAL4::VP16 multiglomerular PN.
In all cases: neuropil was delineated with anti-DN-cadherin staining; all scale bar = 10um.

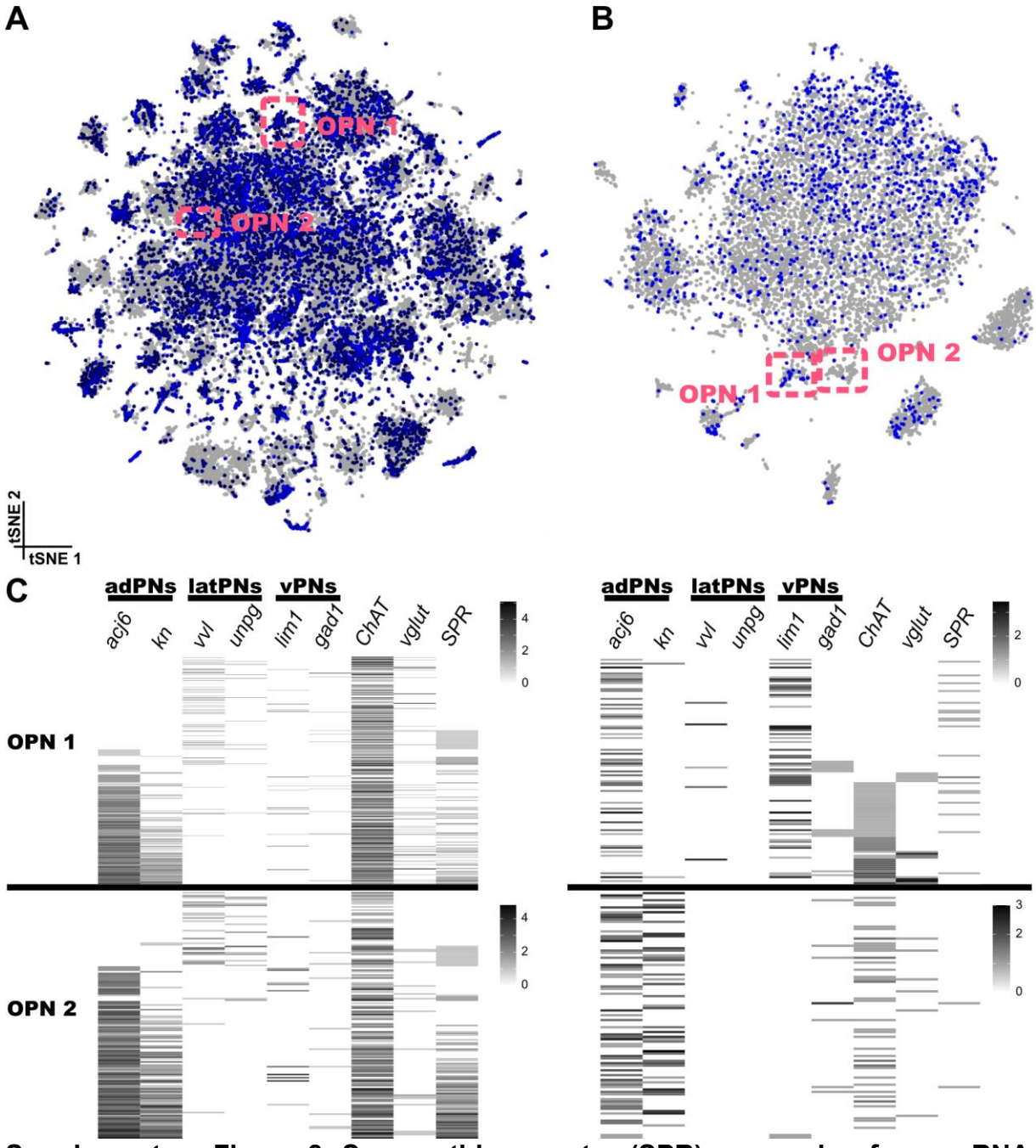

Supplementary Figure 8. Sex peptide receptor (SPR) expression from scRNA-sequencing data.

(A) SPR expression within Davie et al. (2018) scRNA-seq data. Olfactory projection neuron (OPN) cluster boundaries redrawn from previously identified boundaries (Davie et al., 2018).

(B) SPR expression within Croset et al. (2018) scRNA-seq data. OPN cluster boundaries redrawn from previously identified boundaries (Croset et al., 2018).

(C) Expression levels (transcript counts per million, log scale) of known PN-subpopulation markers, neurotransmitter enzymes/transporters, and SPR within each OPN cluster.

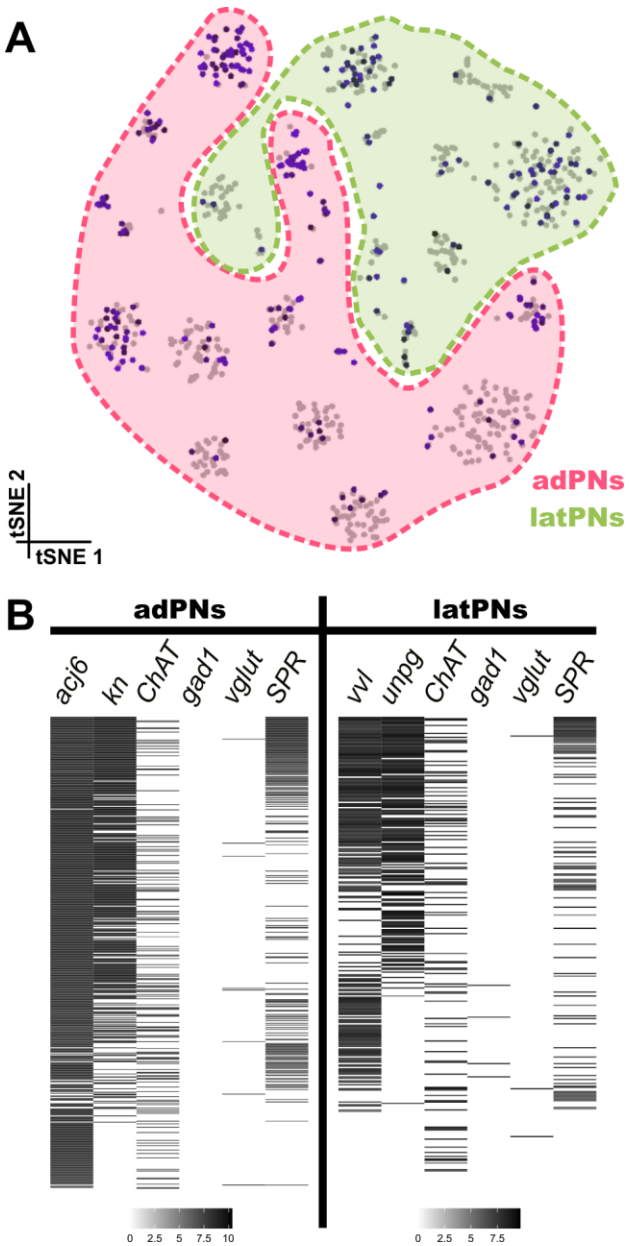

Supplementary Figure 9. Sex peptide receptor (SPR) expression from projection neuron-specific scRNA-sequencing data.
(A) SPR expression within Li et al. (2017) scRNA-seq data. Anterodorsal and lateral projection neuron (adPN & latPN, respectively) cluster boundaries redrawn from previously identified boundaries (Li et al., 2017).
(B) Expression levels (transcript counts per million, log scale) of known PN-subpopulation markers, neurotransmitter enzymes/transporters, and SPR within each PN cluster.

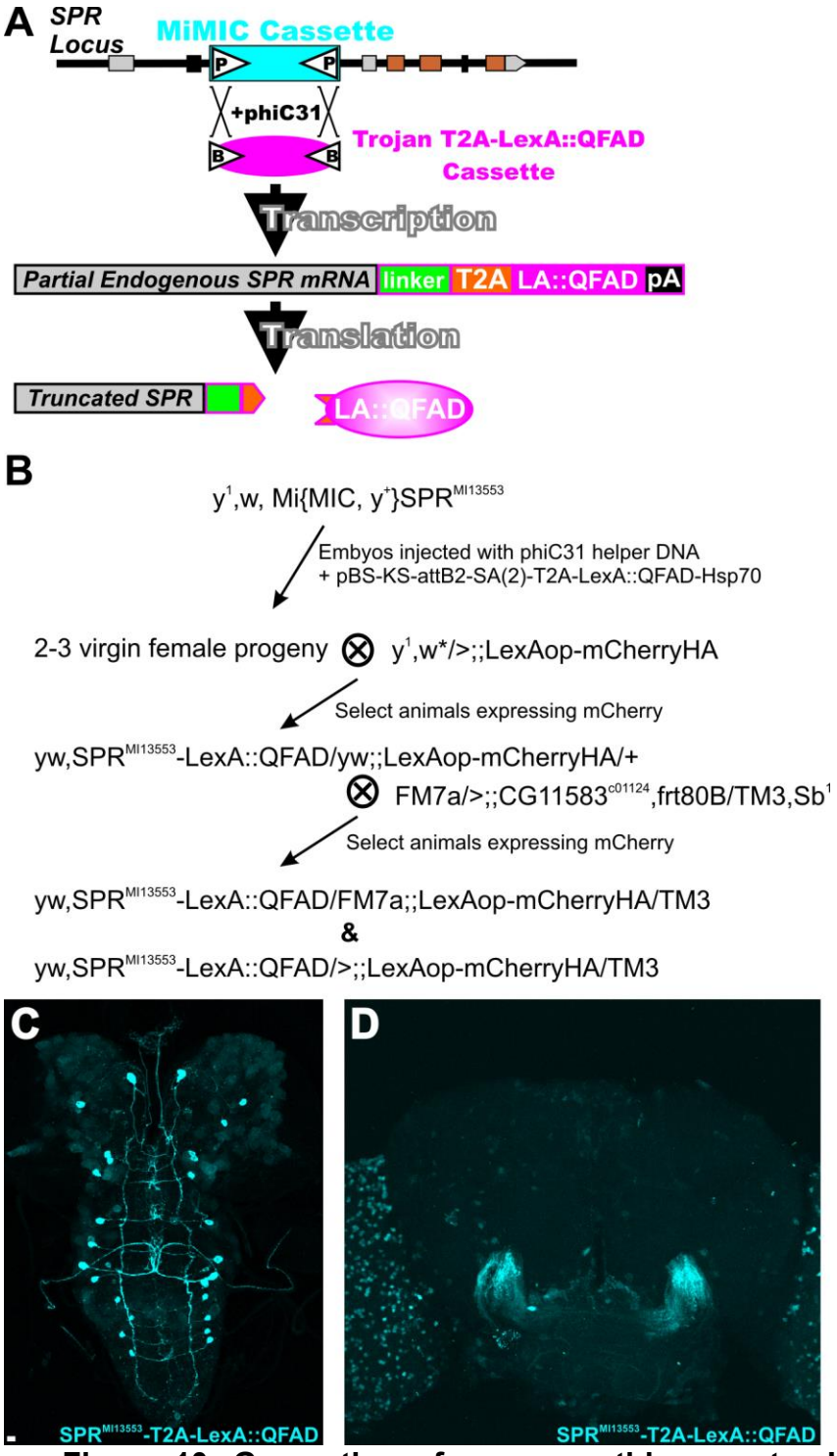

Supplementary Figure 10. Generation of a sex peptide receptor LexA::QFAD driver line via dual microinjection of a Trojan exon construct and phiC31 recombinase.

(A) Cartoon depiction of MiMIC cassette exchange for LexA::QFAD Trojan exon cassette, and subsequent LexA::QFAD expression in all cells that produce the sex peptide receptor (SPR).

(B) Crossing scheme used to establish $SPR^{MI13553}$-T2A-LexA::QFAD transgenics.

(C) $SPR^{MI13553}$-T2A-LexA::QFAD expression (cyan) in the larval central brain and ventral nerve cord.
(D) $SPR^{MI13553}$-T2A-LexA::QFAD expression (cyan) in the adult central brain. Note, the In all cases, scale bars = 10um.

CHAPTER 4

Serotonergic Metamodulation of Central Olfactory Processing

(portions of this chapter are based on my publication Sizemore, T.R., Hurley, L.M., and Dacks, A.M. (2020). Serotonergic modulation across sensory modalities. Journal of Neurophysiology, 123, 6.)

ABSTRACT

The ability of any sensory system to efficiently and effectively switch between which stimuli are salient to the animal's ongoing needs is universal to all modalities. Without the ability to shift between the various streams of stimulus information in this way, a sensory system may become "locked-in" and the animal will likely fail to detect and process stimuli that should far outweigh the stimuli currently most salient to the network (e.g., the scent of a predator vs. the scent of food). Nervous systems typically use diverse neuromodulators to rapidly and fluidly shift network operations toward relevant stimuli according to the animal's ongoing needs. These shifts can be potentiated and dynamically adjusted further still when a neuromodulator modifies the actions of another modulator (so called, "metamodulation"). Here, we reveal a novel metamodulatory pathway wherein the neuromodulator serotonin (5-HT) directly acts on an ensemble of neuropeptidergic LNs, the MIPergic LNs. Using driver and epitope knock-in transgenics and electron microscopy (EM)-level analyses, we reveal all MIPergic LNs express the inhibitory 5-HT1A receptor and receive direct synaptic input from the 5-HTergic CSD neurons. We demonstrate that 5-HT decreases MIPergic LN odor-evoked responses independent of glomerulus identity, which suggests 5-HT acts on MIPergic LNs to broadly inhibit their activity. As MIP is implicated in the animal's olfactory drive towards food-odors (Min et al., 2016), and 5-HT decreases MIPergic LN responses to one such food-odor, this suggests 5-HTergic metamodulation may exert a top-down contingency switch in AL processing by adjusting MIPergic LN activity. However, further behavioral analyses will need to be performed going forward to test this supposition.

INTRODUCTION

Neuromodulation is a universal feature of all nervous systems wherein modulatory

chemicals adjust the biophysical and synaptic properties of individual neurons to support the animal's ongoing external demands and/or internal needs (Marder and Thirumalai, 2002; Bargmann, 2012; Marder, 2012; Bucher and Marder, 2013; Gutierrez and Marder, 2014; Marder et al., 2014; Nadim and Bucher, 2014; Alcedo and Prahlad, 2020). In doing so, neuromodulators can expand the computational capacity of a given neural network to ultimately endow the animal with tremendous behavioral flexibility (Harris-Warrick and Marder, 1991; Kim et al., 2017; Alcedo and Prahlad, 2020; Flavell et al., 2020; Tsuda et al., 2021). However, all networks are influenced by multiple neuromodulators released from intrinsic/extrinsic neurons, whose collective concentrations at any given time can be thought to represent the "modulatory tone" of the network at that time (Hurley et al., 2004; Iwano and Kanzaki, 2005; Berg et al., 2009; Carlsson et al., 2010; Chalasani et al., 2010; Jacob and Nienborg, 2018; Lizbinski et al., 2018; Nassel, 2018; Nässel and Zandawala, 2019). Much like how changes in the collective concentrations of intrinsic/extrinsic factors can have profound consequences on a cell's development (Pearson and Doe, 2004; Doe, 2008), changes in even individual modulators can have profound consequences on the network's ability to rapidly/efficiently adjust activity. This has led to the supposition that changes in a network's modulatory tone may reflect grand shifts in the animal's behavior and/or state (Marder et al., 2014; Delaney et al., 2021). Moreover, given the profound ability of a single neuromodulator to shift overall network states, a neuromodulator acting on another neuromodulator can have long-lived and dramatic consequences in network state and the animal's behavior [e.g., (Chalasani et al., 2010)].

Metamodulation describes second-order neuromodulation, wherein one neuromodulator influences the actions of another neuromodulator (Katz and Edwards, 1999). Such metamodulatory signaling can provide further logarithmic and nonlinear flexibility to the neural network's operations and has been demonstrated in disparate networks, such as the *Tritonia* and crustacean motor systems (Katz and Edwards, 1999; Edwards et al., 2002) and sensory systems (Lizbinski and Dacks, 2018; Flavell et al., 2020). In olfactory systems, 5-HTergic metamodulation acts on interneuron-mediated GABAergic modulation to differentially tune the gain of olfactory input to the brain (Gaudry, 2018; Lizbinski and Dacks, 2018; Sizemore et al., 2020). For example, 5-HT stimulates 5-HT2C expressing juxtaglomerular cells in the olfactory bulb (OB) to increase

the amount of presynaptic inhibition exerted upon OSNs (Petzold et al., 2009). A similar computation occurs in the insect antennal lobe (AL), wherein 5-HTergic metamodulation attenuates afferent inputs by increasing LN-mediated GABAergic presynaptic modulation (Dacks et al., 2009; Zhang and Gaudry, 2016). However, LNs in both the mammalian OB and insect AL also release a diverse array of neuropeptides whose actions in each circuit - for the most part - remains elusive (Baker, 1986; Blakemore et al., 2006; Carlsson et al., 2010; Lepousez et al., 2010; Tobin et al., 2010; Siju et al., 2014). Therefore, this suggests that in addition to modulating LN-mediated GABAergic modulation, 5-HT may also modulate LN-mediated peptidergic modulation of olfactory processing in these systems. In *Aplysia* motor systems and cell culture, 5-HT has been shown to frequently modulate the actions of peptidergic modulation (whim and Lloyd 1992; Vilim et al 1996;). However, 5-HTergic metamodulation of peptidergic modulation (to the best of our knowledge) has never been demonstrated *in vivo* in the olfactory system.

Here, we reveal a novel metamodulatory signaling pathway that likely “rebalances” the level of olfactory input to the central brain. In accordance with our previous observations (Sizemore and Dacks, 2016), we find that the MIPergic LNs exclusively express the inhibitory 5-HT1A receptor subtype (**see Chapters 2 & 3**). Then, we leverage the densely reconstructed hemibrain EM volume (Clements et al., 2020; Scheffer et al., 2020) to demonstrate MIPergic LNs likely receive direct synaptic input from the sole source of synaptic 5-HT in the AL, the CSDns. Moreover, we generally find that CSDn input to these putative MIPergic LNs is concentrated in a food-odor associated glomerulus we previously demonstrated is modulated by MIP-SPR signaling, DM1 (**see Chapter 3**). We, then, tested whether 5-HT modulates MIPergic LN odor-evoked responses and find that 5-HT attenuates MIPergic LN responses in all glomeruli tested independent of glomerulus identity. This result is consistent with 5-HT1A Gαi-coupling, as was demonstrated when this receptor subtype was initially discovered in flies (Saudou et al., 1992). Together, these results suggest that 5-HTergic metamodulation of MIPergic LN modulation may underly a contingency-switch in AL state, based on the animal’s shifts in satiation behaviors. However, this supposition requires further experimentation, which is currently undergoing and will likely continue long past my time at WVU. Regardless, these

results represent the first demonstration of 5-HTergic metamodulation of peptidergic modulation in any primary olfactory center.

RESULTS

All MIPergic LNs Express the Inhibitory 5-HT1A Receptor

The MIPergic LNs are patchy GABAergic LNs that release the neuropeptide myoinhibitory peptide (MIP) and form broad reciprocal connections with principal neurons and their ensemble partners within every glomerulus, such as DM1 and DM2 (**Figure 1A**) (**see Chapter 3**). Moreover, MIP signaling was previously found to decrease and increase afferent responses in DM1 and DM2 (**Figure 1B**) (**see Chapter 3**), presumably in a satiation-state dependent manner. However, are there mechanisms to circumvent peptidergic modulation? We previously used protein-trap T2A-GAL4 insertions in the endogenous 5-HT1A locus to demonstrate that all MIPergic LNs express the inhibitory 5-HT1A receptor (Sizemore and Dacks, 2016) (**Figure 1C**). However, we sought to confirm these results using animals with a CRISPR/Cas9-mediated hemagglutinin-tag (HA-tag) insertion on the C-terminus of the 5-HT1A receptor (5-HT1A::HA) (Alekseyenko et al., 2019). We find that 5-HT1A::HA signal colocalizes with ~9.28 ± 0.52 neurons (n = 7 brains, 12 ALs) labeled by R32F10-GAL4, a driver we previously demonstrated selectively labels MIPergic LNs within the AL (**Figure 1D**) (**see Chapter 3**). These numbers agree with the total number of MIPergic LNs within the AL (**see Chapter 3**). Altogether, these results suggest that 5-HT and MIP form a metamodulatory circuit wherein 5-HTergic modulation decreases MIPergic LN activity (**Figure 1E**).

MIPergic LNs Are Reciprocally Connected to the Serotonergic CSDns

The sole source of synaptic 5-HT within the *Drosophila* AL are the highly conserved serotonin-immunoreactive deutocerebral neurons, or “CSDns” (Salecker and Distler, 1990; Sun et al., 1993; Wegerhoff, 1999; Hill et al., 2002; Dacks et al., 2006; Roy et al., 2007; Zhang and Gaudry, 2016; Coates et al., 2017, 2020). A single CSDn spans the entire olfactory network (both ALs, both MB calyces, and both LHs), and less well-

defined areas which integrate inputs from many modalities (both superior lateral protocerebrums and antlers) (Roy et al., 2007; Coates et al., 2017, 2020; Suver et al., 2019). Within the AL, the CSDns innervate different glomeruli to varying degrees and differentially connect with the various principal neuron types from animal-to-animal (Coates et al., 2017). Previous CSDn connectomic analyses from 9 glomeruli indicate all principal neuron types are consistently targeted by the CSDn, but in each glomerulus the CSDn chiefly targets LNs (Coates et al., 2020). However, recent evidence suggests that CSDn synaptic connections are not necessarily required for some AL LNs to detect 5-HT (Suzuki et al., 2020). Therefore, we took a more comprehensive and targeted approach in order to determine whether MIPergic LNs receive direct CSDn synaptic input, or if MIPergic LNs likely receive 5-HT from another source. To do so, we leveraged the densely reconstructed hemibrain electron microscopy volume (Clements et al., 2020; Scheffer et al., 2020) and our previously identified putative MIPergic LNs (putMIP LNs) (**see Chapter 3**) to determine putMIP LN connectivity with the easily identifiable CSDn (**Figure 2A**).

We first wondered how much of the CSDn's overall output do putMIP LNs represent, if they receive input from the CSDn at all. We, therefore, performed downstream demographics analyses which indicate that the CSDn chiefly targets neurons outside the AL such as those in the LH, MB calyx, nearly every protocerebral region, and the antler ("Others"; ~22% of total output;) (**Figure 2B**). Within the AL, the CSDn targets all principal neuron types to various degrees, these are: ~2% (OSNs), ~6% (PNs), and ~10% of total output to non-putMIP LNs (**Figure 2B**). We find that putMIP LNs represent the majority of CSDn output amongst AL targets (~16% of total CSDn output) (**Figure 2B**). It's notable that a non-insignificant amount of total CSDn output remains unidentifiable (~42% of total CSDn output) (**Figure 2B**), and therefore our results may be overestimates. Regardless, these results demonstrate that putMIP LNs do receive synaptic input from the CSDn, and that putMIP LNs represent the CSDn's greatest targets within the AL.

We wondered whether CSDn input to putMIP LNs were focused in certain olfactory channels more than others. If this were the case, this would suggest 5-HTergic modulation targets specific odor-response properties of MIPergic LNs. Alternatively, if

CSDn input to putMIP LN were evenly distributed over the putMIP LN's processes across all glomeruli, then 5-HT may serve to alter MIPergic LN odor-responses across the entire AL. We find that CSDn input to putMIP LNs is generally greatest in the V glomerulus (218 synapses total), DM1 (120 synapses total), DM4 (101 synapses total), DP1l (84 synapses total), and DL2d (79 synapses total) (**Figure 2C**). These glomeruli have been associated with several aspects of food-odors, such as alcoholic fermentation (V and DP1l), decaying fruit volatiles (DL2d), and yeast volatiles (DM1 and DM4) (Bates et al., 2020b). This suggests that 5-HTergic modulation likely targets MIPergic LN food-odor responses. In contrast, glomeruli where putMIP LNs generally receive no/little CSDn input include VM2 (0 synapses), VC3l and VL2a (1 synapse each), and DA4m and DA4l (2 synapses each) (**Figure 2C**). These glomeruli are mostly associated with aversive olfactory stimuli (VC3, DA4m, and DA4l), which suggests that 5-HT does not target MIPergic LN responses to aversive stimuli for modulation. Altogether, these results indicate 5-HTergic modulation of MIPergic LNs generally targets appetitive (as opposed to aversive) stimulus responses.

In addition to the aforementioned general CSDn-to-putMIP LN connectivity, we also noted several instances where putMIP LNs synapsed back onto the CSDn across several glomeruli (**Figure 2D**). These putMIP LN-to-CSDn connections were largest in the V glomerulus (41 synapses), DM4 (41 synapses), DL2d (41 synapses), DL1 (41 synapses), and DC1 (41 synapses) (**Figure 2D**). Interestingly, these general putMIP LN-to-CSDn connections scale linearly with the amount of CSDn-to-putMIP LN connections. That is to say, generally, if putMIP LNs receives a large amount of input from the CSDn within a glomerulus, they are generally likely to provide more output to the CSDn. In contrast, we found no putMIP LN synapses onto the CSDn in DA4m, VM2, VM3, or VM7d (**Figure 2D**). The lack of putMIP LN-to-CSDn synapses in VM2 and VM3 contrasts with previous connectomic analyses that found the CSDns receive ~60-62% of their LN input in these glomeruli from presumed patchy LNs (Coates et al., 2020). However, this discrepancy likely owes to several features, such as: (1) several glomeruli (19 glomeruli) are truncated within the hemibrain (Schlegel et al., 2021), and (2) the presumed patchy LNs found in this previous work are not necessarily MIPergic patchy LNs. Regardless, all of these results together demonstrate that MIPergic LNs and the CSDn form direct and reciprocal synaptic connections to one another. Moreover, this CSDn "reciprocity motif"

appears to be generalizable across different neuron types and animals, as previous connectomic results found the CSDn forms reciprocal connections to every target neuron (Coates et al., 2020).

Serotonin Decreases MIPergic LN ACV-Responses Across Glomeruli

To this point, we have demonstrated: (1) all MIPergic LNs express the inhibitory 5-HT1A serotonin receptor subtype (**Figure 1**); and, (2) putative MIPergic LNs receive direct synaptic input from the CSDn, and represent the CSDn's greatest downstream target within the AL (albeit based on synapse number) (**Figure 2**). We previously demonstrated that MIPergic LNs are robustly and consistently activated by the innately attractive food-associated odor apple cider vinegar (ACV), and MIP signaling directly decreases and indirectly increases OSN ACV-evoked responses in the food-odor associated glomeruli DM1 and DM2 (**see Chapter 3**). As the only 5-HTR expressed by MIPergic LNs is the inhibitory 5-HT1A (Sizemore and Dacks, 2016), and CSDn input to putMIP LNs in DM1 is generally substantial (see above) (**Figure 2**), we wondered if 5-HT would decrease MIPergic LN odor-evoked responses in glomeruli where MIP signaling had been found to modulate OSN responses (**see Chapter 3**).

To test whether 5-HT can alter MIPergic LN odor-evoked responses in ACV-responsive glomeruli, we first recorded from MIPergic LNs in these glomeruli before, during, and after 5-HT bath application (**see Methods**) (**Figure 3A**). We chose to use this approach, as oppose to stimulating CSDns while recording from MIPergic LNs, to avoid confounds from potential CSDn co-transmitter(s) whose identity remains elusive (**Figure S1**) (Sizemore et al., 2020). However, after laborious effort I was able to identify a LexA driver line that is restrictive to the MIPergic LNs, and establish a novel transgenic for conditional disruption of 5-HT1A production, that may enable such future experiments (**Figure S1**). We find that before 5-HT application MIPergic LN neurites within DM1, DM2, and DP1m robustly respond to ACV, which on average persists in most glomeruli after 5-HT application (the "during" test) (DM1: $p = 0.111$, $n = 3$; DP1m: $p = 0.051$, $n = 3$; Bonferroni-corrected repeated measures one-way ANOVA) (**Figure 3B**). This was not the case in DM2, where MIPergic LN odor-evoked responses were significantly affected by

5-HT application ($p = 0.036$, before vs. during, $n = 3$; Bonferroni-corrected pairwise paired t-tests). Then, after the washout period (the “after” test) MIPergic LN neurite ACV-responses are significantly diminished most glomeruli (DM1: $p = 0.048$, $n = 3$; DM2: $p = 0.03$, $n = 3$, before vs. after; Bonferroni-corrected pairwise paired t-tests) (**Figure 3B**). Although not significant, MIPergic LN neurite responses in DP1m are noticeably diminished by 5-HT application, which may become significant as more animals are tested (i.e., failure of significance likely caused by low power). Regardless, these results suggest, therefore, that 5-HT acts to decrease MIPergic LN odor-evoked responses (albeit directly or polysynaptically) independent of glomerulus identity. Moreover, these results suggest that 5-HT may act to halt or decrease MIPergic modulation of food-associated olfactory channels (i.e., DM1) perhaps in accordance with the animal’s satiation-state. However, this supposition and how MIPergic LN-expression of 5-HT1A contributes to serotonin’s metamodulatory effects here, remain to be tested. Please note, that we attempted to test whether 5-HT diminishes MIPergic LN dense core vesicle (DCV)-release using two different peptide release sensors: preproANF-EMD (Rao et al., 2001) and NPRR-ANP (Ding et al., 2019). However, we were unable to resolve DCV-trafficking or peptide release (i.e., decrease in fluorophore puncta) with either sensor, most likely due to weak expression levels of either sensor when used in combination with our driver.

DISCUSSION

Altogether, our data reveal a novel metamodulatory signaling pathway which has the capacity to inhibit a neuropeptide signaling pathway that mediates olfactory gain control. We have shown that all MIPergic LNs express the inhibitory 5-HT1A receptor subtype, and receive direct synaptic input with the AL’s sole source of synaptic 5-HT, the CSDns. Moreover, we find that this synaptic input is generally strongest in glomeruli whose cognate odor-scenes correspond to several food-odor features, such as fermentation (the V glomerulus) and yeast volatiles (DM1 and DM4) (Bates et al., 2020b). Then, we demonstrate that 5-HT decreases MIPergic LN odor-evoked responses across the food-odor associated glomeruli, such as DM1. We previously determined that MIP-SPR signaling modulates the gain of DM1 OSN odor-evoked responses independent of

odor concentration (**see Chapter 3**). Before that, behavioral analyses independently performed revealed that the activity of these OSNs - and MIP itself - plays a key role in the animal's odor-evoked behavioral responses (see below). Thus, 5-HTergic modulation of MIPergic modulation may contribute to a key circuit switch for behavioral attraction vs. aversion. Below, we expand upon the important features and potential consequences of this metamodulatory signaling pathway as implicated by this work.

Consequences of Metamodulation: From Circuit Logic to Behavior

Modulators, such as neuropeptides, can rapidly and dynamically transform neural network computations over extended epochs and typically do so in accordance with the animal's ongoing needs (De Bono and Bargmann, 1998; Blakemore et al., 2006; Chalasani et al., 2010; Flavell et al., 2013; Komuniecki et al., 2014; Maeda et al., 2015; Kim et al., 2017; Nocera et al., 2019). These modulators can work in a concerted and/or antagonistic manner together to bring about dramatic shifts in network and behavioral output. For example, 5-HT and the neuropeptide pigment dispersing factor (PDF) mutually inhibit and inversely control *C. elegans* food-search activity (Sawin et al., 2000; Ben Arous et al., 2009; Flavell et al., 2013; Iwanir et al., 2016; Ji et al., 2020). Here, a single chemosensory processing neuron (AIA) (Chalasani et al., 2007; Dobosiewicz and Bargmann, 2019) acts on both 5-HTergic (NSM & HSN) and PDF-releasing (AVB) neurons differentially based on the chemosensory cues regarding food abundance in the environment (Fujiwara et al., 2002; Flavell et al., 2013; McCloskey et al., 2017; Ji et al., 2020). When food is plentiful, input from the chemosensory neuron to the 5-HTergic neurons (and inhibitory neurons that impinge on the PDF-releasing neuron) are strongest, thus producing a "dwelling" behavioral state (Ji et al., 2020). Conversely, when food-odor and intake diminish, output from the chemosensory neuron diminishes and inhibitory interneurons suppress 5-HT release (Ji et al., 2020). Even further, the PDF-releasing neurons, now free from the inhibition driven by the chemosensory neuron's activity, become engaged in circuit operation and eventually produce a long-lasting "roaming" state (Flavell et al., 2013; Ji et al., 2020). In this way, the nematode's overall locomotor activity (dwell vs. roam) can dictated by the antagonistic actions of two separate

modulators.

Although our circuit motif differs (here, 5-HT directly acts on the peptidergic neurons), our results suggest a similar terminal consequence may exist. We demonstrate that 5-HT decreases the odor-evoked responses of MIPergic LNs, whose cognate peptide (MIP) modulates the gain of olfactory afferent responses (**see Chapter 3**). Myoinhibitory peptide was previously found to be necessary and sufficient to decrease the fly's attraction to food-odors and their motivation to feed (as measured via proboscis extension assays) (Min et al., 2016). These behavioral analyses therefore suggest that MIP plays a vital role in the fly's drive towards food, such that when the animal is starved MIP signaling decreases and starvation-contingent behavioral programs initiate (albeit in parallel or one-after-the-other). Consistent with this, we previously found that MIP significantly diminishes OSN food-odor evoked responses independent of odor concentration (**see Chapter 4**). Moreover, the glomerulus where these previous results were resolved – DM1 – can be selectively activated (independent of other olfactory channels) and evoke an attractive behavioral response (Bell and Wilson, 2016). Thus, if 5-HT's effects are sufficiently strong enough to halt MIPergic LN MIP-release, then 5-HT may be used here to return each MIPergic modulated olfactory channel to "baseline". This would be a useful and efficient mechanism to bias AL neuronal activity to a more food-odor sensitive state in situations when the animal is hungry. In this situation, perhaps 5-HT is tonically released and scales linearly with the animal's increasing hunger, eventually reaching a "tipping point" where anorexic-like behaviors are induced. Moreover, since 5-HT acts on other AL neurons through many receptors (Dacks et al., 2009; Sizemore and Dacks, 2016; Zhang and Gaudry, 2016), it is plausible that this 5-HTergic metamodulation could efficiently switch-off MIP-induced food-odor avoidance while simultaneously increasing the activity of circuit elements that drive food-odor induced attraction (e.g., disinhibition of DM1 OSNs, increase sensitivity of food-odor sensitive PNs, etc.). Although some of these specific hypotheses are (admittedly) highly-speculative and will need to be followed up in future studies, these results may represent the critical circuit elements of a metamodulatory pathway that impactfully adjusts olfactory processing. As MIPergic LNs likely play several computational roles within the AL (indeed, we previously uncovered circuit topologies indicative of lateral inhibition and output gain modulation), 5-HT likely has the capacity to

adjust nearly every aspect of AL processing simply by acting on this one ensemble.

METHODS

Key Resources Table

REAGENT or RESOURCE	SOURCE	IDENTIFIER
Antibodies		
Rat anti-DN-Cadherin	DSHB, University of Iowa	Catalog #: DN-Ex #8; RRID: AB_528121
Mouse anti-Bruchpilot	DSHB, University of Iowa	Catalog #: nc82; RRID: AB_2314866
Rabbit anti-Myoinhibitory Peptide (MIP)	Christian Wegener (by way of Manfred Eckert)	RRID: AB_2314803
Chicken anti-GFP	Abcam	Catalog #: ab13970; RRID: AB_300798
Rabbit anti-Hemagglutinin	Cell Signaling Technology	Catalog #: 3724; RRID: AB_1549585
Rabbit anti-serotonin	Immunostar	Catalog #: 20080 RRID: AB_572263
Donkey anti-Chicken AlexaFluor 488	Jackson ImmunoResearch Laboratories, Inc.	Catalog #: 703-545-155; RRID: AB_2340375
Donkey anti-Rabbit AlexaFluor 546	Thermo Fisher Scientific, CA	Catalog #: A-10040; RRID: AB_2534016
Goat anti-Rabbit AlexaFluor 633	Thermo Fisher Scientific, CA	Catalog #: A-21070; RRID: AB_2535731
Goat anti-Mouse AlexaFluor 633	Thermo Fisher Scientific, CA	Catalog #: A-21050; RRID: AB_2535718
Donkey anti-Rat AlexaFluor 647	Abcam	Catalog #: ab150155
Experimental Models: Organisms/Strains		
w^-;; GMR32F10-GAL4	Bloomington Stock Center	RRID: BDSC_49725
w^-; GMR32F10-LexA	Bloomington Stock Center	RRID: BDSC_53565
w^*; 10xUAS-IVS-mCD8::GFP	Bloomington Stock Center	RRID: BDSC_32186
y^1,w^*, 10xUAS-IVS-mCD8::RFP, 13xLexAop-mCD8::GFP	Bloomington Stock Center	RRID: BDSC_32229
w^-; 20xUAS-IVS-GCaMP6f	Bloomington Stock Center	RRID: BDSC_42747
w^-, 3xUAS-FLPG5.PEST	Bloomington Stock Center	RRID: BDSC_55808

w^{*};; ChAT ^{MI04508} Trojan LexA::QFAD/TM6B, Tb^{1}	Bloomington Stock Center	RRID: BDSC_60319
$y^{1}w^{*}$;CyO/Sp^{1}; Dr^{1}/TM3, Sb^{1}	Bloomington Drosophila Stock Center	RRID: BDSC_59967
w^{*}; 5-HT1A^{FlpStop_ND}/CyO	This study.	N/A
$y^{1}w^{*}$; 5-HT1A-T2A-GAL4^{MI01140}	Herman Dierick, Baylor College of Medicine	Gnerer et al., 2015
$y^{1}w^{*}$; 5-HT1A-T2A-GAL4^{MI01468}	Herman Dierick, Baylor College of Medicine	Gnerer et al., 2015
$y^{1}w^{*}$; 5-HT1A-T2A-GAL4^{MI04464}	Herman Dierick, Baylor College of Medicine	Gnerer et al., 2015
5-HT1A::HA	E. Kravitz, Harvard University (by way of Olga Alekseyenko, Harvard University)	Alekseyenko et al., 2019 Flybase ID: FBal0353540
Odors		
Paraffin oil	J.T. Baker, VWR	CAS #: 8012-95-1
Apple cider vinegar (ACV)	Heinz	N/A
Recombinant DNA		
pFlpStop-attB-UAS-2.1-tdTom	Fisher et al., 2017	Addgene: #88910
Oligonucleotides		
Orientation-MiL-F: GCGTAAGCTACCTTAATCTCAAGAAGAG	Venken et al., 2011	N/A
FRTspacer_5p_rev: AAATGGTGCAAAGAGAAGTTCC	Fisher et al., 2017	N/A
FRTspacer_3p_for: ACAATCCAGCTACCATTCTGC	Fisher et al., 2017	N/A
Molecular Biology Reagents/Chemicals		
Serotonin (5-HT)	Santa Cruz Biotechnology	Catalog #: SC-201146A
OneTaq DNA Polymerase	New England BioLabs	Catalog #: M0480L
5x OneTaq Standard Reaction Buffer	New England BioLabs	Catalog #: B9022S
Deoxyribonucleotide (dNTP) solution	New England BioLabs	Catalog #: N0447L
Nuclease-free water	New England BioLabs	Catalog #: B1500L
Software and Algorithms		
VAA3D (v.3.20)	Peng et al., 2010	RRID: SCR_002609

FluoRender (v.2.22.3)	Wan et al., 2017	RRID: SCR_014303
FIJI (v.2.0.0)	Open-Source	RRID:SCR_002285
R Studio (v.1.4.1103)	Open-Source	www.rstudio.com
MATLAB 2016b	MathWorks	www.mathworks.com
Python 3	Open-Source	RRID: SCR_008394
CorelDRAW 2021	Corel Corp.	www.corel.com
Adobe Illustrator 2020	Adobe Inc.	www.adobe.com
natverse	Bates et al., 2020; Schlegel et al., 2021	https://natverse.org/
Connectome-neuprint/neuprint-python	Stuart Berg (JRC)	N/A
CloudVolume	William Silversmith (Princeton)	https://github.com/seung-lab/cloud-volume

Contact for Reagent and Resource Sharing. Further information and reasonable requests for reagents and resources should be directed to - and will be fulfilled by - the Lead Contact, Andrew M. Dacks (andrew.dacks@mail.wvu.edu).

Experimental Model and Subject Details. Flies were reared on standard cornmeal and molasses media at 24°C and under a 12:12 light:dark cycle. Equal numbers of male and female animals were used when possible, excluding live-imaging experiments.

Immunocytochemistry, Image Acquisition and Image Analyses. All immunocytochemistry was performed generally as previously described (Sizemore and Dacks, 2016) (**also see Chapter 3**). Briefly, samples were dissected, fixed in 4% paraformaldehyde, then washed with phosphate buffered saline with 0.5% Triton-X 100 (PBST) several times before taking samples through an ascending-descending ethanol was series, then blocking in 4% IgG-free BSA (Jackson Immunoresearch; Cat#001-000-162). Samples were then incubated in primary antibody (see **Key Resources Table**) diluted in blocking solution and 5mM sodium azide. Following primary antibody incubation samples were washed with PBST, blocked, and incubated in secondary antibody diluted in blocking solution and 5mM sodium azide. Finally, samples were washed, cleared using an ascending glycerol series (40%, 60%, 80%), and mounted on well slides in Vectashield® (Vector Laboratories, Burlingame, CA; Cat#H-1200). Images were

collected and analyzed as previously described (Sizemore and Dacks, 2016), with the exception of images captured with a 40x/1.25 Silicone UPlanSApo Olympus objective.

Hemibrain Connectomics Analyses. All connectome analyses leveraged the densely reconstructed Janelia FlyEM *Drosophila* hemibrain electron microscopy volume (version 1.2; https://neuprint.janelia.org/) (Clements et al., 2020; Scheffer et al., 2020), and recently described analysis suites (Bates et al., 2020a; Schlegel et al., 2021). All connectomics analyses were performed as previously described (**see Chapter 3**). Briefly, we identified putative MIPergic LNs (putMIP LNs) based on several previously described stringent criteria. The CSDns were identified based on neuPrint's associated bodyid "name" and the neuron's easily identifiable and highly-conserved neuronal architecture (Dacks et al., 2006). These CSDn bodyids were later confirmed by generating a NBLAST morphological similarity score between our query skeleton ("putative" CSDns) and GMR60F02-GAL4, a driver previously demonstrated to contain the CSDns (Singh et al., 2013). Please note that although both CSDns are present within the hemibrain dataset, only synaptic connections from the contralateral CSDn are considered here as the ipsilateral CSDn makes little-to-no connections within the only AL included in the hemibrain.

***in vivo* Calcium Imaging – animal preparation.** All calcium imaging experiments were performed on female flies ~1-5 days post-eclosion at room temperature, and are generally exactly as described in **Chapter 3**. Animals of the proper genotype were collected and briefly anesthetized on ice. Once anesthetized, an animal was affixed to a custom-built holder with UV curable glue (BONDIC, M/N: SK8024). Our custom-built holder consists of a sheet of aluminum foil with a small hole (the imaging window) affixed to a 3D-printed design derived from similar designs described previously (Weir et al., 2016). Once mounted, a small window exposing the dorsal side of the brain was created, and covered with filtered recording saline (in mM: 2 CaCl2, 5 KCl, 5 HEPES, 8.2 MgCl2, 108 NaCl, 4 NaHCO3, 1 NaH2PO4, 10 sucrose, and 5 trehalose; adjusted pH: ~7.4) (Root et al., 2008). Following this, the air sacs, fat bodies, and trachea covering the dorsal side of the brain were removed with fine forceps. With the exception of minimal epochs during 5-HT

bath application (see below), the brain was continuously perfused with oxygenated (95%O2/5%CO2) recording saline using a Cole-Parmer Masterflex C/L (M/N: 77120-62) at a rate of ~2mL/min.

***in vivo* Calcium Imaging – Image Acquisition.** Functional imaging data were acquired using the same custom-built system previously described (**see Chapter 3**). Briefly, we used a Prior Scientific Open Stand (M/N: H175) microscope mounted on Prior Scientific motorized translational stage (M/N: HZPKT1), and equipped with an Olympus 10x/0.30 UPlanFL N objective and an Olympus 60x/1.00 LUMPlanFL N water-immersion objective. A 470nm CoolLED pE-100 (CoolLED Ltd., Hampshire, UK) was used as the light source. Each trial was captured with a Hamamatsu ORCA-4.0LT camera (Hamamatsu Phototonics, Hamamatsu, Japan), and consists of 40 1,024x1,024 frames acquired at a frame rate of ~9 Hz.

***in vivo* Calcium Imaging - Odor Preparation and Delivery.** All odors were prepared and delivered as previously described (**see Chapter 3**). Here, all odor concentrations are reported as v/v dilutions in paraffin oil (J.T. Baker, VWR #JTS894), or autoclaved and twice-filtered distilled water (for diluting acids). For example, 10^{-2} dilution indicates that one volume of an odor is diluted with 100 volumes of paraffin oil. Dilutions were prepared in 2mL odor vials (SUPELCO; P/N: 6020) that contained a final volume of 1mL of diluted odor in paraffin oil every other day, or after two experiments (whichever came first). Odors were presented as previously described (Bhandawat et al., 2007; Hong and Wilson, 2015; Jeanne et al., 2018). Briefly, a carrier stream of carbon-filtered, dehumidified, air was presented at 2.2 L/min to the fly continuously through an 8mm Teflon tube placed ~1cm away from the fly. A three-way solenoid (The Lee Company, P/N: LHDA1231315H) diverted a small portion of the airstream (0.2 L/min) through the headspace of an odor vial for 200ms after triggering an external voltage command (TTL pulse) at frame 20 of the trial. Considering the above, the odor is diluted further (by 10-fold) prior to delivery to the animal. The odor stream joined the carrier stream 11cm from the end of the tube, and the tube opening measured ~4mm.

Methods for assessing preparation health and performing multiple odor trials

generally conform to previous work (Hong and Wilson, 2015; Jeanne et al., 2018). At the start of each experiment, the animal was presented a test odor (10^{-3} 2-heptanone) to assess the preparation's health. Only the data collected from animals whose responses to this test odor were initially robust were used for further analysis. As 5-HT bath application likely causes network-wide changes in odor-evoked responses (Dacks et al., 2009; Zhang and Gaudry, 2016), the test odor was only initially presented to animals used for 5-HT application experiments, so their initial olfactory response health could be assessed. However, it's notable that no animal was tested longer than the duration of the MIPergic LN odor panel experiments previously discussed (**see Chapter 3**). Each experiment consisted of four odor trials per a preparation which were then averaged to attain a within-animal response. These within-animal averages were subsequently averaged across many animals for subsequent statistical analysis, and "n" is reported as the number of animals. Each odor trial consisted of five 200ms pulses of odor with a 1ms interpulse interval. The same odor was never presented twice within 2min to prevent depletion of the odor vial's headspace. Air entered and exited each odor vial through a PEEK one-way check valve (The Lee Company, P/N: TKLA3201112H) connected to the vial by Teflon tubing. The odor delivery tube was flushed with clean air for 2min when changing between odors/concentrations. As an additional preemptive measure, all odor delivery system components were hooked up to the house vacuum line overnight.

***in vivo* Calcium Imaging – Data Analysis.** All calcium imaging data were analyzed as previously described (**see Chapter 3**). That is, we made use of a custom-made script graciously provided by Marco Gallio (Northwestern University) and has been described previously (Frank et al., 2015, 2017) to analyze all calcium imaging data. With the exception of any preparations that violated the aforementioned criteria (e.g., movement, diminishing prep health, etc.), no data points or outliers were excluded from our analyses. Generally, the number of flies to be used for experiments are not a limiting factor, therefore no statistical power analyses were used to pre-determine sample sizes. Regardless, our sample sizes are similar to those in previous reports that perform similar experiments (Dacks et al., 2009; Zhang and Gaudry, 2016; Suzuki et al., 2020). Before analyzing the data, a Gaussian low-pass filter (sigma=1), bleach correction (exponential

fit), and image stabilizer algorithms were applied to the given trial's raw ΔF/F signal. Calcium transients (ΔF/F) were measured as changes in fluorescence (ΔF) normalized to baseline fluorescence (F, averaged over the first 19 frames before odor delivery). By normalizing this way, we could ensure trivial effects of slight z-axis drifts, GCaMP concentration differences, and variations in the tested neuron's innervation density would be corrected. Responses were pooled for each odor stimulus - and within concentration - by averaging the peak odor-evoked calcium signal across multiple odor presentation trials (4 trials). We used the following formula to derive percent ΔF/F: [(*the calcium transients within a given glomerulus*)/(*the peak odor response averaged across the entire AL tested*)] x 100%. A trial's maximum response (Max %ΔF/F) refers to the average of five consecutive frames centered around that trial's peak response post stimulus presentation. Glomeruli were manually identified post-hoc by comparing acquired images to well-defined three-dimensional maps of the AL (Fishilevich and Vosshall, 2005; Grabe et al., 2015). Only the glomeruli that were reasonably identifiable were considered for analysis.

Serotonin Bath Application Experiments. Serotonin (see **Key Resources Table**) was prepared daily and/or every four hours on ice and under strict low-light protocols (Dacks et al., 2009) to ensure amine concentrations were as intended when tested. To test how 5-HT application adjusts odor-evoked responses, a 10^{-3}M working solution was made by diluting a small portion of the amine in nuclease-free water (Thermo Scientific, #R0581). After testing the initial odor-evoked responses of the neurons being tested for a given experiment, the perfusion system was switched off momentarily so a small portion of our 5-HT working solution could be pressure injected into the AL to a final concentration of 10^{-4}M. This final concentration was chosen in accordance with similar experiments previously reported in flies (Dacks et al., 2009; Zhang and Gaudry, 2016; Suzuki et al., 2020) and other insects (Kloppenburg and Hildebrand, 1995; Mercer et al., 1995; Kloppenburg et al., 1999; Dacks et al., 2008). Ten minutes after 5-HT pressure injection, the animal's odor-evoked responses were tested as before 5-HT injection, and then the perfusion system was switched back on. Ten minutes after turning the perfusion system back on, the animal's odor-evoked responses were once again tested as they were

initially. Re-testing the animal's response to the test odor (10^{-3} 2-heptanone) at the end of these experiments could not be used as a reliable means for assessing prep health due to changes in circuit member responses induced by modulator bath application. The resulting data were generally analyzed as outlined above, but we modified our procedure for deriving percent ΔF/F such that the average peak response within that given glomerulus to ACV presentation before 5-HT application was used as the dividend across treatment groups.

5-HT1A^{FlpStop_ND} Generation. The 5-HT1A^{FlpStop_ND} fly line was established using previously described injection methods (Fisher et al., 2017). Briefly, pFlpStop-attB-UAS-2.1-tdTom and ΦC31 helper plasmid DNA were co-injected into y^1w^*; Mi{MIC}5-HT1A^{MI01140}. Resultant flies were crossed to y^1w^*;CyO/Sp^1; Dr^1/TM3, Sb^1 flies, and screened for loss of the yellow rescue construct from the MiMIC construct. pFlpStop-attB-UAS-2.1-tdTom (Addgene #88910) was a gift from Thomas Clandinin (Stanford University). Embryo injections ("MiMIC injection – Service A") were performed by Rainbow Transgenic Flies, Inc. (Camarillo, CA). PCR-verification of the FlpStop construct orientation was performed using a previously described primer set (Venken et al., 2011; Fisher et al., 2017) (see **Key Resources Table**). Genomic DNA were extracted from a small number of flies using previously described methods (Gloor et al., 1993) and PCR conditions for construct orientation confirmation were: denaturation at 94°C for 10min., 40 cycles at 94°C for 30sec., 51°C for 30sec., and 72°C for 60sec., followed by a post-amplification extension at 72°C for 10min.

Quantification and Statistical Analyses. Statistical analyses were performed using R (v.3.6.2) in R Studio (v.1.4.1103). Values to be analyzed were concatenated in Excel before importing into the relevant analysis software. Statistical results are reported in text and in each figure legend. All statistical tests were two-tailed. The Shapiro-Wilk test was used to evaluate any deviations from a normal distribution. Delta F/F analyses were carried out using the custom MATLAB scripts previously described (Frank et al., 2015, 2017), and are depicted as mean ± SEM. To assess max response (%ΔF/F) differences between MIPergic LN odor-evoked 5-HT treatments, we first determined if normality could

be assumed (as above), then outliers were determined using the “identify_outliers” function in *rstatix* package. If normality could be assumed and no outliers were present, then an omnibus one-way repeated measures ANOVA with a Greenhouse-Geisser sphericity correction was performed (“anova_test” in *rstatix*). If max responses (%ΔF/F) were statistically different at each odor trial, then pairwise paired t-tests with a Bonferroni multiple comparisons correction were performed to identify which groups were statistically different. If normality could not be assumed, then a Kruskal-Wallis rank sum test followed by a pairwise Mann-Whitney U test with a Bonferroni multiple comparisons adjustment were performed. All boxplots display the minimum, 25th-percentile, median, 75th-percentile, and ’maximum’ of the given data. Additional analysis details are provided for each set of experiments above. Values are given as means ± SEM. Statistical significance is defined as $p < 0.05$.

Acknowledgements. We are grateful for the Bloomington Drosophila Stock centers (NIH P40OD018537) and the Janelia Fly Light project for flies. We would also like to thank Herman Dierick and Olga Alekseyenko for providing flies. Christian Wegener kindly provided the MIP antibody that was developed by Manfred Eckert. Marco Gallio provided scripts for analyzing live imaging data. Marta Costa, Greg Jefferis, and Philipp Schlegel graciously instructed connectomic analyses, especially for extracting synapse counts within AL glomeruli. Our connectomic analyses also benefited from discussions in the nat-user community (https://groups.google.com/g/nat-user). Kristyn Lizbinski and James Jeanne graciously provided advice and equipment specifications that lead to the construction and use of the olfactometer system described here. We are grateful to Yvette Fisher for technical advice when determining the FlpStop cassette orientation, and Kevin Daly for kindly loaning equipment and advice regarding their use. This work was supported by a Grant-In-Aid of Research (G20141015669888) from Sigma Xi, The Scientific Research Society (T.R.S.), and a National Institutes of Health R01 DC016293 (A.M.D.).

Author Contributions. T.R.S. conceived and implemented all experiments, analyzed the

subsequent data, prepared figures, and wrote and edited the manuscript. A.M.D. acquired funding and helped with manuscript edits. Please note, this chapter is part of a larger study that will, eventually, include behavioral analyses from authors not listed here.

WORKS CITED

Alcedo J, Prahlad V (2020) Neuromodulators: an essential part of survival. J Neurogenet 34:475–481.

Alekseyenko O V., Chan YB, Okaty BW, Chang YJ, Dymecki SM, Kravitz EA (2019) Serotonergic Modulation of Aggression in Drosophila Involves GABAergic and Cholinergic Opposing Pathways. Curr Biol 29:2145-2156.e5.

Baker H (1986) Substance P and tyrosine hydroxylase are localized in different neurons of the hamster olfactory bulb. Exp Brain Res 65:245–249.

Bargmann CI (2012) Beyond the connectome: How neuromodulators shape neural circuits. BioEssays 34:458–465.

Bates AS, Manton JD, Jagannathan SR, Costa M, Schlegel P, Rohlfing T, Jefferis GSXE (2020a) The natverse, a versatile toolbox for combining and analysing neuroanatomical data. Elife 9:1–35.

Bates AS, Schlegel P, Roberts RJ V, Drummond N, Tamimi IFM, Turnbull RG, Zhao X, Marin EC, Popovici PD, Dhawan S, Jamasb AR, Javier A, Li F, Rubin GM, Waddell S, Bock DD, Costa M, Jefferis GSXE (2020b) Complete connectomic reconstruction of olfactory projection neurons in the fly brain. Curr Biol 30:1–17.

Bell JS, Wilson RI (2016) Behavior Reveals Selective Summation and Max Pooling among Olfactory Processing Channels. Neuron 91:425–438.

Ben Arous J, Laffont S, Chatenay D (2009) Molecular and sensory basis of a food related two-state behavior in C. elegans. PLoS One 4:1–8.

Berg BG, Schachtner J, Homberg U (2009) γ-Aminobutyric acid immunostaining in the antennal lobe of the moth Heliothis virescens and its colocalization with

neuropeptides. Cell Tissue Res 335:593–605.

Bhandawat V, Olsen SR, Gouwens NW, Schlief ML, Wilson RI (2007) Sensory processing in the Drosophila antennal lobe increases reliability and separability of ensemble odor representations. Nat Neurosci 10:1474–1482.

Blakemore LJ, Levenson CW, Trombley PQ (2006) Neuropeptide Y modulates excitatory synaptic transmission in the olfactory bulb. Neuroscience 138:663–674.

Bucher D, Marder E (2013) SnapShot: Neuromodulation. Cell 155:482-482.e1.

Carlsson M a., Diesner M, Schachtner J, Nässel DR (2010) Multiple neuropeptides in the Drosophila antennal lobe suggest complex modulatory circuits. J Comp Neurol 518:3359–3380.

Chalasani SH, Chronis N, Tsunozaki M, Gray JM, Ramot D, Goodman MB, Bargmann CI (2007) Dissecting a circuit for olfactory behaviour in Caenorhabditis elegans. Nature 450:63–70.

Chalasani SH, Kato S, Albrecht DR, Nakagawa T, Abbott LF, Bargmann CI (2010) Neuropeptide feedback modifies odor-evoked dynamics in Caenorhabditis elegans olfactory neurons. Nat Neurosci 13:615–621.

Clements J, Dolafi T, Umayam L, Neubarth N, Berg S, Scheffer L, Plaza S (2020) neuPrint: Analysis Tools for EM Connectomics. bioRxiv:1–20.

Coates K, Calle-Schuler S, Helmick L, Knotts V, Martik B, Salman F, Warner L, Valla S, Bock D, Dacks A (2020) The wiring logic of an identified serotonergic neuron that spans sensory networks. J Neurosci 40:6309–6327.

Coates KE, Majot AT, Zhang X, Michael CT, Spitzer SL, Gaudry Q, Dacks AM (2017) Identified Serotonergic Modulatory Neurons Have Heterogeneous Synaptic

Connectivity within the Olfactory System of *Drosophila*. J Neurosci 37:7318–7331.

Dacks a M, Christensen T a, Hildebrand JG (2008) Modulation of olfactory information processing in the antennal lobe of Manduca sexta by serotonin. J Neurophysiol 99:2077–2085.

Dacks AM, Christensen T a., Hildebrand JG (2006) Phylogeny of a Serotonin-Immunoreactive Neuron in the Primary Olfactory Center of the Insect Brain. J Comp Neurol 498:727–746.

Dacks AM, Green DS, Root CM, Nighorn AJ, Wang JW (2009) Serotonin modulates olfactory processing in the antennal lobe of Drosophila. J Neurogenet 23:366–377.

De Bono M, Bargmann CI (1998) Natural variation in a neuropeptide Y receptor homolog modifies social behavior and food response in C. elegans. Cell 94:679–689.

Delaney K, Hu M, Hellenbrand T, Dickinson PS, Nusbaum MP, Li L (2021) Mass Spectrometry Quantification, Localization, and Discovery of Feeding-Related Neuropeptides in Cancer borealis. ACS Chem Neurosci 12:782–798.

Ding K, Han Y, Seid TW, Buser C, Karigo T, Zhang S, Dickman DK, Anderson DJ (2019) Imaging neuropeptide release at synapses with a genetically engineered reporter. Elife 8:1–15.

Dobosiewicz M, Bargmann CI (2019) Reliability of an interneuron response depends on an integrated sensory state. Elife:1–27.

Doe CQ (2008) Neural stem cells: balancing self-renewal with differentiation. Development 135:1575–1587.

Edwards DH, Yeh SR, Musolf BE, Antonsen BL, Krasne FB (2002) Metamodulation of the crayfish escape circuit. Brain Behav Evol 60:360–369.

Fisher YE, Yang HH, Isaacman-Beck J, Xie M, Gohl DM, Clandinin TR (2017) FlpStop, a tool for conditional gene control in *Drosophila*. Elife 6:1–33.

Fishilevich E, Vosshall LB (2005) Genetic and Functional Subdivision of the Drosophila Antennal Lobe Genetic and Functional Subdivision of the Drosophila Antennal Lobe. Curr Biol 15:1548–1553.

Flavell SW, Pokala N, Macosko EZ, Albrecht DR, Larsch J, Bargmann CI (2013) Serotonin and the neuropeptide PDF initiate and extend opposing behavioral states in C. Elegans. Cell 154:1023–1035.

Flavell SW, Raizen DM, You YJ (2020) Behavioral states. Genetics 216:315–332.

Frank DD, Enjin A, Jouandet GC, Zaharieva EE, Para A, Stensmyr MC, Gallio M (2017) Early Integration of Temperature and Humidity Stimuli in the Drosophila Brain. Curr Biol 27:2381-2388.e4.

Frank DD, Jouandet GC, Kearney PJ, MacPherson LJ, Gallio M (2015) Temperature representation in the Drosophila brain. Nature 519:358–361.

Fujiwara M, Sengupta P, McIntire SL (2002) Regulation of body size and behavioral state of C. elegans by sensory perception and the egl-4 cGMP-dependent protein kinase. Neuron 36:1091–1102.

Gaudry Q (2018) Serotonergic modulation of olfaction in rodents and insects. Yale J Biol Med 91:23–32.

Gloor GB, Preston CR, Johnson-Schlitz DM, Nassif NA, Phillis RW, Benz WK, Robertson HM, Engels WR (1993) Type I repressors of P element mobility. Genetics 135:81–95.

Grabe V, Strutz A, Baschwitz A, Hansson BS, Sachse S (2015) Digital in vivo 3D atlas of

the antennal lobe of Drosophila melanogaster. J Comp Neurol 523:530–544.

Gutierrez GJ, Marder E (2014) Modulation of a Single Neuron Has State- Dependent Actions on Circuit Dynamics 1 , 2 , 3. eNeuro 1:1–12.

Harris-Warrick R, Marder E (1991) Modulation of Neural Networks for Behavior. Annu Rev Neurosci 14:39–57.

Hill ES, Iwano M, Gatellier L, Kanzaki R (2002) Morphology and physiology of the serotonin-immunoreactive putative antennal lobe feedback neuron in the male silkmoth Bombyx mori. Chem Senses 27:475–483.

Hong EJ, Wilson RI (2015) Simultaneous Encoding of Odors by Channels with Diverse Sensitivity to Inhibition. Neuron 85:573–589.

Hurley LM, Devilbiss DM, Waterhouse BD (2004) A matter of focus: Monoaminergic modulation of stimulus coding in mammalian sensory networks. Curr Opin Neurobiol 14:488–495.

Iwanir S, Brown AS, Nagy S, Najjar D, Kazakov A, Lee KS, Zaslaver A, Levine E, Biron D (2016) Serotonin promotes exploitation in complex environments by accelerating decision-making. BMC Biol 14:1–15.

Iwano M, Kanzaki R (2005) Immunocytochemical Identification of Neuroactive Substances in the Antennal Lobe of the Male Silkworm Moth Bombyx mori. Zoolog Sci 22:199–211.

Jacob SN, Nienborg H (2018) Monoaminergic Neuromodulation of Sensory Processing. Front Neural Circuits 12:1–17.

Jeanne JM, Fis M, Wilson RI, Jeanne JM, Fis M (2018) The Organization of Projections from Olfactory Glomeruli onto Higher-Order Neurons. Neuron:1198–1213.

Ji N, Madan G, Fabre G, Dayan A, Baker C, Nwabudike I, Flavell S (2020) A neural circuit for flexible control of persistent behavioral states. BioRxiv:1–74.

Katz PS, Edwards DH (1999) Metamodulation: the control and modulation of neuromodulation.

Kim SM, Su C-Y, Wang JW (2017) Neuromodulation of Innate Behaviors in Drosophila. Annu Rev Neurosci 40:annurev-neuro-072116-031558.

Kloppenburg P, Ferns D, Mercer a R (1999) Serotonin enhances central olfactory neuron responses to female sex pheromone in the male sphinx moth manduca sexta. J Neurosci 19:8172–8181.

Kloppenburg P, Hildebrand JG (1995) Neuromodulation by 5-hydroxytryptamine in the antennal lobe of the sphinx moth Manduca sexta. J Exp Biol 198:603–611.

Komuniecki R, Hapiak V, Harris G, Bamber B (2014) Context-dependent modulation reconfigures interactive sensory-mediated microcircuits in Caenorhabditis elegans. Curr Opin Neurobiol 29C:17–24.

Lepousez G, Mouret A, Loudes C, Epelbaum J, Viollet C (2010) Somatostatin contributes to in vivo gamma oscillation modulation and odor discrimination in the olfactory bulb. J Neurosci 30:870–875.

Lizbinski KM, Dacks AM (2018) Intrinsic and Extrinsic Neuromodulation of Olfactory Processing. Front Cell Neurosci 11:1–11.

Lizbinski KM, Marsat G, Dacks AM (2018) Systematic analysis of transmitter coexpression reveals organizing principles of local interneuron heterogeneity. eNeuro 5.

Maeda T, Nakamura Y, Shiotani H, Hojo MK, Yoshii T, Ida T, Sato T, Yoshida M, Miyazato

M, Kojima M, Ozaki M (2015) Suppressive effects of dRYamides on feeding behavior of the blowfly, Phormia regina. Zool Lett 1:1–10.

Marder E (2012) Neuromodulation of Neuronal Circuits: Back to the Future. Neuron 76:1–11.

Marder E, O'Leary T, Shruti S (2014) Neuromodulation of Circuits with Variable Parameters: Single Neurons and Small Circuits Reveal Principles of State-Dependent and Robust Neuromodulation. Annu Rev Neurosci 37:329–346.

Marder E, Thirumalai V (2002) Cellular, synaptic and network effects of neuromodulation. Neural Networks 15:479–493.

McCloskey RJ, Fouad AD, Churgin MA, Fang-Yen C (2017) Food responsiveness regulates episodic behavioral states in Caenorhabditis elegans. J Neurophysiol 117:1911–1934.

Mercer a R, Hayashi JH, Hildebrand JG (1995) Modulatory effects of 5-hydroxytryptamine on voltage-activated currents in cultured antennal lobe neurones of the sphinx moth Manduca sexta. J Exp Biol 198:613–627.

Min S, Chae HS, Jang YH, Choi S, Lee S, Jeong YT, Jones WD, Moon SJ, Kim YJ, Chung J (2016) Identification of a peptidergic pathway critical to satiety responses in drosophila. Curr Biol 26:814–820.

Nadim F, Bucher D (2014) Neuromodulation of neurons and synapses. Curr Opin Neurobiol 29:48–56.

Nassel DR (2018) Substrates for neuronal cotransmission with neuropeptides and small molecule neurotransmitters in drosophila. Front Cell Neurosci 12:1–26.

Nässel DR, Zandawala M (2019) Recent advances in neuropeptide signaling in

Drosophila, from genes to physiology and behavior. Prog Neurobiol 179:101607.

Nocera S, Simon A, Fiquet O, Chen Y, Gascuel J, Datiche F, Schneider N, Epelbaum J, Viollet C (2019) Somatostatin serves a modulatory role in the mouse olfactory bulb: Neuroanatomical and behavioral evidence. Front Behav Neurosci 13:1–20.

Pearson BJ, Doe CQ (2004) Specification of Temporal Identity in the Developing Nervous System. Annu Rev Cell Dev Biol 20:619–647.

Petzold GC, Hagiwara A, Murthy VN (2009) Serotonergic modulation of odor input to the mammalian olfactory bulb. Nat Neurosci 12:784–791.

Rao S, Lang C, Levitan ES, Deitcher DL (2001) Visualization of neuropeptide expression, transport, and exocytosis in Drosophila melanogaster. J Neurobiol 49:159–172.

Root CM, Masuyama K, Green DS, Enell LE, Nässel DR, Lee CH, Wang JW (2008) A Presynaptic Gain Control Mechanism Fine-Tunes Olfactory Behavior. Neuron 59:311–321.

Roy B, Singh AP, Shetty C, Chaudhary V, North A, Landgraf M, Vijayraghavan K, Rodrigues V (2007) Metamorphosis of an identified serotonergic neuron in the Drosophila olfactory system. Neural Dev 2:20.

Salecker I, Distler P (1990) Serotonin-immunoreactive neurons in the antennal lobes of the American cockroach Periplaneta americana: light- and electron-microscopic observations. Histochemistry 94:463–473.

Saudou F, Boschert U, Amlaiky N, Plassat JL, Hen R (1992) A family of Drosophila serotonin receptors with distinct intracellular signalling properties and expression patterns. EMBO J 11:7–17.

Sawin ER, Ranganathan R, Horvitz HR (2000) C. elegans locomotory rate is modulated

by the environment through a dopaminergic pathway and by experience through a serotonergic pathway. Neuron 26:619–631.

Scheffer L et al. (2020) A connectome and analysis of the adult drosophila central brain. Elife:1–83.

Schlegel P, Bates AS, Stürner T, Jagannathan SR, Drummond N, Hsu J, Capdevila LS, Javier A, Marin EC, Barth-Maron A, Tamimi IFM, Li F, Rubin GM, Plaza SM, Costa M, Jefferis G (2021) Information flow, cell types and stereotypy in a full olfactory connectome. Elife.

Schnütgen F, Doerflinger N, Calléja C, Wendling O, Chambon P, Ghyselinck NB (2003) A directional strategy for monitoring Cre-mediated recombination at the cellular level in the mouse. Nat Biotechnol 21:562–565.

Siju KP, Reifenrath A, Scheiblich H, Neupert S, Predel R, Hansson BS, Schachtner J, Ignell R (2014) Neuropeptides in the antennal lobe of the yellow fever mosquito, Aedes aegypti. J Comp Neurol 522:592–608.

Singh AP, Das RN, Rao G, Aggarwal A, Diegelmann S, Evers JF, Karandikar H, Landgraf M, Rodrigues V, VijayRaghavan K (2013) Sensory Neuron-Derived Eph Regulates Glomerular Arbors and Modulatory Function of a Central Serotonergic Neuron. PLoS Genet 9.

Sizemore TR, Dacks AM (2016) Serotonergic Modulation Differentially Targets Distinct Network Elements within the Antennal Lobe of Drosophila melanogaster. Sci Rep 6:37119.

Sizemore TR, Hurley LM, Dacks A (2020) Serotonergic Modulation Across Sensory Modalities. J Neurophysiol:2406–2425.

Sun XJ, Tolbert LP, Hildebrand JG (1993) Ramification pattern and ultrastructural characteristics of the serotonin-immunoreactive neuron in the antennal lobe of the moth Manduca sexta: A laser scanning confocal and electron microscopic study. J Comp Neurol 338:5–16.

Suver MP, Matheson AMM, Sarkar S, Damiata M, Schoppik D, Nagel KI (2019) Encoding of Wind Direction by Central Neurons in Drosophila. Neuron 102:828-842.e7.

Suzuki Y, Schenk JE, Tan H, Gaudry Q (2020) A Population of Interneurons Signals Changes in the Basal Concentration of Serotonin and Mediates Gain Control in the Drosophila Antennal Lobe Report A Population of Interneurons Signals Changes in the Basal Concentration of Serotonin and Mediates Gain Co. Curr Biol:1–9.

Tobin VA, Hashimoto H, Wacker DW, Takayanagi Y, Langnaese K, Caquineau C, Noack J, Landgraf R, Onaka T, Leng G, Meddle SL, Engelmann M, Ludwig M (2010) An intrinsic vasopressin system in the olfactory bulb is involved in social recognition. Nature 464:413–417.

Tsuda B, Pate SC, Tye KM, Siegelmann HT, Sejnowski TJ (2021) Neuromodulators enable overlapping synaptic memory regimes and nonlinear transition dynamics in recurrent neural networks. bioRxiv.

Venken KJT, Schulze KL, Haelterman N a, Pan H, He Y, Evans-Holm M, Carlson JW, Levis RW, Spradling AC, Hoskins R a, Bellen HJ (2011) MiMIC: a highly versatile transposon insertion resource for engineering Drosophila melanogaster genes. Nat Methods 8:737–743.

Wegerhoff R (1999) GABA and serotonin immunoreactivity during postembryonic brain development in the beetle Tonebrio molitor. Microsc Res Tech 45:154–164.

Weir PT, Henze MJ, Bleul C, Baumann-Klausener F, Labhart T, Dickinson MH (2016) Anatomical reconstruction and functional imaging reveal an ordered array of skylight polarization detectors in drosophila. J Neurosci 36:5397–5404.

Zhang X, Gaudry Q (2016) Functional integration of a serotonergic neuron in the drosophila antennal lobe. Elife 5:1–24.

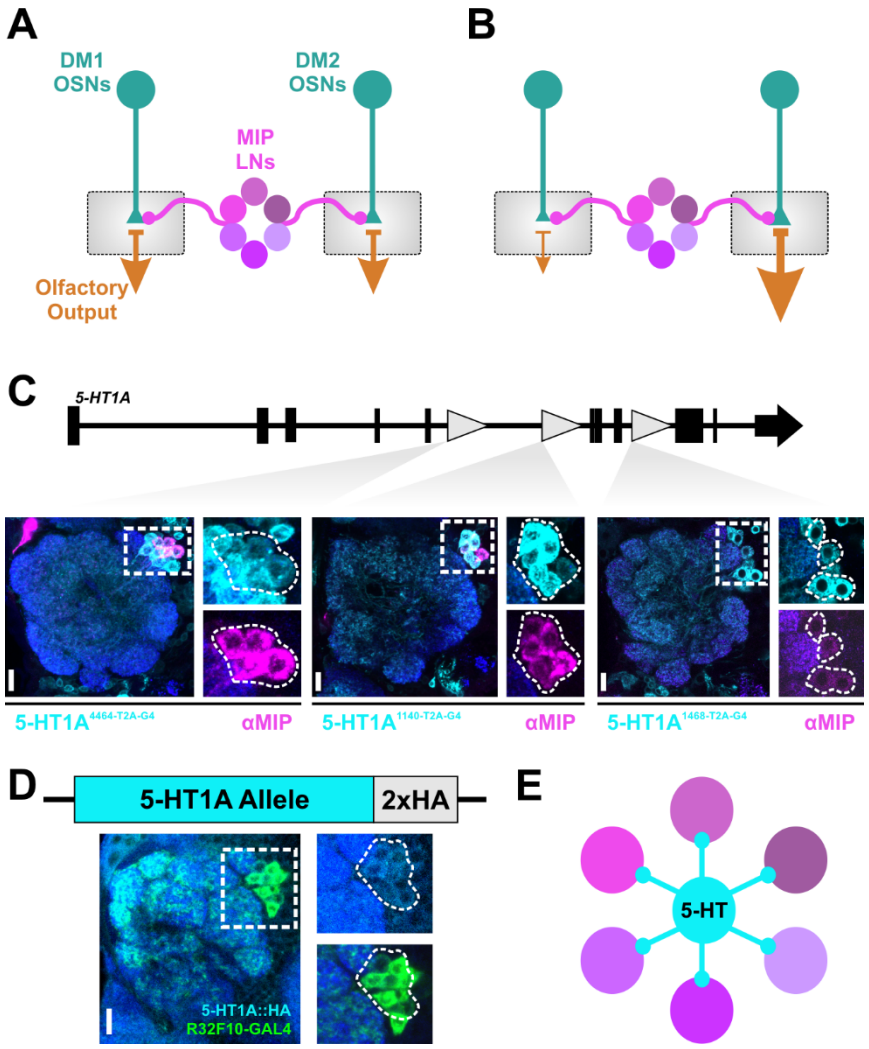

Figure 1. All MIPergic LNs express the inhibitory 5-HT1A receptor.
(A-B) MIPergic LNs (magenta) differentially act on DM1 and DM2 OSNs (blue-green) to decrease and increase their odor-evoked responses, respectively. In doing so, MIPergic LNs can decrease and increase olfactory output (orange) from each glomerulus concordantly.
(C) Three independent protein-trap T2A-GAL4 insertions within the endogenous 5-HT1A locus (cyan) label all MIPergic AL LNs (magenta).
(D) Signal from 5-HT1A::HA (cyan) colocalizes with ~9.28 ± 0.52 MIPergic LNs as revealed through R32F10-GAL4, a driver previously demonstrated to selectively label MIPergic LNs (**see Chapter 3**). Cell count estimates, n = 7 brains, 12 ALs.
(E) Together, these results suggest 5-HTergic modulation acts on MIPergic modulation within the *Drosophila* AL.
In all cases: neuropil was delineated by anti-DN-Cadherin staining; scale bars = 10um.

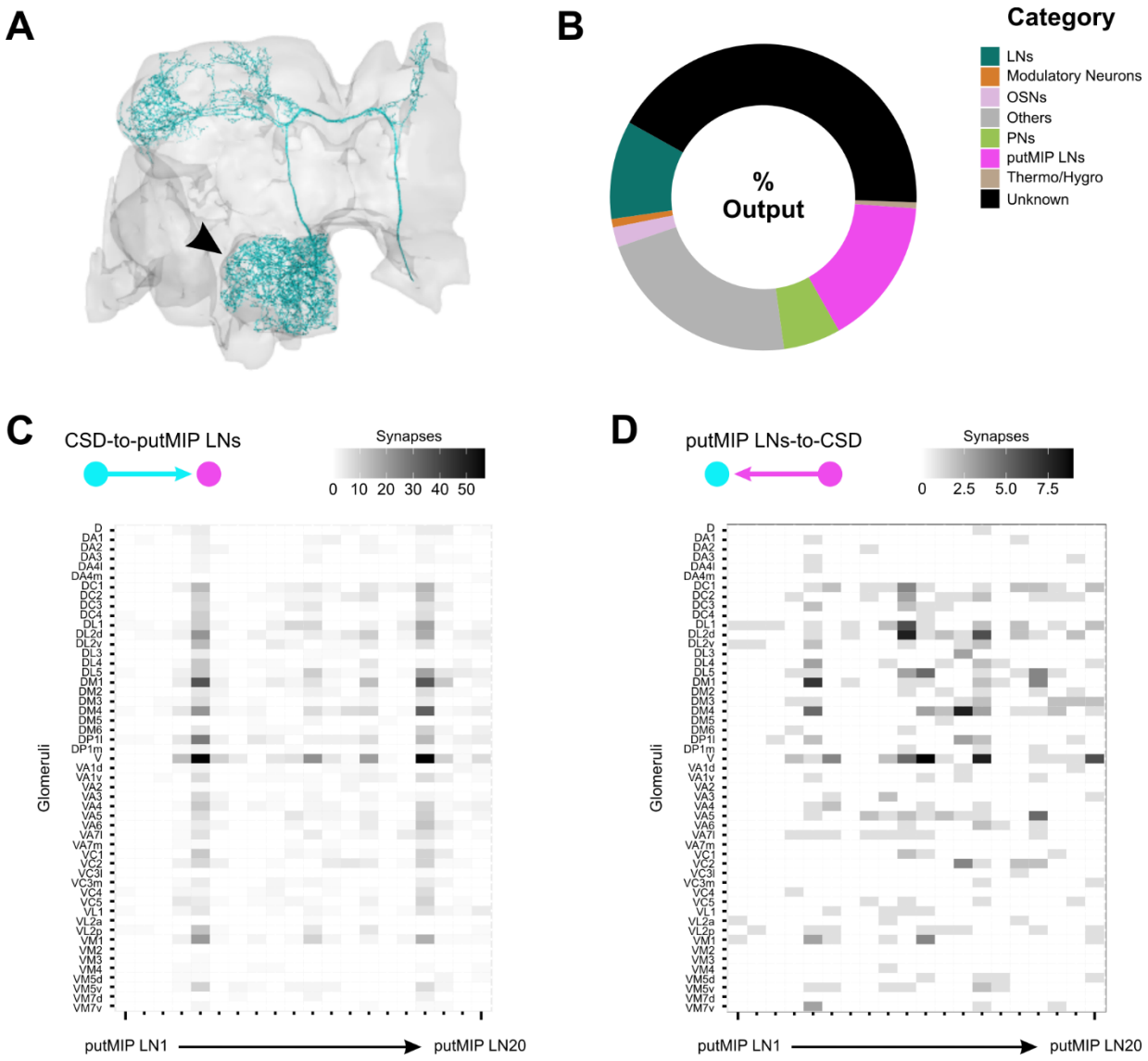

Figure 2. The serotonergic CSDn forms reciprocal synaptic connectivity with all putative MIPergic LNs.

(A) CSDn mesh skeleton (cyan) identified from the FlyEM FIB-SEM hemibrain connectome volume. Black arrowhead = CSDn branches within the AL.

(B) Donut chart of CSDn downstream partners' demographics as function of CSDn overall output. Data are represented as a function of the total amount of output the CSDn sends to all categories.

(C) CSDn synaptic output to each putMIP LN by glomerulus across the entire AL.

(D) Putative MIPergic LN synaptic output onto the CSDn by glomerulus across the entire AL.

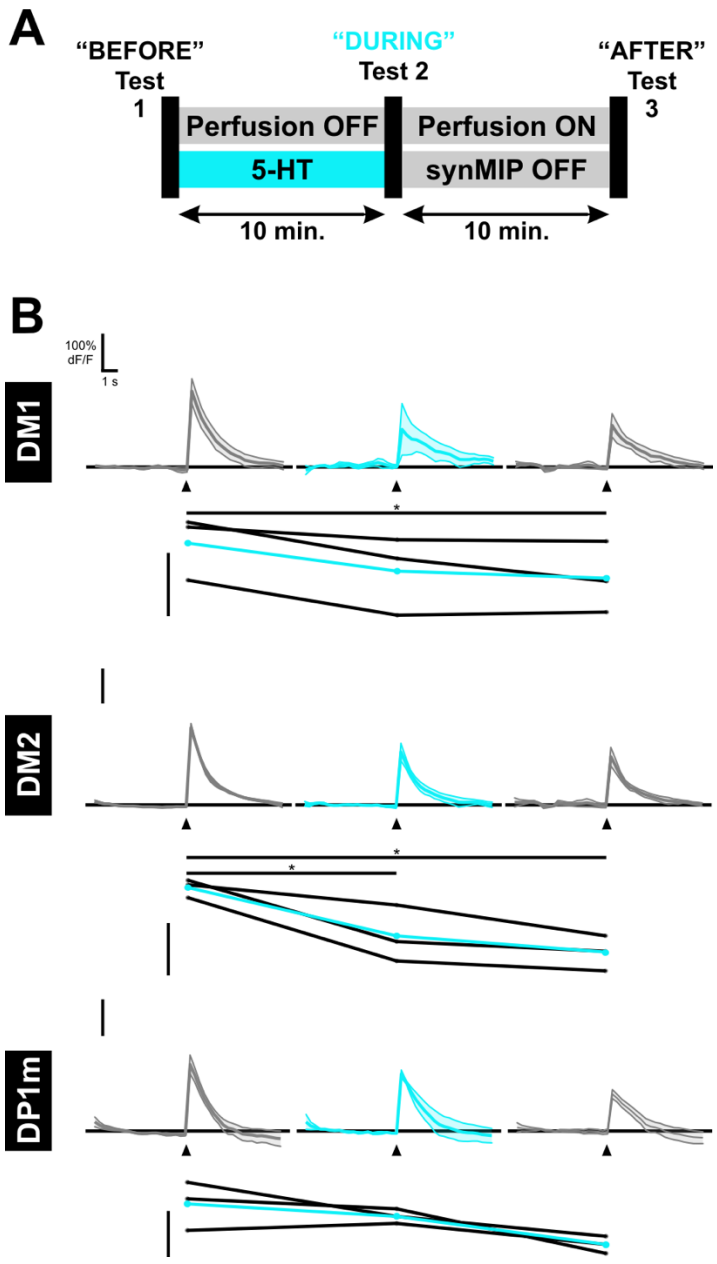

Figure 3. Serotonin decreases MIPergic LN odor-evoked responses to apple cider vinegar (ACV) in most glomeruli tested.

(A) MIPergic LN odor-evoked responses are initially tested under constant perfusion (Test 1; "BEFORE"), then the perfusion system is shut off and 5-HT is pressure injected into the AL. After a 10min incubation period, MIPergic LN odor-evoked responses are tested again (Test 2; "DURING"), after which the perfusion system is turned back on. MIPergic LN responses are tested once more after a 10min washout period (Test 3; "AFTER").

(B) MIPergic LN neurites in DM1, DM2, and DP1m (mean ± SEM) odor-evoked responses to 10^{-2} ACV before 10^{-4} 5-HT application (most left traces), 10min after 10um

5-HT pressure injection (middle traces), and after a 10min washout epoch (far right traces). Serotonin significantly decreases MIPergic LN neurites' responses in DM1 (before vs. after: p = : p = 0.048, n = 3; Bonferroni-corrected repeated-measures pairwise t-tests) and DM2 (before vs. during: p = 0.036, n = 3; before vs. after: p = 0.03, n = 3; Bonferroni-corrected repeated-measures pairwise t-tests).
In all cases: n = 3; traces represent mean ± SEM of the data; scale bars = 100%ΔF/F; repeated measures scatter plot represents each animal's max response (%ΔF/F; black dots) connected across treatments (black lines), and the mean of each test's max response (%ΔF/F) across all animals (cyan dots and lines).

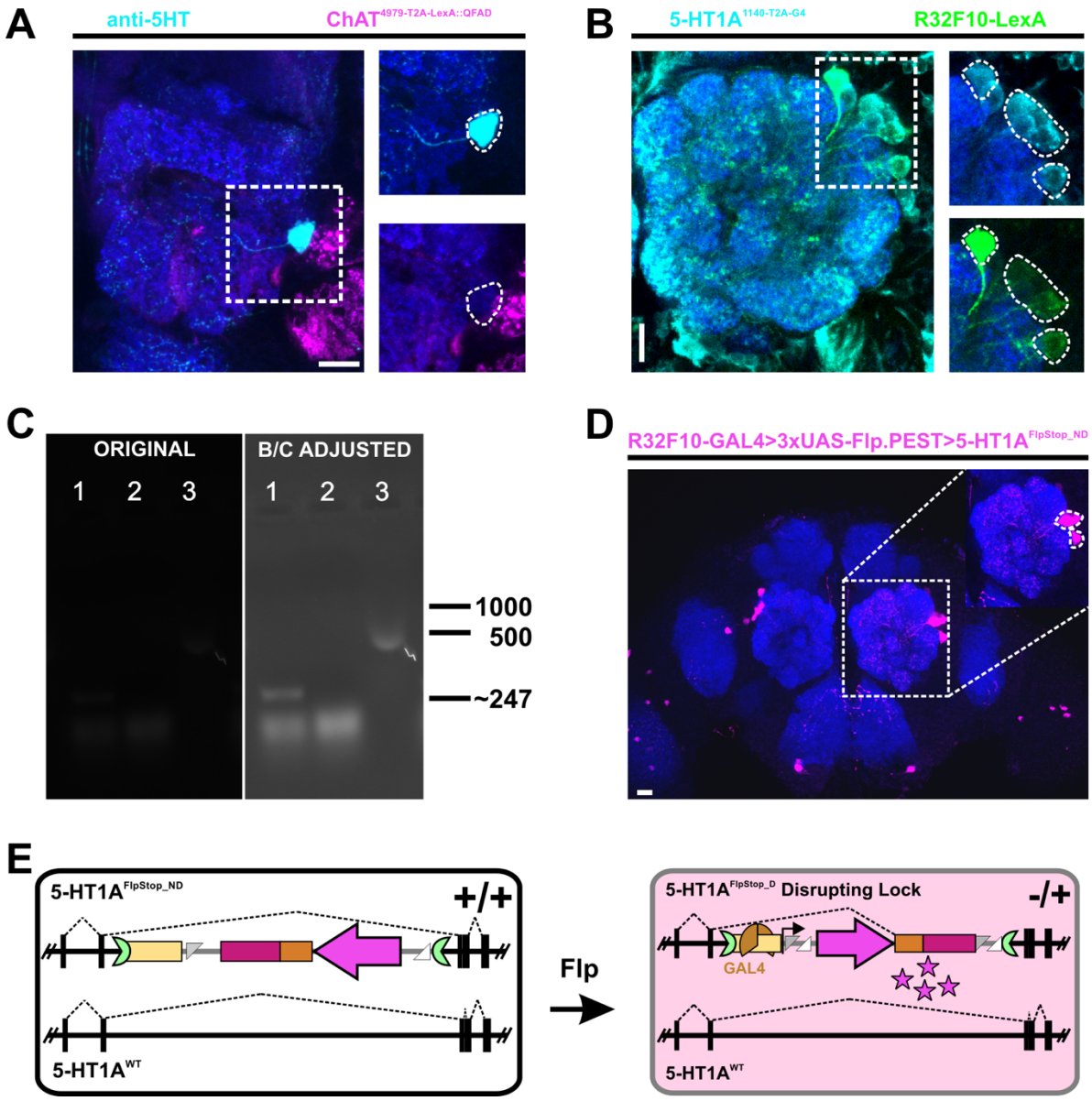

Figure S1. The CSDns do not express choline acetyltransferase and tools for future experiments.
(A) A protein-trap T2A-LexA::QFAD knockin within choline acetyltransferase (ChAT; magenta) does not label the CSDns (as delineated with anti-5HT staining; cyan). This suggests the CSDns do not release acetylcholine.
(B) Intersectional genetics between a 5-HT1A T2A-GAL4 protein-trap knockin (cyan) and R32F10-LexA (green) reveal 100% of R32F10-LexA neurons are 5-HT1A positive. Cell count estimates, ~8.5 ± 0.40 neurons, n = 6.
(C) Original (unmodified) gel and brightness/contrast adjusted (B/C adjusted) gel image of PCR confirmation of 5-HT1A FlpStop transgene orientation, where each lane corresponds to: (1) genomic DNA + MiL-F + 5pRP, (2) genomic DNA + MiL-F + 3pFP,

and (3) diluted DNA-only control (no polymerase, dNTPs, etc.). All genomic DNA depicted were extracted from the same “founder” lineage. The ~247bp band in lane 1 suggests FlpStop cassette integration occurred and is in the “Non-Disrupting” orientation. Values to the right of the gels correspond to base pair values derived from the DNA ladder.

(D) To test (*in vivo*) the orientation of the FlpStop cassette in founders from **(C)**, we crossed these flies to a GAL4 which produced no tdTomato signal (data not shown). This suggests that the FlpStop cassette is not in the “Disrupting” orientation. Then, we crossed these flies to animals where a Flp recombinase is constitutively expressed in R32F10-GAL4 positive neurons. This produced several tdTomato-positive neurons, suggesting the FlpStop cassette is in the “Non-Disrupting” orientation. Inset: two AL LNs where the 5-HT1A^{FlpStop_ND} transgene was induced, thus producing tdTomato (magenta).

(E) Schematic of the theoretical logic for conditional disruption of 5-HT1A via FlpStop induction. Here, the FlpStop cassette (grey backbone) remain inactive within an intron of 5-HT1A. While 5-HT1A^{FlpStop_ND} is in the non-disrupting orientation, the splice acceptor (orange) and stop signals (stop codons and transcriptional terminators; scarlet) are inverted, ignored (and eventually spliced-out), thus avoiding transcriptional disruption until the transgene is induced. When the Flp recombinase is induced/present it can act on the FRT sites (light grey) to invert the once non-disruptive elements, which are then locked into this position by the FLEx switch (Schnütgen et al., 2003). In this “disrupting locked” orientation, the splice acceptor and stop signals are available, thus disrupting expression of 5-HT1A transcription from the allele and eventual translation. Moreover, cells where 5-HT1A^{FlpStop_ND} has been induced (light magenta background) can be identified during or *post hoc* by visualizing tdTomato signal (magenta stars).

In all cases: neuropil was delineated by anti-DN-Cadherin staining; scale bars = 10um.

CHAPTER 5

Discussion and Future Directions

(portions of this chapter were published in my publication Sizemore, T.R., Hurley, L.M., and Dacks, A.M. (2020). Serotonergic modulation across sensory modalities. Journal of Neurophysiology, 123, 6.)

My dissertation addresses three main questions regarding the mechanisms of serotonergic modulation of one sensory modality, olfaction. I began by establishing a "functional atlas" of which principal neuron types express which of the five serotonin receptors (5-HTRs) in the *Drosophila* primary olfactory center, the antennal lobe (AL) **(Chapter 2)**. Here, I found that each 5-HTR is expressed by specific subsets of neurons, suggesting serotonin (5-HT) targets multiple levels of olfactory processing. Generally, the inhibitory 5-HTRs are expressed by inhibitory neurons, while excitatory 5-HTRs are expressed by excitatory neurons. This suggests serotonin's effects on olfactory processing within the AL are mediated by a combination of network-wide disinhibition and glomerulus-specific enhancement. Later, in my final data chapter, I leveraged this "functional atlas" to determine how the activity of one serotonin receptor shapes the activity of a specialized neuropeptidergic signaling pathway **(Chapter 4)**. I found that, despite having a uniform effect on this peptidergic ensemble of interneurons, serotonin could have non-uniform consequences across two glomeruli (namely, DM1 and DM2). However, before I could address how the activity of this serotonin receptor adjusts the activity of this neuropeptidergic pathway, I had to determine how this neuropeptidergic pathway shapes olfactory processing **(Chapter 3)**. I determined the identity, connectivity, odor-tuning properties of the presynaptic local interneurons (LNs) that release this neuropeptide (myoinhibitory peptide, MIP), as well as the downstream MIP receptor expressing partners. Additionally, I demonstrate that MIP has divergent effects on the odor-evoked responses of olfactory receptor neurons (OSNs) across different glomeruli, wherein some OSN odor-evoked responses are decreased (DM1) while others are boosted (DM2). Altogether, my work establishes several key insights that expand our understanding of neuromodulation of sensory processing.

Below, I will expand on these findings and relate them to similar results found across sensory modalities and across disparate taxa. I will end with several looming questions that future investigators should seek to resolve.

i. Serotonergic Modulation of Olfactory Processing

Olfactory networks across disparate taxa are innervated by and modulated by the actions of 5-HTergic neurons (Gaudry, 2018; Lizbinski and Dacks, 2018; Sizemore et al., 2020). These neurons can be heterogeneous in nearly every way and often target different principal neuron types through a diversity of 5-HTRs (Sizemore et al., 2020). For example, the vertebrate olfactory bulb (OB) is innervated by Median and Dorsal Raphe Nuclei (MRN and DRN) serotonergic neurons with varying intrinsic properties, which can have multifaceted consequences for their effects on downstream 5-HTR expressing neurons, like periglomerular, juxtaglomerular, and short axon cells (Mclean and Shipley, 1987; Appel et al., 1990; Shen et al., 1993; Tecott et al., 1993; Wright et al., 1995; Waeber et al., 1998; Watts and Fink, 1999; Bai et al., 2004; Lucaites et al., 2005; Petzold et al., 2009). For instance, 5-HT stimulates 5-HT2C expressing juxtaglomerular cells in the OB to increase the amount of presynaptic inhibition exerted upon OSNs (Petzold et al., 2009). In doing so, 5-HT reduces the gain of OSN responses and thus the amount of sensory input entering the OB (Petzold et al., 2009). Like in the OB, the *Drosophila* AL is differentially innervated by a single source of synaptic 5-HT (the CSDns) that can act on nearly every principal neuron type (Dacks et al., 2006; Sizemore and Dacks, 2016; Coates et al., 2017). For example, I found that OSNs express the 5-HT2B receptor, excitatory and inhibitory PNs/LNs generally express excitatory and inhibitory 5-HTRs (respectively) (Sizemore and Dacks, 2016) (**Chapter 2**). These results have since been independently substantiated from single cell-RNA sequencing (Li et al., 2017; Deanhardt et al., 2021; McLaughlin et al., 2021) and electrophysiology experiments (Suzuki et al., 2020). My results also provide mechanisms for earlier calcium imaging experiments wherein the stimulus-evoked responses of various principal AL neuron populations were assessed before and after 5-HT application (Dacks et al., 2009). For instance, in the aforementioned study, 5-HT application was found to increase LN-mediated GABAergic inhibition of OSN terminals (Dacks et al., 2009), and my results show that ~12 GABAergic LNs express the excitatory 5-HT7 (Sizemore and Dacks, 2016). Therefore, 5-HT (in this instance) likely increases the excitability of these GABAergic LNs by activating their 5-

HT7 receptors, consequently decreasing OSN input. Altogether, these examples demonstrate that general future efforts to understand how a given modulator acts in a neural circuit must consider the modulator's receptor(s) distribution within the circuit. That is to say, the identity of the neuromodulatory molecule itself is mostly dispensable; the effect of any neuromodulator on a cell is dictated by the receptor type/subtype(s) expressed by that cell.

ii. Peptidergic Modulation of Olfactory Processing

Despite their rich abundance across all nervous systems, the mechanism of neuropeptidergic modulation of sensory processing has largely been understudied. Recent technological advances have enabled studies that seek to resolve peptidergic modulatory mechanisms, such as my previously described work (**Chapter 3**) and recent work in the olfactory bulb. In the olfactory bulb, the neuropeptide somatostatin (SST) is released by calretinin-positive GABAergic LNs and sparse GABAergic deep short-axon cells (Lepousez et al., 2010a). Here, SSTergic LNs form reciprocal synapses with several mitral cells (2^{nd}-order relay neurons) and other inhibitory LNs, both of which differentially express the four SST receptors found in the central nervous system (SSTR1-4) (Videau et al., 2003; Martel et al., 2015; Nocera et al., 2019). Moreover, SST signaling through at least one of these receptors (SSTR2) has been shown to play a critical role in the animal's ability to detect and discriminate between olfactory stimuli (Lepousez et al., 2010b; Lepousez and Lledo, 2013; Nocera et al., 2019). Similarly, I find that MIP is released by GABAergic LNs that form reciprocal synapses with OSNs, PNs, non-MIP LNs, and other MIPergic LNs. The MIP receptor (sex peptide receptor, or SPR) is similarly broadly distributed across AL principal neurons, but is also expressed by several food-odor responsive OSNs.

MIP-SPR signaling was previously found to control the fly's sensitivity to food-associated odors and drive to search for food (Min et al., 2016). These investigators found that inactivating all MIPergic neurons increases the animal's drive for food-derived odors in a T-maze assay (Min et al., 2016). This effect was replicated in similar experiments performed with MIP-genetic null mutants and could be reversed by MIP overexpression

in all MIP neurons in this mutant background (Min et al., 2016). In contrast, increasing MIP transmission significantly alters the animal's drive for food-odors - so much so that they display odor-induced aversion (Min et al., 2016). These behavioral observations, are consistent with my finding that individual MIPergic LNs significantly co-innervate several food-odor associated glomeruli and neurons from several of these glomeruli express SPR. Moreover, I find that MIP-SPR signaling significantly diminishes odor-evoked responses from food-odor associated glomeruli (DM1) regardless of odor concentration. As DM1 activation has been shown to elicit potent behavioral attraction (Semmelhack and Wang, 2009; Bell and Wilson, 2016) and MIP-null mutants display significantly greater behavioral attraction to food-odors (Min et al., 2016), my results suggest that the MIPergic AL LNs signaling circuit may represent one of likely several neural substrates whose actions underly the animal's switch in satiety-state driven behaviors. However, future work will need to be done to specifically determine whether MIPergic LN-derived MIP signaling contributes to odor-evoked behavioral responses.

iii. Metamodulation: Large Consequences via Simple Manipulations

To the best of my knowledge, 5-HTergic modulation of peptidergic modulation has not been explored in the OB. In addition to SST, the neuropeptides vasoactive intestinal peptide (VIP), substance P, neuropeptide Y (NPY), vasopressin, and cholecystokinin (CCK) are present in the OB (Fallon and Seroogy, 1985; Baker, 1986; Seroogy et al., 1987; Blakemore et al., 2006; Lepousez et al., 2010a; Tobin et al., 2010). Moreover, the OB is innervated by 5-HTergic fibers from the MRN and DRN (Muzerelle et al., 2016; Ren et al., 2018; Huang et al., 2019). Although whether these neuropeptide-releasing populations express 5-HTRs has not been determined (to the best of my knowledge), work in other modalities has revealed that 5-HT acts on neuropeptide-releasing neurons and in doing so might have significant behavioral consequences. For instance, interneurons of the vertebrate sensory cortex that release vasoactive intestinal peptide (VIP) also express the excitatory ionotropic 5-HT3 receptor (Lee et al., 2010; Rudy et al., 2011; Cardin, 2018). Activating 5-HT3 receptors in VIP interneurons causes a hyperpolarization in 5-HT3-negative inhibitory interneurons, which subsequently

disinhibits pyramidal neurons (Pfeffer et al., 2013; Jiang et al., 2015; Takesian et al., 2018). Moreover, serotonergic stimulation of VIP interneurons also produces a latent, $GABA_B$-receptor mediated hyperpolarization in these same pyramidal cells (Takesian et al., 2018). Therefore, by acting through these interneurons, serotonin can have a large impact on network dynamics and even modulate distinct aspects of sensory processing (Pi et al., 2013). Moreover, the activity of the VIP interneurons appears to be at least one determinant for the changes observed in the activity of visual cortex circuitry according to the animal's ongoing behavioral state (Bennett et al., 2013; Polack et al., 2013; Fu et al., 2014; Pakan et al., 2016; Batista-Brito et al., 2017). Collectively, these results suggest that there may be a serotonin-induced contingency switching module in visual cortex, wherein the animal's locomotor activity induces 5-HTergic activation of VIP interneurons. Then, perhaps after some epoch post-behavior initiation, negative feedback terminates this serotonin-induced module.

My result that 5-HT uniformly inhibits MIPergic LN odor-evoked responses across food-odor associated glomeruli is one of few examples of 5-HTergic metamodulation of olfactory processing. I previously demonstrated that MIPergic LNs are robustly and consistently activated by a food-associated odor, and that MIP application differentially affects afferent input to the relevant olfactory channels. Therefore, several plausible consequences might arise from 5-HTergic modulation of MIPergic modulation here. For instance, if 5-HT's effects are sufficiently strong enough to halt MIPergic LN MIP-release, then 5-HT may be used here to return each MIPergic modulated olfactory channel to "baseline". This would be a useful and efficient mechanism to bias AL neuronal activity to a more food-odor sensitive state in situations when the animal is hungry. In this situation, perhaps 5-HT is tonically released and scales linearly with the animal's increasing hunger, eventually reaching a "tipping point" where anorexic-like behaviors are induced. Moreover, since 5-HT acts on other AL neurons through many receptors (Dacks et al., 2009; Sizemore and Dacks, 2016; Zhang and Gaudry, 2016), it is plausible that this 5-HTergic metamodulation could efficiently switch-off MIP-induced food-odor avoidance while simultaneously increasing the activity of circuit elements that drive food-odor induced attraction (e.g., disinhibition of DM1 OSNs, increase sensitivity of food-odor sensitive PNs, etc.). Although some of these specific hypotheses will need to be followed

up by my successors, my results represent the key beginnings of a metamodulatory pathway that may impactfully adjust olfactory processing. Future investigators should seek to determine whether 5-HT1A expression in MIPergic LNs is required for 5-HT to initiate this switch in behavioral drive.

Future Directions

In **Chapter 2**, I determined the numbers of each principal AL neuron type that expresses each of the five 5-HT receptors. However, while this methodology can tell me if a neuron expresses/recently expressed a given 5-HTR, it could not tell me where along the given neuron any particular 5-HTR localizes. Moreover, these methods rely on 5-HTR expression induction of GAL4 which then induces GFP expression, and a single GFP molecule has a half-life ~26 hours (Corish and Tyler-Smith, 1999). Thus, it is plausible that a given neuron was identified as being 5-HTR positive long after that 5-HTR was no longer expressed. However, my results have been independently substantiated since their publication (Coates et al., 2017; Li et al., 2017; Suzuki et al., 2020; Deanhardt et al., 2021; McLaughlin et al., 2021). Regardless, several questions remain:

1) *What glomeruli do 5-HTR expressing neurons innervate? Are all glomeruli innervated by at least one 5-HTR expressing neuron?*
2) *If a neuron expresses multiple 5-HTRs, are these receptors expressed in different neuronal compartments (e.g., axons, etc.)? Does this spatial pattern of 5-HTR expression hold true for all neurons that co-express the same combinations of 5-HTRs?*
3) *How does 5-HTR expression evolve over the development of the animal? Do neurons express different receptor subtypes at different stages of the animal's life?*
4) *How much of the context-dependent effects of 5-HT arises from the heterogeneous nature of 5-HTergic neurons? How much arises from different 5-HTR expression motifs?*
5) *What sexual dimorphisms exist in 5-HT signaling substrates (e.g., 5-HTergic neurons, 5-HTR distribution, etc.)?*

6) *How do the properties of 5-HTergic neurons and expression patterns of 5-HTRs change in response to different external and/or internal demands?*
7) *Do invertebrate 5-HTRs homodimerize and/or heterodimerize like vertebrate 5-HTRs have been noted to do [e.g.,* (Xie et al., 1999)*]? And, if so, how does this change their ligand affinities, time-course of action, influence on the neuron, etc.?*
8) *How does 5-HTR autoreceptor and heteroreceptor activity [e.g.,* (Sizemore et al., 2020)*] influence 5-HTergic modulation of sensory processing?*

In **Chapter 3**, I described a novel peptidergic signaling pathway that mediates olfactory gain control. I determined that MIP is released by GABAergic LNs that – as individuals – innervate a different compliment of olfactory channels from animal-to-animal. However, these MIPergic LNs reliably innervate all glomeruli across all animals. Moreover, I determined the identity of each synaptic input to and postsynaptic partner that connects with each of my stringently selected putative MIPergic LNs. I identified which downstream partners express the MIP receptor (SPR) and are therefore subject to MIPergic modulation, and then I tested the odor-evoked responses of one SPR-expressing population to one stimulus at multiple concentrations. Through this "simple case study" of OSN ACV-evoked responses, I demonstrated that MIP adjusts the gain of OSN input to glomeruli involved in processing the innately attractive odor ACV. However, several questions remain and should be followed up by future investigations. These include (but are not limited to):

1) *What factor(s) underly the animal-to-animal differences in individual MIPergic LN innervation patterns?*
2) *Do MIPergic LNs have different connectivity from animal-to-animal?*
3) *How do MIPergic LNs respond across a larger odor panel, that include odors that activate very few glomeruli (e.g., cis-vaccenyl acetate, wasp pheromone, etc.)?*
4) *Do individual MIPergic LNs display differing biophysical and electrophysiological properties from animal-to-animal? If you record from a large enough sampling, can you identify the same MIPergic LN based on odor-tuning properties from somatic electrophysiology recordings?*

5) *Are individual MIPergic LNs electrotonically isolated, as was suggested by anatomical evidence included here? For instance, can you detect somatic current changes if you selectively activate a single MIPergic LN's processes in a glomerulus?*
6) *How does MIPergic modulation affect other SPR-expressing neurons that were not tested here?*

In **Chapter 4**, I show that all MIPergic LNs express the 5-HT1A receptor and make robust reciprocal connections with the CSDn. I show that 5-HT uniformly diminishes MIPergic LN odor-evoked responses in DM1 and DM2, two glomeruli whose activation is necessary and sufficient to initiate an odor-evoked attractive behavioral program. These results suggest that 5-HT, by manipulating this single circuit node, can efficiently and effectively transform olfactory driven behaviors. Questions that should be followed up by future investigations include (but are not limited to):

1) *What external stimuli and/or internal demands drive the release of 5-HT onto MIPergic LNs?*
2) *How is odor-evoked behavior influenced by MIPergic LN expression of 5-HT1A? Does decreasing MIPergic LN 5-HT1A expression alter olfactory behaviors?*
3) *Do MIPergic LNs constantly express similar levels of 5-HT1A? Does 5-HT1A preferentially localize to any particular compartments of MIPergic LNs?*
4) *If 5-HT1A protein concentrations along MIPergic LN neurites could be measured, is the concentration of 5-HT1A uniform along MIPergic LN fibers within every glomerulus?*

Conclusion

The near-ubiquitous presence of neuromodulators (such as 5-HT) within sensory regions, coupled with their strong effects on stimulus representation, suggest that these signaling pathways should be considered integral components of all sensory systems. Regardless of modality or species, 5-HTergic systems are heterogeneous at the level of

individual neurons, as well as diverse at the level of whole populations. Moreover, the suite of 5-HT receptors further expands the means with which 5-HT affects select features, such as odor coding. These heterogeneous features of the 5-HT system allow for widespread, nuanced effects of 5-HT on sensory processing that vary in a context dependent manner. Subsequently, these heterogenous features also complicate assignments of a singular role for serotonin. However, 5-HTergic modulation is widespread throughout the animal kingdom, and currently the majority of our understanding regarding the cellular mechanisms underlying 5-HTergic modulation of sensory processing comes from a handful of organisms (e.g., rodents, fruit flies, etc.). By comparing across modalities and diverse taxa, we can reveal convergent adaptations that reveal fundamental molecular, cellular and network mechanisms of sensory modulation. Similar approaches might also reveal divergent adaptations that reveal the selective pressures that sculpt neuromodulation.

WORKS CITED:

Appel NM, Mitchell WM, Garlick RK, Glennon RA, Teitler M, De Souza EB (1990) Autoradiographic characterization of (±)-1-(2,5-dimethoxy-4-[125I] iodophenyl)-2-aminopropane ([125I]DOI) binding to 5-HT2 and 5-HT(1c) receptors in rat brain. J Pharmacol Exp Ther 255:843–857.

Bai F, Yin T, Johnstone EM, Su C, Varga G, Little SP, Nelson DL (2004) Molecular cloning and pharmacological characterization of the guinea pig 5-HT1E receptor. Eur J Pharmacol 484:127–139.

Baker H (1986) Substance P and tyrosine hydroxylase are localized in different neurons of the hamster olfactory bulb. Exp Brain Res 65:245–249.

Batista-Brito R, Vinck M, Ferguson KA, Chang JT, Laubender D, Lur G, Mossner JM, Hernandez VG, Ramakrishnan C, Deisseroth K, Higley MJ, Cardin JA (2017) Developmental Dysfunction of VIP Interneurons Impairs Cortical Circuits. Neuron 95:884-895.e9.

Bell JS, Wilson RI (2016) Behavior Reveals Selective Summation and Max Pooling among Olfactory Processing Channels. Neuron 91:425–438.

Bennett C, Arroyo S, Hestrin S (2013) Subthreshold mechanisms underlying state-dependent modulation of visual responses. Neuron 80:350–357.

Blakemore LJ, Levenson CW, Trombley PQ (2006) Neuropeptide Y modulates excitatory synaptic transmission in the olfactory bulb. Neuroscience 138:663–674.

Cardin JA (2018) Inhibitory Interneurons Regulate Temporal Precision and Correlations in Cortical Circuits. Trends Neurosci 41:689–700.

Coates KE, Majot AT, Zhang X, Michael CT, Spitzer SL, Dacks AM, Spitzer SL, Gaudry Q, Dacks AM (2017) Identified serotonergic modulatory neurons have heterogeneous synaptic connectivity within the olfactory system of Drosophila Title : Identified serotonergic modulatory neurons have heterogeneous synaptic connectivity within the olfactory system of Drosop.

Corish P, Tyler-Smith C (1999) Attenuation of green fluorescent protein half-life in mammalian cells. Protein Eng 12:1035–1040.

Dacks AM, Christensen T a., Hildebrand JG (2006) Phylogeny of a Serotonin-Immunoreactive Neuron in the Primary Olfactory Center of the Insect Brain. J Comp

Neurol 498:727–746.

Dacks AM, Green DS, Root CM, Nighorn AJ, Wang JW (2009) Serotonin modulates olfactory processing in the antennal lobe of Drosophila. J Neurogenet 23:366–377.

Deanhardt B, Duan Q, Du C, Soeder C, Jones C, Volkan P (2021) Changes in splicing and neuromodulatory gene expression programs in sensory neurons with pheromone signaling and social experience. bioRxiv.

Fallon JH, Seroogy KB (1985) The Distribution and Some Connections of Cholecystokinin Neurons in the Rat Brain. Ann N Y Acad Sci 448:121–132.

Fu Y, Tucciarone JM, Espinosa JS, Sheng N, Darcy DP, Nicoll RA, Huang ZJ, Stryker MP (2014) A cortical circuit for gain control by behavioral state. Cell 156:1139–1152.

Gaudry Q (2018) Serotonergic modulation of olfaction in rodents and insects. Yale J Biol Med 91:23–32.

Huang KW, Ochandarena NE, Philson AC, Hyun M, Birnbaum JE, Cicconet M, Sabatini BL (2019) Molecular and anatomical organization of the dorsal raphe nucleus. Elife 8:1–34.

Jiang X, Shen S, Cadwell CR, Berens P, Sinz F, Ecker AS, Patel S, Tolias AS (2015) Principles of connectivity among morphologically defined cell types in adult neocortex. Science (80-) 350.

Lee SH, Hjerling-Leffler J, Zagha E, Fishell G, Rudy B (2010) The largest group of superficial neocortical GABAergic interneurons expresses ionotropic serotonin receptors. J Neurosci 30:16796–16808.

Lepousez G, Csaba Z, Bernard V, Loudes C, Videau C, Lacombe J, Epelbaum J, Viollet C (2010a) Somatostatin interneurons delineate the inner part of the external plexiform layer in the mouse main olfactory bulb. J Comp Neurol 518:1976–1994.

Lepousez G, Lledo PM (2013) Odor Discrimination Requires Proper Olfactory Fast Oscillations in Awake Mice. Neuron 80:1010–1024.

Lepousez G, Mouret A, Loudes C, Epelbaum J, Viollet C (2010b) Somatostatin contributes to in vivo gamma oscillation modulation and odor discrimination in the olfactory bulb. J Neurosci 30:870–875.

Li H, Horns F, Wu B, Luginbuhl DJ, Quake SR, Li H, Horns F, Wu B, Xie Q, Li J, Li T, Luginbuhl DJ, Quake SR (2017) Classifying Drosophila Olfactory Projection Neuron

Resource Classifying Drosophila Olfactory Projection Neuron Subtypes by Single-Cell RNA Sequencing. Cell 171:1206-1207.e22.

Lizbinski KM, Dacks AM (2018) Intrinsic and Extrinsic Neuromodulation of Olfactory Processing. Front Cell Neurosci 11:1–11.

Lucaites VL, Krushinski JH, Schaus JM, Audia JE, Nelson DL (2005) [3H]LY334370, a novel radioligand for the 5-HT1F receptor. II. Autoradiographic localization in rat, guinea pig, monkey and human brain. Naunyn Schmiedebergs Arch Pharmacol 371:178–184.

Martel G, Simon A, Nocera S, Kalainathan S, Pidoux L, Blum D, Leclère-Turbant S, Diaz J, Geny D, Moyse E, Videau C, Buée L, Epelbaum J, Viollet C (2015) Aging, but not tau pathology, impacts olfactory performances and somatostatin systems in THY-Tau22 mice. Neurobiol Aging 36:1013–1028.

McLaughlin CN, Brbić M, Xie Q, Li T, Horns F, Kolluru SS, Kebschull JM, Vacek D, Xie A, Li J, Jones RC, Leskovec J, Quake SR, Luo L, Li H (2021) Single-cell transcriptomes of developing and adult olfactory receptor neurons in drosophila. Elife 10:1–37.

Mclean JH, Shipley T (1987) Serotonergic Afferents to the Rat Olfactory Bulb : I . Origins and Laminar Specificity of Serotonergic Inputs in the Adult Rat. J Neurosci 7.

Min S, Chae HS, Jang YH, Choi S, Lee S, Jeong YT, Jones WD, Moon SJ, Kim YJ, Chung J (2016) Identification of a peptidergic pathway critical to satiety responses in drosophila. Curr Biol 26:814–820.

Muzerelle A, Scotto-Lomassese S, Bernard JF, Soiza-Reilly M, Gaspar P (2016) Conditional anterograde tracing reveals distinct targeting of individual serotonin cell groups (B5–B9) to the forebrain and brainstem. Brain Struct Funct 221:535–561.

Nocera S, Simon A, Fiquet O, Chen Y, Gascuel J, Datiche F, Schneider N, Epelbaum J, Viollet C (2019) Somatostatin serves a modulatory role in the mouse olfactory bulb: Neuroanatomical and behavioral evidence. Front Behav Neurosci 13:1–20.

Pakan JMP, Lowe SC, Dylda E, Keemink SW, Currie SP, Coutts CA, Rochefort NL (2016) Behavioral-state modulation of inhibition is context-dependent and cell type specific in mouse visual cortex. Elife 5:1–18.

Petzold GC, Hagiwara A, Murthy VN (2009) Serotonergic modulation of odor input to the

mammalian olfactory bulb. Nat Neurosci 12:784–791.

Pfeffer CK, Xue M, He M, Huang ZJ, Scanziani M (2013) Inhibition of inhibition in visual cortex: The logic of connections between molecularly distinct interneurons. Nat Neurosci 16:1068–1076.

Pi HJ, Hangya B, Kvitsiani D, Sanders JI, Huang ZJ, Kepecs A (2013) Cortical interneurons that specialize in disinhibitory control. Nature 503:521–524.

Polack PO, Friedman J, Golshani P (2013) Cellular mechanisms of brain state-dependent gain modulation in visual cortex. Nat Neurosci 16:1331–1339.

Ren J, Friedmann D, Xiong J, Liu CD, Ferguson BR, Weerakkody T, DeLoach KE, Ran C, Pun A, Sun Y, Weissbourd B, Neve RL, Huguenard J, Horowitz MA, Luo L (2018) Anatomically Defined and Functionally Distinct Dorsal Raphe Serotonin Sub-systems. Cell 175:472-487.e20.

Rudy B, Fishell G, Lee SH, Hjerling-Leffler J (2011) Three groups of interneurons account for nearly 100% of neocortical GABAergic neurons. Dev Neurobiol 71:45–61.

Semmelhack JL, Wang JW (2009) Select Drosophila glomeruli mediate innate olfactory attraction and aversion. Nature 459:218–223.

Seroogy KB, Mehta A, Fallon JH (1987) Neurotensin and cholecystokinin coexistence within neurons of the ventral mesencephalon: projections to forebrain. Exp Brain Res 68:277–289.

Shen Y, Monsma FJ, Metcalf MA, Jose PA, Hamblin MW, Sibley DR (1993) Molecular cloning and expression of a 5-hydroxytryptamine7 serotonin receptor subtype. J Biol Chem 268:18200–18204.

Sizemore TR, Dacks AM (2016) Serotonergic Modulation Differentially Targets Distinct Network Elements within the Antennal Lobe of Drosophila melanogaster. Sci Rep 6:37119.

Sizemore TR, Hurley LM, Dacks A (2020) Serotonergic Modulation Across Sensory Modalities. J Neurophysiol:2406–2425.

Suzuki Y, Schenk JE, Tan H, Gaudry Q (2020) A Population of Interneurons Signals Changes in the Basal Concentration of Serotonin and Mediates Gain Control in the Drosophila Antennal Lobe Report A Population of Interneurons Signals Changes in the Basal Concentration of Serotonin and Mediates Gain Co. Curr Biol:1–9.

Takesian AE, Bogart LJ, Lichtman JW, Hensch TK (2018) Inhibitory circuit gating of auditory critical-period plasticity. Nat Neurosci 21:218–227.

Tecott LH, Maricq A V., Julius D (1993) Nervous system distribution of the serotonin 5-HT3 receptor mRNA. Proc Natl Acad Sci U S A 90:1430–1434.

Tobin VA, Hashimoto H, Wacker DW, Takayanagi Y, Langnaese K, Caquineau C, Noack J, Landgraf R, Onaka T, Leng G, Meddle SL, Engelmann M, Ludwig M (2010) An intrinsic vasopressin system in the olfactory bulb is involved in social recognition. Nature 464:413–417.

Videau C, Hochgeschwender U, Kreienkamp HJ, Brennan MB, Viollet C, Richter D, Epelbaum J (2003) Characterisation of [125I]-Tyr0DTrp8-somatostatin binding in sst1- to sst4- and SRIF-gene-invalidated mouse brain. Naunyn Schmiedebergs Arch Pharmacol 367:562–571.

Waeber C, Grailhe R, Yu X-J, Hen R, Moskowitz MA (1998) Putative 5-ht5 receptors: localization in the mouse CNS and lack of effect in the inhibition of dural protein extravasation. Ann N Y Acad Sci.

Watts SW, Fink GD (1999) 5-HT2B-receptor antagonist LY-272015 is antihypertensive in DOCA-salt-hypertensive rats. Hear Circ Physiol 276:H944–H952.

Wright DE, Seroogy KB, Lundgren KH, Davis BM, Jennes L (1995) Comparative localization of serotonin1A, 1C, and 2 receptor subtype mRNAs in rat brain. J Comp Neurol 351:357–373.

Xie Z, Lee SP, O'Dowd BF, George SR (1999) Serotonin 5-HT(1B) and 5-HT(1D) receptors form homodimers when expressed alone and heterodimers when co-expressed. FEBS Lett 456:63–67.

Zhang X, Gaudry Q (2016) Functional integration of a serotonergic neuron in the drosophila antennal lobe. Elife 5:1–24.

Abbreviation / Acronym	Meaning
5-HT	Serotonin (5-hydroxytryptophan)
5-HT1A	Serotonin Receptor subtype 1A
5-HT1B	Serotonin Receptor subtype 1B
5-HT2A	Serotonin Receptor subtype 2A
5-HT2B	Serotonin Receptor subtype 2B
5-HT2C	Serotonin Receptor subtype 2C
5-HT3	Serotonin Receptor subtype 3
5-HT4	Serotonin Receptor subtype 4
5-HT5B	Serotonin Receptor subtype 5B
5-HT6	Serotonin Receptor subtype 6
5-HT7	Serotonin Receptor subtype 7
5-HT8	Serotonin Receptor subtype 8
5-HTR(s)	Serotonin Receptor(s)
ACV	Apple Cider Vinegar
adPN(s)	Anterodorsal Projection Neuron(s)
AL(s)	Antennal Lobe(s)
AMPA receptor(s)	α-amino-3-hydroxy-5-methyl-4-isoxazolepropionic acid receptor(s) *an ionotropic glutamate receptor*
AstB / Ast-B	Allatostatin-B
ATP	Adenosine Triphosphate
BENZ	Benzaldehyde
Brp	Bruchpilot
BSA	Bovine Serum Albumin
Cas9	CRISPR-associated protein 9
ChAT	Choline Acetyltransferase
CRISPR	Clustered Regulatory Interspaced Short Palindromic Repeats
CSD / CSDn(s)	The Contralaterally Projecting, Serotonin-Immunoreactive Deutocerebral Neuron(s)

D1 receptor(s)	Dopamine-1 receptor(s)
D2 receptor(s)	Dopamine-2 receptor(s)
DCV(s)	Dense Core Vesicle(s)
DenMark	Dendrite Marker
DFN	Dorsal Flexion Neurons
DRN	Dorsal Raphe Nucleus
DSI	Dorsal Swim Interneurons
ELAV	Embryonic Lethal Abnormal Vision
eLN(s)	Excitatory/Electrically-Coupled Local Interneuron(s)
EM	Electron Microscopy
ePN(s) / e-PN(s)	Excitatory Projection Neuron(s)
EPSP(s)	Excitatory Postsynaptic Potential(s)
Gαi-signaling	G-protein alpha-i signaling
GABA	Gama Aminobutyric Acid
$GABA_A$	Gama Aminobutyric Acid Receptor subtype A
$GABA_B$	Gama Aminobutyric Acid Receptor subtype B
GER. ACETATE	Geranyl Acetate
GFP	Green Fluorescent Protein
GlutLN(s)	Glutamatergic Local Interneuron(s)
GPCR(s)	G-Protein Coupled Receptor(s)
GR(s)	Gustatory Receptor(s)
HA	Hemagglutinin
HEX	1-Hexanol
ICLI	Inferior Contralateral Interneurons
iLN(s)	Inhibitory Local Interneuron(s)
IP_3	Inositol Triphosphate
iPN(s) / i-PN(s)	Inhibitory Projection Neuron(s)
IPSP(s)	Inhibitory Postsynaptic Potential(s)

IR(s)	Ionotropic Receptor(s)
latLN(s)	Lateral Local Interneuron(s)
latPN(s)	Lateral Projection Neuron(s)
LexAop	LexA-Operator Sequence
LH	Lateral Horn
LMlo	Lateral Medial Lobula
LN(s)	Local Interneuron(s)
LOM-MIP	*Locusta migratoria* Myoinhibitory Peptide
MB	Mushroom Body
MBDL	Median Bundle
MCFO	Multicolor Flp Out
MiMIC	Minos-Mediated Insertion Cassette
MIP	Myoinhibitory Peptide
mlALT	Mediolateral Antennal Lobe Tract
MOD-1	Modulation of Locomotion Defective-1
MP	Maxillary Palp
mPN(s)	Multiglomerular Projection Neuron(s)
MRN	Median Raphe Nucleus
MsMIP	*Manduca sexta* Myoinhibitory Peptide
MSN(s)	Medium Spiny Neuron(s)
NBLAST	Neuron BLAST
NCAD	DN-Cadherin
NGS	Normal Goat Serum
NPF	Neuropeptide F
NPRR-ANP	Neuropeptide Release Reporter tagged Atrial Natriuretic Peptide
NPY	Neuropeptide Y
NPY	Neuropeptide Y
OR(s)	Olfactory Receptor(s)

OSN(s) / ORN(s)	Olfactory Sensory Neuron(s) / Olfactory Receptor Neuron(s)
P/N	Part Number
P2X2	P2X Purinoreceptor 2
PBS	Phosphate Buffered Saline
PBST	Phosphate Buffered Saline with Triton-X
PC1	Principal Component 1
PC2	Principal Component 2
PCA	Principal Components Analysis
PDF	Pigment-Dispersing Factor
Pea-MIP	*Periplaneta* Myoinhibitory Peptide
PEEK	Polyether Ether Ketone
pepLN(s)	Peptidergic Local Interneuron(s)
PLC	Phospholipase C
PN(s)	Projection Neuron(s)
preproANF-EMD	GFP-tagged Atrial Natriuretic Factor
PTSP-1	Prothoracicotropic hormone-1
REPO	Reverse Polarity
RFP	Red Fluorescent Protein
RMCE	Recombinase-Mediated Cassette Exchange
SAC(s)	Starburst Amacrine Cell(s)
scRNA-seq	Single Cell RNA-Sequencing
SLP	Superior Lateral Protocerebrum
SMP	Superior Medial Protocerebrum
sNPF	Short Neuropeptide F
SP	Sex Peptide
SPR	Sex Peptide Receptor
SPR	Sex Peptide Receptor
SST	Somatostatin

SSTR(s)	Somatostatin Receptor(s)
STG	Stomatogastric Ganglion
synMIP	Synthetic Myoinhibitory Peptide
syt.eGFP	Synaptotagmin-tagged Enhanced GFP
Thermo/Hygro	Thermosensation and Hygrosensation
TKK	Tachykinin
TRPA1	Transient Receptor Potential Cation Channel subfamily A member 1
UAS	Upstream Activator Sequence
uPN(s)	Uniglomerular Projection Neuron(s)
v.###	Version ###
VGlut / vGlut	Vesicular Glutamate Transporter
VIP	Vasoactive Intestinal Peptide
vLN(s)	Ventral Local Interneuron(s)
vlPN(s)	Ventrolateral Projection Neuron(s)
VP16	VP16 Acidic Activation Domain
vPN(s)	Ventral Projection Neuron(s)
VTA	Ventral Tegmental Area